SERDP

FINAL REPORT

Combined In Situ/Ex Situ Treatment Train for Remediation of Per- and Polyfluoroalkyl Substances (PFAS)-Contaminated Groundwater

Michelle Crimi
Clarkson University

John Kornuc
Naval Facilities Engineering Command (NAVFAC) Expeditionary Warfare Center

Nathan Hagelin
AMEC Foster Wheeler

Steven Woodard
Emerging Compounds Treatment Technologies (ECT2)

Jennifer Guelfo
Brown University

January 2023

SERDP Project ER18-1306

REPORT DOCUMENTATION PAGE

Form Approved
OMB No. 0704-0188

1. REPORT DATE (DD-MM-YYYY)	2. REPORT TYPE	3. DATES COVERED (From - To)
01/23/2023	Final Technical Report	9/27/2018 - 9/27/2023

4. TITLE AND SUBTITLE

Combined In Situ/Ex Situ Treatment Train for Remediation of PFAS-Impacted Goundwater

5a. CONTRACT NUMBER

18-C-0092

5c. PROGRAM ELEMENT NUMBER

6. AUTHOR(S)

Michelle Crimi: Clarkson University
John Kornuc: Naval Facilities Engineering Command (NAVFAC) Expeditionary Warfare Center
Nathan Hagelin: AMEC Foster Wheeler
Steven Woodard: Emerging Compounds Treatment Technologies (ECT2)
Jennifer Guelfo: Brown University

5d. PROJECT NUMBER

ER18-1306

5e. TASK NUMBER

5f. WORK UNIT NUMBER

7. PERFORMING ORGANIZATION NAME(S) AND ADDRESS(ES)

Clarkson University
8 Clarkson Ave
Potsdam, NY 13699

8. PERFORMING ORGANIZATION REPORT NUMBER

ER18-1306

9. SPONSORING / MONITORING AGENCY NAME(S) AND ADDRESS(ES)

Office of the Deputy Assistant Secretary of Defense (Energy Resilience & Optimization)
3500 Defense Pentagon, RM 5C646
Washington, DC 20301-3500

10. SPONSOR/MONITOR'S ACRONYM(S)

SERDP

11. SPONSOR/MONITOR'S REPORT NUMBER(S)

ER18-1306

12. DISTRIBUTION / AVAILABILITY STATEMENT

DISTRIBUTION STATEMENT A. Approved for public release: distribution unlimited.

13. SUPPLEMENTARY NOTES

14. ABSTRACT

Key challenges to treating per- and polyfluoroalkyl substance (PFAS)-impacted sites include the broad range of PFAS present, the presence of polyfluorinated precursors that transform into perfluoroalkyl acids (PFAAs), the recalcitrance of PFAAs, and the current lack of in situ approaches for implementing aggressive chemical treatment processes. The objective of this project was to develop a set of combined in situ/ex situ treatment approaches for the efficient and effective treatment of PFAS-impacted groundwater. The treatment train includes (A) pre-treatment of PFAS and their precursors in situ by oxidation to eliminate or reduce PFAA source zones, and (B) pumping pre-treated groundwater for follow-on ex situ treatment by ion exchange and plasma destruction. Precursor transformation was effective using persulfate and oxygen in both batch tests and transport cells and was found to reduce PFAA source zones. IX regenerant solutions comprised of methanol and brine were explored, and regenerant solution performance was comparable between the solutions even in different resins. Plasma was found to be successful in the treatment of PFAS in groundwater, pre-oxidised groundwater, and in concentrated IX regenerant solution.

15. SUBJECT TERMS

Distillation, groundwater, investigation derived waste, in situ chemical oxidation, ion exchange, PFAS, plasma treatment, resins, treatment train

16. SECURITY CLASSIFICATION OF:			17. LIMITATION OF ABSTRACT	18. NUMBER OF PAGES	19a. NAME OF RESPONSIBLE PERSON
a. REPORT	b. ABSTRACT	c. THIS PAGE			Michelle Crimi
Unclass	Unclass	Unclass	Unclass	171	19b. TELEPHONE NUMBER (Include area code) 315-268-4174

TABLE OF CONTENTS

LIST OF TABLES

LIST OF FIGURES

LIST OF ACRONYMS

4:2 FTS	4:2 Fluorotelomer sulfonic acid
6:2 FTS	6:2 Fluorotelomer sulfonic acid
8:2 FTS	8:2 Fluorotelomer sulfonic acid
10:2 FTS	10:2 Fluorotelomer sulfonic acid
AC	Ambient control
AFFF	Aqueous Film Forming Foam
AGW	Artificial ground water
AHA	Alkaline heat activated
ANOVA	Analysis of variance
BD	Below detection
BDL	Below detection limit
bgs	Below ground surface
BMP	Best management practices
Br	Bromide
BV	Bed volume
$CaCO_3$	Calcium carbonate
CaO_2	Calcium peroxide
CEC	Cation exchange capacity
CIC	Combustion ion chromatography
CO_2	Carbon dioxide
CSTR	Continuous stirred tank reactor
CTAB	Cetrimonium bromide
DC	Direct current
DO	Dissolved oxygen
DOC	Dissolved organic carbon
DoD	Department of Defense
EBCT	Empty bed contact time
EC	Enhanced contact
ECF	Electrochemical fluorination

ECT	Environmental Consulting & Technology, Inc.
ECT2	Emerging Compounds Treatment Technologies, Inc.
EtFOSA	N-ethyl perfluorooctane sulfonamide
EtFOSAA	N-ethyl perfluorooctane sulfonamido acetic acid
F	Fluorine
Fe	Iron
FOSA-1 (or FOSA)	Perfluorooctane sulfonamide
FOSAA	Perfluorooctane sulfonamido acetic acid
FT	Fluorotelomer
GAC	Granular activated carbon
gpm	Gallons per minute
GW	Ground water
HA	Heat activated
HAL	Health advisory level
HDPE	High Density Poly Ethylene
HRQToF	High-resolution quadrupole time-of-flight
HVAC	Heating, ventilation and air conditioning
IC	Ion chromatography
IDW	Investigation derived waste
ISCO	In situ chemical oxidation
IX	Ion exchange
MDL	Method detection limit
MeFOSA	N-methyl perfluorooctane sulfonamide
MeFOSAA	2-(N-Methylperfluorooctanesulfonamido)acetic acid
Mn	Manganese
MS	Mass spectrometry
NaBr	Sodium bromide
NaCl	Sodium chloride

NaOH	Sodium hydroxide
NAVFAC	Naval Facilities Engineering Systems Command
N_2	Nitrogen
NTU	Nephelometric turbidity units
O_2	oxygen
OC	Organic carbon
O&M	Operations and Maintanence
PFAA	perfluoroalkyl acids
PFAS	Per- and polyfluoroalkyl substance
PFBA	Perfluorobutanoic acid
PFBS	Perfluorobutane sulfonate
PFCA	Perfluoroalkyl carboxylic acids
PFDA	Perfluorodecanoic acid
PFNA	Perfluorononanoic acid
PFDS	Perfluorodecanesulfonic acid
PFHpA	Perfluoroheptanoic acid
PFHxA	Perfluorohexanoic acid
PFHpS	Perfluoroheptane sulfonic acid
PFHxS	Perfluorohexane sulfonate
PFNA	Perfluorononanoic acid
PFPeA	Perfluoropentanoic acid
PFPnA	Perfluoropentanoic acid
PFOA	Perfluorooctanoic acid
PFOS	Perfluorooctanesulfonic acid
PFSA	perfluorosulfonic acid
PFUnA	Perfluoroundecanoic acid
pHC	pH control
ppt	Parts per trillion
P&T	Pump-and-treat
PVC	Polyvinyl chloride
Regen	Regenerant

ROS	Reactive oxygen species
SB	Still bottoms
TCE	Trichloroethylene
TDS	Total dissolved solids
TF	Total fluorine
TIP	Total identified precursors
TOC	Total organic carbon
TOD	Total oxidant demand
TOP	Total oxidizable precursors
UCMR	Unregulated contaminant monitoring rule
UPLC	Ultra-performance liquid chromatography
USEPA	United States Environmental Protection Agency
VOC	Volatile organic carbon

KEYWORDS

Distillation

Groundwater

Investigation Derived Waste

In Situ Chemical Oxidation

Ion exchange

PFAS

Plasma Treatment

Resins

Treatment Train

ABSTRACT

INTRODUCTION AND OBJECTIVES

Key challenges to treating per- and polyfluoroalkyl substance (PFAS)-impacted sites include the broad range of PFAS present, the presence of polyfluorinated precursors that transform into perfluoroalkyl acids (PFAAs), the recalcitrance of PFAAs, and the current lack of in situ approaches for implementing aggressive chemical treatment processes. As no single treatment technique can address all of these challenges, the objective of this project was to develop a set of combined in situ/ex situ treatment approaches for the efficient and effective treatment of PFAS-impacted groundwater through the evaluation of the feasibility and effectiveness of a range of treatment train approaches along with cost drivers and challenges for field-scale implementation.

TECHNICAL APPROACH

The treatment train approach centered on a novel plasma PFAS destruction technology includes (A) pre-treatment of PFAS and PFAA precursors in situ to eliminate or reduce PFAA source zones, and (B) pumping pre-treated groundwater for follow-on ex situ treatment. Options for in situ treatment include persulfate oxidation and oxygen addition by sparging. The ex situ treatment approaches for removal of PFAAs, including PFOA and PFOS, were direct plasma treatment of pumped groundwater, and ion exchange (IX) including IX resin regeneration with plasma treatment of IX regenerant solution. Research results were integrated from two sites to develop conceptual designs of viable treatment trains along with the identification of associated cost drivers, limitations, and challenges to field-scale implementation.

RESULTS

Precursor transformation was effective using persulfate and oxygen in both batch tests and transport cells and was found to reduce PFAA source zones. IX regenerant solutions comprised of methanol and brine were explored, and regenerant solution performance was comparable between the solutions even in different resins. Plasma was found to be successful in the treatment of PFAS in groundwater, pre-oxidized groundwater, and in concentrated IX regenerant solution, including PFAA precursors, long-chain, and short-chain compounds under optimized reactor conditions/configurations and under a broad range of groundwater conditions. The incorporation of plasma into treatment trains that include pre-oxidation and concentration by ion exchange individually or combined is appropriate and effective. The conceptual designs enhanced understanding of approaches for and limitations to integrating various PFAS treatment methods.

BENEFITS

The limitations of current PFAS treatment options, such as granular activated carbon (GAC), may be overcome by replacing or combining multiple technologies to obtain a more effective system that results in no waste product which can be implemented fully on site. This project assessed newly developed treatment methods and combinations for both treatment and implementation, resulting in a more protective and efficient treatment option for the DoD.

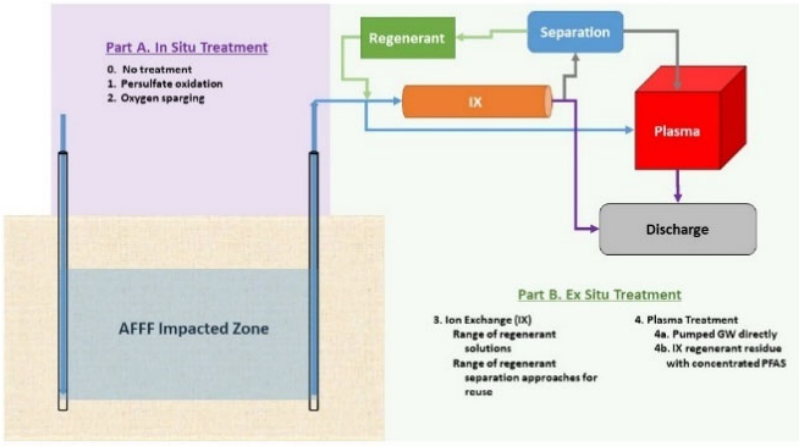

EXECUTIVE SUMMARY

INTRODUCTION

The historical use of aqueous film forming foam (AFFF) formulations containing PFAS for firefighting and training activities at DoD sites has led to concern over the potential for contamination of groundwater at up to 600 sites (Rak and Vogel, 2009). Because regulatory guideline concentrations for PFAAs are 3-4 orders of magnitude lower than concentrations measured to date at several Air Force sites (Schultz et al., 2004), cost effective treatment approaches are needed that consider their unique chemical properties (high solubility, low volatility, emulsification behavior, recalcitrance, and presence as mixtures). We propose a treatment train for treatment of PFAS and common site co-contaminants (e.g., petroleum hydrocarbons, chlorinated solvents). The train involves addressing PFAS and PFAA precursors in situ as a first pre-treatment step to eliminate or reduce secondary sources of PFAAs including the production of PFOS and PFOA. Without addressing these precursors, treatment times could be significantly extended by chasing low concentrations of persistent PFAA precursors. Ex situ plasma treatment, a novel destructive treatment approach, is proposed as a key element of the treatment train. Plasma is effective in destroying PFAS, as well as common co-contaminants. Plasma enables a complete on site treatment approach. To complement plasma treatment and potentially further its treatment efficiency, we propose coupling plasma with IX treatment using regenerable resin proven to efficiently remove and concentrate PFAS. Concentrating PFAS in the regenerant solution prior to destruction may prove more efficient and cost-effective than direct destruction. Both the resin and regenerant solutions can be reused, extending treatment time and minimizing both cost and waste relative to more conventional GAC treatment. These approaches in combination can result in a protective remediation approach that can be fully implemented on-site.

OBJECTIVES

The overall objective of this study was to evaluate the feasibility and effectiveness of a range of treatment train approaches for managing PFAS contaminated groundwater, and estimate and compare the scaled-up design challenges for implementation. The general treatment train approach included (A) pre-treatment of PFAS and PFAA precursors in situ to eliminate or reduce secondary sources of PFAAs including the production of PFOS and PFOA, and (B) pumping pre-treated groundwater for follow-on ex situ treatment. Options for in situ treatment that were evaluated include (1) persulfate oxidation; and (2) oxygen sparging. The ex situ treatment approaches evaluated include (3) IX for removal of PFAAs, incorporating IX resin regeneration; and (4) plasma treatment of (4a) pumped groundwater directly or (4b) IX regenerant solution. This holistic approach seeks to manage the challenge of PFAA precursors, to efficiently separate PFAS from contaminated groundwater using media that can be regenerated and reused, and to ultimately destroy PFAS on site.

TECHNICAL APPROACH

Each major component of the treatment train was investigated in terms of effectiveness, rate, and efficiency under a range of treatment conditions including the presence of common PFAS site co-contaminants. In situ oxidation experiments varied oxidation approaches, including aggressive chemical oxidation and oxygen sparging; oxidant dose; and treatment time in batch tests. The impact of these treatment approaches on post-treatment PFAS mass flux was then evaluated in treatment cells. IX has already been proven effective for removing PFAAs from water sources. This research focused on resin regeneration and optimization of the regenerant solution for maximum treatment, recovery, and reuse. Destructive treatment of PFAS including PFOA and PFOS using plasma has been demonstrated. This project focused on optimizing treatment conditions for a range of site conditions, as well as on treatment of post-oxidation groundwater and treatment of IX regenerant solution residue containing concentrated PFAAs. Research results were integrated from two sites to develop conceptual designs of viable treatment trains and associated cost drivers, and limitations. Challenges to field-scale implementation were identified for future investigations.

RESULTS AND DISCUSSION

Soil and groundwater physiochemical characterization. Groundwater and soil from contaminated sites were found to contain PFAA precursors, short-chain and long-chain PFAS including PFOS and PFOA. Twelve main PFAS were found ranging in concentration from 0.01-650 µg/L. Of the 12 PFAAs , PFOS, PFHpS, PFOA, PFHxS, PFHpA, PFBS, PFPeA and PFBA were found in all of the samples (**Figure E 1**). The sum of PFOA (13.2 ± 26.6 µg/L) and PFOS (54.3 ± 179 µg/L) concentrations was 5 to 10,500 times above the 2016 USEPA lifetime health advisory levels in all of the samples. Average TOP concentrations were high in all of the samples (74 ± 105 µg/L with a range of 20 to 750 µg/L). TOP concentrations were on average ten times higher than the total directly measured precursor concentrations indicating the presence of numerous undefined precursors (the ratio of TOP/ ΣTIP concentration varied from 2.5 to 513). The co-contaminants present included chloroform and dichloroethane (0.003-0.050 µg/L) and metals including manganese, potassium, and iron (0.01-50 µg/L). The pH varied from 5.3-8.0, conductivity ranged from 17.3 – 26300 uS/cm, hardness varied from below detection (BD) to 300 mg as $CaCO_3$ eq/L, alkalinity ranged from 10-550 mg as $CaCO_3$ eq/L, TOC was between 0.11-10.8 mg/L, and turbidity varied from <1-558 NTU.

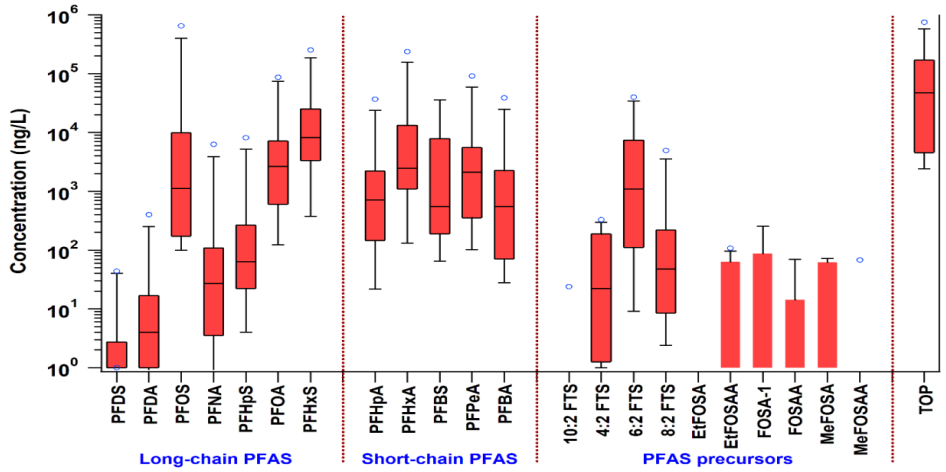

Figure E 1. Concentrations of PFCAs, PFSAs, precursors and total oxidizable precursors (TOP) in 13 unidentified samples. Ends of the boxes represent the first and third quartiles, horizontal lines marked inside the box represent median, whiskers represent minimum and maximum values, and small hollow circles represent the outliers.

In situ oxidative treatment in batch tests. Total PFAS composition and recoveries in batch reactors were evaluated following persulfate pre-treatment (**Figure E 2**). Persulfate oxidation has the potential to convert a complex mixture of PFASs into a simpler and more recoverable mixture of perfluoroalkyl acids (PFAAs). AFFF-impacted soils were treated with heat-activated persulfate in batch reactors and subjected to 7-day leaching experiments. Soil and water were analyzed using a combination of targeted and high resolution liquid chromatography mass spectrometry techniques as well as the total oxidizable precursors assay. Following oxidation, total PFAS composition showed the expected shift to a higher fraction of PFAAs, and this led to higher total PFAS leaching in pre-treated reactors (108-110%) vs. control reactors (62-90%). In both pre-treated and control soils, precursors that remained following leaching experiments were 61-100% cationic and zwitterionic. Results suggest that persulfate pre-treatment of soils shows promise as an enhanced recovery technique for remediation of total PFAS in impacted soils. They also demonstrate that PFAS distribution may have been altered at sites where in situ chemical oxidation was applied to treat co-occurring contaminants of concern

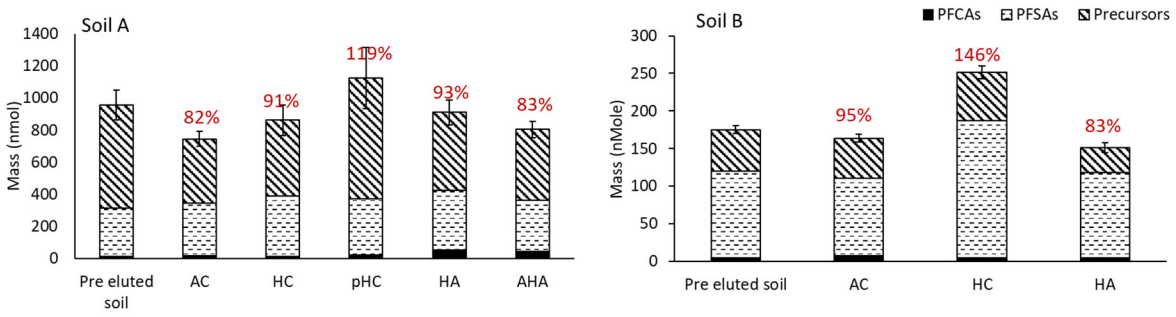

Figure E 2. Composition of PFCAs, PFSAs, and precursors in Soil A (Willow Grove) and B (Jacksonville) Alkaline heat activated (AHA), Heat activated (HA), Ambient Control (AC), Heat Control (HC), and pH Control (pHC). Percentage mass balance for each column shown in red numbers.

Oxygen infusion of groundwater has the potential to result in an enhanced biotransformation rate of less mobile polyfluoroalkyl substances to more mobile PFAA endpoints, and consequently enhance total PFAS recovery during groundwater extraction. Two AFFF impacted soils were used to evaluate PFAS biotransformation and mass transfer in the presence of oxygen infusion using batch experiments. Batch reactors were analyzed using targeted, combination of suspect screening and semi-quantification (SQ) analysis, and total oxidizable precursors (TOP) assay. Batch reactor results showed oxygen infusion increased aerobic biotransformation of precursors to PFAAs (41%) in sparged reactors relative to controls (28%) after 69 days.

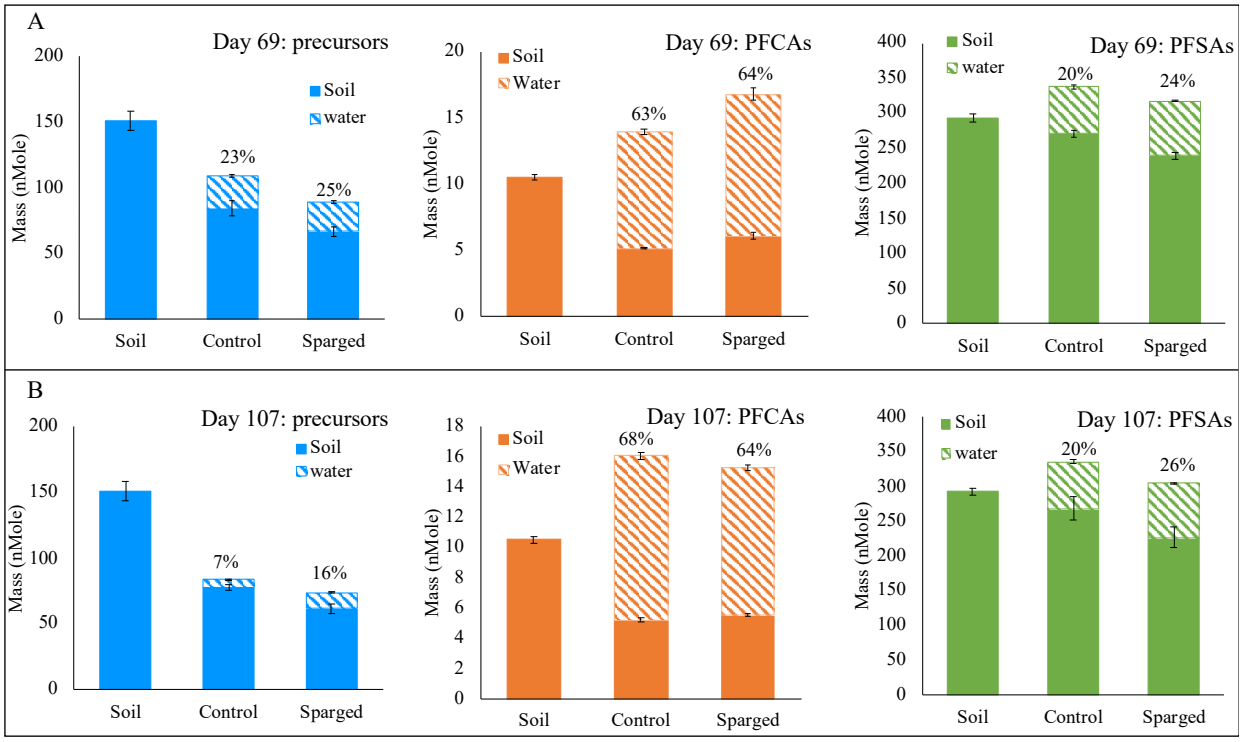

Figure E 3. Total molar mass of precursors, PFCAs, and PFSAs measured in Soil (i.e., original composition) and soil and water phases in sparged and control reactors on Day 69 (panel A) and Day 107 (panel B). Percentages represent the fraction present in the aqueous phase.

In situ oxidative treatment in transport cells. Two AFFF impacted soils were used to simulated PFAS release during heat activated persulfate treatment under saturated condition in packed soil columns (**Figure E 3**). Column effluents and soils were analyzed for PFAS using targeted analysis, high resolution liquid chromatography mass spectrometry technique and total oxidizable precursors (TOP) assay. During oxidation, pulse activated persulfate transformed 42-57% of precursors to perfluoro carboxylic acids (PFCAs) and more mobile oxidation intermediates like 6:2 fluorotelomer sulfonate. Precursor oxidation consequently increased PFAS mass transport relative to controls. Applying heat and highly alkaline pH led to an increase in PFAS release. Applying heat alone led to the highest release of perfluoroalkane sulfonates (PFSAs, 117-128%) and an increase of the pH to 10-12 led to a maximum total PFAS mass recovery in the effluent (104%). Results of this study suggest that by optimizing in-situ persulfate chemical oxidation, PFAS can be released more rapidly in the subsurface and could be used as flushing technique during pump and treat remediation approaches.

Two AFFF impacted soils were used to evaluate PFAS biotransformation and mass transfer in the presence of oxygen infusion using 1-D column experiments. Similarly to the batch reactors, the column solid and liquid phases were analyzed using targeted, a combination of suspect screening and semi-quantification (SQ) analysis, and total oxidizable precursors (TOP) assay. However, results of columns showed incomplete precursors biotransformation in all of columns, and similar PFAS mass released in all column type effluents.

Oxygen, ultrapure nitrogen and artificial ground water (10 mM calcium chloride) were assessed in of flow through reactors. The dissolved oxygen (DO) measurement of the influent line using flowthrough DO sensors illustrated that tubing used to pump sparged artificial groundwater (AGW) to columns was gas permeable and sparged AGW gained/lost oxygen while it was pumped through tubing. Despite this factor, DO concentrations in the O_2-sparged columns were higher than in other column types which can explain more generation of biotransformation intermediates in that type of column. These results suggest that biosparging of the impacted subsurface and increasing groundwater DO can result in the enhanced biotransformation of PFAA precursors and consequently release of PFAS in saturated zones.

Ex situ Ion-exchange regenerant selection and replication. Fifteen ion exchange resin regeneration solutions were tested using a proprietary regenerant solution and varying solvent and salt concentrations (**Figure E 4**). Key take-a-ways of the regenerant solution testing are that (1) salt or solvent alone are ineffective at desorbing PFAS; (2) higher solvent or higher salt concentrations are more effective at PFAS desorption; and (3) there is very little difference between the effectiveness of methanol, ethanol, or isopropanol as the solvent, however, methanol is preferred because salts are more soluble in methanol than either ethanol or ispropanol. Additionally, ethanol and isopropanol form azeotropes with water, making solvent recovery more difficult; methanol does not form an azeotrope with water.

Ex situ Optimization of top performing regenerant for multiple treatment cycles. Of the 15 solutions tested, three different solutions were explored in depth: (1) a mixture of 90% methanol and 2% NaCl, (2) a mixture of 100% methanol with 2.5% NaBr, and (3) a mixture of 90% methanol and 2% NaBr. Regenerant solution performance was comparable between the solutions even for different resins.

Twelve different distillation and membrane separation techniques were applied to recover solvent from the renerant solutions. . Distillation was found to be the best performing recovery method (e.g. maximum regenerant solution recovery and minimum PFAS carry over) for each of the regenerant solutions.

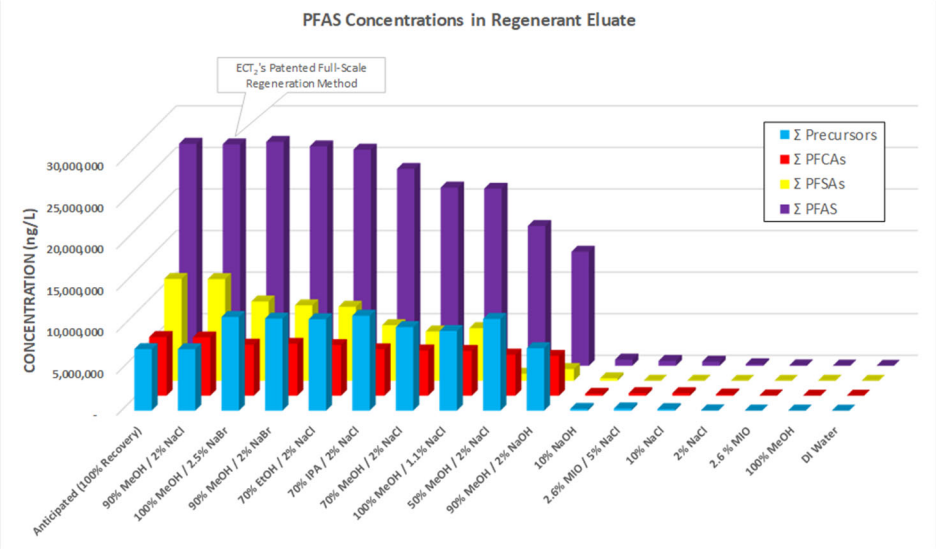

Figure E 4. PFAS concentrations in regenerant eluate.

Ex situ destructive plasma treatment of IDW. For PFOA and PFOS, the removal efficiency of the plasma treatment was > 93% within 5 minutes for 9 of the 13 PFAS-contaminated field samples, 30 minutes for 3 of the samples and 60 minutes for one. Removal efficiencies were generally higher for long-chain PFAAs than for shorter-chain PFAAs (**Figure E 5**). However negative removal (increasing concentrations) were observed for PFPeA, PFBA and MeFOSA which is likely due to the formation of short-chain PFCAs from the degradation of long-chain PFAAs and the oxidation of their precursors. In general, PFSAs were more rapidly removed than PFCAs of similar chain-length and similar initial concentrations. For the ten identified precursors, removal efficiencies were between 95 and 65%. These removal efficiencies were higher than those observed for TOP (65 ± 20%, Figure E 4).

To understand the influence of water quality parameters on treatment of PFAS, a Pearson's correlation analysis was performed on pseudo first order removal rate constants for PFOA and PFOS ($k_{PFOA+PFOS}$). Of these variables, the removal rate of PFOA+PFOS was significantly correlated only with total identified precursors (TIP) ($r = -0.55$, $p = 0.049$) and marginally correlated with total fluorine ($r = -0.49$, $p = 0.087$). TIP was the most influential parameter suggesting that the concentrations of precursors can decrease the PFAAs degradation rate by scavenging reactive species generated by the plasma and also by generating PFOA and PFOS as reaction intermediates. In addition, no correlation with TOC was observed ($r = -0.18$, $p = 0.55$) indicating that the presence of natural organic matter does not affect PFAS removal rates.

Ex situ destructive plasma treatment after oxidative pre-treatment. The efficiency of oxidative pretreatment of PFAS-contaminated groundwater at removing PFAA precursors (defined by TOP assay) using heat-activated persulfate was investigated to determine if pretreatment would improve the efficiency of the plasma process. The percent reduction of TOP after plasma treatment for untreated and pretreated samples were similar (77% and 80%, respectively), indicating that oxidative pretreatment did not impact plasma treatment efficiency.

Ex situ destructive plasma treatment of still bottoms. Plasma treatment was used to degrade PFAS in six different IX regenerant still bottoms (SB) provided by ECT2 (conductivity range from 50 to 80 mS/cm). A high-concentration and a low-concentration bench-scale batch plasma reactors were used sequentially to minimize the impact of PFAS desorption on final concentrations. In the high concentration reactor plasma degradation efficiencies were higher for long-chain PFAAs than short-chain PFAAs. For long-chain PFAAs, plasma treatment resulted in >99% degradation within 120 minutes and the extent of removal was independent of the PFAA chain length.

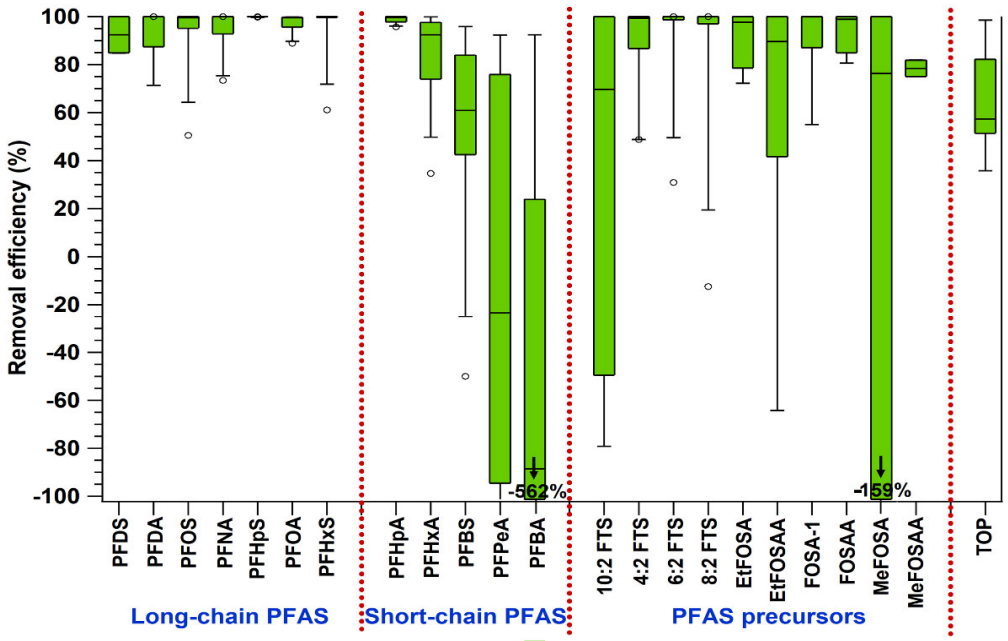

Figure E 5. Removal efficiency of PFAS in plasma treatment. Box and Whisker plot showing the removal efficiency (%) of several long-chain PFAS, short-chain PFAS, PFAA precursors, and total oxidizable precursors (TOP) in unidentified IDW samples treated in pilot-scale plasma reactor. Removal efficiency is shown between +100 and -100%, where negative removal efficiency is due to the formation of short-chain PFAS from degradation products of long-chain PFAS. PFBA and MeFOSA have shown negative removal efficiency of -562 and -159%, respectively, which are indicated by downward pointing arrows in the figure. The IDW treatment volume was 4 L and treatment time was 60 minutes.

In the low concentration reactor all the long-chain PFAAs were removed to BDL after 30 minutes of additional treatment, except for short-chain PFAAs. For short-chain PFAAs removal efficiencies were >99% after 6 hours of treatment except for PFPeA (96.7 ± 5.4%) and PFBA (23 ± 42%). To remove short-chain PFAAs, an additional experiment was performed in which the cationic surfactant CTAB was added initially and after every 30 minutes of treatment for another 210 minutes of treatment. In this experiment all the short-chain PFAAs were removed to BDL in 90 minutes of treatment time, expect PFBA whose concentration decreased from 6,000 to 260 ng/L. For all the SB samples, organically bound fluorine concentration decreased, and free inorganic fluoride ion concentration increased after treatment time of six hours.

Scaled up ex situ destructive plasma treatment of still bottoms. Scaled-up plasma reactors were also tested on still bottom samples generated by ECT2 and treated in two batches in two 35-gallon identical plasma reactors. Each sample was first treated in the high-concentration reactor and further in the low-concentration reactor. In the high-concentration reactor, plasma degradation efficiencies were higher for long-chain PFAAs than for short-chain PFAAs, which is consistent with what was found earlier for our small batch (~750 mL) stillbottoms (SBs) treatment. After CTAB addition in order to move PFAS from the bulk solution to the surface of the solution, a significant decrease in short-chain PFAAs (PFHpA, PFPeS, PFHxA, and PFBS) except PFBA and PFPeA was observed. Treated SB samples were transferred to the low-concentration reactor for further treatment where all the identified precursors were removed by ~99.9%, however, they were not removed to below detection limit (BDL, ~90 ng/L). This additional analysis confirmed that CTAB decreased the degradation efficiency of long-chain PFAAs, but improved the degradation efficiency for short-chain PFAAs.

Conceptual designs for in situ and ex situ treatment trains. Based on experimental results that affirm the technical potential to couple treatment technologies for improved efficiency, conceptual designs of full-scale treatment systems were prepared in order to assess implementation feasibility and challenges. The conceptual designs highlight feasible combinations of in situ and ex situ treatment trains that close PFAS treatment gaps of managing the challenge of PFAA precursors, to efficiently separate PFAS from contaminated groundwater using media that can be regenerated and reused, and to ultimately destroy PFAS implemented fully on-site. Major cost drivers for a holistic treatment approach were identified to be design flow rates, PFAS concentrations, presence of foulants or competing ionic species, PFAS treatment capacity of the treatment media, and regulated PFAS for specific sites.

IMPLICATIONS FOR FUTURE RESEARCH AND BENEFITS

The limitations of current PFAS treatment options, such as granular activated carbon (GAC), may be overcome by replacing the technologies or by combining multiple technologies to obtain a more cost-effective overall treatment system that results in no waste product and which can be implemented fully on site. This project assessed newly developed treatment methods and combinations for both treatment and cost effectiveness, wherein three viable treatment trains were identified and process flow schematics were developed based on a base case resulting in a protective remediation approach. The Site A base case entails an extraction well network with pretreatment of iron with accompanying sludge treatment, organic carbon treatment, ion exchange resin treatment with assumed direct discharge of treated water; resins regeneration with a solvent brine solution, followed by distillation and treatment of the still bottoms with superloaded activated carbon. Site A, option 1 differs from the base case by treating the distilled solution with plasma instead of the superloader, Site B, option 1 differs from Site A, option 1 by forgoing iron pretreatment with accompanying sludge treatment, and Site B, option 2 introduces the ISCO well and injection network before the extraction well network. The conceptual designs highlight feasible combinations of in situ and ex situ treatment trains that close PFAS treatment gaps of managing the challenge of PFAS precursors, to efficiently separate PFAS from contaminated groundwater using media that can be regenerated and reused, and to ultimately destroy PFAS implemented fully on-site. As no single treatment technique can address all of these challenges, implementation challenges and considerations based on these two sites and developed treatment trains provide guidance for the evaluation of any potential site for a holistic PFAS treatment train. Major cost drivers for a holistic treatment approach were identified to be design flow rates, PFAS concentrations, and presence of foulants or competing ionic species, PFAS treatment capacity of the treatment media, and regulated PFAS for specific sites (discharge limits). Due to the fundamental nature of this work, a site-specific pilot testing guided by these conceptual designs is recommended for remedial technology selection and additional treatment scenarios should be evaluated on a case-by-case basis as this research is not mature enough to translate to general guidance. Ultimately, the treatment train approach will result in a more protective and efficient treatment option for the DoD and others.

FINAL REPORT

OBJECTIVE

The overall objective of this proposed work was to develop a set of combined in situ/ex situ treatment approaches using a treatment train approach centered around a novel plasma PFAS destruction technology including (A) pre-treatment of PFAS and their precursors in situ to eliminate or reduce perfluoroalkyl acid (PFAA) source zones, and (B) pumping pre-treated groundwater for follow-on ex situ treatment, and to evaluate their feasibility and effectiveness, and estimate and compare the scaled-up cost and design challenges for implementation for the efficient and effective treatment of per- and polyfluoroalkyl substance (PFAS) contaminated groundwater.

To achieve this overall objective, the eight specific tasks of this SERDP project were to:

1. Characterize soil and groundwater from multiple PFAS contaminated sites in terms of PFAS concentrations and physiochemical properties and quantify and identify the total oxidizable precursors.
2. Determine the rate and extent of precursor transformation by each of the in situ oxidative treatment approaches and identify reaction byproducts in order to optimize treatment conditions for each of the proposed amendments through batch testing.
3. Use laboratory transport cells to obtain a quantitative analysis of in situ oxidative treatment on post-treatment mass flux, verify PFAS transfer rates during reactive transport, and evaluate potential design or implementation challenges.
4. Determine the top two performing regenerant methods/solutions through PFAS quantification and screening for resin regeneration from an active treatment system at a contaminated field site for more detailed testing in Task 5.
5. Determine the consistency of the regeneration approaches for a given site and across sites for the two best performing regeneration methods/solutions from Task 4.
6. Optimize and identify the top performing regenerant solution recovery approaches for its reuse in future resin regeneration cycles
7. Determine an optimal plasma reactor design, quantitatively assess the impact of co-contaminants on the plasma treatment of PFAS, and compare treatment efficiency and effectiveness for contaminated groundwater, in situ pre-treated groundwater, and concentrated IX regeneration solution residue.
8. Determine feasible combinations of in situ and ex situ treatment trains based on Tasks 1-7 for the conceptual designs for two representative sites considering implementation challenges and challenges, and cost drivers for site specific implementation.

P*re-treatment in situ* (**Tasks 1-3**) hypotheses: (1) In situ treatment cannot fully destroy PFAAs, but can enhance transformation of precursors to end point PFAAs; (2) PFAAs are more mobile in saturated, subsurface systems than precursors, so in situ transformation of precursors will mobilize that fraction of total PFAS, allowing it to be recovered and treated via ex situ methods; (3) A fraction of the precursor load will be resistant to transformation within relevant treatment time frames; (4) Overall this approach will reduce PFAA precursors as a secondary PFAA source and decrease time and costs associated with subsequent ex situ treatment. I*on-exchange ex situ* (**Tasks 4-6**) hypotheses: (1) Multiple regeneration options will be identified that are safe and effective; (2) IX regeneration and reuse effectiveness will not be negatively impacted by pre-treatment of groundwater using persulfate or oxygen. P*lasma treatment ex situ* (**Task 7**) hypotheses: (1) Plasma will be an effective PFAS destructive treatment approach for a broad range of PFAS, even in the presence of common co-contaminants; for concentrated or dilute PFAS concentrations; for treating PFAS concentrated in regenerant solutions with varying properties; and within a range of varied groundwater conditions; (2) Plasma will be equally effective in treating contaminated groundwater and concentrated IX regenerant solution. *Treatment train* (**Task 8**) hypotheses: (1) A range of viable coupled in situ/ex situ treatment approaches will be identified and will be more effective at mitigating PFAS than implementing a single treatment approach.

BACKGROUND

TASKS 1-3: PRE-TREATMENT IN SITU

Precursors are polyfluoroalkyl substances that also have a fluoroalkyl tail but are distinguishable from the anionic PFAAs by the presence of carbon bonded to hydrogen elsewhere in their structure and the potential to be cationic or zwitterionic in addition to negatively charged. These differences may cause precursors to be more strongly sorbed and therefore less mobile and challenging to recover during groundwater extraction for subsequent ex situ treatment. Additionally, unlike PFAAs, precursors can undergo transformation but their transformation endpoints include the more recalcitrant PFAAs. This suggests that without in situ intervention, PFAA precursors will serve as a long-term secondary source of PFAAs in groundwater, leading to extended treatment time and costs. Data suggest that PFAA precursors are oxidizable by introduction of oxygen (McGuire et al., 2014) or by heat-activated persulfate (Houtz and Sedlak, 2012). McGuire et al. (2014) found that PFAAs at a former fire training facility were highest near oxygen infusion wells and that total precursors were elevated outside of these infusion zones, suggesting that introduction of oxygen can enhance precursor transformation via aerobic processes. Suthersan et al. (2016) point to the total oxidizable precursor (TOP) assay (Houtz and Sedlak, 2012; Houtz et al., 2013), which rapidly converts PFAS into PFAAs using heat-activated persulfate. Originally developed as a valuable sample preparation tool for determining the total mass of precursors at a contaminated site, there is the potential to apply it to remediation scenarios. Other groups have investigated use of persulfate specifically for PFAS remediation (Park et al. 2016). Though the focus was on treatment of PFOA and PFOS, for which the technique was only partially successful, results did further illustrate enhancement of precursor transformation and found that co-contaminants (e.g. hydrocarbon constituents) did not have a significant impact on treatment rates. As such, these two amendments, oxygen and heat-activated persulfate, are promising for their potential to intentionally transform and mobilize PFAA precursors for subsequent ex situ treatment with the goal of managing source areas and reducing long-term flux of PFAAs into groundwater. There is a significant body of work related to these treatment processes for wide ranges of site conditions in general, but there has been no concerted effort, to our knowledge, to employ these approaches intentionally as part of a treatment train. Nor are there existing studies that can be relied upon to estimate transformation rates or extents as a function of amendment mass and treatment duration.

The technical objectives of pre-treatment in situ involved O-1. Determining if in situ pre-treatment can be used to eliminate PFAA precursors as a secondary source of PFAAs in groundwater; O-2. Quantifying the portion of PFAA precursors transformed and the portion resistant to transformation within a given treatment time frame, and measure the composition of the transformed portion; O-3. Quantifying change in mass flux of PFAAs into the groundwater following in situ pre-treatment; O-4. Comparing heat-activated persulfate, oxygen sparging, and slow-release oxygen for precursor transformation in terms of (1) mass of amendment per mass of transformed PFAS, (2) rate of precursor transformation, (3) cost of amendment per mass of transformed PFAS, (4) estimated treatment time, and (5) design challenges or implementation limitations.

TASKS 4-6: ION-EXCHANGE EX SITU

Commercially available IX resin has been demonstrated to be more effective than GAC at removing PFAAs from water (Appleman et al., 2013). One study completed by project team members Amec Foster Wheeler and ECT2 has shown IX resin is approximately four times more efficient than GAC at removing PFOA, and eight times more efficient at removing PFOS. Additionally, IX may be effective at removing a broader suite of PFAS including short-chain PFAAs, which exhibit little retention in GAC. Unlike GAC, IX resin can be efficiently regenerated and reused on site indefinitely, making it superior to GAC on a cost and sustainability basis. During regeneration, contaminants, in this case PFAAs, are desorbed from the resin by a regenerant solution that is mixed with the PFAAs-saturated resin, drained, and rinsed. The

process is conducted in a controlled manner such that the full amount of PFAAs that had been adsorbed onto the media is removed and can be accounted for through mass-balance calculations. A propriety regeneration procedure using solvent and salt has been proven effective at the bench scale and pilot scale. The process recovered over 99% of the PFAAs collected on the IX resin in the bench scale vessels.

Figure 1 shows results of recent pilot testing at Site 8, the fire training area at the former Pease Air Force Base in Portsmouth, NH. Parallel testing was performed for more than three months, providing a direct comparison of GAC (Calgon Filtrasorb 400) versus ion exchange resin (ECT Sorbix A3F). Figure 1a illustrates the PFOA breakthrough curves for both adsorptive media at a 5-minute empty bed contact time (EBCT). The Sorbix resin clearly out-outperformed the GAC, lasting more than four times longer before initial PFOA breakthrough. Figure 1b is a similar plot for PFOS. The resin's performance for PFOS removal was even more impressive than PFOA. PFOS breakthrough in GAC began at approximately 3,000 bed volumes, whereas the Sorbix still showed no breakthrough at the conclusion of the loading cyle (21,000 bed volumes). Figure 1c demonstrates that the Sorbix resin can be effectively regenerated in place using a proprietary process to restore its PFAS removal capacity. The regeneration procedure uses a brine-solvent blend wherein the used solvent can be recovered and reused in subsequent resin regenerations. The blue line shows the total PFAS breakthrough curve for virgin resin at a 2.5-minute EBCT, while the orange line shows a similar trend for regenerated resin. The Pease pilot testing showed that, in addition to having superior removal capacity for PFOS, PFOA and other all other PFAS detected at Site 8, Sorbix A3F ion exchange resin can also be effectively regenerated and reused without removing it from the vessel. The result is a more cost effective, sustainable treatment technology than the current GAC standard.

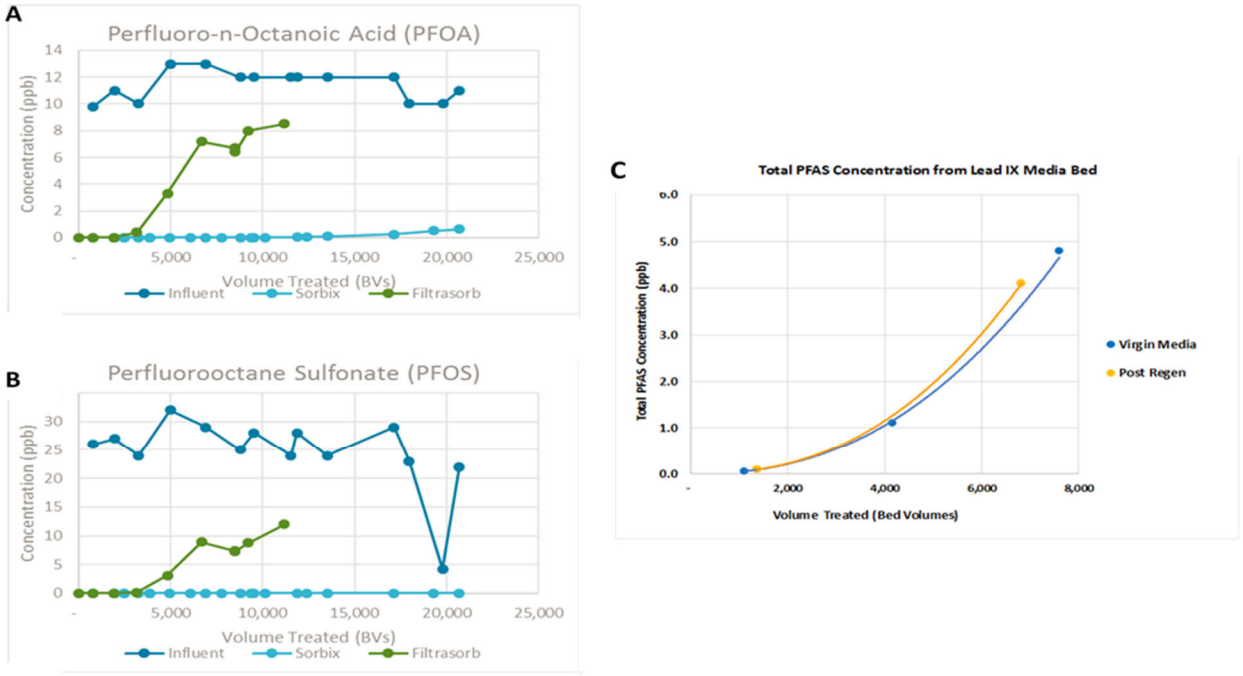

Figure 1. Results of pilot testing of IX and regeneration at former Pease Air Force Base, including (a) PFOA removal, (b) PFOS removal, and (c) restoration of PFAS removal capacity of resin through regeneration.

The proprietary regenerant solution that has been demonstrated to be effective on Sorbix is a solvent brine solution that exceeds flammability thresholds and therefore requires special handling. Although flammability is easily managed, a goal of this proposed project is to evaluate alternative regenerant solutions that are easy to use and inexpensive, as well as effective. Solvents, (e.g., methanol, ethanol, and butanol) will be tested at various concentrations and with various salt mixtures to find the lowest concentration of the least hazardous mixture that achieves complete removal of PFAAs from the IX resin. Another goal is to establish the most effective method of recovering regenerant solution for its reuse.

The technical objectives of ion-exchange ex situ involved: O-5. Screening IX regenerant solutions for their PFAS recovery efficiency from IX resin; O-6. Comparing a limited number of viable IX regeneration procedures in terms of regeneration effectiveness, cost-effectiveness, safety, practicality, and implementability (ease of performance, transferability); O-7. Comparing the effectiveness of regenerant solution recovery techniques for its reuse.

TASK 7: PLASMA TREATMENT EX SITU

Recently, the PIs have developed a novel treatment process based on electrical discharge plasma, the enhanced contact (EC*) electrical discharge plasma reactor* (**Figure 2**), which is highly effective in degrading PFAS at efficiencies significantly better than alternative treatment technologies (Stratton et al., 2015; Stratton et al., 2016). This technology uses electricity to convert water into a mixture of highly reactive species, including $OH^{\bullet}$, O, $H^{\bullet}$, $HO_2^{\bullet}$, $O_2^{\bullet-}$, H_2, O_2, H_2O_2 and aqueous electrons (e^-_{aq}) (i.e., plasma), that rapidly and non-selectively degrade recalcitrant organic contaminants such as pharmaceuticals (Gerrity et al., 2010; Krause et al., 2011), 1,4-dioxane (Even-Ezraa et al., 2009), and a broad spectrum of PFAS (Yasuoka et al., 2011; Stratton et al., 2017).

The EC *plasma reactor* has two high voltage wire electrodes in the gas phase, just above the liquid surface, and three grounded rail electrodes submerged just beneath the liquid surface, so that the plasma streamers primarily rest upon and in contact with the liquid surface. This contact between the plasma and the liquid is critical, as it allows the chemicals in the liquid to be exposed to the reactive species generated by the plasma.

Compared to the traditional gas discharge reactor where plasma is generated in a gas from a point and contacts the liquid and the grounded plate is immersed in water, our bench-scale EC reactor design (**Figure 3**) integrates a submerged gas diffuser, through which argon process gas is pumped, and an argon recirculation system. Argon produces bubbles and forms a layer of foam on the liquid surface without chemical addition. This foam concentrates surfactant-like contaminants and enhances the contact between the liquid and the plasma exposing the contaminant at the interface to reactive species in the plasma (Stratton et al., 2016) Because argon molecules have no charge, its composition is not directly affected by the plasma, allowing it to be recycled, which can significantly reduce operational costs. Air is purposely avoided because its use results in the creation of ozone and nitrogen oxides. **Figure A 1** in the supporting data section describes the external electrical network used to generate plasma.

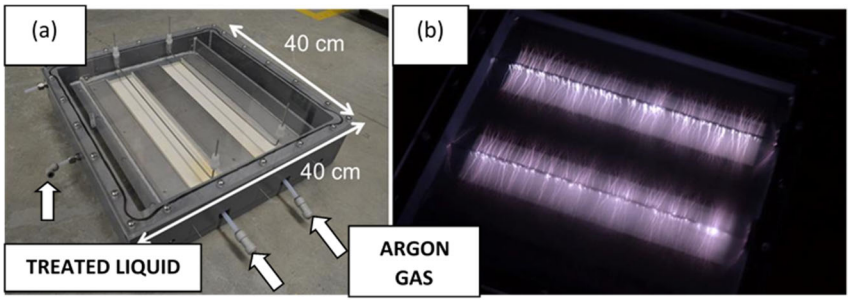

Figure 2. Prototype scale-up continuous flow unit. (a) A single unit plasma reactor and (b) the unit in operation.

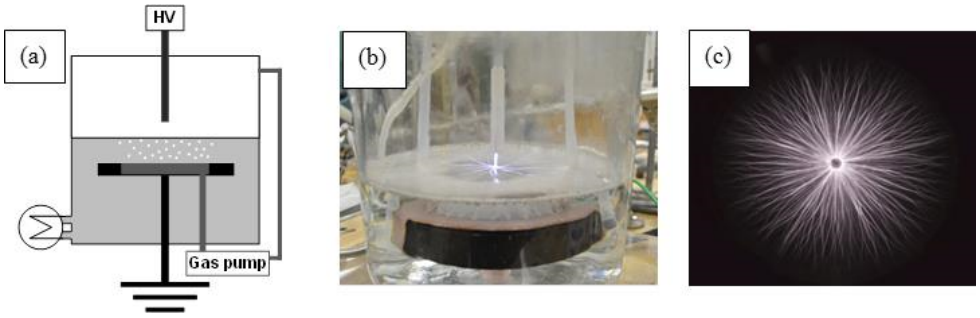

Figure 3. The bench-scale batch EC plasma reactor: (a) General schematic, (b) Reactor in operation, and (c) A picture of the plasma contacting water recorded in dark. Reactor capacity is 1.4 L.

The bench-scale EC plasma reactor rapidly and efficiently degrades several perfluoroalkyl acids (PFAAs) including PFOA, PFOS, and shorter chain PFAA (Stratton et al., 2017). In the case of PFOA, a 30-minute plasma treatment of a 1.4 L aqueous solution (equivalent to 0.012 gpm) removed 90% of the initial PFOA concentration of 20 µM (~11 mgL^{-1}) with an input power of 76.5 W (high removal rate case) or 25% using 4.1 W (high efficiency case) (**Figure 4).** Continuing the treatment for an additional 40 minutes removed PFOA to below detection limits, significantly below the 2016 HAL of 70 ppt.

Furthermore, plasma achieved remarkably high PFOA removal and defluorination efficiencies compared to leading alternative treatment technologies (sonolysis (Vecitis et al., 2008), activated persulfate (Chen and Zhang, 2006) electrochemical treatment (Schaefer et al., 2015) and DC plasma in O_2 bubbles (**Table A 2, supporting data section**) in terms of PFOA removal efficiency, defined as the observed first-order removal rate constant (kobs) divided by the power density (PD = input power/treated volume). Other performance indicators and corresponding experimental parameters for these six processes are also shown in **Table A 2** in the supporting data. Calculations show that the high efficiency plasma-based water treatment (PWT) process performed well compared with the alternative treatment methods, achieving a defluorination efficiency about 30 times greater than that of activated persulfate, 10 times greater than that of sonolysis and 15% greater than electrochemical treatment.

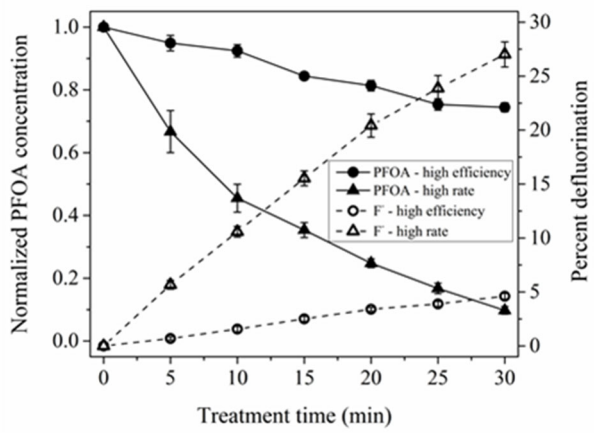

Figure 4. Normalized PFOA concentration and defluorination profiles for the EC reactor configured for high treatment efficiency and high treatment rate.

The high efficiency process was further used to treat groundwater containing PFOA and several co-contaminants including PFOS, TCE and PCE (total TOC concentration was 0.67 mg/L) demonstrating that the process was not significantly affected by co-contaminants and that the process was capable of rapidly degrading PFOS (**Figure 5**).

Because previous studies on the transformation of PFOA and PFOS have cited shorter-chain PFAAs as a major class of byproducts, a preliminary investigation was conducted to quantify shorter-chain PFAAs produced during treatment of a mixture of PFOS and PFOA in the benchscale EC reactor. The anticipated byproducts that were tested for were perfluoroheptanoic acid (PFHpA), perfluorohexanoic acid (PFHxA) and perfluoropentanoic acid (PFPnA). Although shorter-chain PFAAs are clearly being produced (**Figure A 2, supporting data section),** the difference between the sum of the concentrations of PFOA and PFOS and the sum of the concentrations of all PFAS is never greater than 0.1 nmol/L. This indicates that shorter-chain PFAAs account for only about 10% of the degraded PFOA and PFOS, which is much lower than for oxidation-based processes, where shorter-chain PFAAs account for most of the degraded PFOA (e.g., 85-95% for activated persulfate (Chen and Zhang, 2006). PFAAs smaller than PFPnA may also be formed, however, they would be formed via the much slower transformation of PFPnA, thus they are not expected to be produced in significant quantities. Evidence of volatile F containing byproducts has also been observed in the reactor headspace samples (**Table A 2, supporting data section**).

The PFOA treatment efficiency for groundwater (NAWC, Warminster, PA) in the prototype EC plasma reactor (Figure 2) is more than twice that of the bench-scale reactor. The PFAA removal rates also far exceed those attainable in the bench scale version of the reactor. As shown in Table 1, both PFOA and PFOS were removed in < 1 minute when treated continuously at 1 gpm. We believe this is primarily due to much thinner layer of water flowing between the electrodes and the generation of smaller and more numerous bubbles (the diffuser pore size is different between the bench-scale and the prototype reactor) which increased the contact between the plasma and PFAAs concentrated at the bubble interface.

Recently the PIs obtained some ion-exchange regenerant solution residual that had been treating PFAS contaminated groundwater from our partner ECT2 and treated it in the prototype scale-up continuous flow unit. Due to the high concentration of PFAS the solution foamed significantly so the diffuser flowrates had to be very low. In addition, the high solution conductivity caused the plasma streamers to be small and weak. Even with these limitations removal was excellent with PFOA concentrations reaching detection limits within one hour of treatment and PFOS concentrations reaching detection limits within two hours of treatment (**Figure 6**).

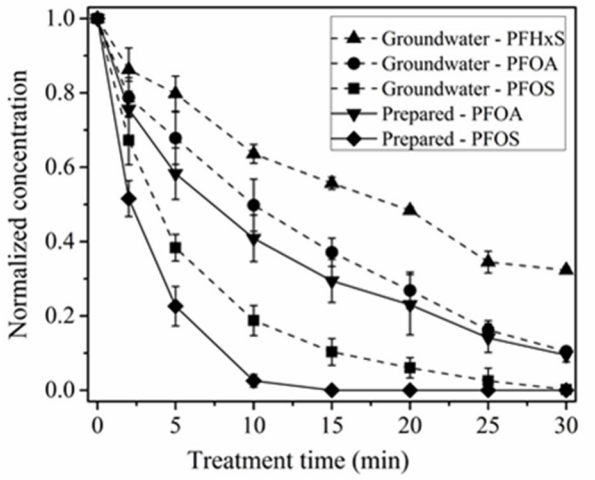

Figure 5. Normalized concentration profiles for PFAS in the contaminated groundwater and prepared solution. Groundwater experiments were conducted using unmodified samples from the effluent of an air stripper within the Former NAWC Warminster Groundwater Treatment Plant in Warminster, Pennsylvania. Initial PFOA concentration in groundwater was 0.0014 mgL-1 and PFOS 0.00035 mgL-1. Initial concentrations of PFOA and PFOS in prepared solutions were 0.0018 mgL-1 and 0.00014 mgL-1, respectively.

Table 1. Results of treatment of PFAS-contaminated groundwater (NAWC, Warminster, PA) by the prototype EC plasma reactor.

Compound	$C_{0\ min}$ (µg/L)	$C_{60\ min}$† (µg/L)	Removal (%)
Perfluorooctanoic acid (PFOA)	0.89	0.0035*	99.6
Perfluorooctane sulfonate (PFOS)	0.18	0.0026*	98.5
Perfluoroheptanoic acid (PFHpA)	0.11	0.0002	99.8
Perfluorohexanoic acid (PFHxA)	0.27	0.024	91.1
Perfluoropentanoic acid (PFPnA)	0.22	0.16	26.4
Perfluorohexane sulfonate (PFHxS)	0.32	0.0041	98.7

†Samples concentrated using solid-phase extraction.
*Concentration dropped below the detection limit in the first minute of treatment.

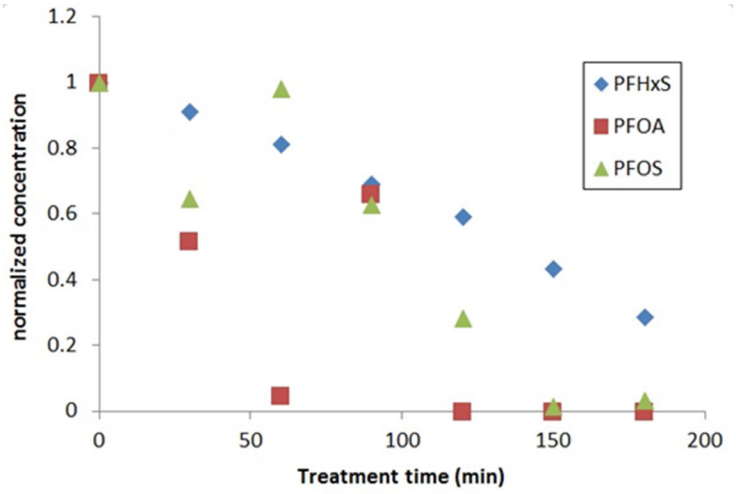

Figure 6. Removal of concentrated PFHxS, PFOA, and PFOS from IX exchange regenerant solution residual.

The technical objectives of plasma treatment ex situ involved: O-8. Quantifying the destruction of PFAS at varied concentrations, in varied ratios, and in the presence of common co-contaminants (petroleum hydrocarbons and chlorinated solvents); O-9. Comparing the efficiency and effectiveness of treating contaminated groundwater, pre-treated groundwater (in situ), and concentrated IX regenerant solution using plasma; O-10. Determining the influence of groundwater conditions (total solids, pH, dissolved organic carbon, key metals, and common co-contaminants) on treatment of PFASs.

TASK 8: TREATMENT TRAIN

Key challenges to treating PFAS contaminated sites include (1) the broad range of PFAS typically present (Place and Field, 2012; Backe et al, 2013); (2) the common presence of polyfluorinated precursors that can transform into PFAAs such as PFOA and PFOS by natural or anthropogenic biological or chemical processes, serving as a long-term source of these compounds in groundwater; (3) the recalcitrance of PFAAs, particularly perfluoroalkyl sulfonates such as PFOS which can only be destroyed by very

aggressive chemical treatment processes; (4) the presence of challenging co-contaminants; and (5) the current lack of in situ approaches for implementing aggressive chemical treatment processes. Because no single treatment technique can address all of these challenges, treatment train approaches are necessary to address PFAA precursors, implement cost-effective ex situ treatment, and ultimately result in contaminant destruction. Conceptual designs of feasible combinations of in situ and ex situ treatment trains were prepared in order to consider implementation challenges and major cost drivers for site-specific implementation. Conceptual designs of feasible combinations of in situ and ex situ treatment trains can be adapted to site-specific designs considering implementation challenges, anticipated treatment effectiveness, safety considerations, sustainability, and cost for each treatment approach and compared to currently employed treatment approaches.

The technical objectives of the treatment train involved: O-11. Based on data collected related to Objectives 1-10, determining viable combinations of in situ and ex situ treatment trains, and determine their potential implementation limitations challenges and cost drivers for implementation.

MATERIALS AND METHODS

The project was completed by a collaborative team from Clarkson University, Texas Tech University, Wood, ECT2, and NAVFAC.

TASK 1: SOIL AND GROUNDWATER PHYSIOCHEMICAL CHARACTERIZATION

For Task 1, soil and groundwater from multiple PFAS contaminated sites (further described in the Results and Discussions section) were obtained and characterized in detail, including contaminant concentrations (PFAS and co-contaminants), organic carbon content, pH, particle size distribution, and concentrations of key metals (e.g., Fe, Mn). Total oxidizable precursors were quantified and identified using the TOP assay and ultra-performance liquid chromatography – high resolution quadrupole time-of-flight mass spectroscopy (UPLC-HRQToFMS), described in the supporting data. Throughout this project, the total precursor concentrations were calculated using TOP, individual target precursors were quantified using target analysis, and individual other precursor concentrations were calculated using high-resolution mass spectrometry results.

Soil A from Willow Grove and Soil B from Jacksonville were received at Texas Tech University prior to batch experiments. Soil B was found to have low PFAS concentrations but was selected to be used in experiments as a representative media low in precursors. Based on batch results, column experiments were designed to focus on media high in precursor concentration therefore Soil B was replaced with Soil C from a second site in Jacksonville.

TASK 2: IN SITU OXIDATIVE TREATMENT IN BATCH TESTS

For **Task 2**, batch laboratory tests with impacted media from Task 1 were used to optimize treatment conditions for each amendment (**Table 2**): heat-activated persulfate, slow-release oxygen, and sparged oxygen. Optimized parameters included amendment dosing and reaction time. Prior to batch experiments, field media were characterized for PFAAs by TOP and HRQToFMS.

Table 2. Summary of batch reactor experiments to optimize amendment conditions.

Treatment	Variables to Optimize
Persulfate	Oxidant concentration, reaction time
Air Sparge	Sparge rate, reaction time

Persulfate batch experiments were conducted in 50 mL polypropylene centrifuge tubes containing 1 g of Soil A (Willow Grove) or B (Jacksonville) (dried, homogenized) and 45 mL of PFAS-free deionized (DI) water. Alkaline heat-activated reactors (denoted $OH^{\cdot-}$ pretreated) were amended with 50 mM potassium persulfate ($K_2S_2O_8$) and 110 mM sodium hydroxide (NaOH) and activated in a hot water bath. The oxidant dose was selected from a range of 18.5-111mM recommended for use when optimizing persulfate chemistry (Guelfo et al., 2018). The mid-point was selected because the current study investigates feasibility, and dose optimization is targeted for future efforts. This dose is also consistent with prior studies of persulfate oxidation as a PFAS remediation technique (Liang and Su, 2009; Park et al. 2016). Alkaline conditions were maintained in order to prevent PFCA degradation, which occurs primarily at pH $\leq$ 3, (Liang and Su, 2009) and maintain a constant total PFAS concentration in the reactors. Closing the mass balance in reactors was necessary to evaluate persulfate impacts on total PFAS mobilization only. In the presence of PFCA degradation, the impacts of leaching and degradation on reduction of PFAS soil concentrations would be combined. A series of control experiments were conducted to evaluate PFAS composition and mobilization in unamended soils (controls) and the impacts of ambient pH (heat activated, denoted $SO_4^{\cdot-}$ pretreated), heat (heat controls), and elevated pH (pH control) on total PFAS

mobilization. Following pre-treatment, all reactors were brought to room temperature, centrifuged (Beckman Coulter, Avanti J-E, 5000 rpm, 20 min), and the soil and aqueous phase retained for analysis. For a subset of experiments additional replicate reactors were retained following pretreatment for use in leaching experiments. After centrifugation, the soil was retained and the aqueous phase replaced with 45 mL of clean DI water, and placed on a shaker table (VWR, 3500STD). Every 24 hours of the leaching period, reactors were centrifuged, the supernatant was separated, retained for analysis, and replaced with 45 mL of clean DI. This was done to maximize desorption of PFAS, which may slow or stop as reactors approach equilibrium. At the end of the leaching period, soils were retained and analyzed. All batch experiment soil and water samples were analyzed using targeted analysis and total oxidizable precursors (TOP) plus targeted analysis. A subset of soil extracts and aqueous samples were also analyzed using a suspect screening technique.

Oxygen sparging batch experiments were used to screen for the potential of enhanced precursor transformation during air sparging. Air sparge batch reactors (9 total) were prepared in 1L glass bottles using 200 g of Soil A (Table E2) and 1L of clean, deionized (DI) water. Six reactors were connected to an air sparge manifold consisting of a 6-way splitter, flow meter, low pressure regulator, and high purity oxygen cylinder. The tubing in each reactor terminated at a T-junction connected to two pieces of horizontal, perforated tubing placed horizontally at the bottom of each reactor beneath the soil. Hose barb plugs were used to stopper the end of both pieces of perforated tubing forcing a slow and uniformly distributed flow of oxygen through the perforations without causing turbulent mixing. The remaining three reactors were controls maintained at ambient oxygen conditions. The reactor aqueous phase was sampled each day for the first week and approximately every three days thereafter. Reactor sampling was carried out by transferring two 1,260 µL aliquots of water into glass autosampler vials, and the volume replaced with an equal volume of clean, DI water. The first aliquot was used for targeted analysis and the second for suspect screening, each implemented in triplicate. One control reactor and one sparged reactor were sampled at each time point, and sampling rotated through each replicate reactor before returning to a previously sampled reactor. Reactors were sacrificed for full aqueous and solid characterization when results of aqueous phase analysis suggested that in increases in the concentrations of terminal degradation product (i.e., PFCAs and PFSAs) had occurred. Full characterization of soil and water in sacrificed reactors included targeted analysis, TOP assay plus targeted analysis, and suspect screening of aqueous samples and soil extracts. Briefly, TOP provides a total molar oxidizable precursor concentration (Houtz et al., 2013; Houtz and Sedlak, 2012).

For all treatments, each amendment and condition tested consisted of duplicate reactors. Controls with no amendment were used to monitor losses due to natural degradation. Biologically inactivated controls were also used to determine losses or additions of compounds to or from each type of reactor used. Following experiment completion, an aliquot of the aqueous phase was sampled for PFAA analysis. The remaining aqueous phase was analyzed for TOP to determine if any oxidizable precursors remain. The soil was extracted using previously established methods (Sepulvado, 2011). An aliquot of the resulting extract underwent analysis of target analytes and the remaining extract was analyzed for TOP. Select samples underwent HRQToFMS analysis to identify any precursors that are resistant to conversion. The rate and extent of precursor transformation by each of the in situ oxidative treatment approaches, and identification of reaction byproducts were determined.

TASK 3: IN SITU OXIDATIVE TREATMENT IN TRANSPORT CELLS

In **Task 3**, Laboratory transport cells were used to test effective amendments optimized in batch systems under more field-relevant conditions. Contaminated soil collected in Task 1 was packed into laboratory transport cells, in duplicate. Media were treated using each of the three amendments used in Task 2 that was proven to be effective for precursor transformation in separate cells (6 treatment cells, plus duplicate control cells). Results from Task 2 were used to identify the optimum amendment mass and treatment duration for this task.

Transport cell columns for oxidative persulfate experiments were conducted in 2.5 x 15 cm Kontes glass chromatography columns (Kimble Chase, Vineland, NJ) with a fritted, glass bed support in the influent end of the column. Columns were dry-packed in 1cm increments, and each increment was tamped and scored prior to the next increment. Clean sand (1.5 cm) and glass wool were used as additional bed support and to uniformly distribute flow in the influent end of the column. Stainless steel mesh, a 1 cm increment of clean sand, and a 2 cm increment of 5 mm glass beads were used as additional bed support in the effluent end cap. Packed columns were saturated with CO_2 for 4-hrs prior to saturation in up-flow mode with artificial groundwater (10 mM calcium chloride). Soil bulk density, porosity and pore volume were determined gravimetrically. Columns were attached to a multi-channel, high-accuracy peristaltic pump (Ismatec) and influent and effluent samples were collected from three-way valves installed ~ 5 cm prior to and downstream of the column inlet and outlet. Columns were prepared in duplicate, and a sacrificial column was prepared for bromide (Br^-) tracer tests that determined the hydrodynamic properties of the column. The latter was required because experiments were evaluated for PFAS leaching from field-collected, AFFF-impacted soils, and a degree of flushing would occur during the tracer test if conducted prior to column experiments.

Five column types (2 experimental and 3 control types) were each packed in duplicate. Column types were 1) treated with alkaline, heat-activated persulfate (AHA) 2) treated with heat activated persulfate (HA), 3) controls run under ambient conditions (ambient control, AC), 4) controls that were treated only with heated (heat controls, HC), and 5) controls evaluating impacts of alkaline pH (pH controls, pHC). AHA and HA columns were injected with 50mM persulfate 110mM sodium hydroxide (NaOH) was used to achieve alkaline conditions in AHA and pHC columns. AHA, HA, and HC columns were wrapped with heat tape and fiberglass insulation and heated to an internal column temperature of 60ºC. Preliminary experiments in sacrificial columns were used to evaluate eluant persulfate concentrations to ensure full persulfate activation. Persulfate was not detected indicating that the column temperature was sufficient for activation.

After saturation, columns were operated at flow rate of 0.2 ml/min in 2-phases. Oxidation pulses were conducted for 6 hours (2.3-2.6 pore volumes) (Shojaei et al., 2021). Effluents (5 mL) were sampled in 8 mL glass vials and prepared for analysis. Following oxidation pulses, column effluents were sampled every 3 hours for the first 12 hours and then every 6 hours during desorption phase. Column effluent also were sampled, in the middle, and at the end of oxidation pulses for analysis of dissolved organic carbon. Following completion of column tests, columns soils were sectioned in 2.5-3 cm increments and extracted and analyzed for PFAS and total organic carbon (TOC). All column experiment soil samples were extracted and analyzed using targeted analysis, TOP plus targeted analysis, and suspect screening.

Transport cell columns for oxygen sparging experiments were conducted using two AFFF-impacted soils and 2.5 x 15 cm Kontes glass chromatography columns (Kimble Chase, Vineland, NJ) with a fritted, glass bed support in the influent end of the column. Columns were dry packed in 1cm increments, and each increment was tamped prior to the next increment. Clean sand (1.5 cm) and glass wool were used as additional bed support to uniformly distribute flow in the influent end of the column. Stain steel mesh, 1cm clean sand and 5 mm glass beads were used as additional bed support in the effluent end cap. Packed columns were saturated with carbon dioxide (CO2) for 4-hrs prior to saturation in up-flow mode with artificial groundwater (10 mM calcium chloride in DI water). Soil bulk density, porosity and pore volume were determined gravimetrically. Columns were attached to a multi-channel, high-accuracy peristaltic pump (Ismatec) and influent and effluent samples were collected from three-way valves installed ~ 5 cm prior to and downstream of the column inlet and outlet. Columns were prepared in duplicate, and a sacrificial column was prepared for bromide (Br-) tracer tests that determined the hydrodynamic properties of the column. Tracer tests were conducted in separate columns because this study is evaluating PFAS leaching from field-collected, AFFF-impacted soils, and a degree of flushing occurs during the tracer test. Br- was measured with Thermo Orion Br- electrode connected to a Thermo Orion star 421 meter. Br- solution (100 mg/L) was prepared using potassium bromide (KBr) and injected into

columns at pore water velocities listed in Table E3 until effluent Br- concentration reached 100 mg/L. Tracer test columns were then flushed with sparged artificial groundwater (AGW, 10 mM calcium chloride) until effluent Br- concentration decreased to background levels. Br- breakthrough curves were fit using the nonlinear, least-squares model CFITIM (Bruton and Sedlak, 2017). To evaluate if hydrodynamic conditions changed during air sparge experiments, Br- tracer tests were conducted on all columns following collection of all PFAS samples.

After saturation, columns were operated at pore water velocities listed in Table E3 using 1 of 3 conditions. Two columns were connected to an AGW reservoir (20 L) equipped with an air sparge manifold that consisted of polyvinyl chloride (PVC) tubing, low pressure regulator and high purity oxygen cylinder. Oxygen was slowly sparged into the reservoir by connecting tubing to a shower head in the bottom of reservoir. Two additional columns were connected to a reservoir sparged with ultrapure nitrogen in the same manner. Two control columns were connected to a reservoir containing AGW at ambient oxygen levels.

Column effluents were sampled every 3 hours for the first 12 hours, every 12 hours for the first week, daily for 3 weeks, and every 3 days thereafter. Column effluent samples were analyzed using targeted analysis and suspect screening, and a subset of effluents were analyzed for TOP plus targeted analysis. Samples (5 mL) were collected in 8 mL glass vials, then 2 mL of effluent was transferred to separate vial for TOP analysis. Prior to subsampling, 8 mL vials were sonicated for 30 min. Methanol was added to the remaining volume to achieve a final vial composition of 70% water and 30% methanol. Two autosampler vials were prepared from this solution for targeted analysis and suspect screening as described for batch systems. The aliquot for TOP assay was removed prior to methanol amendment because methanol will interfere with persulfate oxidation. Columns were operated for 1210-1920 pore volumes (~188 days).

Following completion of column experiments and subsequent Br- tracer tests, soils were retained, sampled in 3cm increments, extracted, and analyzed. Extracts were analyzed using target analysis, suspect screening, and TOP plus targeted analysis. As an ancillary benefit, PFAS breakthrough in columns were measured with a program such as HYDRUS-1D (Simunek, 1998) to provide additional insights into PFAS fate and transport during in situ treatment. Additional analyses included a quantitative analysis of in situ oxidative treatment on post-treatment mass flux; verification of PFAS transfer rates during reactive transport; and an evaluation of potential design or implementation challenges.

TASK 4: IX REGENERANT SELECTION

In **Task 4**, the effectiveness of multiple resin regeneration methods were screened by collecting 1.5 liters of PFAS-loaded, ion exchange resin (ECTs Sorbix A3F resin) from an active treatment system at a contaminated field site. The resin was divided and packed into 15 laboratory PVC chromatography columns, each 100 ml in volume. The fittings were PVC construction and the tubing was HDPE. Up to 15 different regenerant solutions, some of which are proprietary, were tested by passing 10 bed volumes (BVs) of regenerant solution through a resin column at a rate of 2 BVs per hour, followed by passing 10 BVs of deionized rinse water through the column at a rate of 10 BV per hour. Some of the regenerant solutions contained organic solvents (e.g. methanol, ethanol, butanol) at various concentrations, mixed with various concentrations of brine. The column test setup was fabricated by ECT and the testing was executed in ECT's Rochester, New York laboratory. Composite samples of each regenerant/rinse water solution was collected, packaged and shipped to Clarkson University, where PFAS concentrations were measured to determine the relative effectiveness of each regenerant solution. Duplicate testing was not performed during this task because it is a screening step. This task provided data support for the selection of the top two performing regenerant methods/solutions for more detailed testing in Task 5.

TASK 5: IX REGENERANT REPLICATION

In **Task 5**, the two best performing regeneration methods/solutions from Task 4 were repeated in triplicate. Results were reported as the average (and variability) of the three tests. Additionally, a second resin from a different active resin treatment system was collected, and the experiment was repeated in triplicate with the second resin. This task provided an improved understanding of the consistency of the regeneration approaches for a given site and across sites.

TASK 6: OPTIMIZATION OF TOP PERFORMING REGENERANT FOR MULTIPLE TREATMENT CYCLES

In **Task 6**, this task focused on optimizing the recovery of the regenerant solution for reuse during future resin regeneration cycles. Up to 10 different recovery techniques were applied to the two regenerant solutions from Task 5. As described in Task 4, the volume of regeneration solution was 10 BV of a solvent/salt solution or salt only solution; in this case 1 liter. The primary recovery techniques tested were distillation for the solvent/salt regenerant solutions, and membrane separation for both solvent/salt and salt only regenerant solutions. Variables for the distillation recovery approach included, 1) temperature set-point of the heating apparatus (e.g., boiling point of solvent, 10 °C lower than the solvent boiling point, and 10 °C higher than the solvent boiling point); and 2) distillation time, which determined the amount of water carry-over, pressure (e.g., atmospheric and under vacuum). The variables for the membrane separation approach included: 1) membrane material (solvent vs salt resistant) and applied solution pressure to the membrane. Up to 20 samples were collected and analyzed for PFAS to determine the extent of regenerant solution recovery and PFAS carry over. The best performing recovery method (e.g. maximum regenerant solution recovery and minimum PFAS carry over) for each of the two regenerant solutions were then retested in triplicate, and up to 6 additional samples were analyzed for PFAS. Results were reported as the average and variability of triplicate tests. The top performing regenerant solution recovery approaches for its reuse were identified.

TASK 7: DESTRUCTIVE PLASMA TREATMENT OF EFFLUENTS

In **Task 7**, the broad range of PFAS-containing effluents generated in Tasks 1, 2 and 5, which included untreated and pre-treated groundwater along with spent regenerant solution residue (i.e., the residual or bottoms that were not recycled and which contain concentrated PFAS), were treated in the plasma reactor to determine and compare individual removal efficiencies, optimize the processes for PFAS degradation, and elucidate reaction mechanisms.

The effect of operational parameters including input power (10-100 W), distance between the high voltage electrode and the liquid surface (3-10 mm), argon recirculation rate (0.5-3 L/min) and liquid flowrate (0.1-1 gpm for continuous operation and 0.1-1 gallon for batch operation) on optimum functioning of the system were determined. For the spent regenerant solutions containing high concentrations of PFAS, the argon bubbling rate was adjusted to increase gradually as high surfactant concentrations and high argon bubbling rates produce significant amounts of foam which can interfere with the formation of plasma.

Feed solutions were (i) circulated through the CSTR reactor in a semi-batch mode and (ii) treated continuously with samples collected at regular time (e.g., 5 minutes) intervals for chemical analyses. Byproducts including gaseous products, short-chain acids, and other byproducts including F^- were measured to confirm transformations and to develop a mechanistic understanding of the degradation pathways.

In addition to assessing short-term system treatment performance, the plasma reactor was also evaluated for reliability and energy and cost requirements. The latter, along with the process treatment effectiveness, informed our recommendation on whether to directly plasma-treat PFAS contaminated groundwater or to couple the technology to IX and treat concentrated regenerant streams. Plasma reactor

design (i.e., high voltage electrode configuration); a quantitative assessment of the impact of co-contaminants on plasma treatment of PFAS; and a comparison of treatment efficiency and effectiveness for contaminated groundwater, in situ pre-treated groundwater, and concentrated IX regeneration solution residue were determined.

In order to determine whether the oxidative pre-treatment using heat activated persulfate makes a difference in the plasma treatment of PFCAs, Two HDPE containers designated as control or heat activated persulfate were filled with 1.5 kg of soil and equilibrated with 1500 mL of tap water based on a 1 g soil/ 1 mL water ratio. For the control sample, the mixture was tumbled at room temperature for six hours. For the heat activated persulfate sample, 50 mM potassium persulfate was added to the sample and heated in the oven at 85°C for 24 hours, with shaking every 6 hours. Both sets of solutions were decanted, centrifuged to settle finer particles and decanted again for further plasma treatment.

TASK 8: CONCEPTUAL DESIGNS FOR IN SITU AND EX SITU TREATMENT TRAINS

In **Task 8**, based on results for Tasks 1-7, feasible combinations of in situ and ex situ treatment trains were determined for design. Conceptual designs were prepared for two representative sites. The conceptual designs evaluated implementation considerations and challenges, and cost drivers. The conceptual design output included diagrams of each configuration that were carried into detailed site-specific design.

RESULTS AND DISCUSSION

TASK 1: SOIL AND GROUNDWATER PHYSIOCHEMICAL CHARACTERIZATION

Detailed characterization of groundwater. PFAS-contaminated groundwater was collected from monitoring wells in fire training areas, burn pits, and various other water sources as part of ongoing field investigations at U. S. Air Force installations. In total, 15 samples were collected in 18.9 L high density polyethylene (HDPE) containers, secured in coolers, and shipped to Clarkson University packed on ice. Samples were stored at 4 °C upon receipt. The IDW solution electrical conductivities ranged between 22 and 26,300 µS/cm, and the pH between 5.3 and 8.0. The information on the other characteristics of the IDWs including total organic carbon (TOC), pH, conductivity, total alkalinity, total hardness, turbidity and total fluorine (F) measured by combustion ion chromatography (CIC) is provided in **Table 3**. We have identified 12 main PFAS ranging from 0.01-650 µg/L. Main co-contaminants including chloroform and dichloroethane in range of 0.003-0.050 µg/L and metals including manganese, potassium, and iron in range of 0.01-50 µg/L. Moreover, pH is in range of 5.3-8.0, conductivity ranges from 17.3 – 26300 uS/cm, hardness varies from below detection (BD) to 300 (mg as $CaCO_3$ equ/L), alkalinity ranges from 10-550 (mg as $CaCO_3$ equ/L), TOC lies between 0.11-10.8 mg/L, and turbidity varies from <1-558 NTU.

Table 3. Water Quality Characteristics of IDW Samples

Sample	Total organic carbon (mg/L)	pH	Conductivity (µS/cm)	Total alkalinity (mg/L)	Total hardness (mg/L)	Turbidity (NTU)	Total fluorine (µg/L)
IDW1	1.01	7.2	748	352	360	<1	245
IDW2	3.97	6.7	17.3	10	0	<1	290
IDW3	5.16	7.1	1665	550	548	<1	1050
IDW4	0.74	7.2	268	76	68	<1	248
IDW5	4.69	7.5	310	156	192	<1	720
IDW6	0.112	5.3	25.1	10	30	<1	320
IDW7	13.6	6.9	283	160	144	6	242
IDW8	3.03	6.7	22.1	10	110	13	244
IDW9	268	7.6	515	210	210	20	252
IDW10	1.34	7.2	1170	380	364	<1	1360
IDW11	2.50	7.3	26300	190	1130	<1	98
IDW12	4.19	7.5	344	125	130	13	1530
IDW13	10.8	8.0	2700	340	630	2	4900
WG	1.38	6.7	339	135	140	27	--
JV	26.8	6.3	285	190	230	558	--

PFAS concentrations in IDW samples. Throughout this project, the 2016 USEPA lifetime HAL was used due to analytical limitations wherein the method detection limits (MDLs) ranged between 3-7 ng/L and could not measure 2022 HALs for PFOA (0.004 ng/L) and PFOS (0.02 ng/L). Of the 12 PFAAs analyzed, PFOS, PFHpS, PFOA, PFHxS, PFHpA, PFHxS, PFBS, PFPeA and PFBA were found in all of the samples. PFDS, PFDA, and PFNA were below detection limits (approximately 9 ng/L) in IDW samples 11, 4 and 3, respectively (**Figures 7 and 8)**. Total PFAAs concentrations ranged from 2.7 to

1440 µg/L (mean 151 ± 392 µg/L); ΣPFCAs ranged from 0.3 to 500 µg/L (mean 55 ± 136 µg/L) and ΣPFSAs ranged from 0.3 to 950 µg/L (mean 96 ± 256 µg/L). Individual PFAA concentrations ranged from 3 to 7400,000 ng/L (**Figure 7 and 8**). The mean concentration was the highest for PFOS (54.3 ± 179 µg/L) and the lowest for PFDS (5.3 ± 13.9 µg/L). For the other PFAAs, concentrations decreased in the order of PFHxS (33 ± 69 µg/L), PFHxA (25 ± 65 µg/L), PFOA (13 ± 27 µg/L), PFPeA (9 ± 25 µg/L), PFBS (7 ± 13 µg/L), PFBA (4 ± 10 µg/L), PFHpA (4 ± 10 µg/L), PFHpS (0.8 ± 2 µg/L), PFNA (0.5 ± 1.7 µg/L), and PFDA (0.04 ± 0.11 µg/L) (Figure 7). 6:2 FTS had a mean concentration of 6 ± 11 µg/L which was the highest of PFAA precursors and higher than some measured PFAAs (Figure 7). The sum of PFOA (13.2 ± 26.6 µg/L) and PFOS (54.3 ± 179 µg/L) concentrations was 5 to 10500 times above the 2016 USEPA lifetime HAL in all the samples. One IDW sample (IDW 13) had extremely high concentrations of PFOA (87 µg/L) and PFOS (650 µg/L). PFNA, PFHxS, PFHpA, and PFBS which fall under the USEPA's third Unregulated Contaminant Monitoring Rule (UCMR3) were also detected at mean ratios of 25, 1100, 400, and 78 times higher than their minimum reporting levels of 0.02, 0.03, 0.01, and 0.09 µg/L, respectively. Initial PFAS concentrations in individual IDW samples are shown in **Tables 4 and 5**.

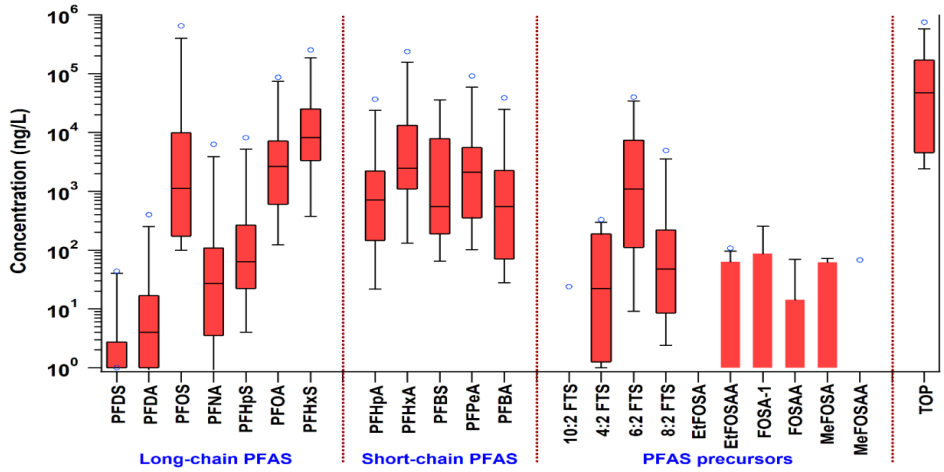

Figure 7. Concentrations of PFCAs, PFSAs, targeted precursors and total oxidizable precursors (TOP) in 13 unidentified samples. Ends of the boxes represent the first and third quartiles, horizontal lines marked inside the box represent median, whiskers represent minimum and maximum values, and small hollow circles represent the outliers.

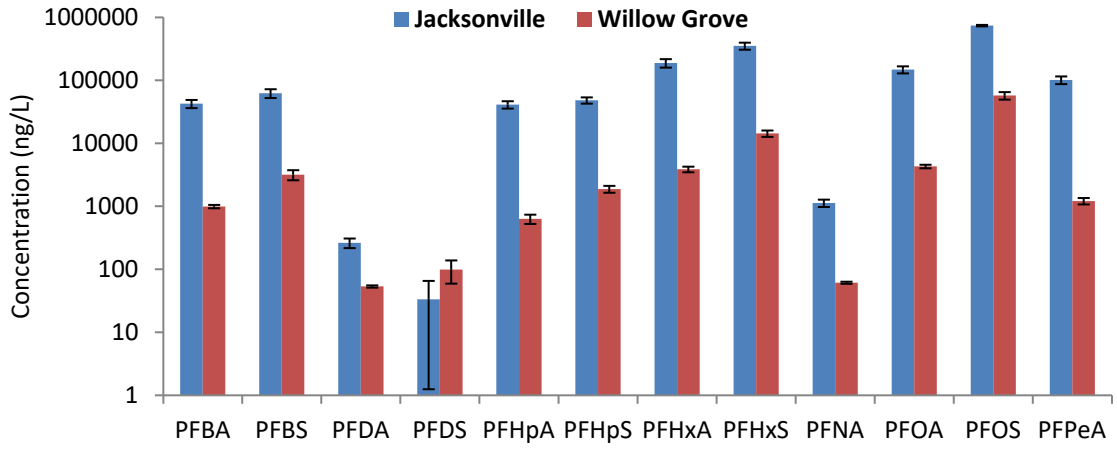

Figure 8. PFAS Concentrations in Willow Grove and Jacksonville samples.

Table 4. Initial concentrations of perfluorinated alkyl acids (PFAAs), precursors and total oxidizable precursors (TOP) quantified in different IDW samples. All the values are shown in ng/L

	IDW 1	IDW 2	IDW 3	IDW 4	IDW 5	IDW 6	IDW 7	IDW 8	IDW 9	IDW 10	IDW 11	IDW 12	IDW 13
PFDS	BDL*	BDL	BDL	BDL	BDL	BDL	44	BDL	BDL	8	BDL	BDL	BDL
PFDA	7	BDL	4	5	6	3	27	BDL	BDL	BDL	3	28	400
PFOS	21780	1001	113	1119	11052	145	8681	848	200	8308	91	2264	649876
PFNA	120	11	15	54	276	7	98	BDL	BDL	27	BDL	84	6320
PFHpS	167	BDL	10	28	780	35	141	72	16	63	54	364	8184
PFOA	6336	1153	252	1111	55728	4727	3942	104	150	2660	947	7924	86636
PFHxS	12796	1348	5389	6544	81292	12121	8232	912	24	5252	15272	34836	253224
PFHpA	1085	282	54	462	4436	1333	712	60	BDL	232	987	3088	36776
PFHxA	8867	2267	604	1560	33808	2466	2743	256	49	1580	10477	15936	237548
PFBS	2209	1844	299	537	5188	248	547	128	48	91	10526	38316	32248
PFPeA	2436	821	157	699	7108	2652	2114	244	64	467	4043	10452	91496
PFBA	1059	27	73	187	2452	649	547	68	29	170	2049	3684	38940
10:2 FTS	BDL	BDL	BDL	BDL	BDL	BDL	BDL	BDL	BDL	24	BDL	BDL	BDL
4:2 FTS	30	BDL	BDL	BDL	196	BDL	5	56	14	BDL	159	328	236
6:2 FTS	1946	8	BDL	371	8856	3180	1743	44	28	307	438	22384	39840
8:2 FTS	344	BDL	8	11	84	10	245	BDL	11	106	8	148	4948
EtFOSA	BDL	BDL	BDL	BDL	68	BDL	BDL	BDL	BDL	BDL	BDL	132	116
EtFOSAA	BDL	BDL	BDL	BDL	108	BDL	BDL	64	14	BDL	BDL	68	60
FOSA-1	BDL	12	BDL	BDL	64	BDL	282	28	BDL	139	BDL	36	216
FOSAA	BDL	BDL	BDL	BDL	BDL	BDL	BDL	BDL	19	BDL	BDL	BDL	72
MeFOSA	BDL	BDL	BDL	BDL	72	BDL	BDL	BDL	32	BDL	BDL	72	72
MeFOSAA	BDL	BDL	BDL	BDL	BDL	BDL	BDL	BDL	BDL	68	BDL	BDL	BDL
TOP (TOP in nM)	318129 (784)	3042 (6)	4104 (11)	70272 (152)	749496 (2419)	57572 (146)	47454 (147)	4984 (11)	2007 (5)	23177 (68)	255649 (740)	10574 (12)**	86551 (202)

* BDL – Below detection limit, **TOP concentration may be underestimated due to incomplete oxidation of 6:2 FTS which is present at higher concentration than used in the method validation experiment.

Table 5. Initial concentrations PFAS quantified in four IDW samples. All the values are shown in ng/L.

	California	Willow Grow	Wurtsmith	Jacksonville
4:2 FTS	880	70	330	BDL
6:2 FTS	62030	2970	46090	3180
8:2 FTS	2160	BDL	3930	BDL
FOSA-1	43330	180	60	70
MeFOSAA	1080	700	710	80
PFBA	29171	625	1380	933
PFPeA	71950	970	7970	1370
PFBS	117749	4295	3526	2536
PFHxA	519770	3420	36410	3090
PFPeS	70100	1600	3370	1890
PFHpA	34190	460	5370	80
PFHxS	215600	9140	99370	9800
PFOA	56770	1440	76070	1410
PFHpS	38750	1720	2990	1290
PFNA	170	60	300	50
PFOS	431100	39850	29520	19890
PFDA	BDL	BDL	50	BDL
PFNS	9420	200	130	90
PFDS	750	BDL	BDL	BDL

TOP in PFAS Samples. Average TOP concentrations were high in all of the samples (74 ± 105 µg/L with a range of 20 to 750 µg/L) (**Figures 7 and 9**). The ratio of average total PFAA concentrations to average TOP concentrations varied from 0.11 to 5.75. Most IDWs had a higher TOP concentration than target PFAA concentration which is expected accounting for the conversion of PFAA precursors to PFAAs after TOP. However, in some aged groundwater samples it is possible to have low PFAA precursor concentrations due to natural oxidation over time resulting in low PFAA precursor concentrations before TOP and low PFAA production after TOP. Total fluorine concentration (organic fluorine + fluoride) measured by CIC ranged from 98 to 4900 µg F/L, which on average was 90 times higher than organic fluorine measured in the TOP assay. Of the 10 individual PFAS precursors and precursors to PFAA investigated, fluorotelomer sulfonates (6:2 FTS, 8:2 FTS and 4:2 FTS) were detected in 13 samples, with mean concentrations of 7.2 ± 12.7, 0.5 ± 1.5, and 0.1 ± 0.1 µg/L, respectively. Other PFAS precursors and precursors to PFAA such as FOSA-1, EtFOSAA, EtFOSA, MeFOSA, and FOSAA were detected in a few samples (2 to 6) at very low concentrations (120 ± 110, 60 ± 30, 120 ± 10, 60 ± 20 and 50 ± 30 ng/L, respectively). MeFOSAA was detected at a concentration of 68 ng/L in only one sample. TOP concentrations were on average ten times higher than the total directly measured precursor concentrations indicating the presence of numerous undefined precursors (the ratio of TOP/ΣTIP concentration varied from 2.5 to 513).

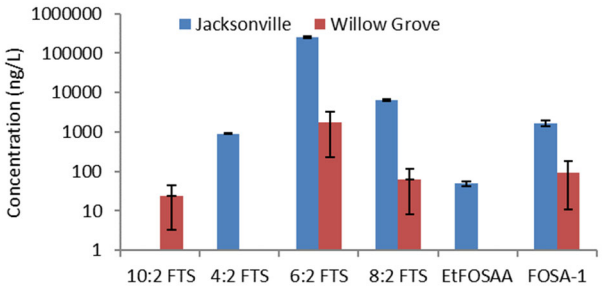

Figure 9. Concentrations of PFAS precursors and precursors to PFAA in Willow Grove and Jacksonville IDW samples.

Soil Characterizations. Soil samples were collected from AFFF impacted sites and sent to Clarkson University and Texas Tech University. Soil A from Willow Grove and Soil B from Jacksonville were received at Texas Tech University prior to batch experiments. Soil B was found to have low PFAS concentrations but was selected to be used in experiments as a representative media low in precursors. Based on batch results, column experiments were designed to focus on media high in precursor concentration therefore Soil B was replaced with Soil C from a second site in Jacksonville.

Soils were analyzed for total organic carbon (TOC) in TTU using a carbon analyzer (Elementar, vario TOC select, **Table 6**). Potassium (K), Magnesium (Mg), and Calcium (Ca), and CEC were analyzed by ammonium acetate saturation (e.g. ASTM D7503, **Table 6**), and soil pH was analyzed in a soil water slurry (e.g. ASTM D4972, **Table 6**). All were obtained via commercial laboratory analysis.

Table 6. Summary of soil characteristics.

Soil Property	Soil A	Soil B	Soil C
[1]K (mg/kg)	95	76	18
[1]Mg (mg/kg)	225	150	23
[1]Ca (mg/kg)	1564	1233	974
[1]Soil pH	7.5	6.6	7.4
[1]CEC (meq/100g)	10.2	8.1	5.2
[2]f_{oc} %	2.2	0.12	0.2
% Sand	79	63	91
% Silt	5	24	4
% Clay	16	13	5

PFAS in Soils. Individual PFAS concentrations and total precursor concentrations in Soils A (Willow Grove), B (Jacksonville) and C (Jacksonville) were within the range reported in previous studies of AFFF-impacted source zones (**Figure 10**, **Table 7**). Results of targeted analysis on pre- and post TOP soil extracts indicate that Soil A contained 2.6% PFCAs (0.05 $\mu mol/kg$), 66% PFSAs (1.28 $\mu mol/kg$), and 31.4% total precursors (0.61 $\mu mol/kg$). Soil B was 62.7% PFCAs (0.84 $\mu mol/kg$), 29.9% PFSAs (0.4 $\mu mol/kg$), and 7.4% precursors (0.1 $\mu mol/kg$). Soil C contained 1% PFCAs (0.08 nmol/g),

32% PFSAs (2.71 nmol/g), and 67% precursors (5.70 nmol/g). Although Soils A and B were similar in total PFAS concentration, Soil A was elevated in PFSAs and precursors relative to Soil B, which was dominated by PFCAs. This suggests that PFCAs were elevated in the AFFF formulations applied to Soil B and/or that precursors originally present in the foams degraded to terminal PFCAs. Previous studies indicate PFCAs were constituents of AFFF prior to 1988 but were not a primary component in more recent foams (Place and Field, 2012).

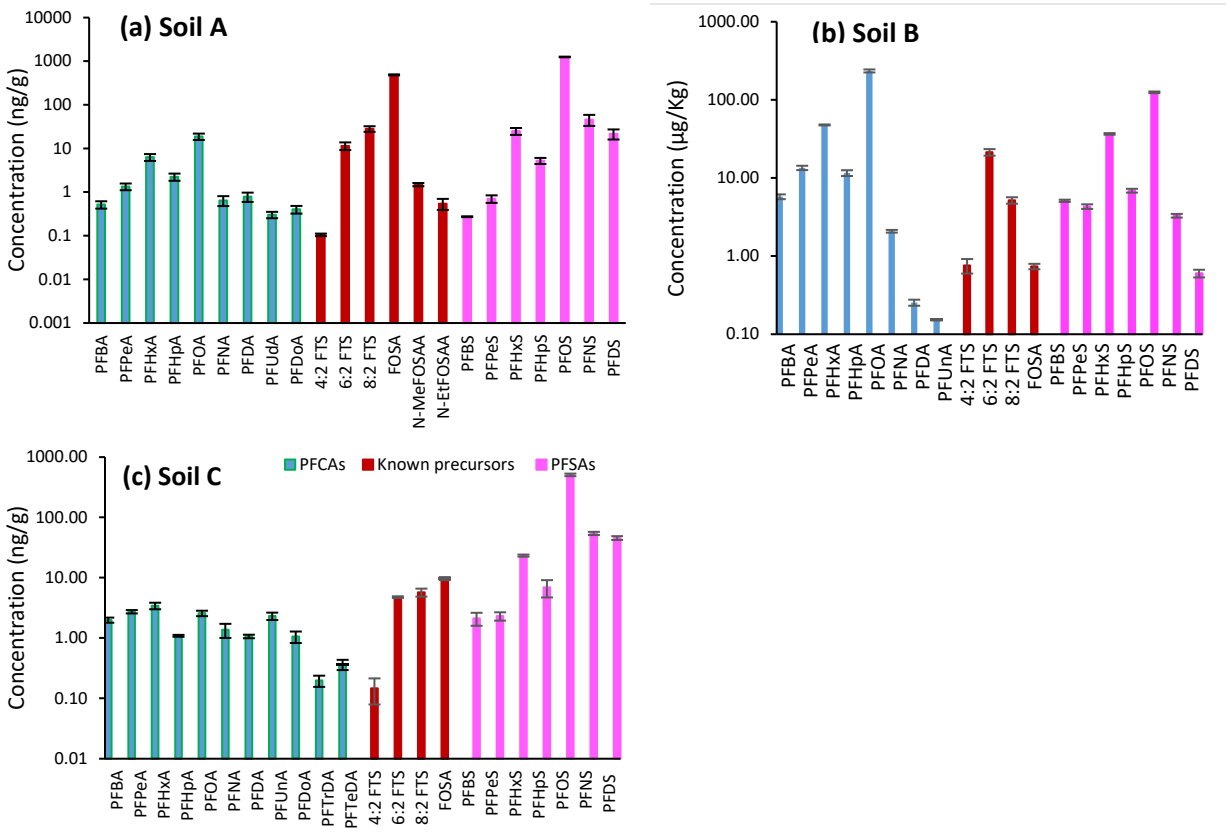

Figure 10. Concentrations of targeted analytes in a) Soil A (panel A), Soil B (panel b) and Soil C (panel c). Only detected compounds are included. Error bars represent the standard deviation of triplicate analysis.

Table 7. Results of targeted analysis and TOP for Soils A, B and C with select values from the literature.

Compound	**Soil A (µg/kg)**	**Soil B (µg/kg)**	**Soil C (µg/kg)**	**Literature Range (µg/kg)***	**References**
PFBA	2.1±0.17	5.75±0.4	0.52±0.10	0.32-456	1, 2-6
PFPeA	2.7±0.17	13.49±0.84	1.34±0.23	0.455-1421	1, 2-6
PFHxA	3.4±0.43	47.83±0.63	6.31±1.12	0.189-2761	1, 2-7
PFHpA	1.1±0.04	11.58±0.96	2.24±0.42	0.14-323	1, 2-6
PFOA	2.6±0.30	235±10.6	18.8±3.14	0.258-11484	1, 2-7
PFNA	1.4±0.36	2.08±0.08	0.64±0.16	0.29-59.4	1, 2-6
PFDA	1.1±0.07	0.25±0.02	0.78±0.19	0.21-23.4	1, 3, 5-6
PFUdA	2.3±0.33	0.15±0.003	0.30±0.05	0.5-3.04	1, 5-6
PFDoA	1.1±0.23	<0.01	0.40±0.08	0.09-1.6	1, 5-6
PFTrDA	0.20±0.04	<0.1	<0.1	0.22	6
PFTeDA	0.37±0.07	<0.1	<0.2	0.37	6
PFBS	2.1±0.51	5.11±0.18	0.27±0.01	0.029-1672	1, 2-6
PFPeS	2.3±0.37	4.30±0.30	0.71±0.14	0.08-51.06	1, 2, 6
PFHxS	23.2±0.93	36.7±0.87	25.1 ±4.49	0.1-23875	1, 2-7
PFHpS	3.8±2.20	6.89±0.39	5.25±0.85	0.08-24.11	1, 6
PFOS	508±25.90	125±2.9	1252±23.1	0.95-4100	1, 2-7
PFNS	54.2±3.29	1.61±0.26	45.9 ±12.9	0.13-6300	1, 6
PFDS	45.6±3.43	0.60±0.07	21.7±5.65	0.02-3500	1, 3, 6
4:2 FTS	0.15±0.07	0.76±0.16	0.11±0.01	1.43-5.71	1
6:2 FTS	4.77±0.15	21.4 ±2.04	11.5 ±2.29	044-6200	1, 4, 6
8:2 FTS	6.7±0.65	5.18±0.48	28.3 ±4.12	0.2-800	1, 4, 6
FOSA	9.7±0.88	0.74±0.06	486 ±12.4	0.21-3400	1, 4-7
MeFOSAA	<0.2	<0.1	1.49±0.12	0.149-3.35	8
EtFOSAA	<0.2	<0.1	0.55±0.16	0.428-0.745	8
TOP (**µmol/kg**)	0.61±0.02	0.1±0.09	5.70±0.83	0.04-291.4	1, 4, 8

*Compounds not reported were non-detect in both soils. *Values are as a range of low to high concentration reported in studies. Less than limit of quantitation (<LOQ); Not applicable (NA). References: (1) Nickerson et al., 2020; (2) Eberle et al., 2017; (3) McGuire et al., 2014; (4) Houtz et al., 2013; (5) O'Carroll et al., 2020; (6) Munoz et al., 2020; (7) Filipovic et al., 2015 (8) Nickerson et al., 2021.*

Suspect screening of Soils A and B identified a total of 70 additional PFAS in Soil A and 12 in Soil B, and the majority have previously been reported in AFFF or PFAS-impacted media (**Table 8**). Four suspect PFAS were detected in Soils A and B, however, that have never been confirmed in AFFF or PFAS-impacted media (**Figure 11**). Prior studies identified the potential for PFTrD-OS, 8:2 UFTS, 9:1 PFDS, and MeEtCMeAMPr-FPeAD to occur based on factors such as occurrence of homologues and predicted structures in prior studies (**Table 8**) (Barzen-Hanson et al., 2017; Schymanski, 2014), but this study is the first to our knowledge that confirms their environmental occurrence.

A previously published semiquantitative method was used to estimate concentrations of PFAS identified in Soil A suspect screening analysis (**Figure 12**) (Nickerson et al., 2020). In Soil A, 22.5% of precursors were ESI- PFAS (i.e., primarily anionic and noncharged), and the remaining fraction were ESI+ PFAS (i.e., primarily cationic and zwitterionic). C4-C6 ECF-based and C6-C8 FT-based PFAS comprised 78% and 22% of the total suspect PFAS concentration in Soil A, respectively (**Table 8**, **Figure 13**). This suggests a prevalence of ECF-based AFFF formulations or more rapid biodegradation of FT-based PFAS. In Soil B, approximately 54% of suspect PFAS present are ESI+ (**Figure 12**). The 26 PFAS detected in Soil B were primarily ECF in origin. In both soils, PFAS with positive moieties dominate the precursor fraction, which highlights the potential for a stronger sorbing and less mobile and recoverable fraction under ambient or remedial leaching scenarios.

Suspect analysis of Soil C resulted in detection 107 PFAS from 52 classes. In Soil C, 35% of precursors were detected in ESI- mode (primarily anionic and neutral PFAS) and 65% in ESI+ (primarily cationic and zwitterionic PFAS, **Figure 12**). Based semiquantitative estimates, 75% of Soil C suspects were C4-C10 ECF-based PFAS (**Figure 13**), and C6 was the predominant chain length (61%). The remaining 25% of precursors were C4-C8 FT based precursors, also dominated by the C6 chain length (91%). This suggests that chemical oxidation and biotransformation of Soil C to terminal endpoints would result in generation of PFHxA and lesser amounts of shorter-chain PFCAs from FT-based PFAS, and PFHxS from ECF-based PFAS.

Table 8. Suspect PFAS, and associated PFAS classes detected in Soils A and B.

Compound	Acronym	Class Acronym	Chain Length	Extract detected Soil A	Extract detected Soil B	Extract detected Soil C	ESI mode	Confidence Level	KMD	RT
1-hydroxy-8:2 fluorotelomer sulfonate	1OH-8:2 FTS	1OH-X:2 FTS	8	B[a]	B/C[b]	B/C	ESI-	2a	0.991	8.57
4:2 fluorotelomer thia propanoamido dimethyl ethyl sulfonate	4:2 FTTh-PrAd-DiMeEtS	X:2 FTTh-PrAd-DiMeEtS	4	NA[d]	NA	C[c]	ESI-	2a	0.078	7.47
6:2 fluorotelomersulfonyl propanoic acid	6:2 FTSO2PrA	X:2 FTSO2PrA	6	NA	B	NA	ESI-	4a	0.025	7.58
6:2 fluorotelomer sulfonamido propyl betaine	6:2 FTSA-PrB	X:2 FTSA-PrB	6	B/C	NA	NA	ESI-	2a	0.113	7.58
6:2 fluorotelomer sulfonamido propyl methyl amine	6:2 FTSA-Pr-MeAn	X:2 FTSA-Pr-MeAn	6	NA	NA	B/C	ESI-	4a	0.089	6.99
6:2 fluorotelomer sulfinyl propanamido dimethyl ethyl sulfonate	6:2 FTSO-PrAd-DiMePrS	X:2 FTSO-PrAd-DiMePrS	6	B/C	NA	NA	ESI-	2a	0.070	7.83
8:2 fluorotelomer sulfinyl propanamido dimethyl ethyl sulfonate	8:2 FTSO-PrAd-DiMePrS	X:2 FTSO-PrAd-DiMePrS	8	B/C	NA	NA	ESI-	2a	0.071	9.14
6:2 fluorotelomer sulfonyl propanoamido-dimethylethyl sulfonate	6:2 FTSO2PrAd-DiMeEtS	X:2 FTSO2PrAd-DiMeEtS	6	B/C	B/C	B/C	ESI-/ESI+[e]	4a	0.069	7.92
8:2 fluorotelomer sulfonyl propanoamido-dimethylethyl sulfonate	8:2 FTSO2PrAd-DiMeEtS	X:2 FTSO2PrAd-DiMeEtS	8	B/C	NA	B/C	ESI-/ESI+	4a	0.069	9.22
7:3 fluorotelomer carboxylic acid	7:3 FTCA	X:3 FTCA	7	C	NA	NA	ESI-	2a	0.024	8.65
10:2 fluorotelomer sulfonate	10:2 FTS	X:2 FTS	10	B	NA	NA	ESI-	2a	0.994	7.84
9:1 perfluorodecane sulfonate	9:1 PFDS	X:1 PFAS	9	B/C	NA	NA	ESI-	4a	0.986	9.76
10:1 perfluoroundecane sulfonate	10:1 PFUdS	X:1 PFAS	10	B/C	NA	NA	ESI-	4a	0.985	10.22
8:2 unsaturated fluorotelomer sulfonate	8:2 UFTS	X:2 UFTS	8	B/C	NA	NA	ESI-	4b	0.987	8.43
N-dimethyl ammonio propyl perfluorobutane sulfonamide	AmPr-FBSA	AmPr-FASA	4	B/C	B/C	B/C	ESI-	2a	0.072	6.25
N-dimethyl ammonio propyl perfluorohexane sulfonamide	AmPr-FHxSA	AmPr-FASA	6	B/C	C	B/C	ESI-/ESI+	2a	0.072	7.47

Compound	Acronym	Class Acronym	Chain Length	Extract detected Soil A	Extract detected Soil B	Extract detected Soil C	ESI mode	Confidence Level	KMD	RT
N-dimethyl ammonio propyl perfluorohexane sulfonamido propanoic acid	AmPr-FHxSA-PrA	AmPr-FASA-PrA	6	B/C	NA	B/C	ESI-/ESI+	2a	0.097	6.87
Chloro-perfluorooctane sulfonate	Cl-PFOS	Cl-PFAS	7	B/C	B/C	B/C	ESI-	2a	0.935	8.4
N-Carboxymethyldimethylammoniopropyl - perfluorohexanesulfonamide	CMeAmPr-FHxSA	CMeAmPr-FASA	6	NA	B/C	B/C	ESI-/ESI+	4b	0.082	7.21
N-Carboxymethyldimethylammoniopropyl -perfluorooctanesulfonamide	CMeAmPr-FOSA	CMeAmPr-FASA	8	B/C	NA	B/C	ESI-/ESI+	4a	0.096	7.22
N-dihydroxybutyl dimethylammoniopropyl perfluorobutane sulfonamide	diOHBAmPr-FBSA	diOHBAmPr-FASA	4	NA	NA	B/C	ESI-	2a	0.131	5.975
N-dihydroxybutyl dimethylammoniopropyl perfluoropentane sulfonamide	diOHBAmPr-FPeSA	diOHBAmPr-FASA	5	NA	NA	B/C	ESI-	2a	0.130	6.451
N-dihydroxybutyl dimethylammoniopropyl perfluorohexane sulfonamide	diOHBAmPr-FHxSA	diOHBAmPr-FASA	6	NA	NA	B/C	ESI-	2a	0.130	6.997
N-dihydroxybutyl dimethylammoniopropyl perfluorooctane sulfonamide	diOHBAmPr-FOSA	diOHBAmPr-FASA	8	NA	NA	C	ESI-	4a	0.130	8.16
N-dihydroxy propyl dimethyl ammonio hydroxymethyl propyl-perfluoropentanesulfonamide	diOHPrAm-MeOHPr-FPeSA	diOHPrAm-MeOHPr-FASA	5	NA	NA	B/C	ESI-	2a	0.126	6.39
N-dihydroxy propyl dimethyl ammonio hydroxymethyl propyl-perfluorohexanesulfonamide	diOHPrAm-MeOHPr-FHxSA	diOHPrAm-MeOHPr-FASA	6	B/C	NA	NA	ESI-	2a	0.126	6.953
N-dihydroxy propyl dimethyl ammonio hydroxymethyl propyl-perfluorohexanesulfonamide	diOHPrAm-MeOHPr-FHxSAPrS	diOHPrAm-MeOHPr-FASAPrS	6	NA	NA	B/C	ESI-	2a	0.138	7.151
N-ethylperfluoro-1-octane sulfonamide	EtFOSA	EtFASA	8	B/C	NA	NA	ESI-	2a	0.009	9.27
PentaFluoroSulfide PerFluorooctanoic Acid	F5S-PFOA	F5S-PFCA	7	NA	NA	B/C	ESI-	2a	0.965	8.896

Compound	Acronym	Class Acronym	Chain Length	Extract detected Soil A	Extract detected Soil B	Extract detected Soil C	ESI mode	Confidence Level	KMD	RT
PentaFluoroSulfide PerFluorononanoic Acid	F5S-PFNA	F5S-PFCA	8	NA	NA	B/C	ESI-	2a	0.958	9.438
PentaFluoroSulfide perfluoroheptane sulfonate	F5S-PFHpS	F5S-PFAS	7	B/C	NA	B/C	ESI-	2a	0.934	8.768
PentaFluoroSulfide perfluorooctane sulfonate	F5S-PFOS	F5S-PFAS	8	B/C	B/C	B/C	ESI-	2a	0.934	9.485
PentaFluoroSulfide perfluorononane sulfonate	F5S-PFNS	F5S-PFAS	9	B/C	NA	B/C	ESI-	2a	0.934	10.014
Perfluoropropane sulfonamide	FPrSA	FASA	2	NA	NA	B	ESI-	2a	0.978	5.797
Perfluorobutane sulfonamide	FBSA	FASA	4	B/C	NA	B/C	ESI-	2a	0.977	6.51
Perfluoropentane sulfonamide	FPeSA	FASA	5	C	NA	B/C	ESI-	2a	0.978	6.935
Perfluorohexane sulfonamide	FHxSA	FASA	6	B/C	B/C	B/C	ESI-	2a	0.978	7.56
Perfluoroheptane sulfonamide	FHpSA	FASA	7	B/C	NA	B/C	ESI-	2a	0.978	8.20
Perfluorononane sulfonamide	FNSA	FASA	9	NA	NA	B/C	ESI-	4a	0.978	9.16
Perfluorohexane sulfonamido acetic acid	FHxSAA	FASAA	6	NA	B	B/C	ESI-	2a	0.987	7.55
Perfluorooctane sulfonamido acetic acid	FOSAA	FASAA	8	B/C	NA	B/C	ESI-	2a	0.987	8.45
Hydrogen-substituted perfluorodecananoic acid	H-PFDA	H-PFCA	8	NA	B/C	NA	ESI-	4a	0.001	7.64
Hydrogen-substituted PerFluoroOctane Sulfonate	H-PFOS	H-PFSA	6	NA	B/C	NA	ESI-	2a	0.97	7.398
Hydrogen-substituted PerFluoroNonane Sulfonate	H-PFNS	H-PFSA	7	NA	NA	B/C	ESI-	2a	0.97	7.60
Hydrogen-substituted PerFluoroDecane Sulfonate	H-PFDS	H-PFSA	8	NA	B/C	B/C	ESI-	2a	0.97	8.279
Unsaturated perfluorononane unsaturated ether/alcohol	H-UPFN-O/OH	H-UPFA-O/OH	9	B/C	NA	NA	ESI-	4b	0.001	7.81
Keto-perfluorohexane sulfonate	K-PFHxS	K-PFAS	4	NA	B/C	NA	ESI-	2a	0.959	6.646
Keto-perfluorooctane sulfonate	K-PFOS	K-PFAS	6	NA	C	NA	ESI-	2a	0.958	7.81
Keto-perfluoroundecane sulfonate	K-PFUdS	K-PFAS	9	B/C	NA	NA	ESI-	2a	0.959	9.55
Keto-perfluorododecane sulfonate	K-PFDoS	K-PFAS	10	B/C	NA	B	ESI-	2a	0.958	10.04
Keto-perfluorotridecane sulfonate	K-PFTrDS	K-PFAS	11	B/C	NA	NA	ESI-	4a	0.958	10.51

Compound	Acronym	Class Acronym	Chain Length	Extract detected Soil A	Extract detected Soil B	Extract detected Soil C	ESI mode	Confidence Level	KMD	RT
Keto-perfluorotetradecane sulfonate	K-PFTeDS	K-PFAS	12	B/C	NA	NA	ESI-	4a	0.959	10.87
N-methyl perfluoro-1-hexane sulfonamide	MeFHxSA	MeFASA	6	NA	NA	B/C	ESI-	4a	0.994	8.55
N-methylperfluoropropane sulfonamido acetic acid	MeFPrAA	MeFASAA	3	NA	NA	B/C	ESI-	2a	0.003	7.30
N-methylperfluorobutane sulfonamido acetic acid3	MeFBSAA	MeFASAA	4	NA	B/C	B/C	ESI-	2a	0.004	7.66
N-methylperfluorohexane sulfonamido acetic acid	MeFHxSAA	MeFASAA	6	NA	B	NA	ESI-	2a	0.004	8.97
N-methylperfluorodecane sulfonamido acetic acid	MeFDSAA	MeFASAA	10	NA	B	NA	ESI-	4a	0.003	11.15
N-methylperfluorotridecane sulfonamido acetic acid	MeTrDSAA	MeFASAA	13	NA	NA	B/C	ESI-	4b	0.005	7.64
N-methylethyl-carboxymethyl dimethyl ammonio propyl perfluoropentane amide	MeEtCMeAmPr-FPeAd	MeEtCMeAmPr-FAAd	5	B/C	NA	B/C	ESI-/ESI+	4b	0.141	7.79
Perfluoro Ether nonane sulfonate	PFENS	PFESA	7	NA	NA	B/C	ESI-	2a	0.956	8.40
Perfluoro Ether decane sulfonate	PFEDS	PFESA	8	NA	NA	B/C	ESI-	2a	0.958	8.81
Perfluoro Ether pentaecane sulfonate	PFEPeDS	PFESA	13	B/C	NA	NA	ESI-	2a	0.958	11.27
Oxa-Unsaturated-PerFluoroHexanoic Acid	UPFEHxA	UPFECA	0	NA	B/C	NA	ESI-	2a	0.989	5.67
PentaHydrogen-substituted fluoroheptane sulfate	PeH-FHpOS	PeH-FAOS	6	NA	B	NA	ESI-	4b	0.998	6.42
Perfluorononane sulfate	PFN-OS	PFA-OS	9	B/C	NA	NA	ESI-	4a	0.956	8.993
Perfluorodecane sulfate	PFD-OS	PFA-OS	10	B/C	NA	B/C	ESI-	4a	0.957	9.35
Perfluorododecane sulfate	PFDo-OS	PFA-OS	12	B/C	NA	NA	ESI-	4a	0.958	10.48
Perfluorotridecane sulfate	PFTrD-OS	PFA-OS	13	B/C	NA	NA	ESI-	4a	0.957	10.85
Perfluorohexane sulfinate	PFHxSi	PFASi	6	B/C	B/C	B/C	ESI-	2a	0.966	7.29
Perfluoroheptane sulfinate	PFHpSi	PFASi	7	NA	NA	B	ESI-	2a	0.966	7.934
Perfluorooctane sulfinate	PFOSi	PFASi	8	B/C	B	B/C	ESI-	2a	0.966	8.598
Perfluoropropane sulfonate	PFPrS	PFSA	3	NA	B/C	NA	ESI-	2a	0.962	5.44
Perfluoroundecane sulfonate	PFUdS	PFSA	11	B/C	NA	C	ESI-	2a	0.960	9.93

Compound	Acronym	Class Acronym	Chain Length	Extract detected Soil A	Extract detected Soil B	Extract detected Soil C	ESI mode	Confidence Level	KMD	RT
Perfluorododecane sulfonate	PFDoS	PFSA	12	B/C	NA	NA	ESI-	2a	0.960	10.41
Perfluorotridecane sulfonate	PFTrDS	PFSA	13	B/C	NA	NA	ESI-	2a	0.961	10.78
Perfluoropentadecane sulfonate	PFPeDS	PFSA	15	B/C	NA	NA	ESI-	4a	0.962	11.63
Perfluorononadecane sulfonate	PFODS	PFSA	18	NA	NA	B//C	ESI-	4a	0.962	8.81
Unsaturated perfluorohexane sulfonate	UPFHxS	UPFAS	3	NA	B/C	NA	ESI-	2a	0.961	6.51
Unsaturated perfluorooctane sulfonate	UPFOS	UPFAS	5	B/C	B/C	NA	ESI-	2a	0.962	7.74
perfluoro propyl cyclohexane sulfonate	UPFNS	UPFAS	6	B/C	NA	B/C	ESI-	2a	0.962	8.21
Unsaturated perfluorodecane sulfonate	UPFDS	UPFAS	7	B/C	B/C	B/C	ESI-	2a	0.962	8.72
Unsaturated perfluoroundecane sulfonate	UPFUdS	UPFAS	8	B/C	NA	B/C	ESI-	2a	0.962	9.32
Unsaturated perfluorododecane sulfonate	UPFDoS	UPFAS	9	B/C	NA	NA	ESI-	4a	0.961	9.93
N-sulfo propyl perfluorohexane sulfonamide	SPr-FHxSA	SPr-FASA	6	NA	B/C	B/C	ESI-	2a	0.989	7.75
N-sulfo propyl perfluorononane sulfonamide	SPr-FNSA	SPr-FASA	9	NA	B	NA	ESI-	4a	0.990	11.18
N-sulfo propyl dimethyl ammonio propyl perfluoropropane sulfonamide	SPrAmPr-FPrSA	SPrAmPr-FASA	3	NA	B/C	NA	ESI-	2a	0.086	5.51
N-sulfo propyl dimethyl ammonio propyl perfluorobutane sulfonamide	SPrAmPr-FBSA	SPrAmPr-FASA	4	NA	B/C	NA	ESI-/ESI+	2a	0.083	5.97
N-sulfo propyl dimethyl ammonio propyl perfluoropentane sulfonamide	SPrAmPr-FPeSA	SPrAmPr-FASA	5	NA	B/C	NA	ESI-	2a	0.082	6.48
N-sulfo propyl dimethyl ammonio propyl perfluorohexane sulfonamide	SPrAmPr-FHxSA	SPrAmPr-FASA	6	B/C	B/C	B/C	ESI-/ESI+	2a	0.083	7.10
N-sulfo propyl dimethyl ammonio propyl perfluoroheptane sulfonamide	SPrAmPr-FHpSA	SPrAmPr-FASA	7	NA	NA	B/C	ESI-	2a	0.084	7.62
N-sulfo propyl dimethyl ammonio propyl perfluorooctane sulfonamide	SPrAmPr-FOSA	SPrAmPr-FASA	8	B	NA	C	ESI-	2a	0.084	8.17
N-sulfopropyl dimethylammoniopropyl perfluoropentane sulfonamido propyl sulfonate	SPrAmPr-FPeSAPrS	SPrAmPr-FASAPrS	5	C	NA	NA	ESI-	2a	0.103	7.54
2:2 fluorotelomer sulfonyl ethano amido propyl trimethyl ammonium	2:2 FTSO2-EtAdPrTAm	X:2 FTSO2-EtAdPrTAm	2	NA	NA	B/C	ESI+	4b	0.148	12.23

Compound	Acronym	Class Acronym	Chain Length	Extract detected Soil A	Extract detected Soil B	Extract detected Soil C	ESI mode	Confidence Level	KMD	RT
4:2 fluorotelomer sulfonyl ethano amido propyl trimethyl ammonium	4:2 FTSO2-EtAdPrTAm	X:2 FTSO2-EtAdPrTAm	4	NA	B/C	NA	ESI+	4b	0.148	11.01
4:2 fluorotelomer sulfonamido propyl methyl amine	4:2 FTSA-Pr-MeAn	X:2 FTSA-Pr-MeAn	4	NA	NA	B/C	ESI+	4a	0.104	5.93
4:2 fluorotelomer sulfonamido propyl dimethyl amine	4:2 FTSAPr-DiMeAn	X:2 FTSAPr-DiMeAn	4	NA	NA	B/C	ESI+	2a	0.121	5.98
6:2 fluorotelomer sulfonamido propyl dimethyl amine	6:2 FTSAPr-DiMeAn	X:2 FTSAPr-DiMeAn	6	B/C	NA	B/C	ESI+	2a	0.120	7.05
8:2 fluorotelomer sulfonamido propyl dimethyl amine	8:2 FTSAPr-DiMeAn	X:2 FTSAPr-DiMeAn	8	B/C	NA	B/C	ESI+	2a	0.120	8.20
6:2 fluorotelomer sulfonamido propyl methyl amino acetic acid	6:2 FTSA-Pr-MeAA	X:2 FTSA-Pr-MeAA	6	NA	C	B/C	ESI+	4b	0.114	7.42
6:2 fluorotelomer sulfonamido propyl amine	6:2 FTSA-PrAn	X:2 FTSA-PrAn	6	NA	NA	B/C	ESI+	4b	0.088	7.47
8:2 fluorotelomer sulfonamido propyl amine	8:2 FTSA-PrAn	X:2 FTSA-PrAn	8	NA	NA	B/C	ESI+	4b	0.088	8.80
6:2 fluorotelomer thia ethanamido propyl dimethyl ammonium	6:2 FTTh-EtAdPrAm	X:2 FTTh-EtAdPrAm	6	C	NA	NA	ESI+	4b	0.143	6.42
9:3 fluorotelomer betaine	9:3 FTB	X:3 FTB	9	NA	NA	B/C	ESI+	2a	0.124	8.20
N-betaine propyl perfluoropropane amide	BPr-FPrAd	BPr-FAAd	2	NA	NA	B/C	ESI+	4a	0.128	12.59
N-betaine propyl perfluoropentane amide	BPr-FPeAd	BPr-FAAd	4	C	NA	NA	ESI+	4a	0.126	8.01
N-carboxyethyl dimethyl ammonio propyl perfluorohexane sulfonamide	CEtAmPr-FHxSA	CEtAmPr-FASA	6	NA	C	B/C	ESI+	2a	0.114	7.42
N-carboxyethyl dimethylammoniopropyl-N-ethyl perfluorohexane sulfonamide	CEtAmPr-N-EtFHxSA	CEtAmPr-N-EtFASA	6	NA	NA	B/C	ESI+	2a	0.147	7.30
N-carboxyethyl dimethylammoniopropyl-N-ethyl perfluorooctane sulfonamide	CEtAmPr-N-EtFOSA	CEtAmPr-N-EtFASA	8	NA	NA	C	ESI+	4b	0.147	8.38
Class 38 (Cn+9H22O2SN2F2n+1)	Class_38_C11	Class 38 (n+9H22O2SN2F2n+1)	2	NA	NA	B/C	ESI+	4a	0.153	5.54

Compound	Acronym	Class Acronym	Chain Length	Extract detected Soil A	Extract detected Soil B	Extract detected Soil C	ESI mode	Confidence Level	KMD	RT
Class 38 (Cn+9H22O2SN2F2n+1)	Class_38_C12	Class 38 (n+9H22O2SN2F2n+1)	3	NA	NA	B/C	ESI+	4a	0.153	5.93
Class 38 (Cn+9H22O2SN2F2n+1)	Class_38_C13	Class 38 (n+9H22O2SN2F2n+1)	4	NA	NA	B/C	ESI+	2a	0.153	6.38
Class 38 (Cn+9H22O2SN2F2n+1)	Class_38_C14	Class 38 (n+9H22O2SN2F2n+1)	5	NA	NA	B/C	ESI+	4a	0.153	6.85
Class 38 (Cn+9H22O2SN2F2n+1)	Class_38_C15	Class 38 (n+9H22O2SN2F2n+1)	6	NA	C	NA	ESI+	2a	0.153	7.42
Class 38 (Cn+9H22O2SN2F2n+1)	Class_38_C16	Class 38 (n+9H22O2SN2F2n+1)	7	NA	NA	B/C	ESI+	4a	0.153	7.95
Class 38 (Cn+9H22O2SN2F2n+1)	Class_38_C17	Class 38 (n+9H22O2SN2F2n+1)	8	NA	NA	B/C	ESI+	4a	0.153	8.50
Class 38 (Cn+9H22O2SN2F2n+1)	Class_38_C18	Class 38 (n+9H22O2SN2F2n+1)	9	NA	NA	B/C	ESI+	4a	0.153	8.78
Class 38 (Cn+9H22O2SN2F2n+1)	Class_38_C19	Class 38 (n+9H22O2SN2F2n+1)	10	NA	NA	B	ESI+	4a	0.151	9.19
N-carboxymethyl dimethylammoniopropyl-perfluoropentane sulfonamido acetic acid	CMeAmPr-FPeSAA	CMeAmPr-FASAA	5	NA	NA	C	ESI+	4a	0.101	6.90
N-carboxymethyl dimethylammoniopropyl-perfluorohexane sulfonamido acetic acid	CMeAmPr-FHxSAA	CMeAmPr-FASAA	6	NA	NA	B/C	ESI+	4a	0.103	8.12
N-dihydroxyethyl amino propyl-perfluoropentane amide	diEtOH-APr-FPeAd	diEtOH-APr-FAAd	4	NA	C	C	ESI+	4b	0.144	8.01
N-dimethylaminohydroxybutyl-perfluorohexanesulfonamidopropylsulfonate	DiMeA-MeOHPr-FHxSAPrS	DiMeA-MeOHPr-FASAPrS	6	NA	NA	B/C	ESI+	2a	0.112	7.07

Compound	Acronym	Class Acronym	Chain Length	Extract detected Soil A	Extract detected Soil B	Extract detected Soil C	ESI mode	Confidence Level	KMD	RT
N-dihydroxybutyl dimethylammoniopropyl perfluoroheptane sulfonamide	diOHBAmPr-FHpSA	diOHBAmPr-FASA	7	NA	NA	B/C	ESI+	4a	0.146	7.33
N-hydroxyethyl dimethylammoniohydroxypropyl perfluoropentanesulfonamide	EtOH-Am-OHPr-FPeSA	EtOH-Am-OHPr-FASA	5	NA	NA	B/C	ESI+	2a	0.130	6.39
N-hydroxyethyldimethylammoniopropyl perfluorobutanesulfonamide	EtOH-AmPr-FBSA	EtOH-AmPr-FASA	4	C	NA	NA	ESI+	2a	0.115	5.35
N-hydroxyethyldimethylammoniopropyl perfluoropentanesulfonamide	EtOH-AmPr-FPeSA	EtOH-AmPr-FASA	5	B/C	NA	B/C	ESI+	2a	0.117	6.38
N-hydroxyethyldimethylammoniopropyl perfluorohexanesulfonamide	EtOH-AmPr-FHxSA	EtOH-AmPr-FASA	6	B/C	NA	B/C	ESI+	2a	0.116	6.91
N-hydroxyethyldimethylammoniopropyl perfluoroheptanesulfonamide	EtOH-AmPr-FHpSA	EtOH-AmPr-FASA	7	B/C	NA	B/C	ESI+	2a	0.117	7.56
N-hydroxyethyldimethylammoniopropyl perfluorooctanesulfonamide	EtOH-AmPr-FOSA	EtOH-AmPr-FASA	8	B/C	NA	B/C	ESI+	2a	0.117	8.07
N-hydroxyethyldimethylammoniopropyl perfluorodecanesulfonamide	EtOH-AmPr-FDSA	EtOH-AmPr-FASA	10	NA	C	NA	ESI+	4b	0.113	7.08
N-hydroxyethyldimethylammoniopropyl perfluoropentanesulfonamidoethanol	EtOH-AmPr-FPeSA-EtOH	EtOH-AmPr-FASA-EtOH	5	NA	NA	B/C	ESI+	2a	0.146	6.33
N-hydroxyethyldimethylammoniopropyl perfluorohexanesulfonamidoethanol	EtOH-AmPr-FHxSA-EtOH	EtOH-AmPr-FASA-EtOH	6	C	NA	B/C	ESI+	2a	0.145	6.82
N-hydroxyethyldimethylammoniopropyl perfluoroheptanesulfonamidoethanol	EtOH-AmPr-FHpSA-EtOH	EtOH-AmPr-FASA-EtOH	7	B/C	NA	NA	ESI+	2a	0.143	7.47
N-hydroxyethyldimethylammoniopropyl perfluorooctanesulfonamidoethanol	EtOH-AmPr-FOSA-EtOH	EtOH-AmPr-FASA-EtOH	8	C	NA	B/C	ESI+	2a	0.146	7.88
N-hydroxyethyl dimethylammoniopropyl perfluorohexane sulfonamido propylsulfonate	EtOH-AmPr-FHxSAPrS	EtOH-AmPr-FASAPrS	6	NA	C	B/C	ESI+	2a	0.128	7.17
N-hydroxyethyl dimethylammoniopropyl perfluoroheptane sulfonamido propylsulfonate	EtOH-AmPr-FOSAPrS	EtOH-AmPr-FASAPrS	8	NA	NA	B/C	ESI+	2a	0.129	8.48
N-oxidedimethylammoniopropyl-perfluoroheptanesulfonamide	OAmPr-FHpSA	OAmPr-FASA	7	NA	NA	B	ESI+	4	0.082	6.96

Compound	Acronym	Class Acronym	Chain Length	Extract detected Soil A	Extract detected Soil B	Extract detected Soil C	ESI mode	Confidence Level	KMD	RT
N-oxidedimethylammoniopropyl-perfluorooctanesulfonamide	OAmPr-FDAd	OAmPr-FAAD	10	NA	NA	B/C	ESI+	4	0.115	8.19
N-sulfohydroxypropyl dimethylammonio propyl perfluorobutane sulfonamido hydroxy propyl sulfonate	S-OHPrAmPr-FBSA-OHPrS	S-OHPrAmPr-FASA-OHPrS	4	NA	C	NA	ESI+	2a	0.102	5.61
N-sulfopropyldimethylammoniopropyl-perfluoropentane sulfonamido acetic acid	C15H21O7S2N2F11	NA	5	NA	NA	B	ESI+	2a	0.108	8.15
N-sulfopropyldimethylammoniopropyl-perfluorohexane sulfonamido acetic acid	SPrAmPr-FHxSAA	SPrAmPr-FASAA	6	NA	C	B/C	ESI-/ESI+	2a	0.109	7.13
N-sulfopropyl dimethylammoniopropyl perfluorobutane sulfonamido propyl sulfonate	C15H25O8S3N2F9	NA	4	B/C	NA	B/C	ESI+	4b	0.117	8.07
N-hydroxyethyldimethylammoniopropyl perfluorodecanesulfonamide	SPrAmPr-FHxSAPrS	SPrAmPr-FASAPrS	6	B	B/C	NA	ESI-/ESI+	2a	0.111	7.08
N-sulfopropyl dimethylammoniopropyl perfluoroheptane sulfonamido propyl sulfonate	SPrAmPr-FHpSAPrS	SPrAmPr-FASAPrS	7	NA	NA	B/C	ESI+	2a	0.112	7.69
N-sulfopropyl dimethylammoniopropyl perfluorooctane sulfonamido propyl sulfonate	SPrAmPr-FOSAPrS	SPrAmPr-FASAPrS	8	NA	NA	B/C	ESI+	2a	0.111	8.33
N-sulfopropyldimethylammonio-propyl N-methyl perfuorooctanesulfonamide	SPrAmPr-N-Me-FOSA	SPrAmPr-N-Me-FASA	8	NA	NA	B/C	ESI+	4b	0.116	8.42
N-Trimethylammoniopropyl perfluoropentane sulfonamide	TAmPr-FPeSA	TAmPr-FASA	5	B/C	B/C	B/C	ESI+	2a	0.104	6.41
N-Trimethylammoniopropyl perfluorohexane sulfonamide	TAmPr-FHxSA	TAmPr-FASA	6	B/C	NA	B/C	ESI+	2a	0.104	6.94
N-Trimethylammoniopropyl perfluoroheptane sulfonamide	TAmPr-FHpSA	TAmPr-FASA	7	B/C	NA	B/C	ESI+	2a	0.104	7.52
N-Trimethylammoniopropyl perfluorooctane sulfonamide	TAmPr-FOSA	TAmPr-FASA	8	B/C	NA	B/C	ESI+	2a	0.103	8.12
N-trimethylammoniopropyl perfluorohexane sulfonamido propanoic acid	TAmPr-FHxSAPrA	TAmPr-FASAPrA	6	C	NA	NA	ESI+	2a	0.129	7.35

Compound	Acronym	Class Acronym	Chain Length	Extract detected Soil A	Extract detected Soil B	Extract detected Soil C	ESI mode	Confidence Level	KMD	RT
N-trimethylammoniopropyl N-methylperfluoropentanesulfonamide	TAmPr-N-MeFPeSA	TAmPr-N-MeFASA	5	C	NA	B/C	ESI+	2a	0.120	6.46
N-trimethylammoniopropyl N-methylperfluoroheptanesulfonamide	TAmPr-N-MeFHpSA	TAmPr-N-MeFASA	7	NA	NA	B/C	ESI+	4a	0.121	7.58
N-trimethylammoniopropyl N-methylperfluorooctanesulfonamide	TAmPr-N-MeFNSA	TAmPr-N-MeFASA	9	NA	NA	B/C	ESI+	4a	0.121	8.52

PFTrD-OS

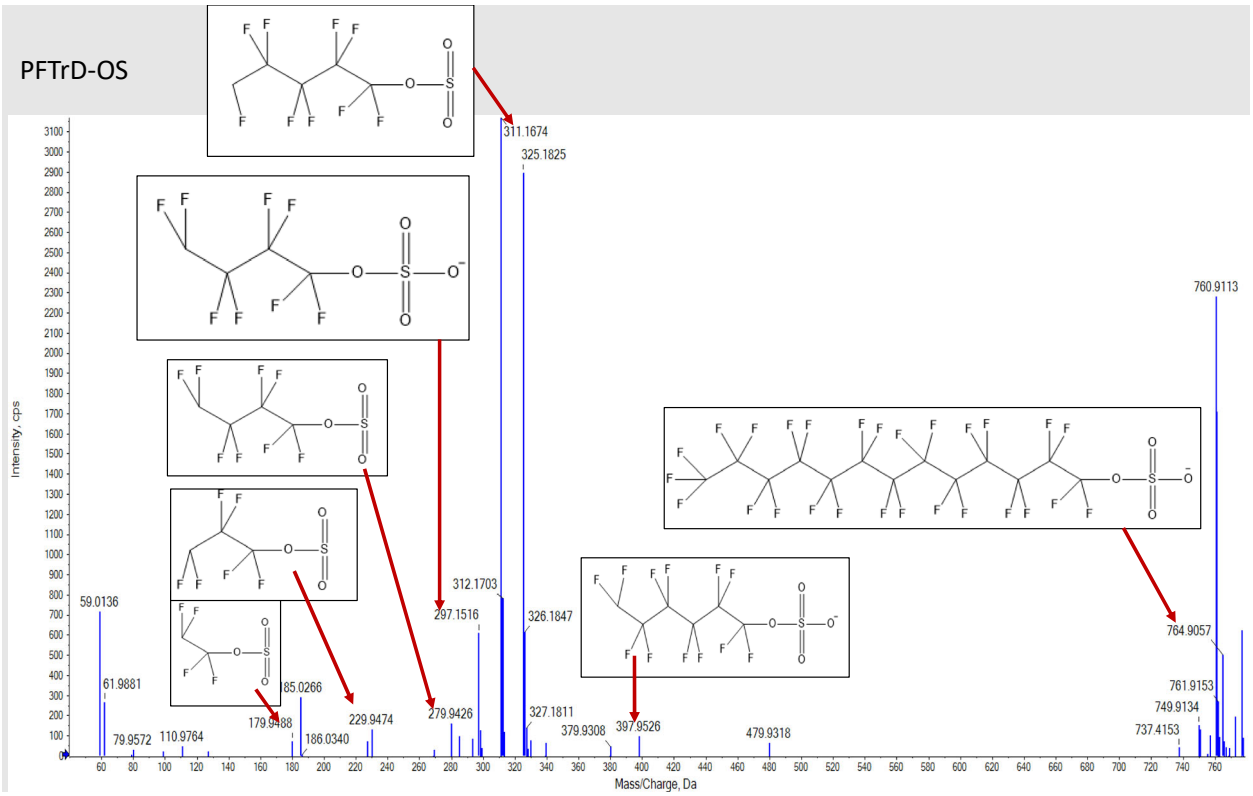

8:2 UFTS

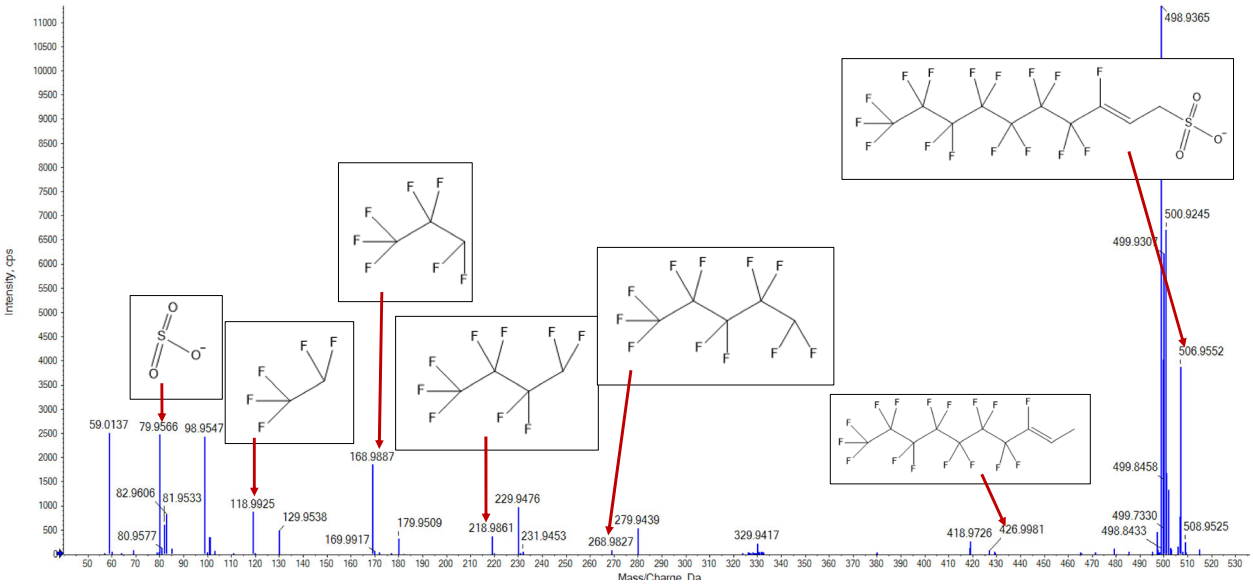

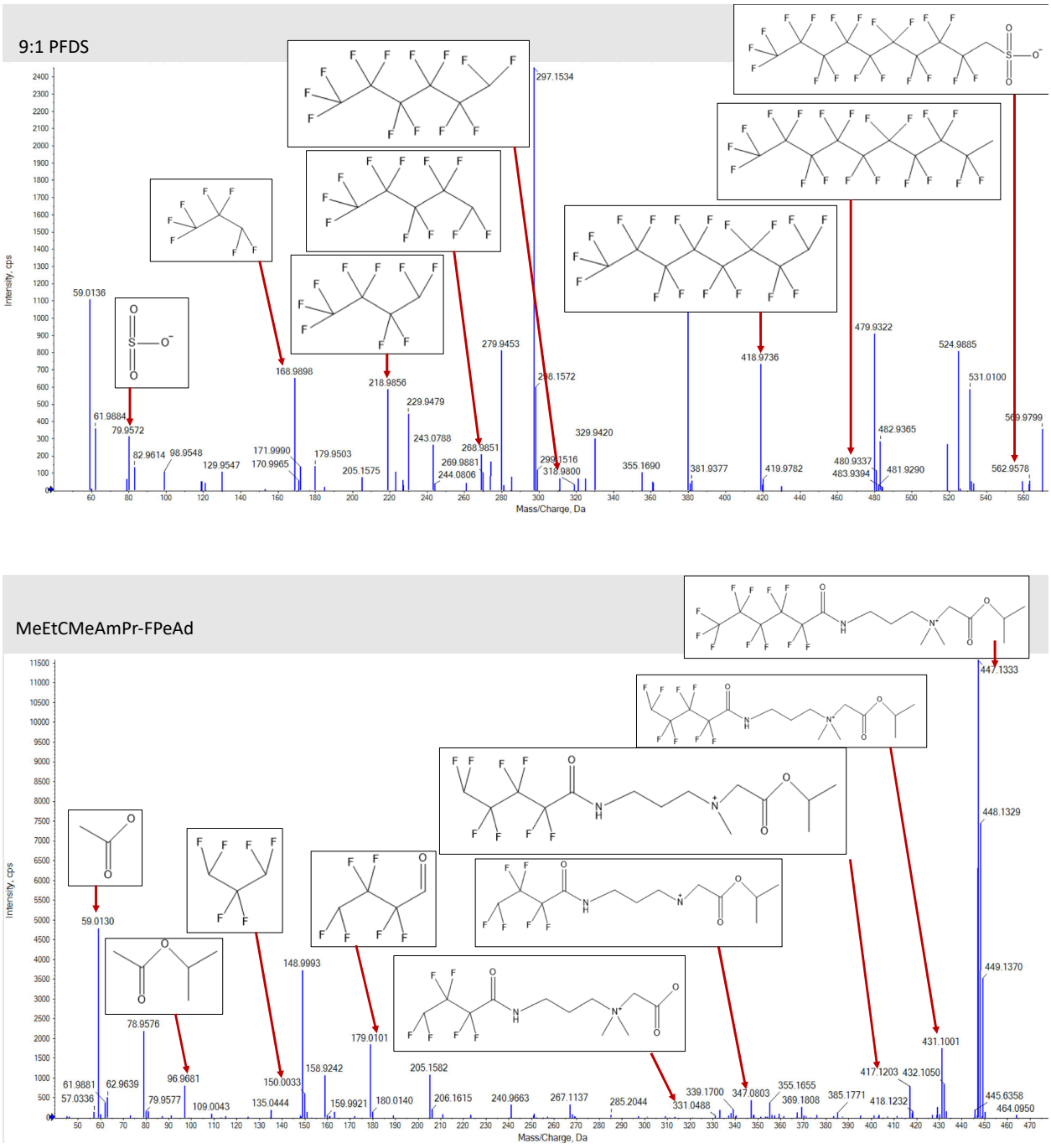

Figure 11. MS/MS spectra of compounds never been reported in AFFF or AFFF-impacted groundwater and soil. Concentrations estimated using SQ analysis were 0.2 (PFTrD-OS), 9.60 (8:2 UFTS), 0.3 (9:1 PFDS), and 11.15 (MeEtCMeAmPr-FPeAd) ng/g.

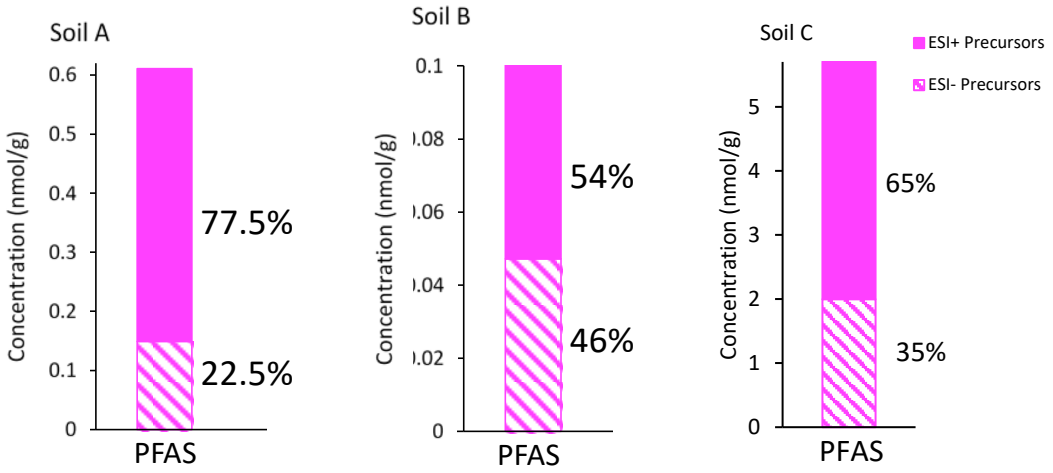

Figure 12. Distribution of total PFAS concentration detected in ESI- vs. ESI+ in Soils A, B and C. Fractions were estimated using semiquantitative (SQ) analysis and legend percentages are the fraction in relative to the total mass originally presented in soil. Note differences in Soil A and B y-axes.

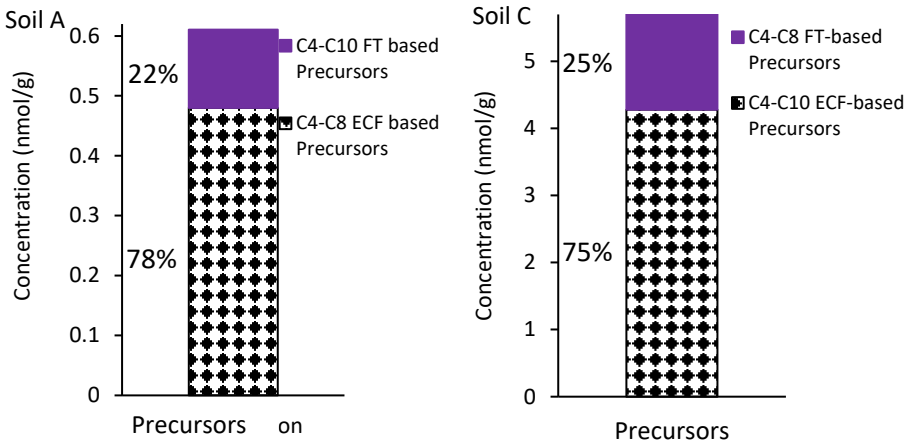

Figure 13. Concentration and distribution of suspect PFAS detected in Soil A based on chain length and manufacturing origin. Concentrations were calculated using semiquantitative analysis and legend percentages are the fraction in relative to the total mass originally presented in soil.

TASK 2: IN SITU OXIDATIVE TREATMENT IN BATCH TESTS

Batch Persulfate Oxidative Experiments.

PFAS Composition Following Pretreatment. Total PFAS composition and mass balances in batch reactors were evaluated immediately following persulfate pre-treatment. Persulfate concentrations were also measured and were found to be non-detect, indicating complete decomposition following the 6h treatment period. Total PFAS mass balances were calculated according to Equation 4 in order to determine mass balance in pre-treated and control reactors (**Table 9**). Mass balances for all $OH^{\cdot-}$ pretreated and control reactors were within the target range of 70-130% suggesting that there was not significant mineralization of PFAS at elevated pH or under any control conditions. This is consistent with previous studies of hydroxyl radical based oxidation of PFAS (Houtz and Sedlak, 2012; Bruton and Sedlak, 2017; D'Agostino and Mabury et al., 2014; Zhang et al., 2020; Liang and Su, 2009; Sun et al., 2016). As expected, mass balances in $SO_4^{\cdot-}$ pretreated reactors (e.g. no NaOH addition) was lower, particularly in Soil B. This is likely due to PFCA mineralization, volatilization, or breakdown of PFAS to short-chain products not included in our analysis (<C2), as documented in previous studies of $SO_4^{\cdot-}$ -based oxidation (Liang and Su, 2009; Qian et al., 2016; Park et al., 2016; Javed et al., 2020). Since our primary objective was to evaluate the ability of oxidative pre-treatment to mobilize (and not degrade) total PFAS, no attempt was made to close the mass balance on $SO_4^{\cdot-}$ pretreated reactors using fluoride analysis.

In all reactors, the PFSA mass balances were 82-107%, consistent with previous work that found no impact of persulfate treatment on PFSA concentrations (Park et al., 2016; Liang and Su, 2009; Qian et al., 2016). In $OH^{\cdot}$ pretreated reactors, the fraction of total PFAS present as PFCAs demonstrated the expected increase following pretreatment in both Soils A and B. The mass of PFCAs increased from 0.051 to 0.88 nmol in Soil A (**Figure 14**), with the largest increases occurring in concentrations of PFHxA (3600%), PFPeA (2600%), and PFOA (1500%, **Figure 15**). This suggests PFCA generation from conversion of either FT-based PFAS with 5-10 fluorinated carbons or ECF-based PFAS with 5-8 fluorinated carbons (Houtz and Sedlak, 2012). This is consistent with soil suspect screening data described above, that show precursors of this size account for approximately 77.4% of the total precursor mass (**Figure 13**). In Soil B, PFCAs increased from 0.84 to 1 nmol **(Figure 14**) and largest increases were observed for PFPeA (164%) and PFHxA (192%, **Figure 15**). Smaller increases relative to Soil A are attributable to the lower concentration of precursors. Increases in PFPeA and PFHxA are consistent with suspect screening data which show that all precursors present in Soil B are C6 and C8, FT-based precursors and C5 and C6 ECF-based precursors except MeFBSAA (**Table 8**). Finally, in $SO_4^{\cdot-}$ pretreated reactors, the PFCA mass either decreased (Soil B) or increased to a smaller degree than increases observed in $OH^{\cdot}$ pretreated reactors (Soil A) due to PFCA losses that may occur at low pH, as described above.

Table 9. Summary of total PFAS mass balance relative to controls in all reactor types immediately following pre-treatment.

Soil	$OH^{\cdot}$ pretreated (%)	$SO_4^{\cdot-}$ pretreated (%)	Control (%)	Heat control (%)	pH control (%)
Soil A	104.5±6.0	76±5.0	100±11.0	83± 3.0	101±8.0
Soil B	118± 11.0	68±7.0	100±8.0	99± 9.3	104± 10

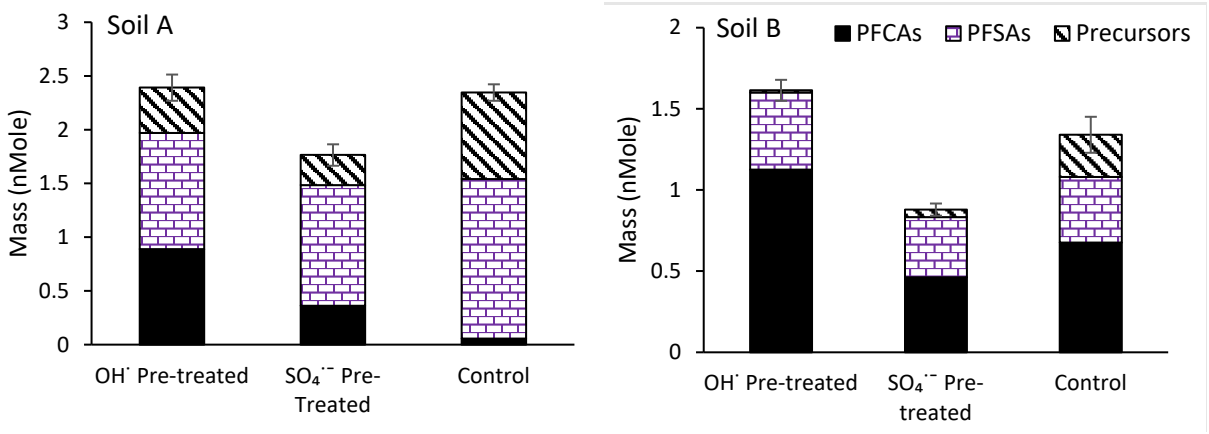

Figure 14. Composition of PFCAs, PFSAs, and precursors in $OH^{\cdot}$ pretreated, $SO_4^{\cdot-}$ pretreated, and control reactors in Soil A (left panel) and Soil B (right panel). Note differences in Soil A and B y-axes.

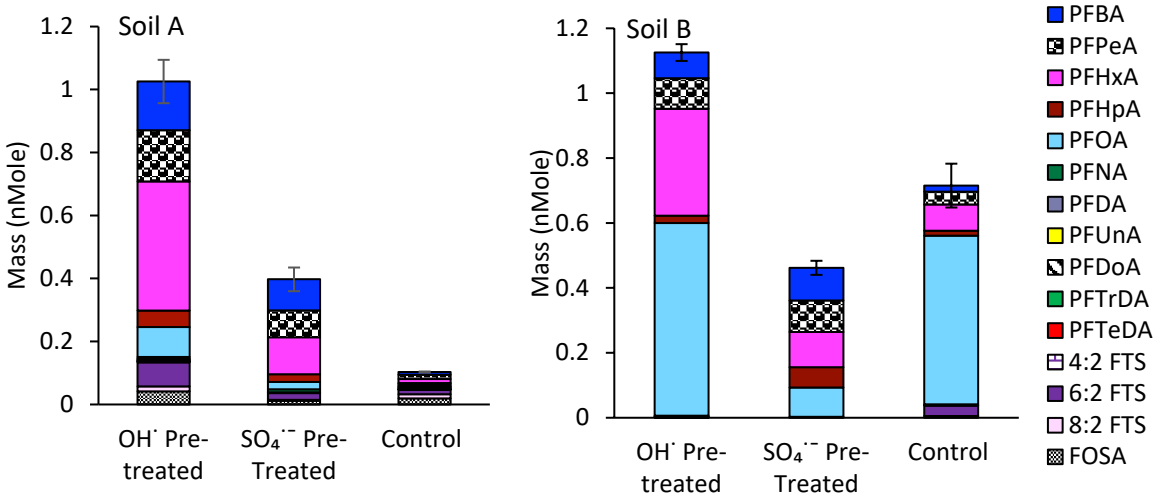

Figure 15. Mass of targeted PFAS present in $OH^{\cdot}$ pretreated, $SO_4^{\cdot-}$ pretreated, and control reactors in Soil A (left panel) and Soil B (right panel).

Immediately following oxidation, 5% (Soil B, $SO_4^{\cdot-}$ pretreated) to 52.5% of PFAA precursors (Soil A, $OH^{\cdot}$ pretreated) remained in soils. In some cases, individual precursor concentrations in Soil A increased following pre-treatment (e.g., 6:2 FTS and FOSA, see **Figure 15**), and this is due to partial transformation of PFAA precursors originally present in soil, as seen in other studies (Hori et al., 2010). For example, a number of PFAS that may potentially transform to 6:2 FTS during oxidation were identified in suspect screening (e.g., 6:2 FTSA-PrB, **Table 8**). A primary objective of this work is to transform PFAA precursors to terminal PFAAs in order to increase the overall mobility of the total PFAS mass in impacted soils. Although not all precursors were fully converted, anionic intermediate products such as 6:2 FTS are still likely to be more mobile than zwitterionic and cationic precursors in many soils. So even partial transformation may be of benefit for total PFAS recovery during remediation.

Impacts of Pre-treatment on PFAS Leaching. Following the 7-day leaching experiments, total PFAS leaching from soils in all reactors was 88% (Soil A heat control) to 116% (Soil A $OH^{\cdot}$ pre-treated),

illustrating that no losses of PFAS occurred during the leaching experiments (**Table 10**). Leaching experiments demonstrated rapid, initial desorption followed by slower desorption over the 7-day period in all reactors, and leaching was greatest in $OH^{\cdot}$ pre-treated reactors (**Figure 16**, **Table 11**). Over the 7-day period, 108% of total PFAS originally present in Soil A mobilized into the aqueous phase of pre-treated reactors as compared to heat controls (73%) and controls (62%). Aqueous PFAS fractions were validated by extracting PFAS remaining in soils on Day 7 of leaching experiments (**Figure 16**). Only 8% remained in pre-treated reactors as compared to 15%, and 27% in heated controls and controls, respectively, which validates the aqueous PFAS fractions. In the soil fraction, precursors dominated (55-68%) followed by PFSAs (31-44%, e.g., **Figure 17**). Minimal PFCAs were recovered in soils of all reactors.

Table 10. Summary of total PFAS mass balance relative to the mass of PFAS in control reactors immediately following pre-treatment.

Soil	$OH^{\cdot}$ pre-treated (%)	Control (%)	Heat control (%)
Soil A	116±5	89±5.0	88± 5.0
Soil B	111± 12	93±13	103± 12

Table 11. Summary of total PFAS recovery in the aqueous phase immediately following pre-treatment and following the end of the desorption experiments. Percentages were calculated as the mass recovered in the aqueous phase relative to the total mass originally present in soil.

Soil	Day 0 $OH^{\cdot}$ pre-treated (%)	Day 7 $OH^{\cdot}$ pre-treated (%)	Day 0 pH control (%)	Day 0 Control (%)	Day 7 Control (%)	Day 0 Heat control (%)	Day 7 Heat control (%)
Soil A	84 ± 6	108 ± 5	73 ± 2	55 ±2	62 ± 3	59 ± 2	73 ± 5
Soil B	118 ± 11	110 ± 12	107 ±5	70 ± 11	90 ± 13	98 ± 11	103 ± 12

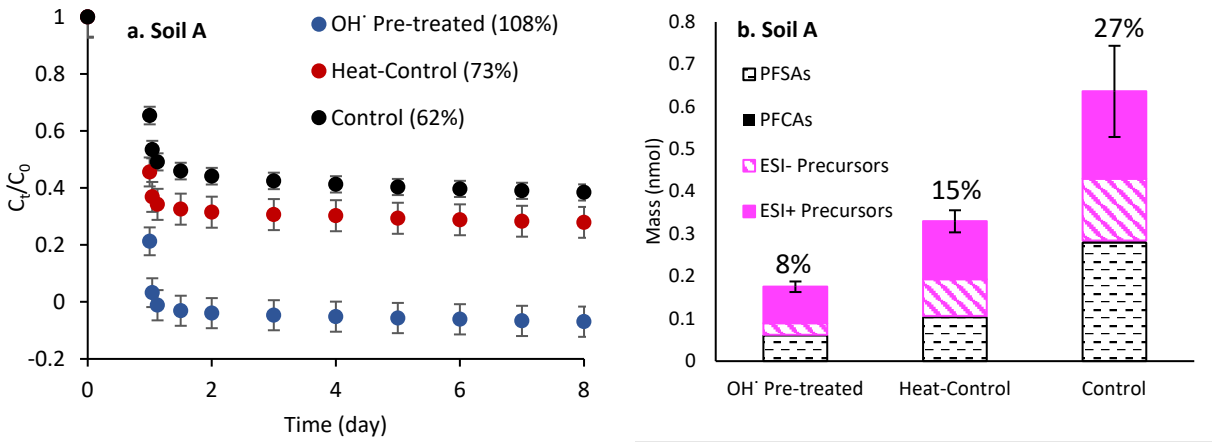

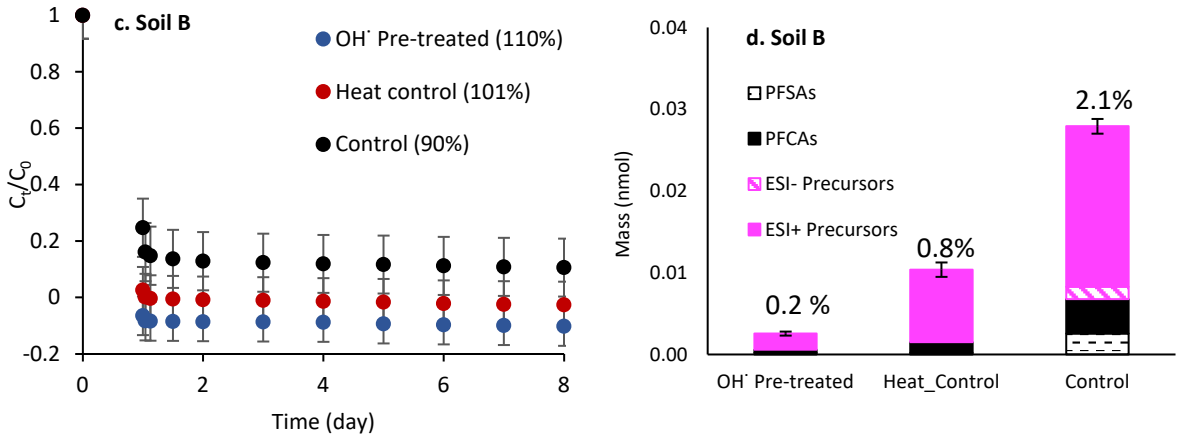

Figure 16. PFAS fraction remaining (Ct/C0) in Soils A and B over the duration of leaching experiments (a,c), and the PFAS composition in remaining in Soils A and B (b,d) following the experiments. Legend percentages (a,c) are the fraction of total mass originally in soil that were recovered in soils. Note the overlap in time 0 points for all three conditions (a,c) and differences in y-axes scales (b,d).

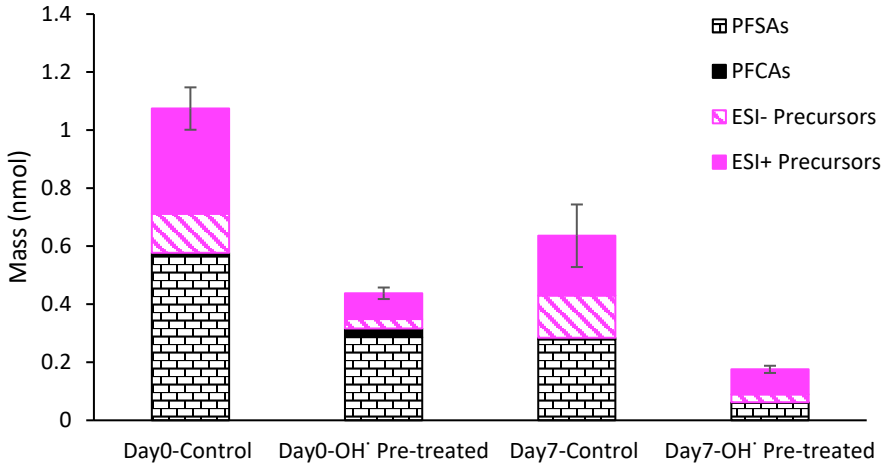

Figure 17. Mass of PFAS in Soil A immediately after treatment (Day0) and after completion of the desorption period (Day 7). Total precursors concentrations were calculated by using TOP assay and cationic and anionic precursors percentages were estimated using suspect PFAS peak areas. Bars are propagated standard errors of triplicate samples.

In Soil A, greater PFAS leaching in pre-treated reactors relative to controls supports the potential for persulfate oxidation to facilitate mobilization of total PFAS during remediation. Additionally, PFAS remaining in soils after leaching are dominated by precursors, which supports the hypothesis that increased leaching is attributable to conversion of stronger sorbing cationic and zwitterionic PFAS to more mobile and anionic PFAAs. Suspect screening further confirms this hypothesis. ESI+ PFAS dominate the remaining precursor fraction in soils of all reactor types immediately following pre-treatment, but concentrations are much lower in $OH^{\cdot}$ pre-treated reactors (**Figure 17**, **Table 12**). Importantly, the total concentration of precursors remaining in soil was not different between Days 0 and 7 when standard deviations were considered, suggesting that minimal additional desorption occurred over this period (**Figure 17**). In contrast, minimal PFCAs remained in soils of all reactors (i.e., near total desorption), and PFSAs desorbed over the entire 7-day period (**Figure 17**). Whereas PFAAs were

recoverable, strongly sorbing precursors were retained in soils, and this supports use of pre-treatment to enhance overall PFAS mobility. In contrast to Soil A, the impacts of persulfate pre-treatment on mobilization of total PFAS in Soil B were less clear. This is likely due to lower precursor concentrations and fraction of organic carbon (f_{oc}, 0.12% in Soil B and 2.2% in Soil A) in Soil B. Despite this, greater leaching in Soil B pre-treated reactors was observed (**Figure 16**, **Table 11**), and precursors remaining in Soil B were zwitterionic (**Table 13**).

Table 12. Precursors detected in Soil A suspect screening after Day 7 of desorption.

Compound name	Acronym	$OH^{\cdot}$ pre-treated Peak Area	Control Peak area	Charge state
ESI- suspect PFAS				
6:2 fluorotelomer sulfonate	6:2 FTS	NA	1.18E+05 ± 1.68E+04	-
8:2 fluorotelomer sulfonate	8:2 FTS	7.77E+04 ± 1.98E+04	4.45E+05 ± 2.94E+04	-
perfluorohexane sulfonamide	FHxSA	4.45E+04 ± 2.30E+03	1.55E+05 ± 2.56E+04	-
perfluorooctane sulfonamide	FOSA	1.66E+04 ± 2.85E+03	7.23E+04 ± 1.22E+04	-
N-dimethyl ammonio propyl perfluorohexane sulfonamide	AmPr-FHxSA	NA	1.02E+05 ± 1.93E+04	+/-
6:2 fluorotelomer sulfonyl propanoamido-dimethylethyl sulfonate	6:2 FTSO2PrAd-DiMeEtS	5.36E+04 ± 7.42E+02	5.14E+04 ± 1.71E+04	+/-
8:2 fluorotelomer sulfonyl propanoamido-dimethylethyl sulfonate	8:2 FTSO2PrAd-DiMeEtS	NA	1.92E+04 ± 2.70E+03	+/-
6:2 fluorotelomer sulfinyl propanamido dimethyl ethyl sulfonate	6:2 FTSO-PrAd-DiMePrS	2.12E+04 ± 1.15E+04	1.60E+04 ± 4.35E+03	+/-
8:2 fluorotelomer sulfinyl propanamido dimethyl ethyl sulfonate	8:2 FTSO-PrAd-DiMePrS	1.58E+04 ± 3.41E+03	2.36E+04 ± 1.16E+04	+/-
N-dihydroxybutyl dimethylammoniopropyl perfluoropropane sulfonamide	diOHBAmPr-FPrSA	1.22E+04 ± 1.06E+03	1.38E+04 ± 8.71E+02	+/-
ESI+ suspect PFAS				
N-methylethyl-carboxymethyl dimethyl ammonio propyl perfluoropentane amide	MeEtCMeAmPr-FPeAd	1.53E+06 ± 1.71E+05	1.71E+05 ±	+/-
N-Trimethylammoniopropyl perfluorohexane sulfonamide	TAmPr-FHxSA	1.11E+05 ± 8.57E+04	2.40E+05 ± 4.68E+04	+/-
N-Trimethylammoniopropyl perfluoroheptane sulfonamide	TAmPr-FHpSA	NA	5.36E+03 ± 1.33E+03	+/-
N-hydroxyethyldimethylammoniopropyl perfluoropentanesulfonamide	EtOH-AmPr-FPeSA	NA	5.18E+03 ± 1.12E+03	+/-
N-hydroxyethyldimethylammoniopropyl perfluorohexanesulfonamide	EtOH-AmPr-FHxSA	8.12E+04 ± 5.21E+04	2.22E+05 ± 3.90E+04	+/-
6:2 fluorotelomer sulfonamido propyl dimethyl amine	6:2 FTSAPr-DiMeAn	3.76E+04 ± 9.88E+03	3.51E+04 ± 6.36E+01	+

Compound name	Acronym	$OH^{\cdot}$ pre-treated Peak Area	Control Peak area	Charge state
N-hydroxyethyldimethylammoniopropyl perfluorohexanesulfonamidoethanol	EtOH-AmPr-FHxSA-EtOH	3.21E+04 ± 1.26E+04	2.24E+04 ± 5.82E+03	+/-
N-dimethyl ammonio propyl perfluorohexane sulfonamido propanoic acid	AmPr-FHxSA-PrA	NA	1.17E+04 ± 6.22E+02	+/-
N-methylethyl-carboxymethyl dimethyl ammonio propyl perfluoropentane amide	MeEtCMeAmPr-FPeAd	1.53E+06 ± 1.71E+05	1.49E+06 ± 1.08E+05	+/-
N-carboxyethyl dimethyl ammonio propyl perfluorobutane sulfonamido propanoic acid	CEtAmPr-FBSA-PrA	NA	2.41E+04 ± 4.13E+03	+/-
N-betaine propyl perfluoropentane amide	BPr-FPeAd	1.86E+04 ± 8.14E+03	1.00E+05 ± 1.37E+05	+
N-hydroxyethyl dimethylammoniohydroxypropyl perfluoropentanesulfonamide	EtOH-Am-OHPr-FPeSA	NA	1.00E+05 ± 2.35E+04	+/-
N-ethyl dimethyl ammonio propyl perfluoropropane N-ethyl sulfonamide	EtAmPr-FPr-N-EtSA	1.91E+04 ± 2.13E+03	1.87E+04 ± 1.87E+04	+

Not applicable (NA) indicated not detected in $OH^{\cdot}$ pre-treated reactors; anionic (-), cationic (+), zwitterionic (+/-)

Table 13. Precursors detected in Soil B suspect screening after Day 7 of desorption.

Compound name	Acronym	$OH^{\cdot}$ pre-treated Peak Area	Control Peak area	Charge state
ESI- suspect PFAS				
N-sulfo propyl dimethyl ammonio propyl perfluorohexane sulfonamide	SPrAmPr-FHxSA	NA	1.12E+05 ± 5.52E+03	+/-
ESI+ suspect PFAS				
N-betaine propyl perfluoropentane amide	BPr-FPeAd	2.79E+05 ± 1.22E+04	2.76E+05 ± 3.92E+04	+
N-methylethyl-carboxymethyl dimethyl ammonio propyl perfluoropentane amide	MeEtCMeAmPr-FPeAd	NA	1.16E+06 ± 4.67E+04	+/-
6:2 fluorotelomer sulfonyl propanoamido-dimethylethyl sulfonate	6:2 FTSO2PrAd-DiMeEtS	NA	2.24E+04 ± 5.07E+03	+/-

Not applicable (NA) indicated not detected in $OH^{\cdot}$ pre-treated reactors; anionic (-), cationic (+), zwitterionic (+/-)

Impacts of Organic Carbon. Prior studies have found that persulfate oxidation can impact the composition and concentrations of total organic carbon (TOC) in soils, and solution chemistry (e.g. pH) may lead to changes in concentrations of dissolved organic carbon (DOC) (Crownover et al., 2019; Weber et al., 1999; Cuypers et al., 2022). Studies have documented that f_{oc} is a key factor influencing PFAS sorption (Guelfo and Higgins, 2002; Tavakkoli et al., 2015; Li et al., 2018; Higgins and Luthy, 2007). Thus, it is important to understand how changes in the concentration, composition, or distribution of organic carbon following persulfate oxidation may impact total PFAS mobility in pre-treated systems. The mass balance of OC (soil TOC plus aqueous DOC) in all control reactors in Soil A (70-83%) and all reactors in Soil B (77-98%) was >70% of the total organic carbon (TOC) originally present in soils; however, $OH^{\cdot}$ and $SO_4^{\cdot-}$ pre-treatment led to degradation of 50% and 37% of the OC in Soil A (**Figure 18**). Total PFAS in Soil A accounted for ~0.03% of TOC demonstrating that even complete PFAS mineralization would not account for the loss of OC in pre-treated reactors. Additionally, representative data from previous site investigations (data not shown) suggest that <0.5% of Soil A TOC may be associated with co-contaminants. This indicates that TOC losses following persulfate oxidation were due to oxidation of soil organic carbon in Soil A pre-treated reactors. This is consistent with at least one prior study where persulfate treatment led to reductions in TOC in excess of those attributable to oxidation of AFFF components (Park et al., 2016). The decrease in soil f_{oc} following oxidation may lead to greater PFAS leaching in pre-treated soils due to a loss of sorption sites, which is further discussed below.

In both Soils A and B, DOC concentrations were higher in pH controls relative to other reactor types (**Figure 18**). Solubility of organic carbon is enhanced at higher pH (Cuypers et al., 2002). The pH of the pH-controls was 12, while other reactors ranged from pH 1.5-8, which likely explains higher DOC. Due to the affinity of many contaminants for organic matter, elevated levels of DOC in water can enhance the apparent solubility of contaminants leading to lower sorption and colloid-facilitated transport (You et al., 2010; Ryan et al., 1998). Colloid-facilitated transport of PFAS is not well-studied; however these results highlight an increase in available colloidal material under alkaline conditions. Trends in colloid-facilitated transport of PFAS are complex, since pH-dependent changes in DOC are coupled with pH-dependent sorption of PFAS (Barzen-Hanson et al., 2017; Higgins and Luthy, 2006; Cheng and Saiers, 2010). Colloid-facilitated transport is not likely to contribute to greater mobilization of total PFAS in pre-treated relative to control reactors (**Figure 16**) because DOC concentrations in pre-treated and heat controls in both Soils A and B were similar (**Figure 18**).

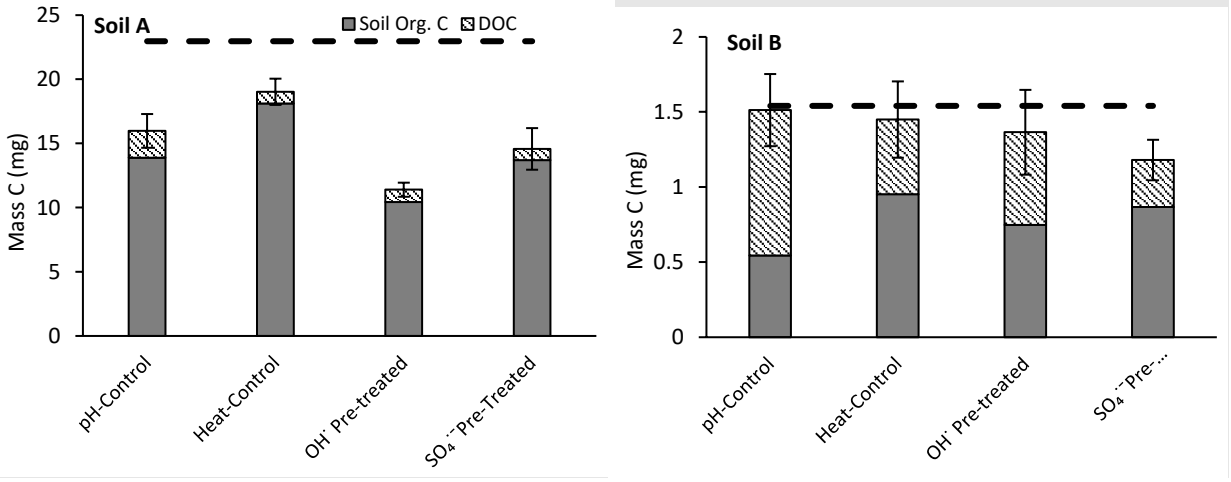

Figure 18. Distribution of organic carbon in Soils A and B organic carbon in pre-treated samples and controls. TOC line is the original OC in the reactor soils based on a foc of 2.2% (±0.03) in Soil A and 0.12% (±0.03) in Soil B.

The impacts of changes in OC composition and distribution in $OH^{\cdot}$ pretreated reactors were investigated using the following equation for the organic carbon-water distribution coefficient (K_{oc}), as seen in previous studies of the impacts of oxidation on OC (Guelfo et al., 2018; Mejia-Avendaño et al., 2020):

$$K_{oc} = \frac{C_s}{C_w f_{oc}}$$

where PFAS concentrations in soil (C_s) and water (C_w) were measured in reactors immediately after pre-treatment. Reactors may not have been at equilibrium, so these values of K_{oc} were used only for comparisons between experimental conditions. $OH^{\cdot}$ pre-treated, heat controls, and controls were all pH 7-8 following the pre-treatment period, so changes in K_{oc} should be attributable to other factors such as composition and amount of OC and/or inorganic ion concentration. The comparison of K_{oc} in the subsequent paragraph is limited to heat controls and pre-treated reactors because they were subjected to the same temperature conditions. Impacts of pH observed in pH control reactors are discussed in a subsequent section.

K_{oc} values of C5, C8 and C9 PFCAs in Soil A, C5-C9 PFCAs in Soil B, and C4-C7 PFSAs in both soils in $OH^{\cdot}$ pre-treated and control reactors were similar when standard deviations were considered (**Figure 19**, **Figure 20**) suggesting that oxidation of organic matter in pre-treated reactors did not change the relative affinity of these PFAAs to the remaining organic carbon. In Soil A, K_{oc} values of C10 and C11 PFCAs and C8 - C10 PFSAs were higher in pre-treated samples and the values of the C4, C6, and C7 PFCAs were lower (**Figure 19**). The same trends were observed for the C4 PFCA and C8 PFSA in Soil B (C10-C11 PFCAs and C9-C10 PFSAs were not detected, **Figure 20**). These trends may be attributable to changes in solution chemistry, competitive sorption (e.g., due to changes in PFAS composition), and/or the nature of the organic matter present (e.g., amorphous vs. condense) that may occur with oxidation. Though the relative affinity of some PFAAs for the remaining organic carbon in Soil A appears to have changed, loss of organic carbon in pre-treated reactors may have led to an overall reduction in the number of sites available for sorption. Because these effects occurred concurrently in the reactors, the existing dataset cannot be used to separately evaluate the impacts of both factors.

Effect of pH on PFAS Desorption. Prior studies have demonstrated that solution pH impacts PFAS sorption (Barzen-Hanson et al., 2017; Higgins and Luthy, 2006; Pan et al., 2012). The aqueous pH of reactors in the current study ranged from 1.5 ($SO_4^{\cdot-}$ pre-treated) to 12 (pH controls). The final pH of controls, heat controls, and $OH^{\cdot}$ pretreated reactors was 7-8; however, $OH^{\cdot}$-pretreated reactors were initially at pH ~12 and decreased to circumneutral by the end of the 6-hr oxidation period. $SO_4^{\cdot-}$ pretreated reactors began at circumneutral pH and were acidified over the course of the activation period. Following pre-treatment, all reactors were circumneutral through the 7-day leaching period because the aqueous phase was replaced daily with clean, deionized water. Although the alkaline period was only a short fraction of the experimental duration, pH controls were used to investigate potential impacts of alkaline pH on desorption.

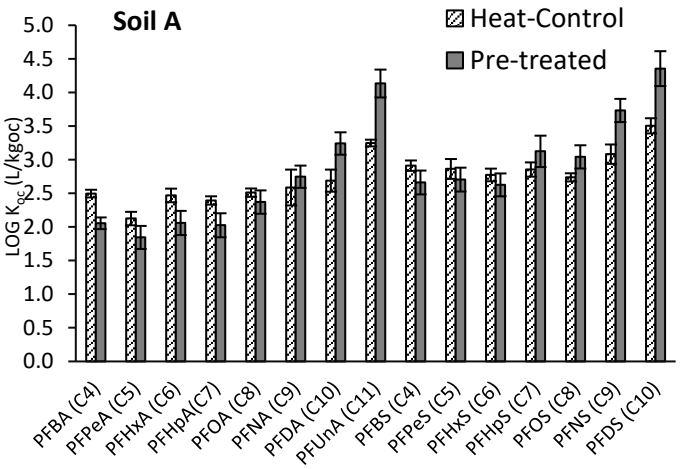

Figure 19. Log K_{oc} values of PFAAs in Soil A (reactor pH was 7-8 in both conditions). Numbers in parentheses indicate the total carbons in each PFAA.

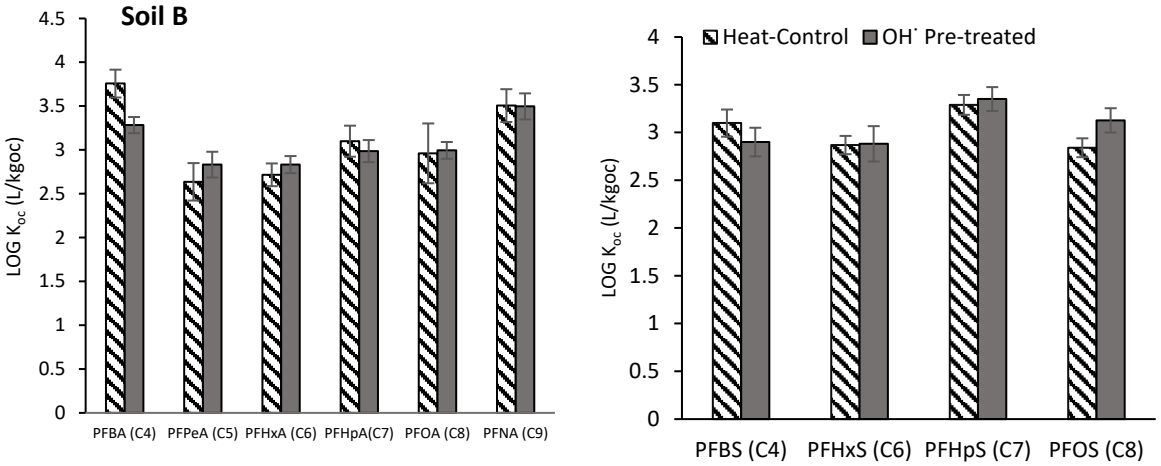

Figure 20. Log Koc values of PFAAs in Soil B. Numbers in parentheses indicate the total carbons in each PFAA. Note that pre-treated reactors were compared to heat controls to ensure that observed differences are due to oxidation and not due to impacts of temperature.

Comparison of the aqueous PFAS fraction in the pH controls to other experimental conditions, suggests that elevated pH may lead to increased mobilization. PFAS leaching in Soil A immediately following treatment was higher in pH controls (73%) relative to controls (55%). The greatest leaching occurred in $OH^{\cdot}$ pre-treated reactors (84%), so pH changes cannot fully explain mobilization. In Soil B, the aqueous PFAS fraction was also higher in pH controls (107%) vs. controls (70%). The aqueous fraction in $OH^{\cdot}$ pre-treated reactors (108%) was similar to that of the pH controls (107%), which suggests the potential for pH changes to account for all of the increased total PFAS mobilization in Soil B. However, it is notable that composition of these aqueous fractions (PFCAs, PFSAs, precursors) was different at various pH due to pre-treatment, and Soil B was comprised of a higher initial fraction of PFAAs relative to Soil A. Data from PFCAs, PFSAs, and precursors were separately investigated to further elucidate the impacts of pH on PFAS mobility.

In Soil A, the aqueous fractions of PFSAs and precursors increased with increasing pH, and it was nearly 100% for PFCAs across the entire pH range (**Figure 21**). The mass of PFSAs remained unaltered in magnitude and composition across all experimental types since they are not impacted by oxidation. The greatest aqueous fraction of PFSAs occurred in pH controls (75%). The aqueous fraction of PFSAs in the $OH^{\cdot}$ pretreated reactors (54%) was ~10% lower than the aqueous fraction in controls and heat controls (63-64%). This suggests that the brief alkaline period in $OH^{\cdot}$-pretreated reactors did not increase PFSA desorption or that the increases in long-chain PFSA K_{oc} values in $OH^{\cdot}$ pretreated reactors (**Figure 19**) were the dominant effect. PFSA mobilization was lowest in $SO_4^{\cdot-}$ pretreated reactors (i.e., lowest pH). Total precursor composition and masses were constant in all control types but altered in pre-treated reactors. In controls, the aqueous precursor fraction increased from 38-45% at pH 7 (controls and heat controls, respectively) to 69% at pH 12 (pH controls). Aqueous phase data demonstrate that the increased aqueous fraction of precursors is due to increased desorption of anionic/neutral PFAS (**Figure C9**). $OH^{\cdot}$ pretreated reactors had a similar aqueous precursor fraction (72%) as pH controls, despite having a lower pH similar to controls and heat controls. This could be attributable to the brief alkaline period during pre-treatment or to conversion of the original precursors present to more mobile intermediates. The lowest aqueous precursor fraction occurred at pH 1.5 in $SO_4^{\cdot-}$ pretreated reactors (**Figure 21**), but these reactors also had the lowest fraction of precursors remaining (65% of the original precursor mass was degraded). As noted, PFCAs exhibited aqueous fractions greater than 80% across the entire pH range (**Figure 21**), demonstrating the overall mobility of PFCAs and supporting precursor to PFCA conversion as a tool for total PFAS mobilization.

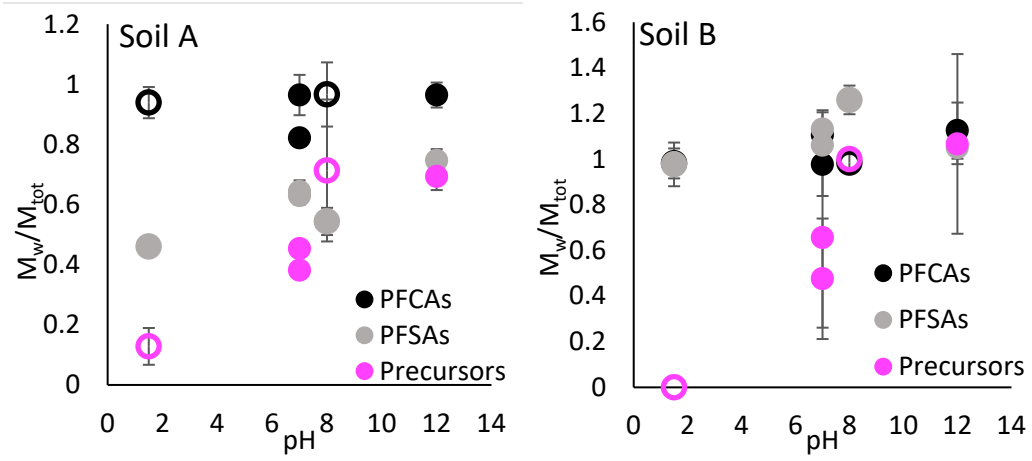

Figure 21. The fraction (M_w/M_{tot}) of PFCAs, PFSAs, and precursors recovered in the aqueous phase at pH 1.5 ($SO_4^{\cdot-}$ pre-treated), 7 (controls and heat controls), 8 ($OH^{\cdot}$ pretreated) and 12 (pH control), where M_{tot} is the total mass (soil + water) of each class in the reactor. Precursors refer to precursors concentrations in reactor aqueous phase and calculated by using TOP assay. Open symbols denote data from persulfate treated reactors where composition and total mass of PFAS within the class changed relative to the original soil due to oxidative pre-treatment.

In Soil B, aqueous fractions of both PFCAs and PFSAs were approximately 100% across the entire pH range (**Figure 21**). Precursor trends in controls were similar to those seen in Soil A. The aqueous precursor fraction increased from 48%-66% at pH 7 (controls and heat controls, respectively) to approximately 100% at pH 12 (pH controls). Aqueous data demonstrate that this increase was dominated by increased desorption of anionic/neutral PFAS although the mass of cationic/zwitterionic PFAS in the aqueous phase also increased (**Figure 22**). As seen in Soil A, $OH^{\cdot}$ pretreated reactors had a similar aqueous precursor fraction as pH controls. No precursors were detectable in suspect screening data for the aqueous phase of Soil B $SO_4^{\cdot-}$ pretreated reactors.

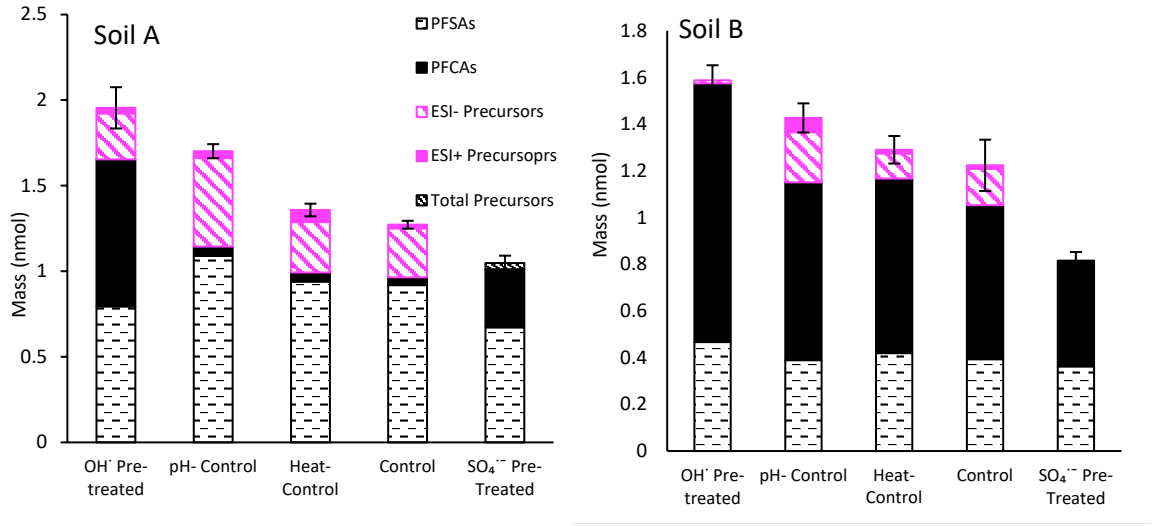

Figure 22. Soil A and B aqueous phase PFAS composition after persulfate treatment (Day 0). Total precursors concentrations were calculated by using TOP assay and ESI- and ESI+ precursors fractions were estimated using suspect screening results. No precursors were detectable during suspect screening of the aqueous phase of $SO_4^{\cdot-}$pretreated reactors, so ESI- precursor and ESI+ precursor fractions could not be determined. The concentration of precursors in the aqueous phase of $SO_4^{\cdot-}$pretreated was determined by TOP and was shown in the figure. No precursors were recovered in Soil B $SO_4^{\cdot-}$pretreated reactors. Reactor pH values were as follows: 12 (pH control), 7 (Controls and Heat Controls), 8 ($OH^{\cdot}$-pretreated reactors), and 1.5 ($SO_4^{\cdot-}$ pre-treated).

Previous studies of PFAS sorption at varying pH can help elucidate results of the current study. Sorption of PFAAs and some anionic precursors (e.g. FTSs) increases with decreasing pH (Barzen-Hanson et al., 2017; Higgins and Luthy, 2006; Pan et al., 2012), which leads to higher potential for mobility of these PFAS under alkaline conditions. This is consistent with observed PFSA (Soil A) and precursor (Soil A and B) trends discussed above, and is likely attributable to increased electrostatic repulsion between anionic PFAS and increasingly negative organic matter surfaces as pH increases (Barzen-Hanson et al., 2017; Higgins and Luthy, 2006). Because DOC increases are also observed at elevated pH, it is also possible that sorption of PFSAs and precursors onto colloidal material contributes to increases in aqueous concentrations observed at pH 12. In prior studies, sorption of PFCAs also increases with decreased pH (Higgins and Luthy, 2006), but that trend was not evident in PFCA data in the current work. However, at least one prior study of PFAA sorption with pH utilized a sediment with an f_{oc} of 0.0434% compared to 0.001-0.002% in the current study (Higgins and Luthy, 2006). Results presented here demonstrate that weak overall sorption of PFCAs in Soil A, and both PFCAs and PFSAs in Soil B (which has lower

organic carbon), leads to high mobility regardless of pH. This suggests that aqueous pH may not play a meaningful role in determining PFAA mobility (especially PFCAs) at sites where f_{oc} is low.

Trends associated with cationic and zwitterionic PFAS are potentially more complex. In addition to changes in the charge of the surface, there could be changes to the charge of the PFAS, particularly at very high pH (e.g., > 9). For example, PFAS with sulfonamide and amine functionality (e.g. fluorotelomer sulfonamido propyl dimethyl amines) will be predominantly cationic at pH < ~9, neutral at pH ~9-10.5, and predominantly anionic at pH > ~10.5 (Barzen-Hanson et al., 2017). Despite these potential complexities, mobilization of cationic and zwitterionic PFAS was similar (and relatively low) at all pH levels. Additionally, precursors remaining in soil (**Figure 16**) were dominated by cationic and anionic PFAS under all conditions. This suggests that mobility of PFAS with positive moieties may be low under a wide range of pH conditions, although studies in additional soil types are warranted before making additional conclusions.

Batch Oxygen Sparging Oxidative Experiments in Soils.*Soil PFAS Characteristics.* Soils A and C used for these experiments contained total PFAS concentrations of 1.94 nmol/g and 8.49 nmol/g, respectively. Soil A contained 1.28 nmol/g (66%) PFSAs, 0.05 nmol/g (2.5%) PFCAs, and 0.61 nmol/g (31.4 %) precursors. In Soil A, 78% of precursors were C4-C8 ECF- based PFAS, and 22% were C4-C10 FT based PFAS. In Soil A, 77.55% of precursors detected in ESI+. Soil C contained 2.71 nmol/g (32%) PFSAs, 0.08 nmol/g (1%) PFCAs, and 5.7 nmol/g (67%) precursors. Moreover, 75% of precursors in Soil C were C4-C10 ECF- based and the rest were C4-C8 FT based PFAS. In Soil C, 65% of precursors were detected in ESI+ and 35% were ESI- precursors.

Batch Experiment Results. Batch reactors prepared using Soil A were operated for 176 days. Results of aqueous phase targeted analysis showed faster generation of terminal PFAAs in O_2-sparged reactors relative to controls (**Figure 23 and 24**). There was also rapid generation and subsequent decrease of the precursors captured during targeted analysis relative to controls (i.e., 6:2 FTS and FOSA, **Figure 25**). Notably, these precursors are documented intermediate transformation products (Harding-Marjanovic et al., 2015; Liu and Mejia Avendaño, 2013). It is possible that mixing in sparged reactors contributed to concentration increases via more rapid desorption, but it is also likely that these trends attributable to faster degradation of precursors not captured in targeted analysis. One sparged and one control reactor were sacrificed on Days 69, and 107, analyzed and used to determine PFAS composition and recovery. Day 69 reactors exhibited faster generation of 6:2 FTS in sparged reactors (57% increase) vs control (20% increase). 6:2 FTS can be intermediate biotransformation of precursors such as 6:2 fluorotelomer sulfonyl propanoamido-dimethylethyl sulfonate (6:2 FTSO2PrAd-DiMeEtS) and then can be biotransformed to 5:3 FTCA and C4-C6 PFCAs (Harding-Marjanovic et al., 2015). Between day 69 and 107 6:2 FTS mass decreased in sparged reactors (45%) and increased in control reactors (64%). FOSA mass, however, was not changed on day 69 and exhibited minimal generation (12-29%) in both controls and sparged reactors.

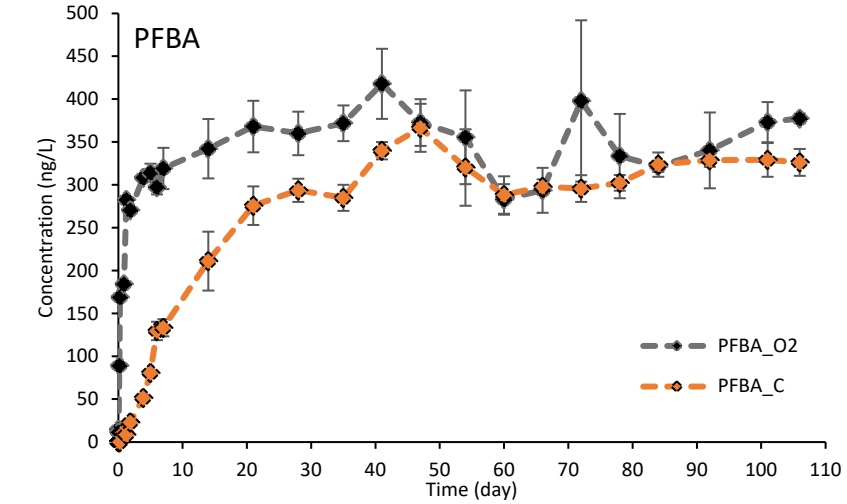
PFBA
Concentration (ng/L)
Time (day)
PFBA_O2
PFBA_C

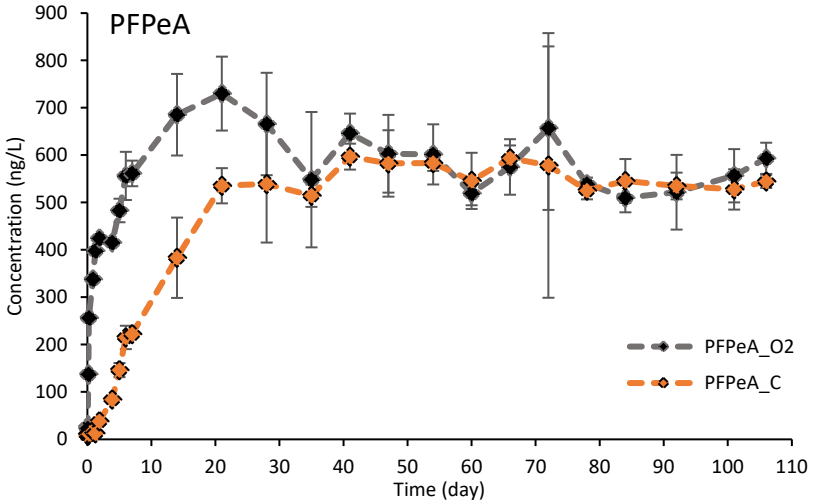
PFPeA
Concentration (ng/L)
Time (day)
PFPeA_O2
PFPeA_C

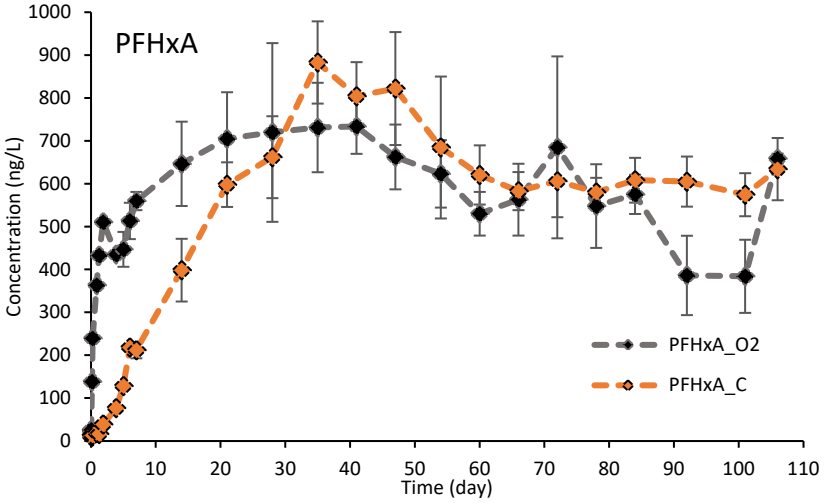
PFHxA
Concentration (ng/L)
Time (day)
PFHxA_O2
PFHxA_C

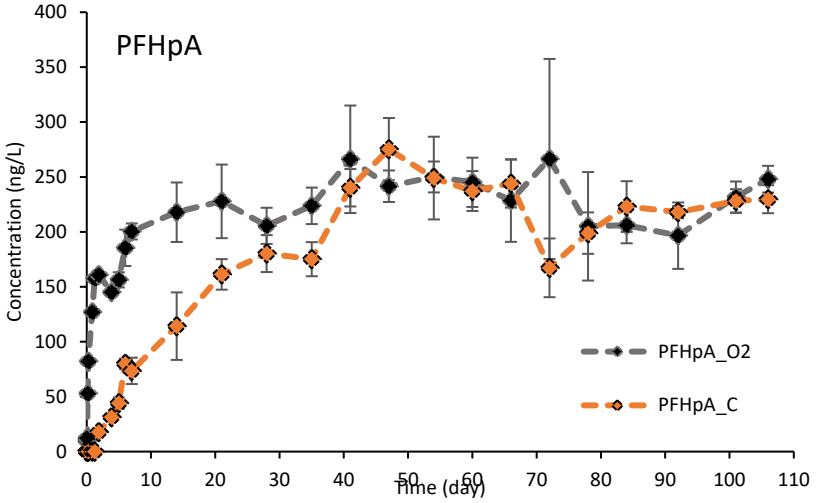
PFHpA
Concentration (ng/L)
Time (day)
PFHpA_O2
PFHpA_C

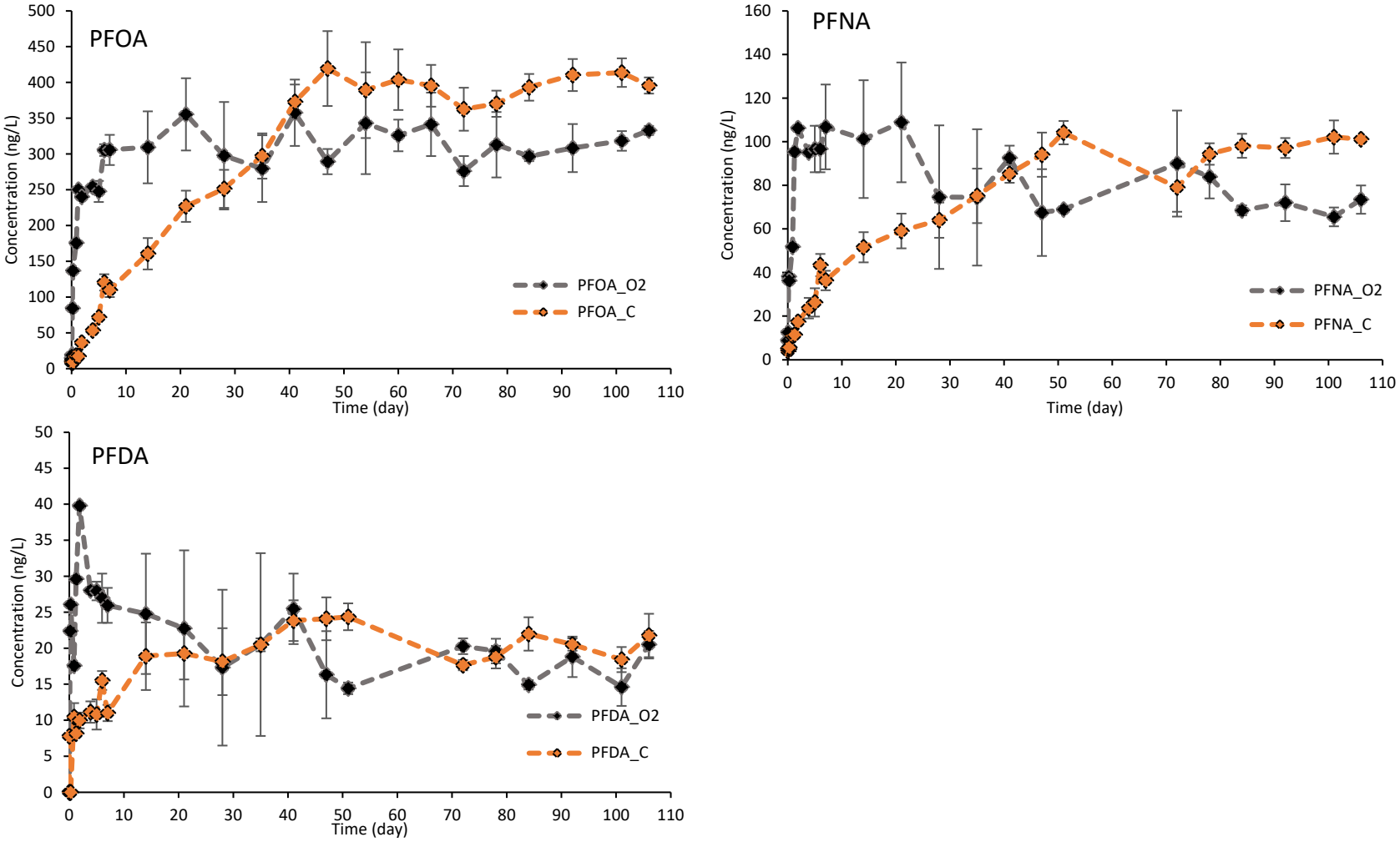

Figure 23. Concentrations of C4 (PFBA)-C10 (PFDA) PFCA in the aqueous phase of sparged (O2) and control (C) batch reactors through Day 107. Note PFNA and PFDA data were lost through Day 54-69 because of retention time shift.

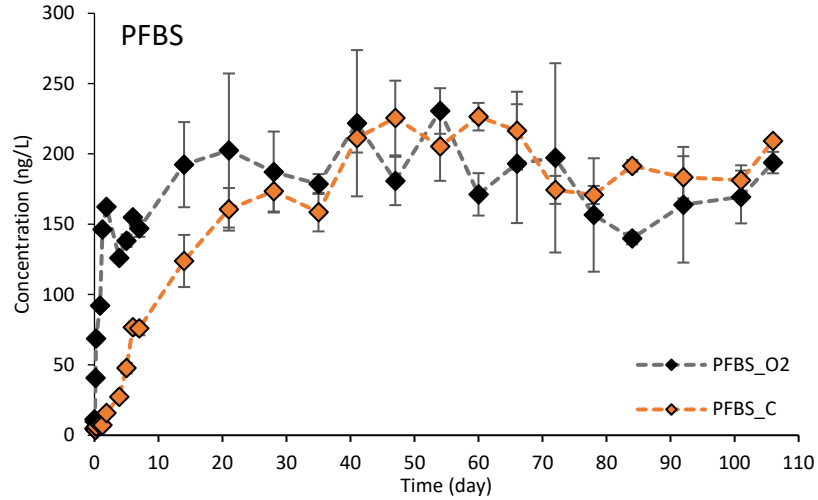
PFBS
Concentration (ng/L)
Time (day)
PFBS_O2
PFBS_C

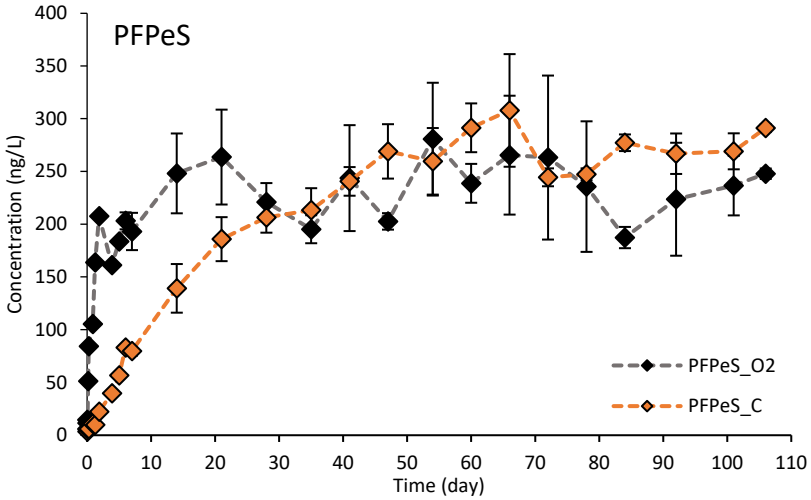
PFPeS
Concentration (ng/L)
Time (day)
PFPeS_O2
PFPeS_C

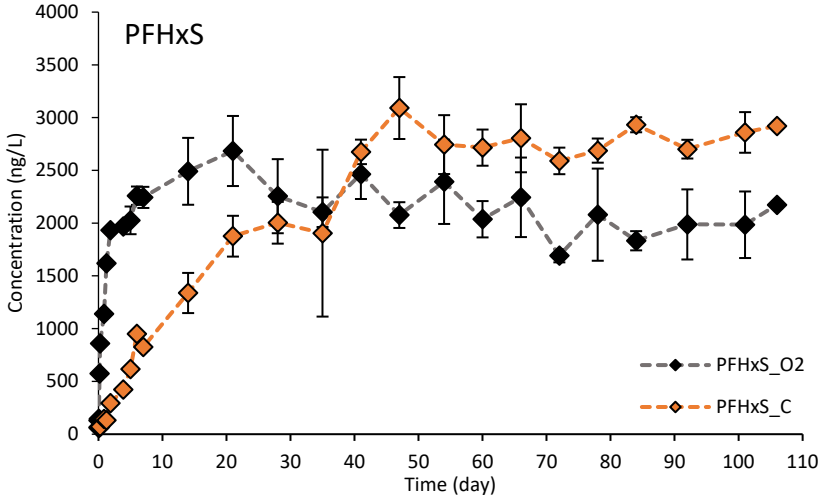
PFHxS
Concentration (ng/L)
Time (day)
PFHxS_O2
PFHxS_C

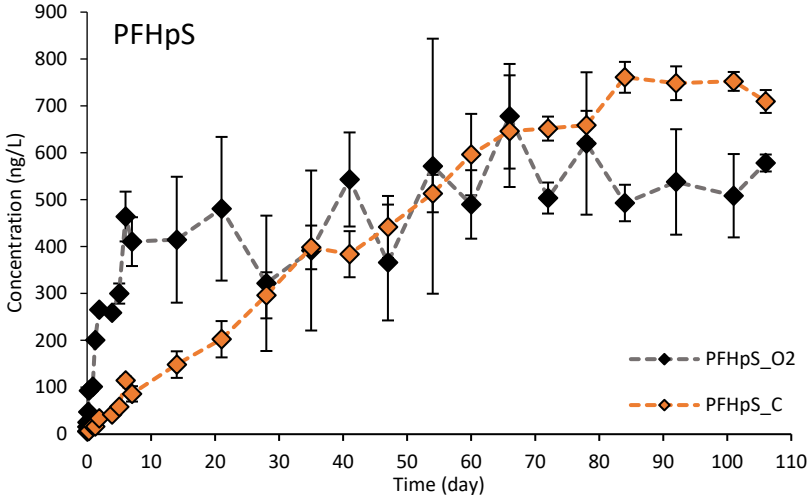
PFHpS
Concentration (ng/L)
Time (day)
PFHpS_O2
PFHpS_C

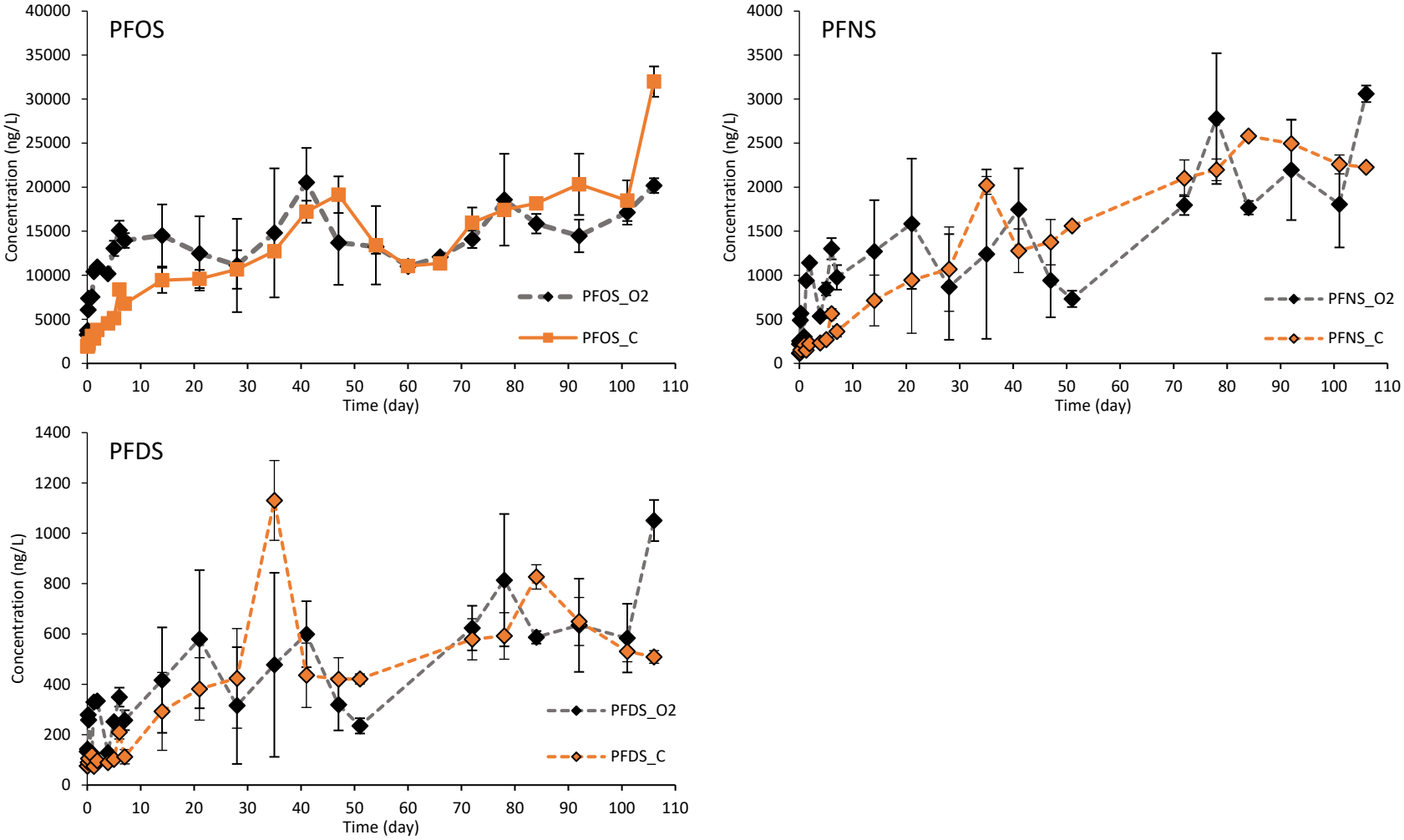

Figure 24. Concentrations of C4 (PFBS)-C10 (PFDS) PFSA in the aqueous phase of sparged (O2) and control (C) batch reactors through Day 107. Note PFNS and PFDS data were lost through Day 54-69 because of retention time shift.

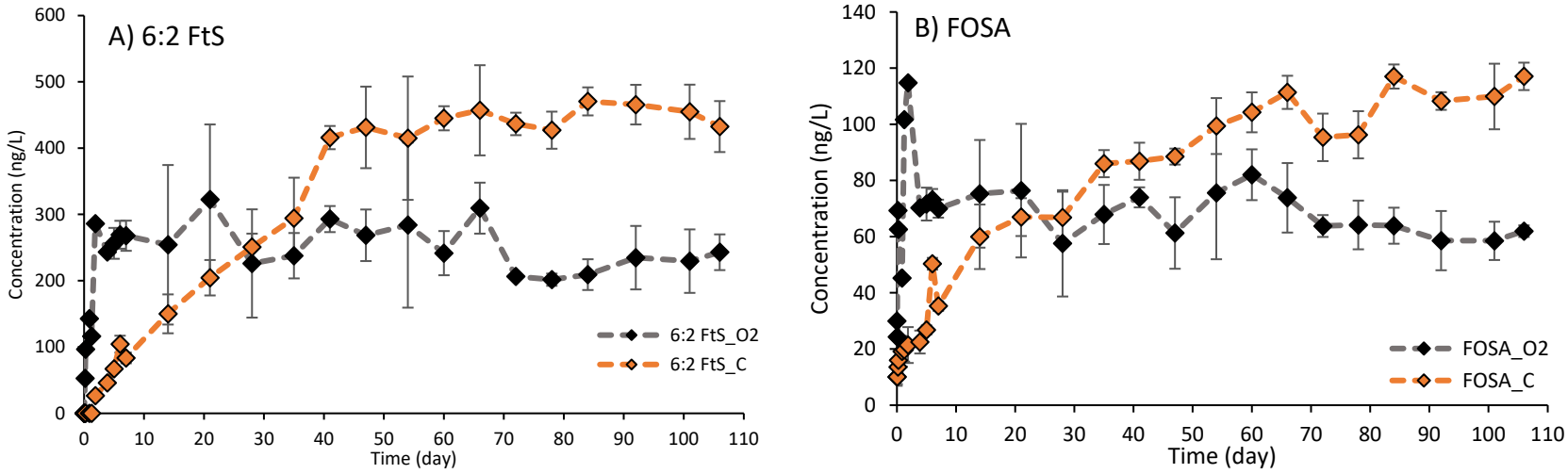

Figure 25. Concentrations 6:2 FTS (Panel A), and FOSA (Panel B) in the aqueous phase of sparged (O2) and control (C) batch reactors through Day 107. Note that 6:2 FTS is an intermediate transformation product and fluorotelomer (FT)-based C4-C6 PFCAs precursor and FOSA is an intermediate transformation product and electrochemical electrochemical fluorination (ECF)-based PFOS precursor.

Suspect screening of the aqueous samples was used to further elucidate trends observed in targeted data by providing data for a large suite of PFAS, including precursors, for which analytical standards were not available. Based on previous studies on PFAS biotransformation, parent precursors originally detected in Soil A were selected, then the data set was searched for additional PFAS that are known or hypothesized to represent intermediate and terminal PFAS during transformation of those precursors. Data showed in Soil A reactors, based on structurally similar PFAS (Kim et al., 2014; Mejia Avendaño and Liu, 2015), it is possible that N-oxide dimethyl ammoniopropyl-perfluorohexane sulfonamide (OAmPr-FHxSA) converts to perfluorohexane sulfonamido acetic acid (FHxSAA), and the transformation pathway to terminal PFHxS after the formation of FHxSAA is documented (Kim et al., 2014; Mejia Avendaño and Liu, 2015). Notably, OAmPr-FHxSA was not present in the original Soil A, and represents an intermediate product that appeared on Day 6 in sparged reactors and not until Day 20 in controls (**Figure 26**). This suggests that O_2-sparging accelerated generation of this compound. Faster degradation of some intermediates was also observed in O_2-sparged reactors. For example, perfluorohexane sulfinate (FHxSi) was not detected in sparged reactors after Day 28 but was still detected in control reactors at Day 107 (**Figure 26**). Reactors aqueous phase suspect screening data was processed for FT-based and other ECF-based precursors, however no other example could be found.

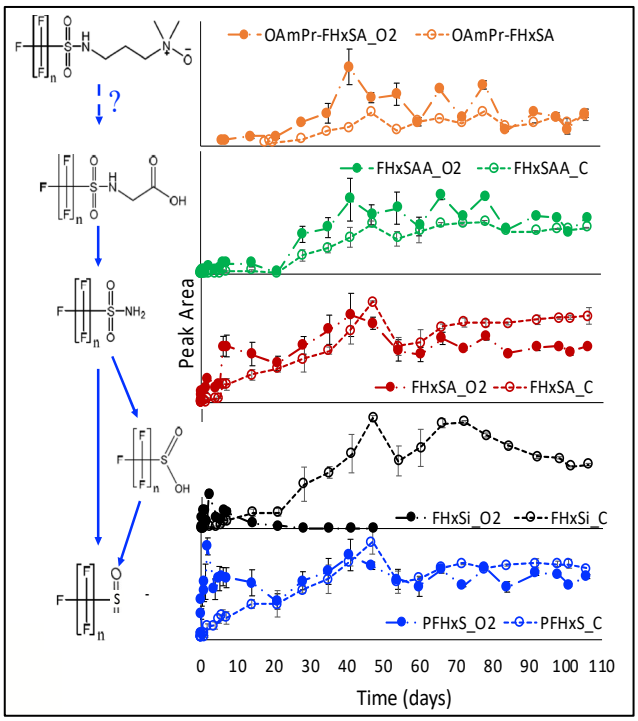

Figure 26. A subset of intermediate ECF-based precursors detected in sparged (O2) and control (C) reactors using suspect screening. Y-axes are peak areas (i.e., a proxy for concentration). OAmPr-FHxSA transformation pathways are not documented; the pathway is hypothesized based on similar PFAS (Shojaei et al., 2021; Liu and Mejia Avendaño, 2013).

Results of sacrificed reactors on Days 69, and 107 were used to determine total PFAS composition and recovery. Total PFAS recoveries on Days 69 and 107 were 80-98%, which were within the target range of 70-130% considered to be full recovery (**Table E5**). Although considered full recovery, mass balances in Day 107 sparged reactors (80%) were lower than that of control reactors (97%). This may be attributable to analytical and/or experimental variability; however, it is also possible that sparging enhanced the air-water partitioning of semi-volatile PFAS (e.g., fluorotelomer alcohols, FTOHs). Analysis of semi-volatile PFAS would require an alternate analytical method (e.g., gas chromatographic techniques), which was beyond the scope of this work, but these results suggest it would merit further investigation in future work.

Overall, trends observed in individual PFAS, and bulk analysis of sacrificial reactors demonstrated early accelerated precursor transformation and PFAA generation in O_2-sparged reactors. Generation of PFSAs (8-10% increase) was minimal and similar in both controls and sparged reactors. Precursors, however, exhibited enhanced degradation in O_2-sparged reactors (**Figure 27**). In day 69 O_2-reactors, precursors decreased 41% vs. 28% in controls and exhibited an overall decrease of 51% in O_2-sparged reactors by day 107 vs. 45% in controls. Between days 69 and 107, additional decreases in precursors were attributable to loss in the aqueous phase. Soil concentrations remained relatively unchanged, which suggests that there is a fraction of precursors in soil that are less accessible for transformation during sparging.

In addition to enhanced precursor loss, day 69 reactors exhibited enhanced PFCA generation (31-60% increase) in sparged reactors vs. controls (**Table 14, Figure 27**). In prior work, FT-based precursor biodegradation to PFCAs was faster than ECF-based precursor biotransformation to PFSAs (Liu and Mejia Avendaño, 2013, Nickerson et al., 2021). So, rapid degradation of FT-based precursors via biotransformation may explain bigger increases in PFCAs in comparison with PFSAs. Studies have shown that ECF-based precursors primarily generate PFSAs, although some generation of PFCAs has been documented (Liu and Mejia Avendaño, 2013; Lange, 2000). It is also possible that transformation occurred via O_2-induced increases in reactive oxygen species (ROS) and oxidation of precursors, which would generate PFCAs and not PFSAs (Plumlee et al., 2009). Early accelerated precursor transformation and PFCA generation support the hypothesis that O_2-sparging will enhance transformation to intermediate transformation products and more mobile PFAAs relative to ambient conditions. As discussed in prior work using persulfate oxidation (Shojaei et al., 2021), conversion of precursors to terminal PFAAs can enhance PFAS recovery from impacted soils.

Table 14. PFSAs, PFCAs, precursors, and total PFAS recovery in sacrificed sparged and control rectors on Days 69 and 107. All values are calculated relative to original concentrations in soil.

Day-Reactor	PFSAs	PFCAs	Precursors	Total PFAS
Day 69-Sparged	108±4%	160±5%	59±4%	93±3%
Day 69-Control	110±5%	131±4%	72±5%	98±4%
Day 107-Sparged	94±7%	145±5%	49±3%	80±5%
Day 107-Control	116±8%	153±5%	55±2%	97±5%

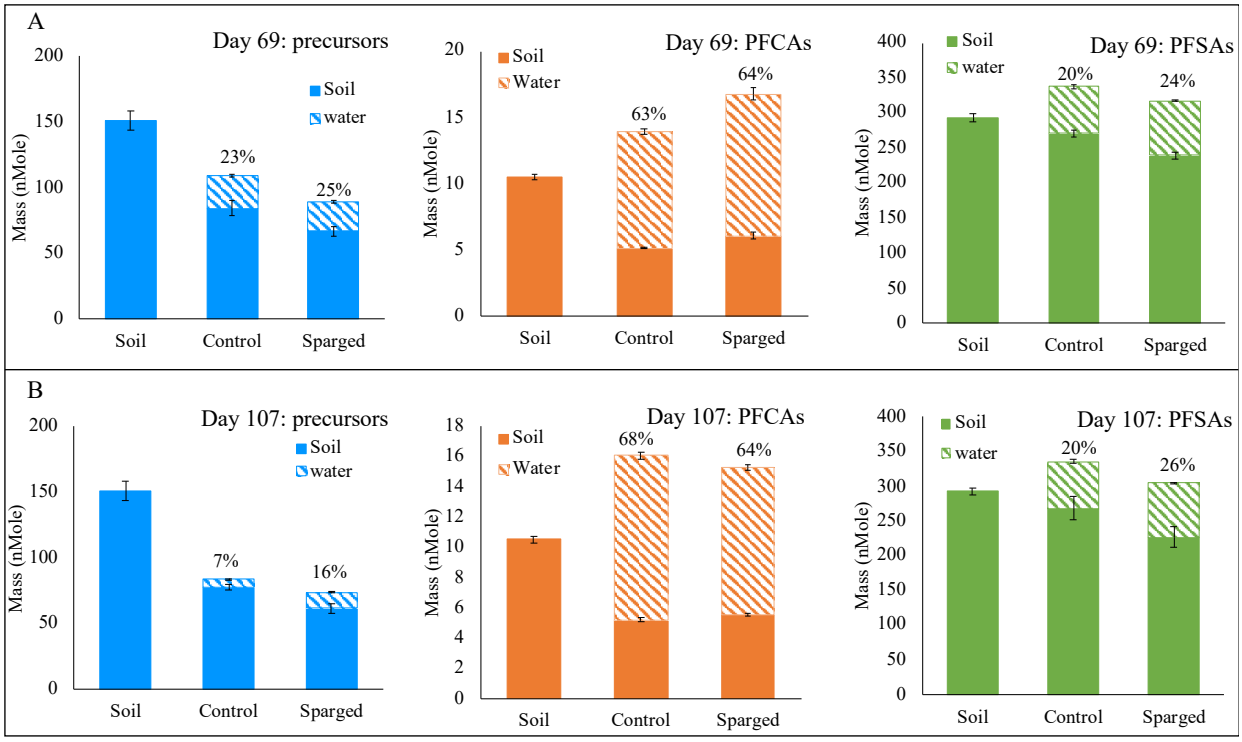

Figure 27. Total molar mass of precursors, PFCAs, and PFSAs measured in Soil (i.e., original composition) and soil and water phases in sparged and control reactors on Day 69 (panel A) and Day 107 (panel B). Percentages represent the fraction present in the aqueous phase.

TASK 3: IN SITU OXIDATIVE TREATMENT IN TRANSPORT CELLS

Transport Cell Column Persulfate Oxidative Experiments

PFAS Mass Balance. Mass balance results (Eq 4) showed total PFAS recoveries of all Soil C columns were in the range of 80-120% (**Table 15, Figure 28**). Soil A pHC and AHA columns clogged after 2 pore volumes. This was attributable to mobilization of soil organic carbon (OC) that occurs at alkaline pH (Weber et al., 1999; Cuypers et al., 2002), which then blocked the effluent end of the column (**Figure 29**). Total PFAS recovery in the remaining Soil A columns (HA, HC, and AC), which were operated for the full experimental duration, were in the range of 80-150% (**Table 15, Figure 28**).

Table 15. Summary of PFAS mass balance relative to pre-elution soils in all column types.

Soil	Ambient Control (%)	Heat Control (%)	pH Control (%)	Heat Activated (%)	Alkaline Heat Activated (%)
Soil C					
PFCAs	162	123	201	510	455
PFSAs	106	125	116	117	103
Precursors	62	74	117	72	68
Total	82	91	119	93	83
Soil A					

PFCAs	159	109	NA*	92	NA
PFSAs	92	160	NA	97	NA
Precursors	96	117	NA	58	NA
Total	95	146	NA	83	NA

*NA= Not Applicable

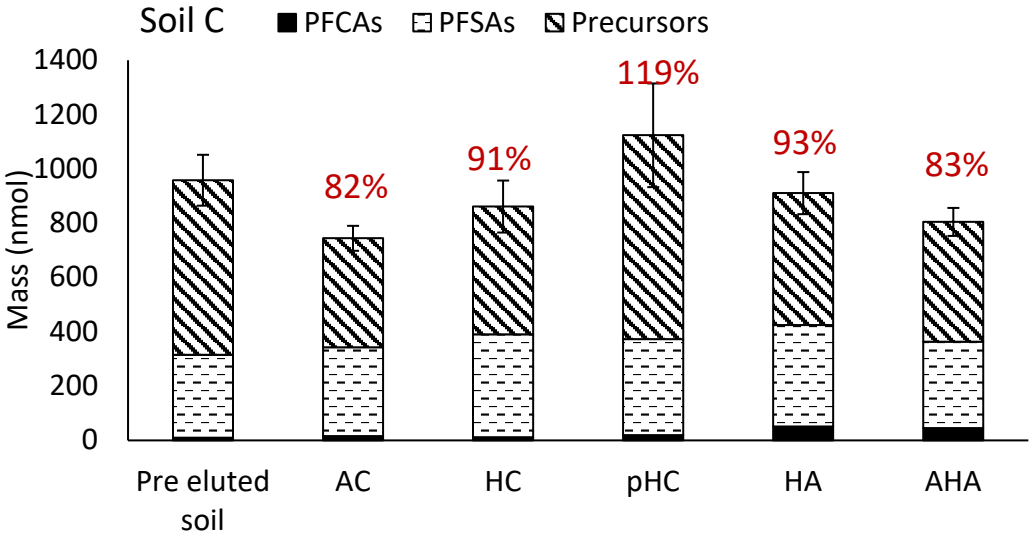

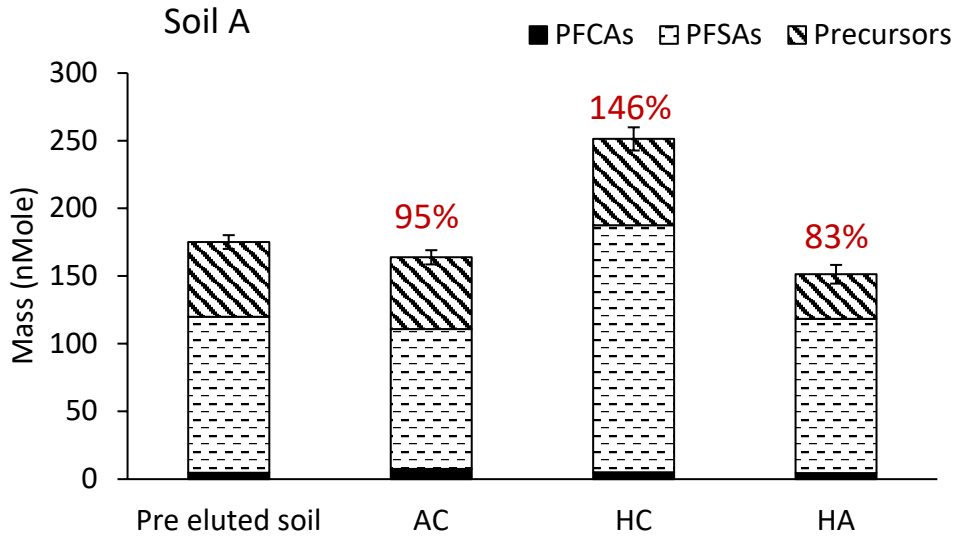

Figure 28. Composition of PFCAs, PFSAs, and precursors in Soil C Alkaline heat activated (AHA), Heat activated (HA), Ambient Control (AC), Heat Control (HC), and pH Control (pHC) and in Soil A AC, HC and HA columns. Percentage mass balance for each column shown in red numbers.

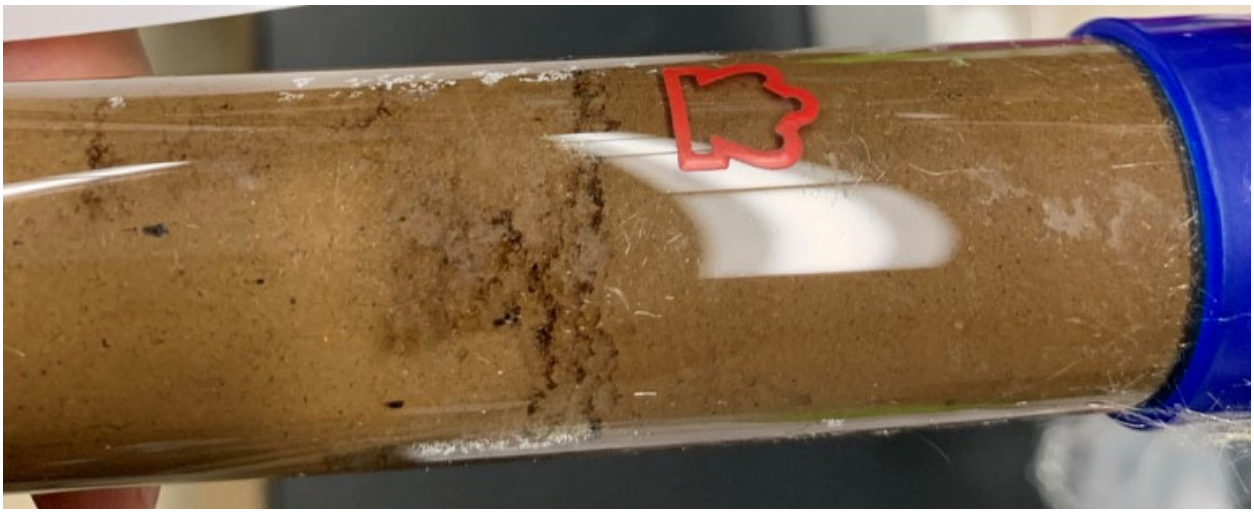

Figure 29. Soil A alkaline heat activated column effluent end.

Due to results of prior batch experiments, mass balances in HA columns were investigated for evidence of PFCA mineralization. Specifically, mineralization was observed in batch experiments treated with non-alkaline heat-activated persulfate (Shojaei et al., 2021) (i.e., the batch equivalent to HA columns), attributable to PFCA degradation that can occur at acidic pH (Bruton and Sedlak, 2017; Bruton and Sedlak, 2018). Soil C HA columns had total PFAS and total PFCA recoveries of 93% and 510%, respectively, and unlike batch experiments, HA conditions did not lead to pH drops in Soil C. The effluent pH during the oxidant pulse of HA columns was the same as the pH in HC and AC effluent (~6.5), likely due to soil buffering capacity. Under these conditions PFCA mineralization would not be expected. Total PFAS recovery in Soil A HA columns was lower than Soil C (83%), but still within 70-130% (considered full mass balance), so potential for degradation was unclear. Total PFCA recovery was 92%, but only 58% of total precursor concentration was recovered. The decrease in precursor recovery without a corresponding increase in PFCA concentration suggests that precursors were transformed to PFCAs and a fraction subsequently degraded resulting in no overall change to the PFCA concentration. Additionally effluent pH in Soil A HA columns was lower (~5) during the oxidant pulse relative to the pH of flushing periods and AC columns (pH ~7). These relatively more acidic conditions may have facilitated PFCA degradation in Soil A HA columns. Finally, changes in PFCA chain length distribution also support PFCA degradation in Soil A HA columns. Whereas under recoveries were observed for PFAS such as PFBA (64%) and PFPeA (68%), masses of other PFCAs such as PFOA and PFNA increased (125% and 134% recovery, respectively).

The mass balances of PFSAs in Soil C were 103-125%, indicating that, as expected, no PFSAs were generated or degraded under any column conditions over the duration of the 14 day experiment. In Soil A HA and AC columns, the mass balances of PFSAs were also in the range of 70-130%; however, the mass balance in the HC was 160%, suggesting over recovery. This was primarily attributable to high recovery of PFOS, which might be due to hydrolysis of C8 precursors to PFOS (Lakshminarasimman et al., 2021; Lazcano, et al., 2019). Additionally, based on TOP data in soil and column effluents, sum of PFOA generation in the heat control post TOP was only ~45% of the generation observed in ambient columns, suggesting that C8 precursors may have been lost in the heat control columns due to transformation mechanisms.

The total PFCA mass increased as a result of oxidation in all columns with circumneutral pH (Soil C HA and AHA columns; note that Soil A AHA columns clogged) as anticipated based on prior batch studies

(Shojaei et al., 2021). The total PFCA mass increased ~5x in Soil C HA and AHA columns (**Figure 30, Table 15**), and the largest increases were observed for PFBA (1107-1442%), PFHxA (1007-1145%) and PFPeA (724-837%; **Figure 31**). Moreover, PFHxA recovery comprised 54-58% of total PFCAs recovered in HA and AHA columns. These results are consistent with the predominance of C6 ECF and FT-based precursors identified in suspect screening results. In Soil C HA and AHA columns and Soil A HA columns, nearly all of the PFCA mass (92-95% and 85% in Soil C and A, respectively) was mobilized during oxidation and subsequent flushing. In Soil C, this includes the original PFCA mass plus PFCAs generated in effluent. Although no PFCA generation was observed in Soil A as discussed above, nearly all of the PFCA mass was also recovered in the aqueous phase (85%). This demonstrates that PFCAs are readily mobilized, and are ideal terminal degradation products for enhanced PFAS recovery based on oxidative conversion.

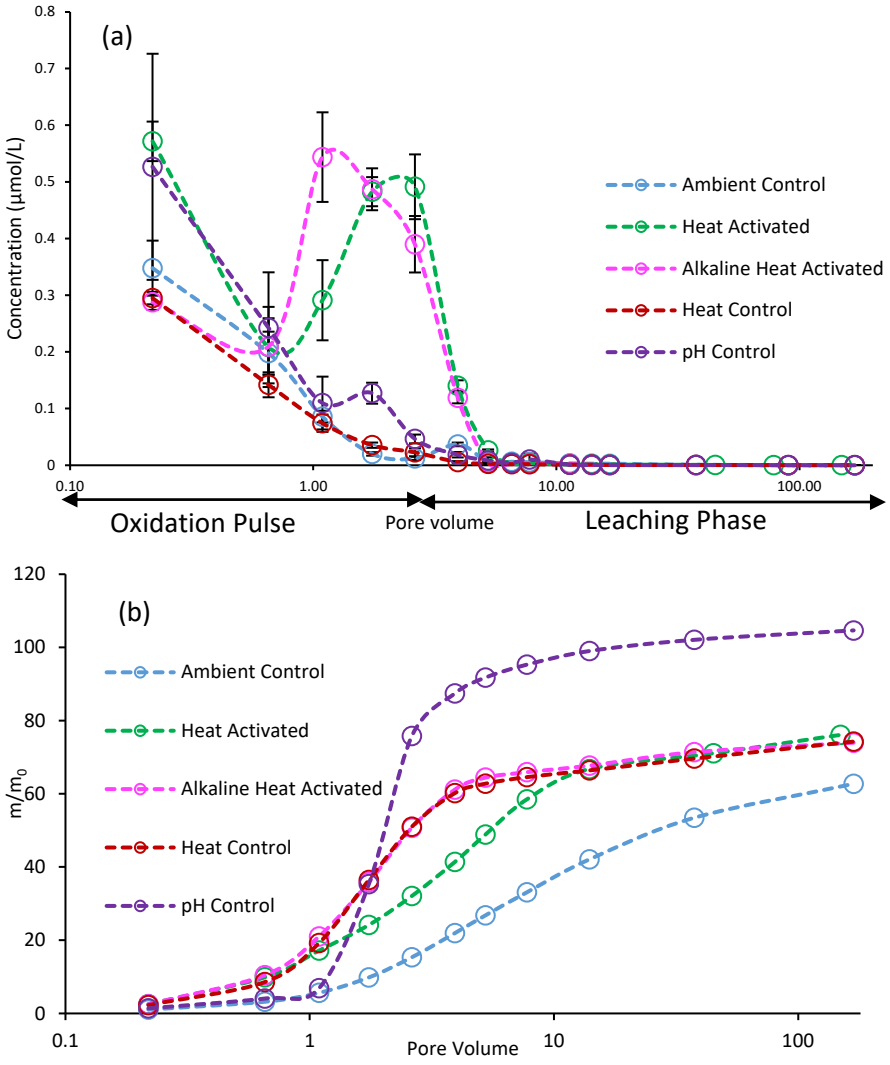

Figure 30. Total PFCA concentration (panel a) and fraction (m/m0) of total PFAS recovered in Soil C column effluents.

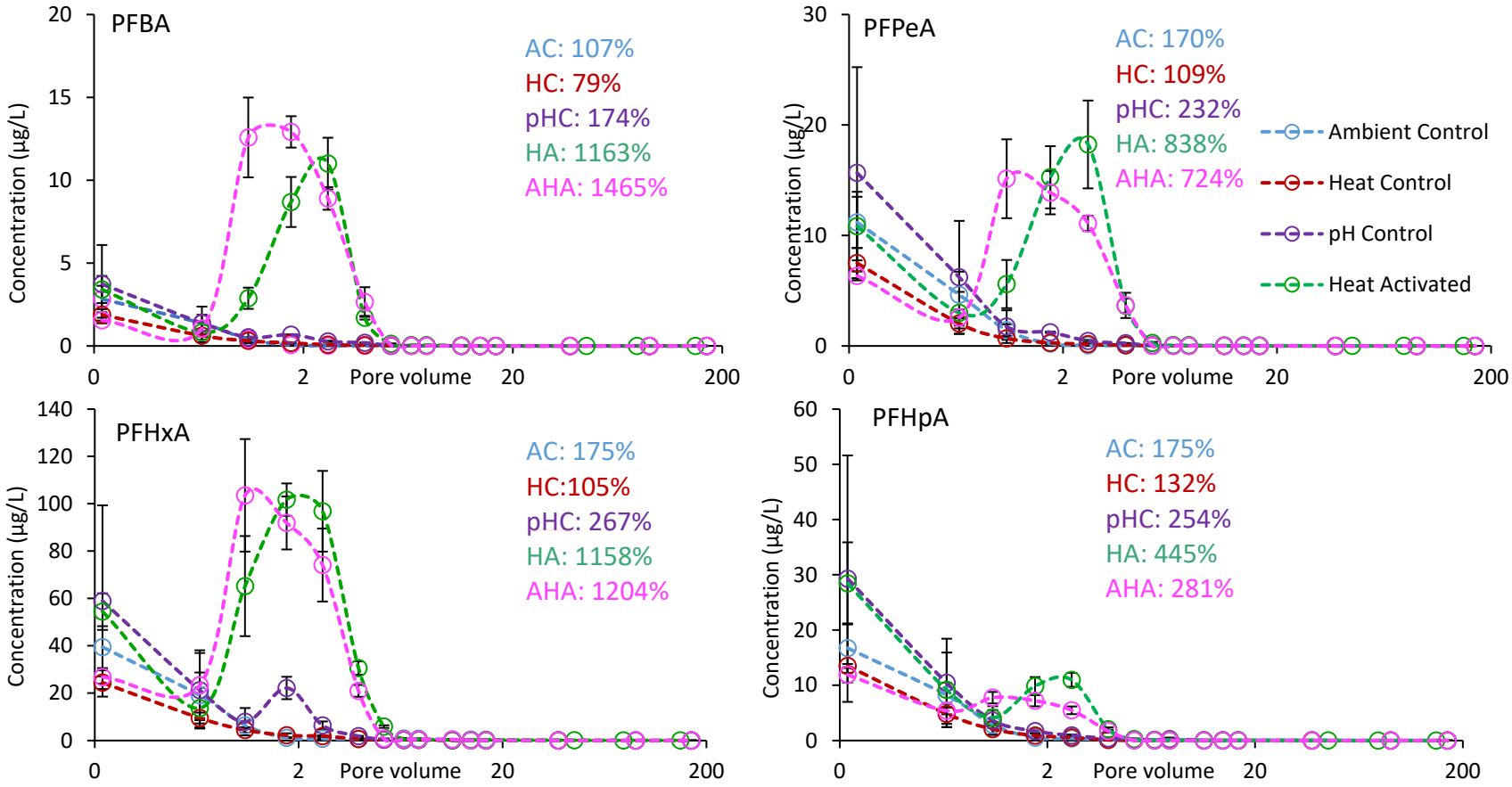
PFBA
AC: 107%
HC: 79%
pHC: 174%
HA: 1163%
AHA: 1465%
PFPeA
AC: 170%
HC: 109%
pHC: 232%
HA: 838%
AHA: 724%
PFHxA
AC: 175%
HC:105%
pHC: 267%
HA: 1158%
AHA: 1204%
PFHpA
AC: 175%
HC: 132%
pHC: 254%
HA: 445%
AHA: 281%
Concentration (µg/L)
Pore volume
Ambient Control
Heat Control
pH Control
Heat Activated

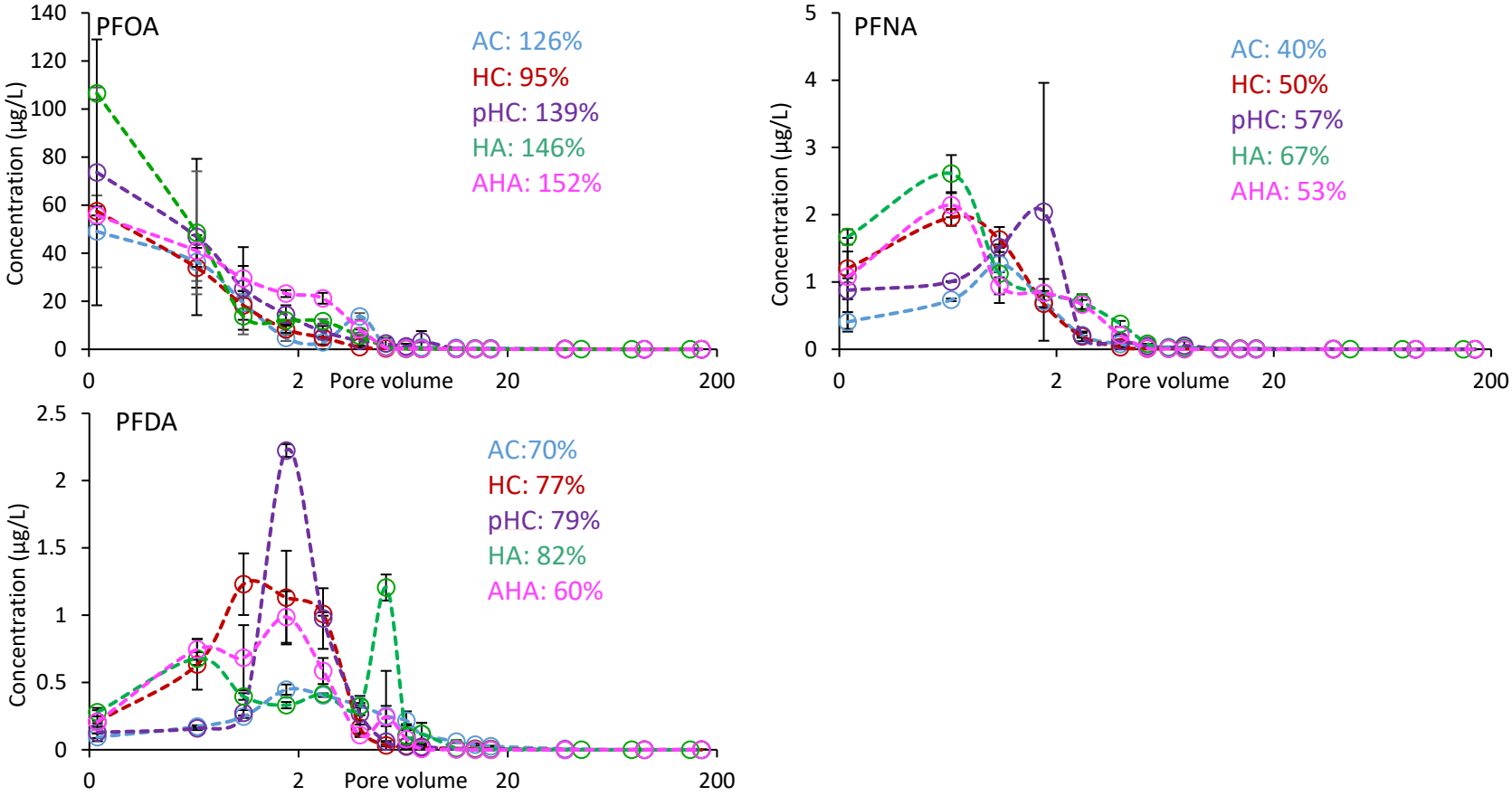

Figure 31. PFCAs breakthrough in Soil C ambient control (AC), heat control (HC), pH control (pHC), heat activated (HA) and alkaline heat activated (AHA) columns. Percentages reflect fraction of original soil mass recovered in column effluents.

Total precursor recovery and composition in oxidized columns (AHA and HA) reflected precursor transformation as anticipated based on batch (Shojaei et al., 2021) and previous studies (Bruton and Sedlak, 2017; Park et al., 2016). In Soil A HA columns, low precursor recovery supports transformation, as discussed above. In Soil C HA and AHA columns, precursor mass balances were 72% and 68%, respectively, and these recoveries meet or approach the 70-130% criteria used to determine full recovery. However, shifts in the composition of precursors reflect oxidation of parent precursors to transformation intermediates. For example, 6:2 fluorotelomer sulfonate (6:2FTS), perfluorohexane sulfonamide (FHxSA) and perfluorooctane sulfonamide (FOSA) increased 269%, 228% and 190% respectively in HA columns, and they increased 258%, 315%, and 122%, respectively in AHA columns. These PFAS classes can be oxidized to PFCAs during persulfate oxidation (Shojaei et al., 2021; Bruton and Sedlak, 2017; Houtz, 2013), so this mass increase is attributable to incomplete oxidation coupled with generation as intermediate transformation products of parents such as N-hydroxyethyldimethylammonio propyl perfluoroalkane sulfonamide (EtOH-AmPr-FASA) and n:2 fluorotelomer sulfonamido propyl dimethyl amine (n:2FTSA-DiMeAn) present in the soil (Bruton and Sedlak, 2017; Schaefer et al., 2018). Generation of transformation intermediates was also observed in the batch experiments. Perfluoroalkane sulfonamides (FASAs), which are the PFAS class inclusive of FOSA, comprised 54% and 43% of the total precursor mass recovered in HA and AHA columns, respectively. If the increased masses of known intermediate transformation products such as FASAs and n:2 FTSs are removed from the precursor mass balance, then only 55-57% of the total precursor mass was recovered in oxidized (i.e., HA and AHA) columns. As noted in batch experiments, although not all precursors were fully converted, intermediate products such n:2 FTSs and FASAs may still be more mobile than their parent precursors (depending on pKa of the intermediate and pH of the system) due to reduced hydrophobic effects and their charge (typically anionic) relative to zwitterionic and cationic precursors. So even partial transformation may be of benefit for total PFAS recovery during remediation.

Ambient PFAS Transport. Numerous studies have established that sorption of PFAS increases with increasing chain length, and the same trends were observed herein (Guelfo and Higgins, 2013; Kabiri et al., 2022; Higgins and Luthy, 2006). In the AC columns of both Soils A and B, short-chain PFAS (e.g., C4, C6 PFCAs and PFSAs) demonstrated rapid elution. In Soil C, maximum eluent concentrations of short-chain PFAS were observed at the onset of column operation, and leaching of >90% of the total mass occurred before 1.75 pore volumes of column operation (**Figure 32**). Alternatively, long-chain PFAS (e.g., PFDA and PFDS) reached maximum eluant concentrations in Soil C at 1.75 and 4 pore volumes, respectively, and after 168 pore volumes only 70% and 28%, respectively, of the total mass was recovered (**Figure 31**). Similar desorption trends were observed in Soil A for PFAAs (**Figure 33**). Chain length dependent trends were also observed in the FASAs and zwitterionic precursors (**Figure 32 e-h** and **Figure 33e-f**).

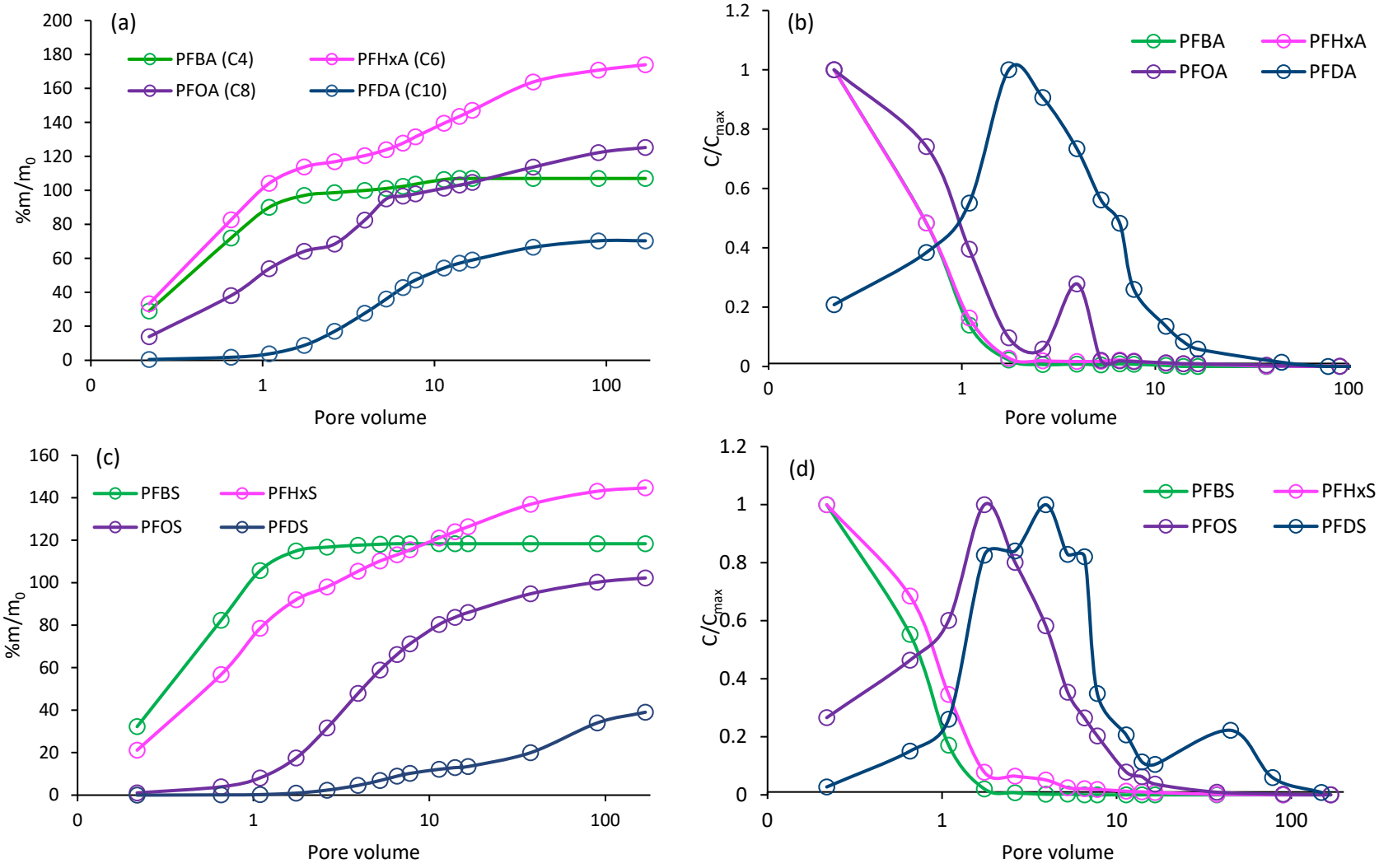
(a)
PFBA (C4)
PFHxA (C6)
PFOA (C8)
PFDA (C10)
%m/m0
Pore volume
(b)
PFBA
PFHxA
PFOA
PFDA
C/Cmax
Pore volume
(c)
PFBS
PFHxS
PFOS
PFDS
%m/m0
Pore volume
(d)
PFBS
PFHxS
PFOS
PFDS
C/Cmax
Pore volume

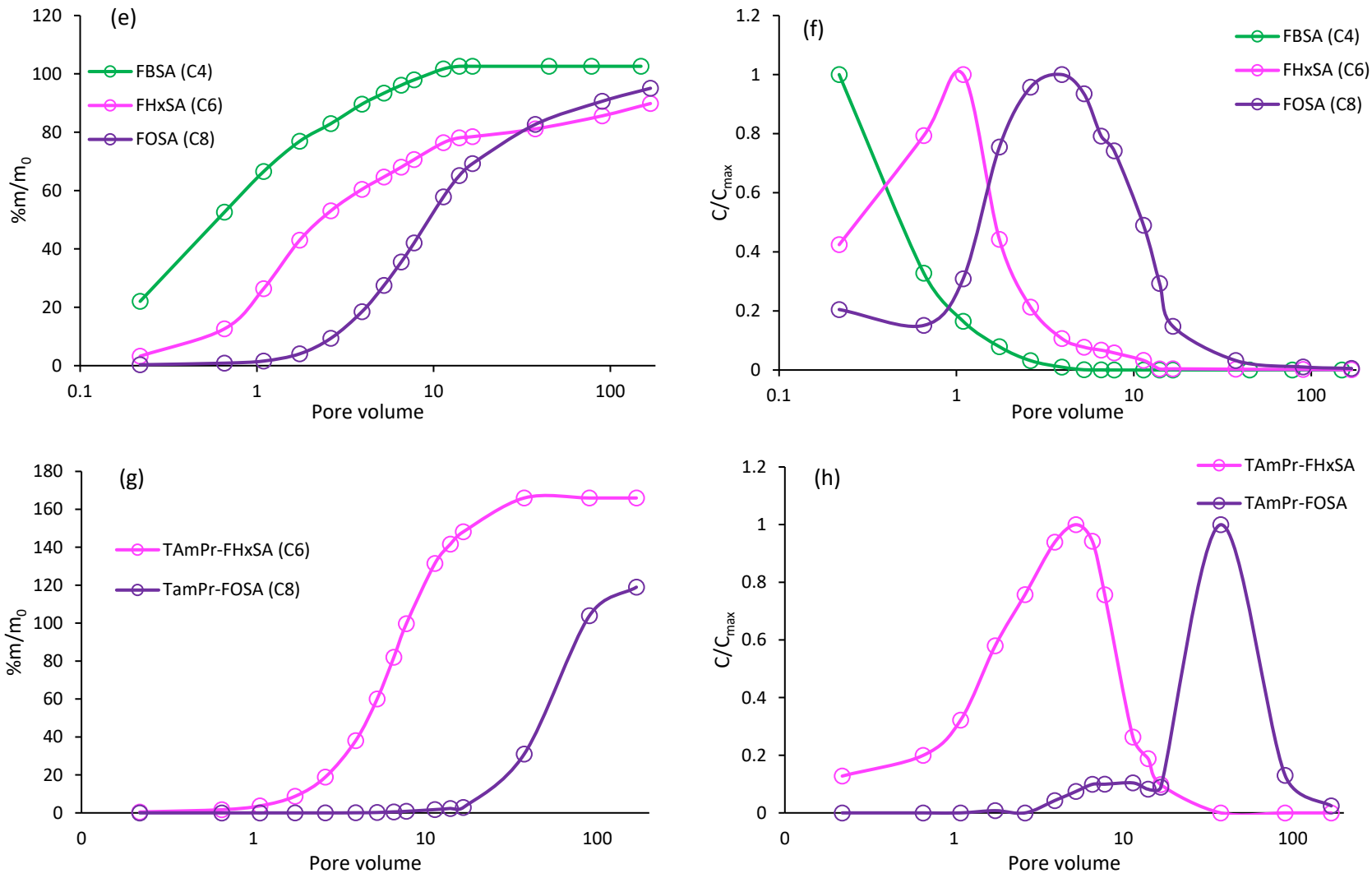

Figure 32. The mass fraction recovered (m/m_0; left column) and breakthrough (C/C_{max}, right panel) of PFCAs (top row), PFSAs (second row), FASAs (third row), and TAmPr-FASAs (fourth row) in Soil C AC columns. Note that C_{max} is maximum concentration measured in effluent.

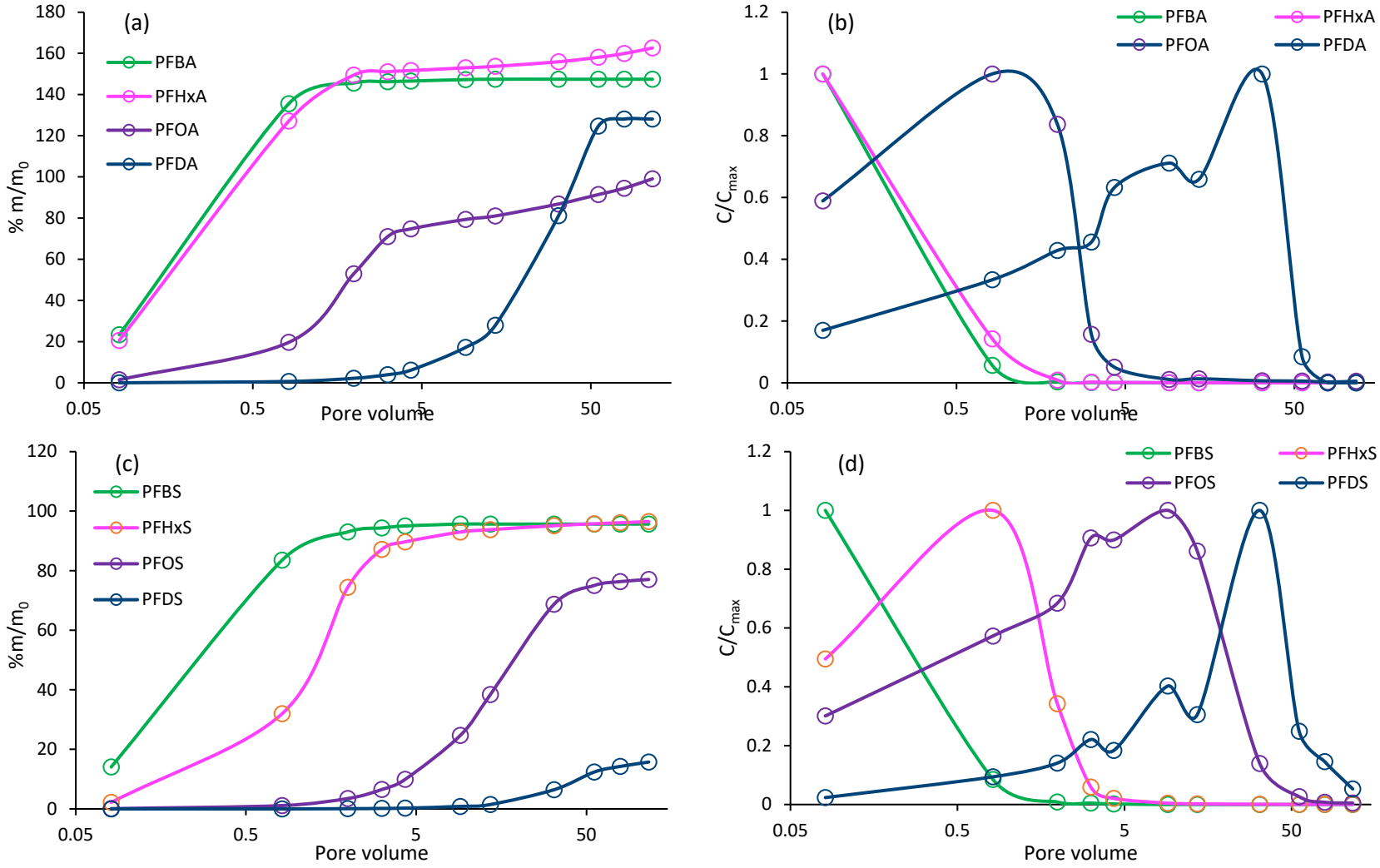
(a)
PFBA
PFHxA
PFOA
PFDA
% m/m0
Pore volume
(b)
PFBA
PFHxA
PFOA
PFDA
C/Cmax
Pore volume
(c)
PFBS
PFHxS
PFOS
PFDS
%m/m0
Pore volume
(d)
PFBS
PFHxS
PFOS
PFDS
C/Cmax
Pore volume

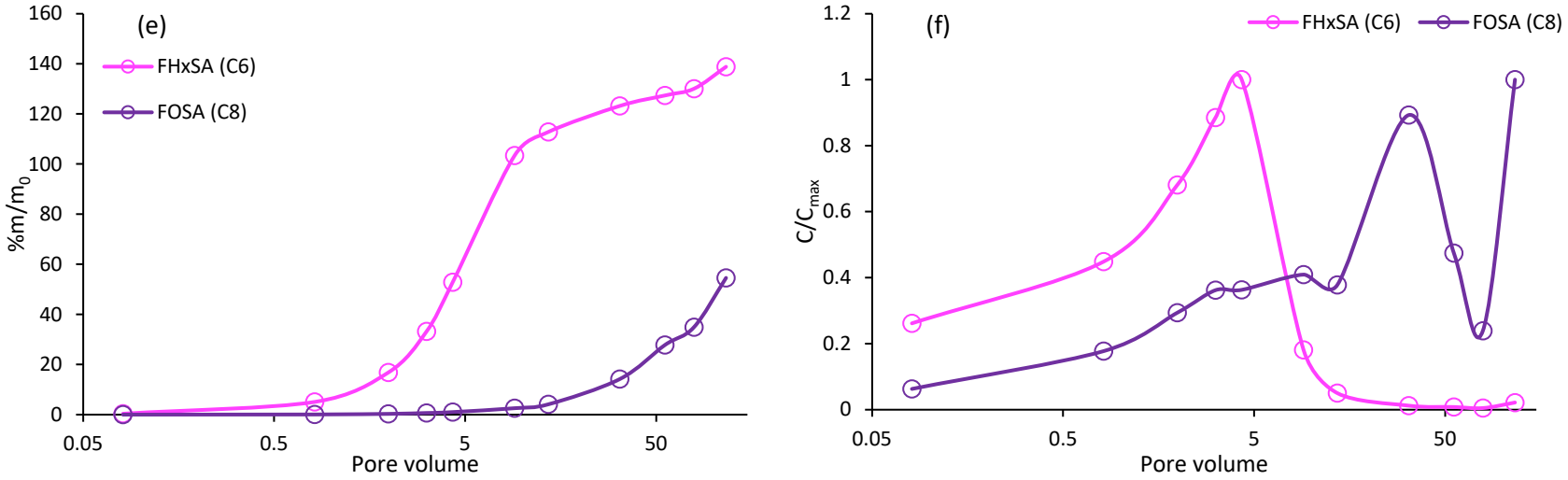

Figure 33. The mass fraction recovered (m/m_0; left column) and breakthrough (C/C_{max}, right panel) of PFCAs (top row), PFSAs (second row), and FASAs (third row) in Soil A AC columns. Note that C_{max} is maximum concentration measured in effluent.

Studies have also shown that PFAS functional group impacts desorption. For example, studies have shown that PFSAs exhibit stronger sorption than PFCAs with the same length of perfluoroalkyl tail (Guelfo and Higgins, 2013; Higgins and Luthy, 2006), and other studies have shown that zwitterionic PFAS sorb stronger than anionic PFAS (Barzen-Hanson et al., 2017; Xiao et al., 2019; Xiao et al., 2017).

The charge of PFAS is another factor that influence their recovery in AGW, cationic and zwitterionic PFAS desorbed slower than anionic PFAS as a result of stronger sorption on soil negatively charged surface. Comparing fraction of PFAS mass recovered in Soil C AC effluent showed that anionic PFHxSi and FHxSA (anion/neutral) eluted faster than zwitterionic EtOH-AmPr-FHxSA. 70% of PFHxSi and 132% of FHxSA masses eluted in Soil C AC during 168 pore volumes while only 30% of EtOH-AmPr-FHxSA mass measured in the effluent (**Figure 34a**). All of these compounds have close retention time in LC C18 columns which compounds were eluted base on their hydrophobicity. As it is shown in **Figure 34b**, zwitterionic TAmPr-FOSA started to elute in effluent after 4 pore volumes, while anionic PFOSi, 8:2 FTS and neutral FOSA have been detected in the effluent in the first measured pore volume (0.22). Maximum 8:2 FTS concentration in AC effluent was measured at 1.75 pore volume and more than 90% of 8:2 FTS eluted before pore volume 12. However, maximum concentration of TAmPr-FOSA was measured later in 11.4 pore volume and in 90 pore volume more than 90% of its mass recovered in effluent. The same trend was observed in soil A, for example 92% of 6:2 FTS mass recovered in AC effluent while only 26% TamPr-FHxSA recovered after eluting 116 pore volume. Charge related desorption of PFAS also reported in prior studies. Maizel et al. (2021) reported that PFAS containing positive charged moiety desorbed slower than anionic and neutral PFAS (Maizel et al., 2021). Therefore, transformation of zwitterionic and cationic precursors to PFCAs and more mobile oxidation intermediate can lead to increased PFAS mobility.

PFAS Transport in Treated Columns. Eluant concentrations were used to calculate total PFAS mass recovered in the aqueous phase over the duration of the column experiments and accelerated mobilization of total PFAS in treated columns (i.e., AHA and HA) was evident relative to recovery in AC columns in Soil C (Figure 1b). Maximum total PFAS mass recovery (104%) was observed in pHC columns, which are further discussed below. The total mass recovered in the eluants of AHA and HA columns was the same (~70%), and was higher than the total recovery AC columns (63%). AHA columns approached maximum recovery at a faster rate than HA columns (i.e., Figure 1b, pore volumes 1-13). Interestingly, elution of PFAS in AHA and HC columns were nearly identical when total PFAS were considered (Figure 1b). Although similar in total PFAS recovery, differences in transport of individual PFAS under AHA, HA, and HC conditions in Soil C were very evident. For example, generation of PFHxA was evident in HA and AHA columns as a result of persulfate oxidation of precursors, but PFHxA was not generated under conditions of heat only (HC; **Figure 29**). In contrast, PFOS transport in HA, AHA, and HC columns demonstrated similar, but slightly offset, pulses (**Figure 35**). Because PFSAs are not generated or degraded during oxidation, these observations are due to impacts of heat and pH, as discussed below. In contrast to effluent results, the cumulative impacts of persulfate treatment on PFAS mobilization were more evident in post elution soil results, and these are discussed below. In Soil B, similar PFAS mass recovered in eluents of HA and AC (68%), however, in 1- 14 pore volumes higher PFAS mass recovered in HA columns which could be due to oxidative treatment (**Figure 36a**). Higher PFAS mass was recovered in HC eluant vs. HA and AC columns which attribute to higher PFSA recovery in HC (**Figure 36b**). PFCA mineralization occurred under non-alkaline conditions and lower PFAS mass was measured in Soil A HC columns.

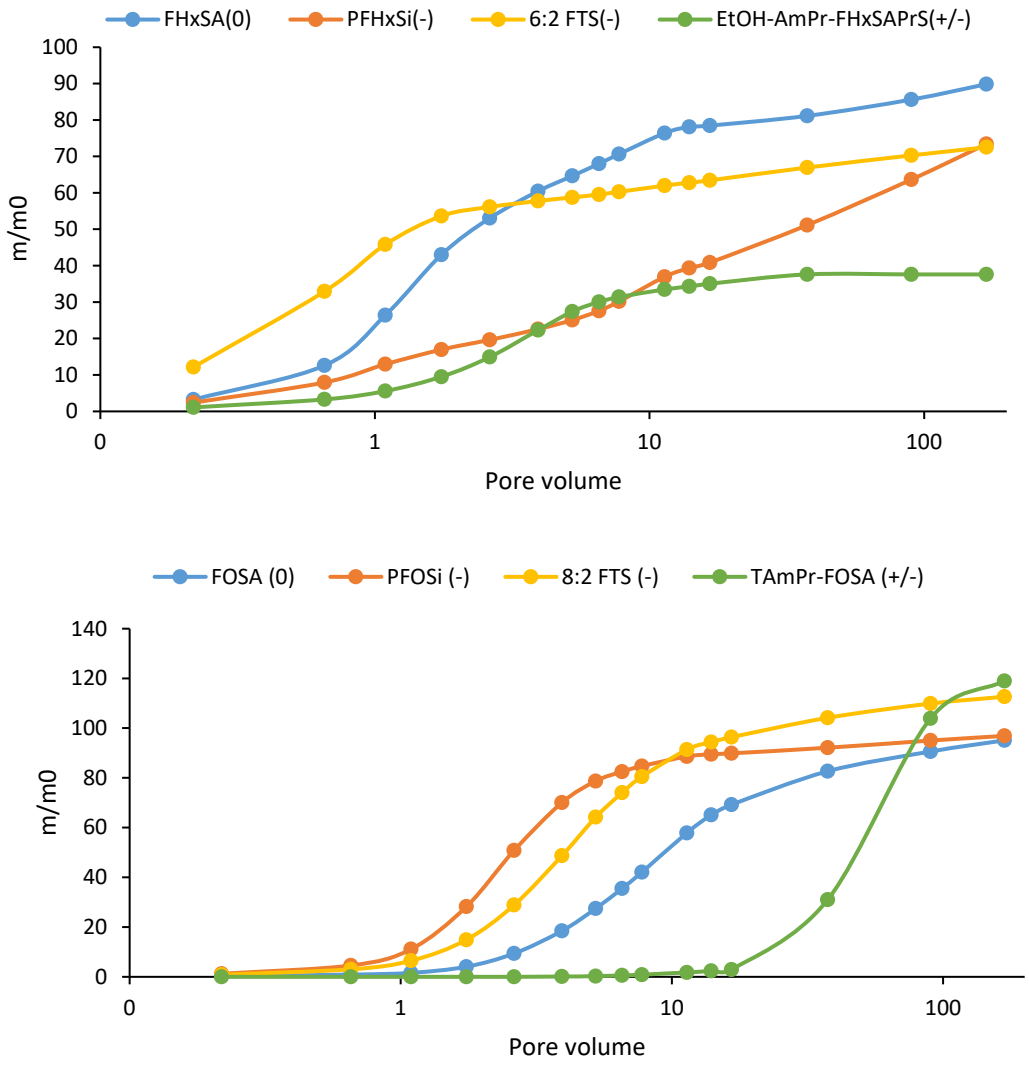

Figure 34. Fraction of anionic (-), neutral (0), and zwitterionic (+/-) precursors (m/m_0) recovered in Soil C ambient control effluents.

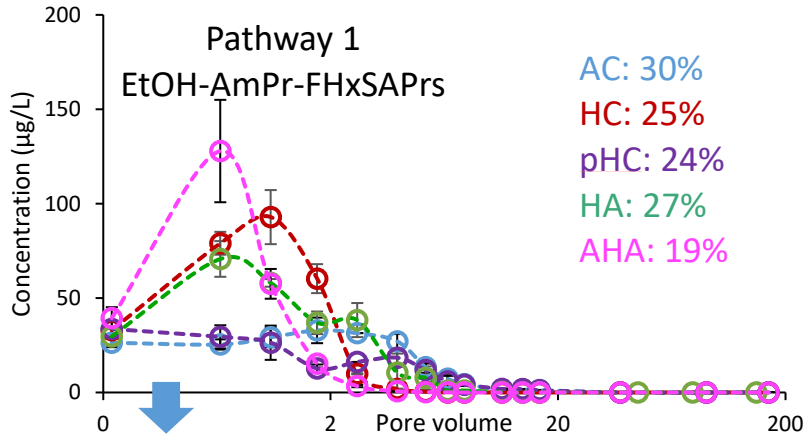
Pathway 1
EtOH-AmPr-FHxSAPrs
AC: 30%
HC: 25%
pHC: 24%
HA: 27%
AHA: 19%
Concentration (µg/L)
Pore volume
0
50
100
150
200
2
20

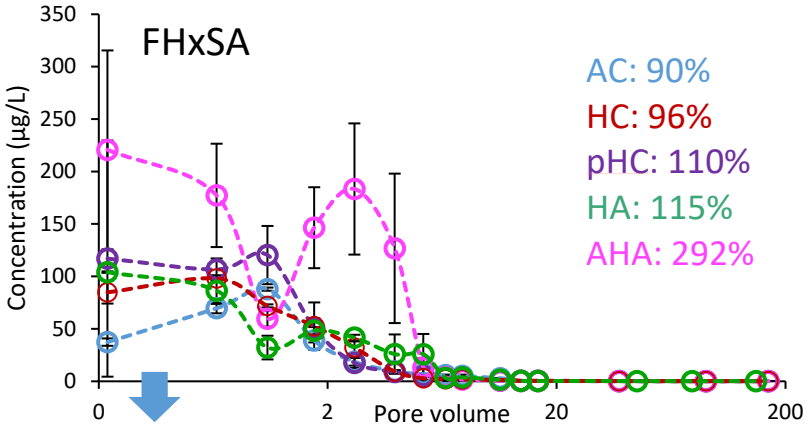
FHxSA
AC: 90%
HC: 96%
pHC: 110%
HA: 115%
AHA: 292%
Concentration (µg/L)
Pore volume
0
50
100
150
200
250
300
350
2
20

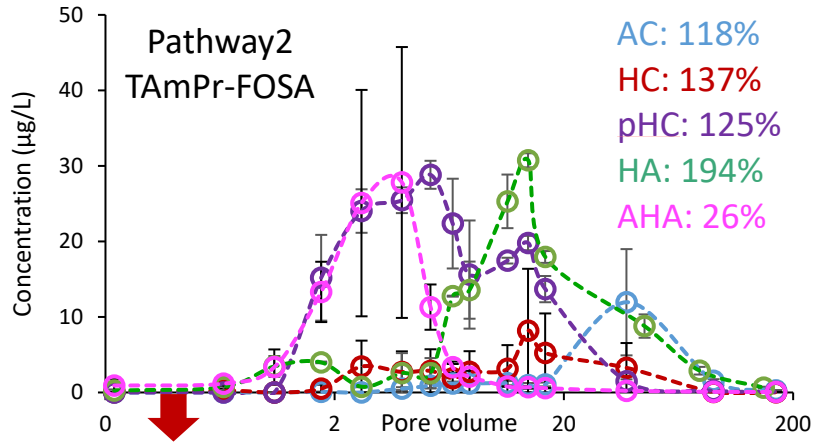
Pathway2
TAmPr-FOSA
AC: 118%
HC: 137%
pHC: 125%
HA: 194%
AHA: 26%
Concentration (µg/L)
Pore volume
0
10
20
30
40
50
2
20

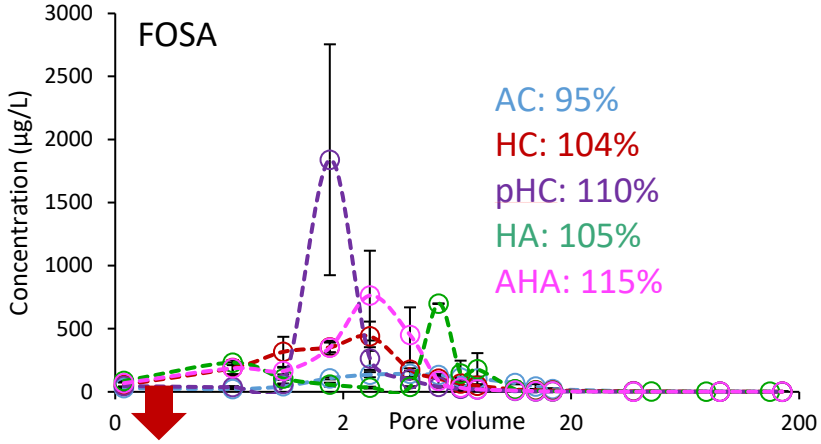
FOSA
AC: 95%
HC: 104%
pHC: 110%
HA: 105%
AHA: 115%
Concentration (µg/L)
Pore volume
0
500
1000
1500
2000
2500
3000
2
20

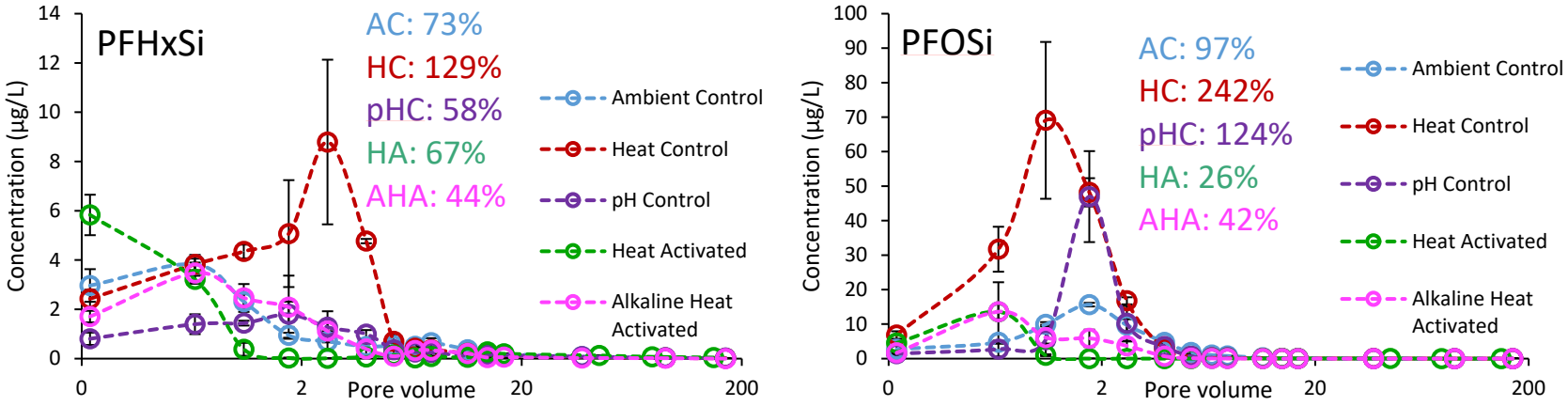

Figure 35. Effluent concentration of PFAS in hypothesized oxidation pathway 1 (blue arrow) and 2 (red arrow) in Soil C heat and alkaline heat activated columns. Percentages are mass fraction of each compounds recovered in the column effluent.

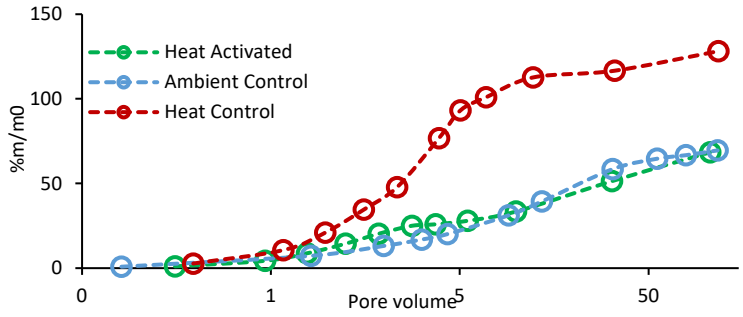

Figure 36. Fraction (m/m_0) of total PFAS recovered in Soil A column effluents.

PFAS in Post Elution Soils. Following completion of column experiments, column soils were sectioned, extracted, and analyzed using targeted analysis, TOP, and suspect screening. Data from the influent, middle, and effluent ends of the columns show that concentrations varied through the length of the column although there were no systematic trends. In Soil C, total PFAS concentrations remaining in all Soil C column types were similar except for AHA columns which showed decreased concentrations in the influent and middle sections of the column (**Figure 37**). AHA columns also had the lowest total PFAS mass remaining in the columns (10%) relative to the other column types which had 14% (pHC) to 21% (HA) remaining. In Soil A, HA columns had the lowest total PFAS mass remaining (15%; **Figure 38**); however, AHA columns failed and were not included in the comparison. Additionally, as noted in Section 3.2, some PFCAs were lost in Soil A HA columns due to mineralization.

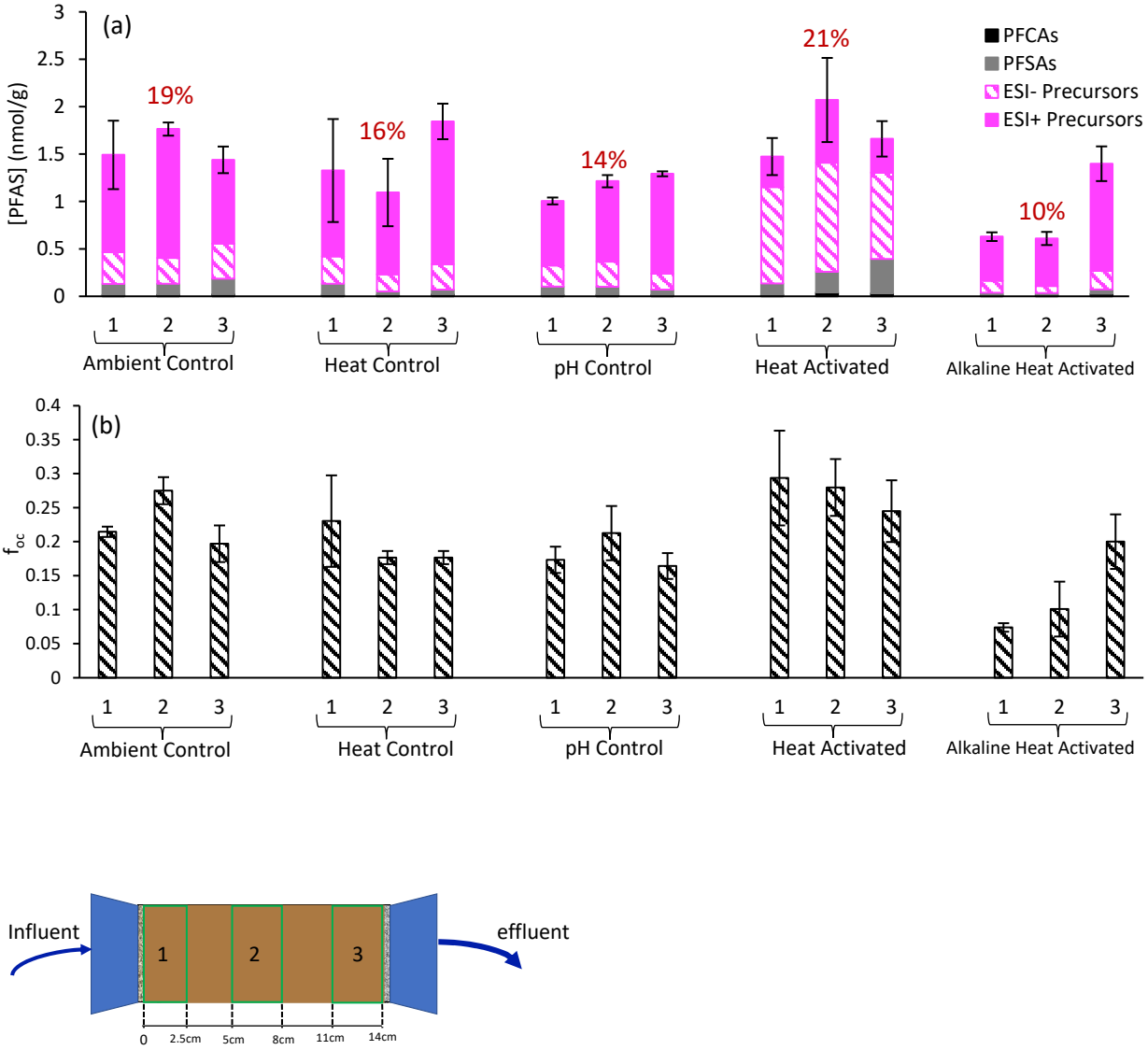

Figure 37. PFAS total Concentration (panel a) and f_{oc} (panel b) in post elution soil in Soil C columns. Percentages in panel a are fraction of total PFAS remained in post elution soils.

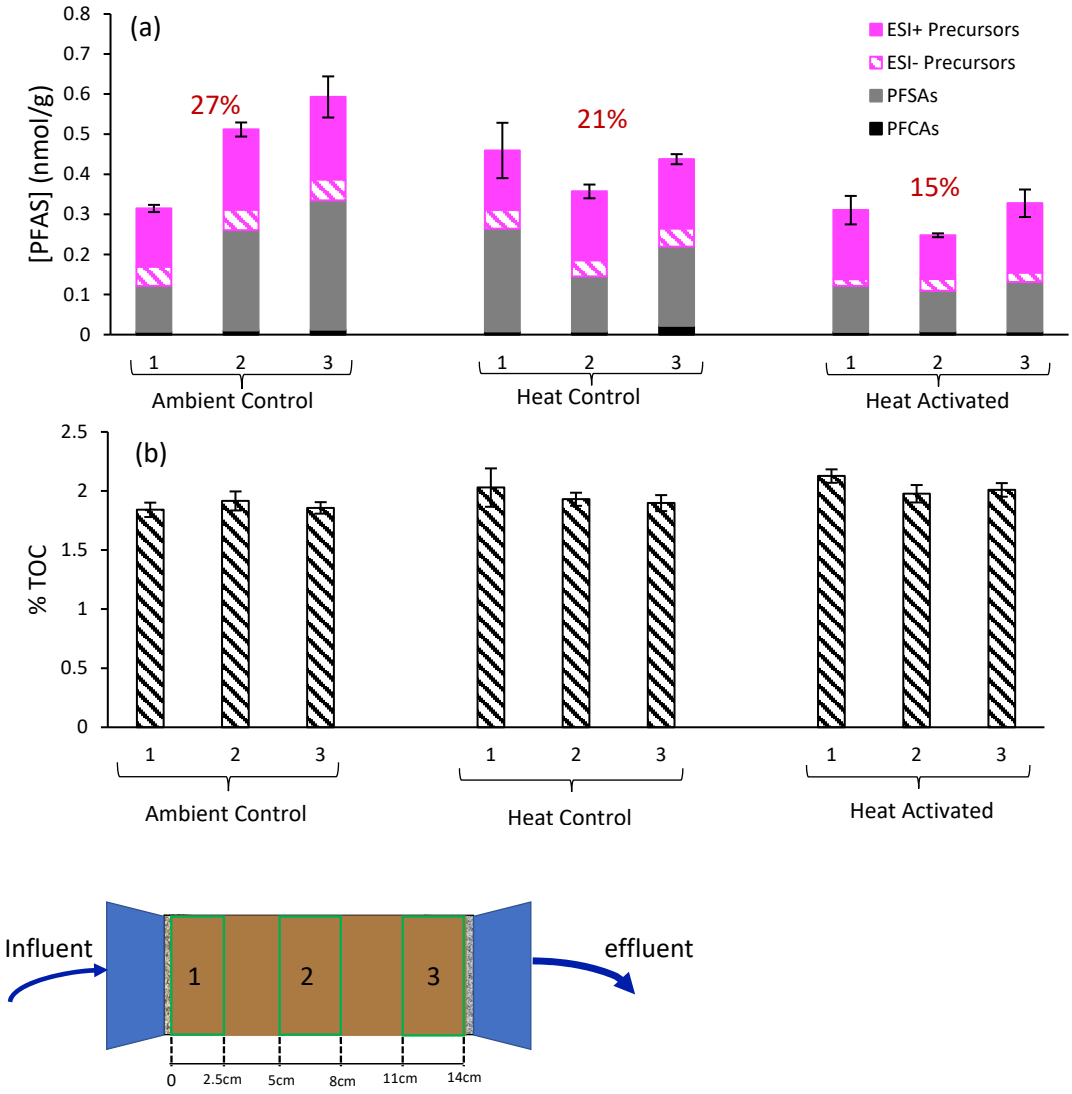

Figure 38. PFAS total Concentration (panel a) and f_{oc} (panel b) in post elution soil in Soil A columns. Percentages in panel a are fraction of total PFAS remained in post elution soils. Note that some PFCAs were lost due to mineralization in HA columns.

The impacts of oxidative treatment in Soil C columns are evident in looking at the composition of precursors remaining in soil. In all column types for Soil C, the dominant PFAS fraction (85-95%) remaining in soils were precursors, and of those precursors, the majority (76-84%) were ESI+ PFAS (i.e., a proxy for stronger-sorbing cationic and zwitterionic PFAS) in all but HA columns. Further, concentrations of ESI+ PFAS were lower in AHA columns relative to AC and HC columns. This demonstrates impacts of persulfate that are not observed under ambient conditions and cannot be explained by heat alone. Of total precursors remaining in HA columns, ESI- PFAS were dominant (70%), and this is further discussed below. Retention of ESI+ PFAS supports observations in earlier batch work (Shojaei et al., 2021) and the overall hypothesis that stronger-sorbing ESI+ PFAS will be the most difficult to recover during groundwater extraction. Lower concentrations remaining in AHA columns also support results of batch experiments which demonstrated the potential for persulfate to convert stronger-sorbing PFAS to more mobile and recoverable PFCAs (Shojaei et al., 2021). As noted above, nearly all

PFCA mass was recovered in column eluants, and this is supported by the minimal PFCA mass that remained in the soils of all column types after completion of experiments (**Figure 37**).

As noted, a large fraction of precursors remaining in Soil C HA columns were identified in ESI- mode (i.e., a proxy for anionic and neutral PFAS), and in addition, a larger fraction of the total PFAS mass (21%) remained in these soils relative to AHA soils (10%) despite receiving oxidative treatment (**Figure 37**). This is likely attributable to combined impacts of partial precursor conversion and the pH of HA columns. As noted in Section 3.2, incomplete precursor oxidation increased the masses of FHxSA (228-315% recovery) and FOSA (122-190% recovery) in HA and AHA columns. The pH of AHA columns was ~8 during the oxidation pulse as compared to ~6.5 in HA columns. The estimated pKa values of FHxSA and FOSA are 6.92 and 7.01 (calculated using Advanced Chemistry Development software, ACD/Lab), suggesting that a higher fraction of both FOSA and FHxSA were present in anionic form in AHA columns vs. HA columns where speciation was primarily neutral. Neutral FHxSA and FOSA are expected to undergo less electrostatic repulsion and higher sorption relative to the deprotonated species, resulting in decreased mobilization at lower pH. FOSA and FHxSA comprised 55% and 12%, respectively of the remaining precursor mass in Soil C HA columns. Despite generation of similar pulses of FHxSA and FOSA, these PFAS represented only 3% and 9% of the remaining PFAS in soils of AHA columns. These trends were also supported by data in AC vs. pHC columns. As noted above, incomplete oxidation to anionic intermediates (e.g. n:2 FTSs) may still yield enhanced mobilization of total PFAS relative to ambient conditions. However, these results also demonstrate that under some pH conditions, incomplete oxidation, particularly of ECF-based PFAS that yield FASA intermediates, may change PFAS composition but yield intermediates that are not relatively more mobile, resulting in total PFAS retention similar to ambient conditions (**Figure 37**).

Differences in DOC may also have contributed to observed differences in the final soil PFAS composition of AHA and HA columns. During the oxidation pulse, the AHA column effluent had DOC concentrations that were 19 times higher than concentrations in HA columns. Differences between the AHA and HA DOC are likely attributable to the impacts of both pH and oxidation. Studies have shown that DOC can be mobilized at alkaline pH (Weber et al., 1999; You et al., 1999). The AHA column pH during the oxidation pulse (~8) exceeded that of the HA columns (~6.5). AHA column pH was much lower than pHC columns (~12), but despite this, the DOC was higher in AHA vs. pHC columns. This indicates that some of the DOC mobilization in AHA columns was attributable to the effects of oxidation, which has been shown to change the organic carbon content of soil (Cuypers et al., 2002). Differences in soil organic carbon in AHA vs. HA columns are also evident in the remaining f_{oc} of soil at the completion of experiments wherein AHA f_{oc} was lower than that of HA columns (**Figure 37**). Deceased organic carbon content of the AHA soils may have led to less available sites for PFAS sorption, and this may also have contributed to the overall higher total PFAS recovery in AHA vs. HA columns.

Impacts of persulfate treatment were less evident in Soil A columns. Following completion of column experiments, 15% of the total PFAS mass remained in the HA columns compared to 21% and 25% in the HC and AC columns, respectively (**Figure 38**). As seen in Soil C columns, the majority (>80%) of precursors remaining in the soils were identified in ESI+ mode (**Figure 38**). Slightly lower (~10%) precursors retained in Soil A HA than HC, and AC. However, differences in the total PFAS remaining in Soil A were primarily attributable to differences in PFSA recovery among the 3 column types. Lower PFSA mass retained in HA and HC columns in compared with AC columns which could be because of thermal desorption of PFSA in HA and HC columns. Higher PFSA mass in HC than HA columns could attribute to generation of PFOS in HC which resulted in slightly higher (6%) PFSA mass remaining in post elution soil. In contrast with Soil C, Soil A columns soil f_{oc} did not change following oxidation, however lower amount of PFAS retained in HA post elution soils, suggesting higher PFAS release in those columns was result of oxidation treatment.

Overall, the suspect screening results (i.e., ESI-/ESI+ PFAS) in AHA (Soil C) and HA columns (Soils A and B) highlight that multiple oxidant pulses may be needed in order to achieve maximum recovery of the PFAS mass in AFFF-impacted soils. Dominant PFAS remaining in Soil C AHA and HA columns were 6:2 FTSAPr-DiMeAn and FOSA. 6:2 FTSAPr-DiMeAn is a cationic FT based precursor which carry positive charge at pH<8 and is net neutral at 8<pH<10 (Barzen-Hanson et al., 2017). FOSA sulfonamide functional group has a calculated pKa 6-7 (Barzen-Hanson et al., 2017), therefore at circumneutral pH could carry negative charge or be neutral. In Soil A, the dominant ESI+ PFAS were C6 and C8, zwitterionic TAmPr-FASAs, which are thought to have a terminal cationic charge and a central negative charge (i.e., net neutral) at circumneutral pH (Mejia-Avendaño et al., 2020). These precursors have the potential to transform to terminal C6 and C8 PFCAs, suggesting that it would be beneficial to consider application of multiple oxidant pulses under field scenarios.

Effect of pH. Changes in column pH could lead to changes in PFAS mobilization via multiple mechanisms. For example, studies have shown that increasing pH can increase the negative charge soil surfaces, which will increase electrostatic repulsion between surfaces and anionic charges on PFAS (Barzen-Hanson et al., 2017; Higgins and Luthy, 2006; Du et al., 2014). For multi-protic PFAS (i.e., zwitterions), pH-dependent interactions depend on the combined impacts of changes in surface charge and charge state of each acidic functional group. Studies have also shown that alkaline pH leads to increases in DOC, so for contaminants with organic carbon interactions, this can lead to facilitated transport in the aqueous phase (Weber et al., 1999; You et al., 1999). Some studies have shown that increasing pH to 10-12 enhanced rate of abiotic hydrolysis of fluorotelomer-based polymers to PFCAs (Lakshminarasimman et al., 2021; Washington and Jenkins, 2015; Washington et al., 2015). Lastly, some studies have shown that increasing pH to 10-12 enhanced rate of abiotic hydrolysis of fluorotelomer-based polymers to PFCAs (Lakshminarasimman et al., 2021; Washington and Jenkins, 2015; Washington et al., 2015). In the current study, NaOH solution was used to increase the column aqueous phase to a pH of 10-12 (**Figure 39**). This pH was selected because it was the maximum pH of the influent of AHA columns; however, the pH of Soil C AHA columns dropped to pH 8 during treatment (**Figure 39**). Nevertheless, differences in pH across AC, HA, pHC, and AHA columns in Soil C, AC present an opportunity to evaluate the impacts of pH-dependent effects on PFAS mobilization. Detailed discussion of Soil A columns is not included in this section due to failure of the pHC and AHA columns.

An interesting outcome of this study that was not evident in prior batch systems, was that alkaline pH alone led to the most rapid and complete recovery of total PFAS in Soil C eluants relative to any other condition (e.g., AC, HC, HA, and AHA). Mobilization of individual groups of PFAS (e.g., PFSAs, PFCAs, precursors) differed, and this is discussed further below. Application of highly alkaline conditions in an in-situ scenario may not be practical, but these results suggest that alkaline soil washing might be a viable approach to ex situ soil remediation. Although, alkaline pH was the most effective at total PFAS recovery in Soil C, this may not always be the case for soils high in zwitterionic PFAS, as will be discussed below.

Increased total PFSA recovery at elevated pH was primarily attributable to C7 and higher homologues. In the first 2 pore volumes of both AC and pHC columns, 100% of PFBS (C4) and PFHxS (C6) were recovered. In contrast, 100% of PFOS (C8) was recovered in the first 4 pore volumes of pHC columns but not until 78 pore volumes in AC columns. Similarly, 100% of PFDS (C10) was recovered by the completion of column experiments (168 pore volumes) in pHC columns, but only 18% of total PFDS mass was recovered over the entire experimental duration in AC columns. As mentioned above, both electrostatic factors and DOC-facilitated transport may contribute to increased mobilization of anionic PFAS at alkaline pH. The two mechanisms cannot be separated from each with the current data set, but aqueous organic carbon analysis did demonstrate enhanced DOC with increasing column pH (**Figure 40**).

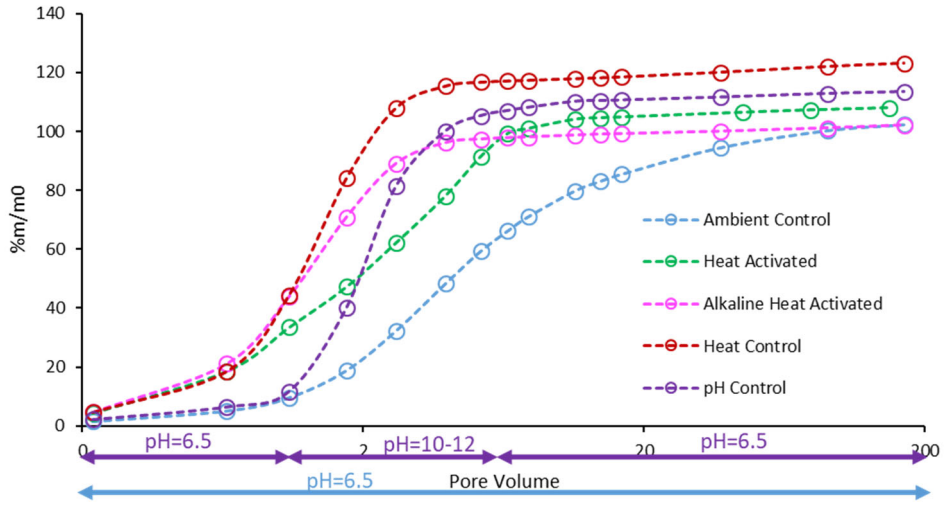

Figure 39. Percent PFSA mass eluted in Soil C column effluents. Note, the purple arrows show change in pH of PHC effluent and blue arrow shows pH of AC effluents.

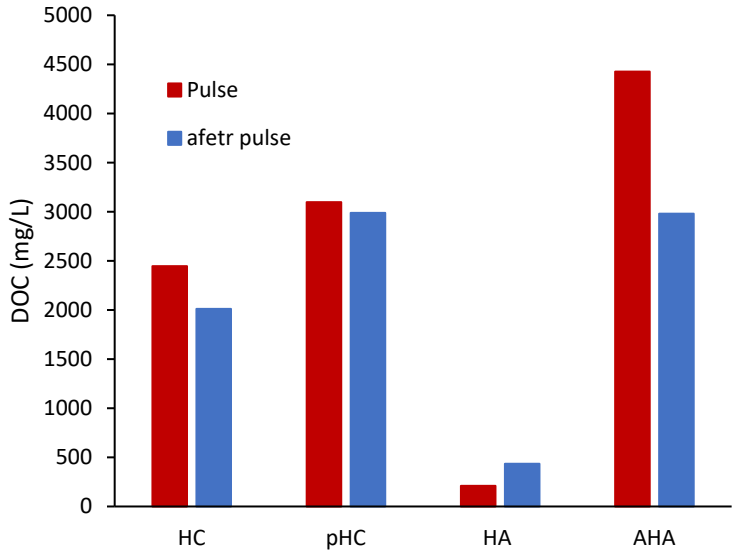

Figure 40. Effluent DOC during pulse (0.2<pore volume<2.6) and after pulse (2.6<pore volume< 5.2) in Soil C columns.

Overall, precursors also demonstrated enhanced recovery in pHC columns, but this is largely attributable to the individual precursors present, and may not be universally true in soils with different precursor composition. In pHC columns, 87% of the total precursor mass was recovered by pore volume 8 and 97% by pore volume 168. Only 37% of total precursors in AC columns were recovered by pore volume 168. Analysis of the individual precursors present demonstrated that this mobilization was due to enhanced recovery of 2 PFAS classes, n:2 FTSs and FASAs, which are both anionic under the conditions of pHC columns and comprised 125-172% (n:2 FTS) and 109-111% (FASAs) of the total precursors in Soil C AC and pHC columns. Under all pH conditions studied, n:2 FTSs are anionic, so enhanced mobilization observed in pHC columns (**Figure 41**) has the same potential mechanistic explanation as PFSAs (e.g.,

electrostatic, DOC-facilitated). As discussed in Section 3.5, the estimated pKa values of FASAs are in the range of the pH of AC columns indicating that these PFAS may be present in a less mobile, neutral form under ambient conditions. Therefore, mobilization of FASAs in pHC columns (**Figure 41**) was likely due to combined effects of deprotonation and the potential for electrostatic repulsion and DOC-facilitated transport.

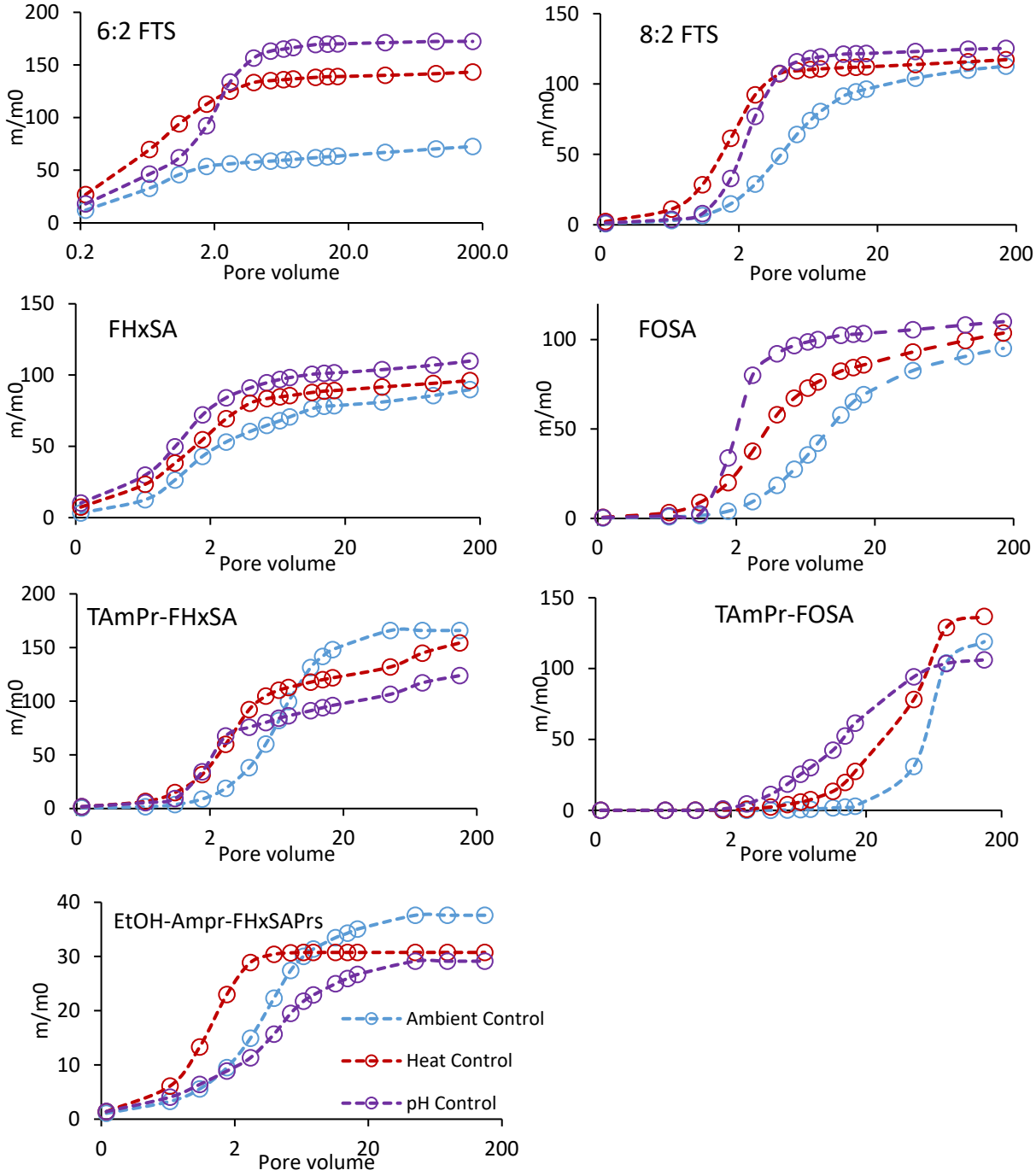

Figure 41. 6:2 FTS, 8:2 FTS, FHxSA, FOSA, TAmPr-FHxSA, TAmPr-FOSA and EtOH-AmPr-FHxSAPrS Mass fraction eluted in Soil C ambient, heat and pH controls.

High fractions of n:2 FTSs and FASAs led to overall mobilization of precursors at alkaline pH in Soil C, but data for zwitterionic PFAS demonstrate that such mobilization may not always be observed in soils with different PFAS composition. In pHC columns, rates of C6 and C8 TAmPr-FASAs desorption were enhanced in pHC columns relative to AC columns during the alkaline pH pulse (Figure S16). In contrast, desorption of EtOH-AMPr-FHxSAPrS was slower under alkaline conditions in pHC columns relative to AC columns and overall recovery decreased from 37% at lower pH (AC columns) to 29% at elevated pH (pHC columns; **Figure 41**). These trends are likely due to changes in protonation of these zwitterionic classes. For example TAmPr-FASAs have net neutral charge at pH>6.8 (negative sulfanomide functional group and positive terminal positive dimethyl amino group, **Figure 42a**), therefore the majority of C6 and C8 TAmPr-FASA are net neutral at alkaline pH of pHC. EtOH-AMPr-FHxSAPrS was also zwitterion at pH of pHC control (negative sulfonyl group and positive dimethyl amino group, **Figure 42b**), however sulfonyl is a terminal functional group located on the propyl sulfonyl branch while dimethyl amino group is located in fluorinated molecule backbone. Slower desorption of this compound at alkaline pH suggests probable significant increasing ionic interaction between positive amino group and negatively charged soil surface at alkaline pH and insignificant ionic repulsion because of sulfonyl group. These results demonstrate that in soils containing a high fraction of zwitterionic classes of PFAS (e.g., some AFFF source zones), alkaline pH alone may not be an effective mobilization or soil washing approach, whereas combination with persulfate transformation to terminal PFCAs would enhance mobilization.

In both pHC and AC columns of Soil C, 90% or more of total PFCAs were recovered in the first 3 pore volumes of column operation. These results are consistent with observations in batch studies that demonstrated that PFCAs were highly mobile at all pH levels, again highlighting PFCAs as transformation endpoint for total PFAS mobilization (Shojaei et al., 2021). However, in pHC columns, the total PFCA mass increased 200%, including PFBA (208% recovery), PFPeA (253% recovery), PFHxA (300% recovery), and PFHpA (269% recovery). Additionally, in pHC columns 6:2 FTSAPr-DiMeAn precursors had a recovery of 67%. This suggests PFCA generation, and as mentioned, studies have shown that abiotic hydrolysis of FT-based PFAS is possible at pH 10-12 (Lakshminarasimman et al., 2021; Washington and Jenkins, 2015; Washington et al., 2015). We hypothesize that this led to the increases in PFCAs observed in Soil C pHC columns indicating that while alkaline pH alone may not be able to enhance desorption of all precursors, it could potentially provide a mechanism of transformation to more mobile transformation products.

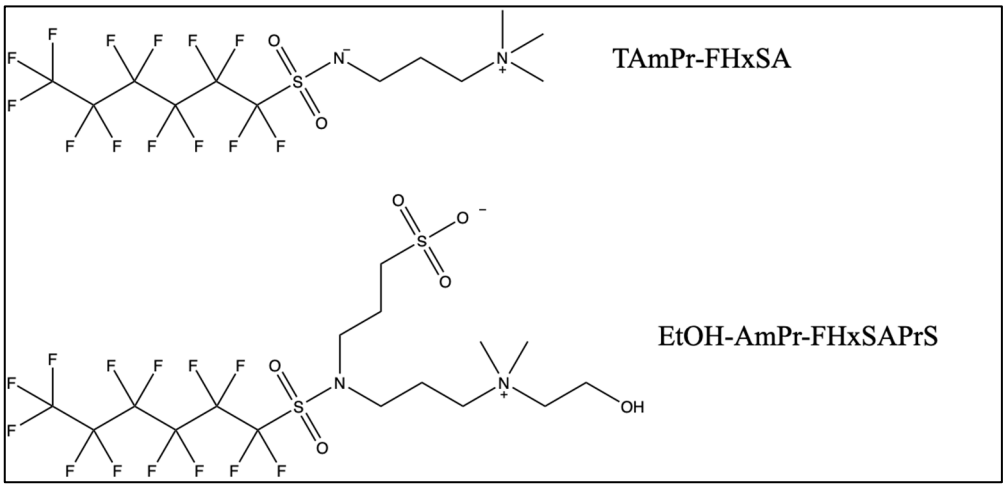

Figure 42. Ionization of TAmPr-FHxSA and EtOH-AmPr-FHxSA in pHC.

Effect of Heat. In the current study, HC columns were used to isolate the impacts of heat on PFAS transport similar to prior batch studies (Shojaei et al., 2021). Heat in the absence of any other treatment (i.e., persulfate) may impact mobilization by increasing the rate of desorption. Studies have also shown that application of heat (85-90 °C) during sludge pelletization led to degradation of the hydrocarbon portions of precursors and subsequent generation of PFSAs and PFCAs (Lakshminarasimman et al., 2021; Washington and Jenkins, 2015; Washington et al., 2015; Tebes-Stevens et al., 2017). In prior batch work, heat primarily influenced the desorption rates of C4-C8 PFSAs and some precursors. Similar results were observed in columns. PFCAs did not exhibit overall enhanced desorption in the presence of heat in either soil (**Figure 43**). In both Soils C and B, total PFSA recovery increased in HC relative to AC columns (**Figure 44**). Total PFSA recovery increased by 68% in the HC columns of Soil C and by 46% in Soil A, primarily due to increases in desorption of C7-C10 PFSAs. Shorter PFSAs exhibited similar desorption in AC and HC columns. Heat also increased recovery of total precursors in Soil C by 18% in HC columns relative to AC. Data from individual precursors demonstrated that this mobilization applied to PFAS with varied charge including n:2 FTSs, FASAs, TAmPr-FASAs, and EtOH-AmPr FHxSAs during the heat pulse (**Figure 41**). Precursor desorption in Soil A did not change significantly in the presence of heat, but Soil A had minimal precursor concentration relative to Soil C.

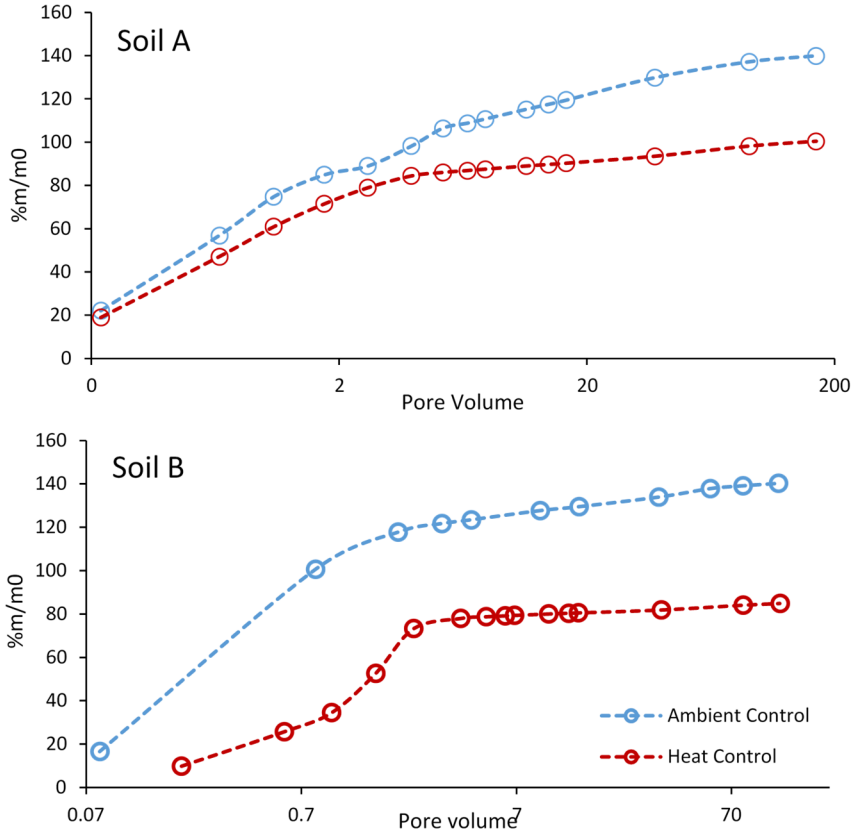

Figure 43. PFCA percent mass fraction eluted in Soil C and A ambient and heat controls.

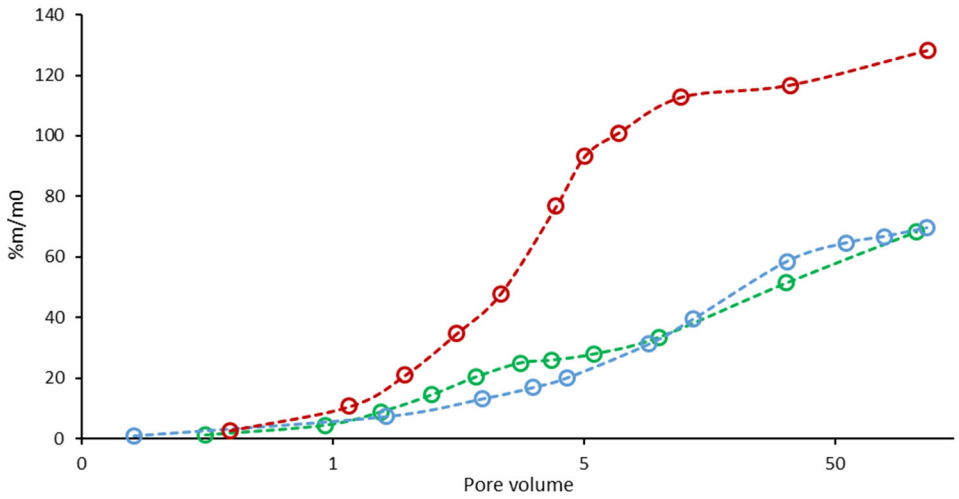

Figure 44. Percent PFSA mass eluted in Soil A column effluents.

The total mass balance of PFSAs in HC columns of Soil A was 160%, suggesting generation. One potential explanation is high temperature, abiotic hydrolysis, which has been observed during pelletization of biosolids (Lakshminarasimman et al., 2021; Washington and Jenkins, 2015; Washington et al., 2015; Tebes-Stevens et al., 2017). In Soil A, total PFSA recovery was primarily attributable to PFOS (176%) and PFHxS (149%), which is consistent with the dominant precursor chain lengths present in the untreated soil. Enhanced recovery of PFSAs was not observed in Soil C HC columns, but intermediate transformation products including PFHxSi and PFOSi increased by 190% and 250%, respectively, potentially due to partial abiotic transformation under heated conditions. Additional work with simpler (i.e., single PFAS precursor) systems would be needed to better evaluate if abiotic hydrolysis explains these trends in HC columns. Overall, the extent of precursor degradation in HC columns was minimal. Mass balances on the soil and eluant recovery of total precursors in Soils A and B HC columns were 74% and 117%, respectively (**Table 15**). Overall, results support prior conclusions of batch work which indicated that heat alone may have utility as a tool for enhanced desorption, particularly in soil washing scenarios where temperature control may be more feasible. High-temperature, abiotic hydrolysis may occur, but at temperatures in this study (60°C), this is likely to provide only a minimal additional contribution to overall PFAS mobilization.

Release Simulation. Release simulations focused on two PFSAs in Soil C columns and used model fits to PFOS and PFNS data to obtain values of K_d under the various control conditions (**Figure 45 and 46**). PFSAs were used because their total mass remained constant under all conditions in Soil C (e.g., they were not degraded or generated during persulfate treatment). Simulations of PFAS within other classes (e.g., PFCAs) were not conducted because their total mass changed under certain column conditions and because the objective of simulations was to further explore impacts of heat and pH. Simulation results indicated that all treatments (heat, pH, heat activated persulfate, and alkaline heat activated persulfate) led to decreases in K_d and a corresponding increase in recovery of both PFOS and PFNS (**Table 16**). The greatest reductions in K_d occurred under heated (HC) and alkaline (pHC) conditions. Since HC, HA, and AHA columns all received the same level and duration of heat, it was expected that the largest reductions in K_d would occur in AHA columns of Soil C, which had the highest pH and DOC concentrations and the greatest soil f_{oc} reduction of these 3 column types. However, lower PFOS and PFNS K_d was calculated in HC than AHA columns which is consistent with results of the batch experiment**.** Stronger sorption of long chain PFSAs in AHA columns vs. HC may be due to i) increasing concentration of divalent cations like Ca^{2+} during oxidation treatment (Higgins and Luthy, 2006; McKenzie et al., 2015), ii) change in soil OC

composition by oxidizing polar amorphous OC while less polar hard condense OC stays unchanged (Weber et al., 1999; Cuypers et al., 2002), iii) less competition for sorption on sites after degradation of precursors to more mobile PFCAs. Modelled K_d values for PFOS and PFNS in pHC columns were lower than AHA columns. This suggests that the highly alkaline pH (10-12) in pHC columns was a greater factor in mobilizing PFSAs than combined effects of heat and organic carbon mobilization in AHA columns. Of the two persulfate treated conditions (AHA and HA), the greatest reductions in K_d occurred in AHA columns, which had a higher pH relative to HA conditions. Overall, these results highlight that applying oxidation pre-treatment can result in increasing mass transport of long chain PFSAs. However, if the objective is washing impacted soil, applying heat or highly alkaline pH alone may lead to higher desorption of long chain anionic PFAS from impacted soils.

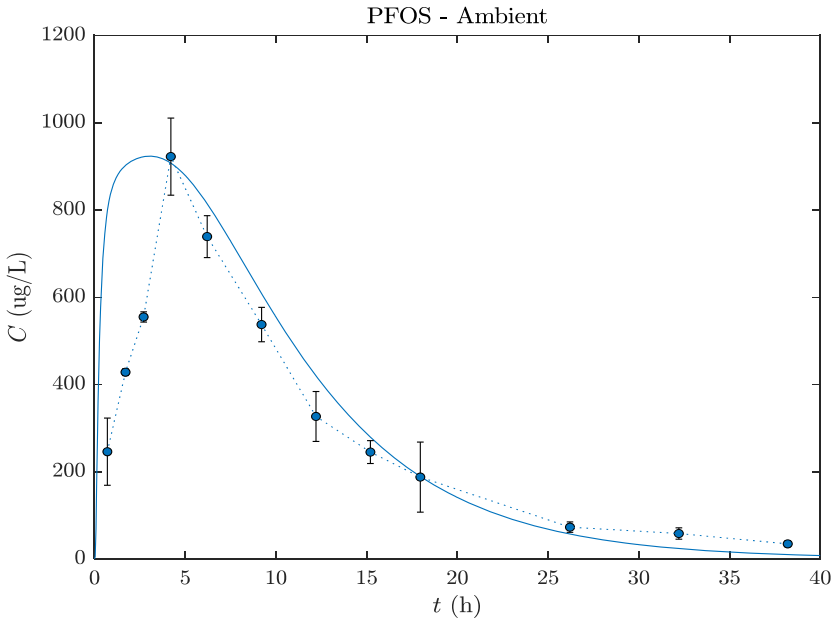
PFOS - Ambient
C (ug/L)
t (h)

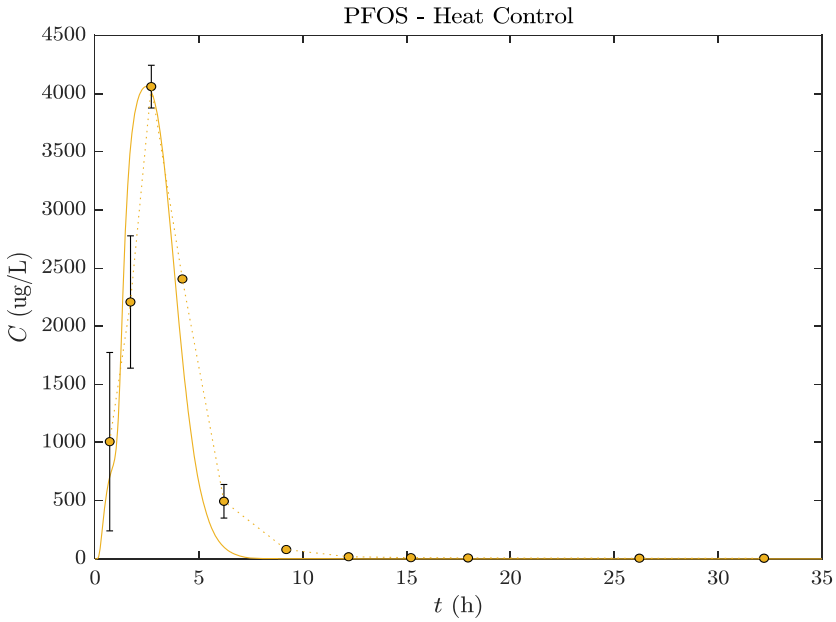
PFOS - Heat Control
C (ug/L)
t (h)

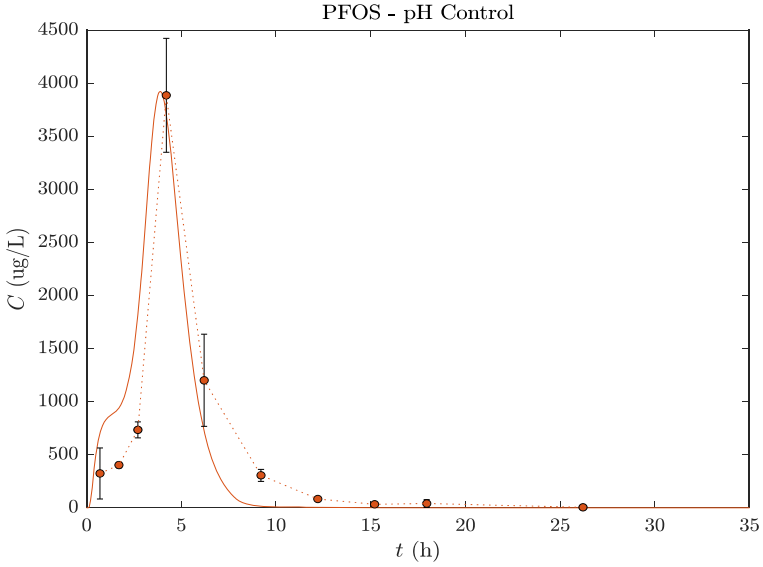
PFOS - pH Control
C (ug/L)
t (h)

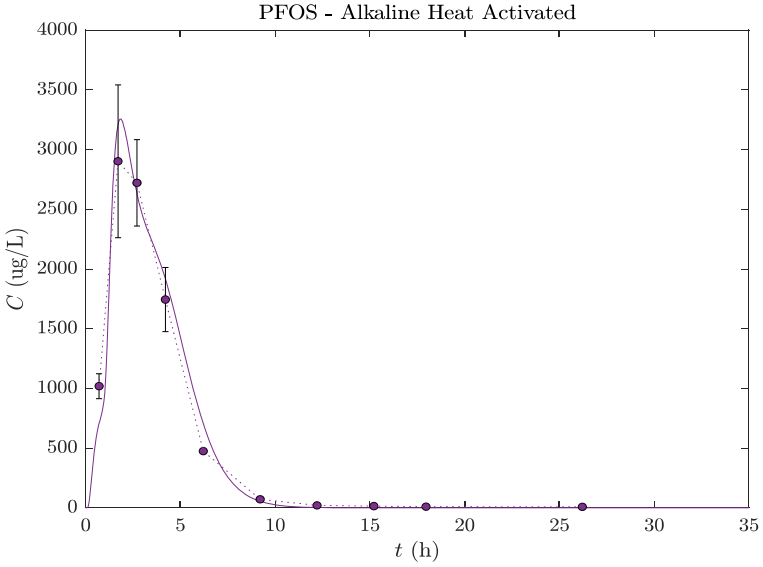
PFOS - Alkaline Heat Activated
C (ug/L)
t (h)

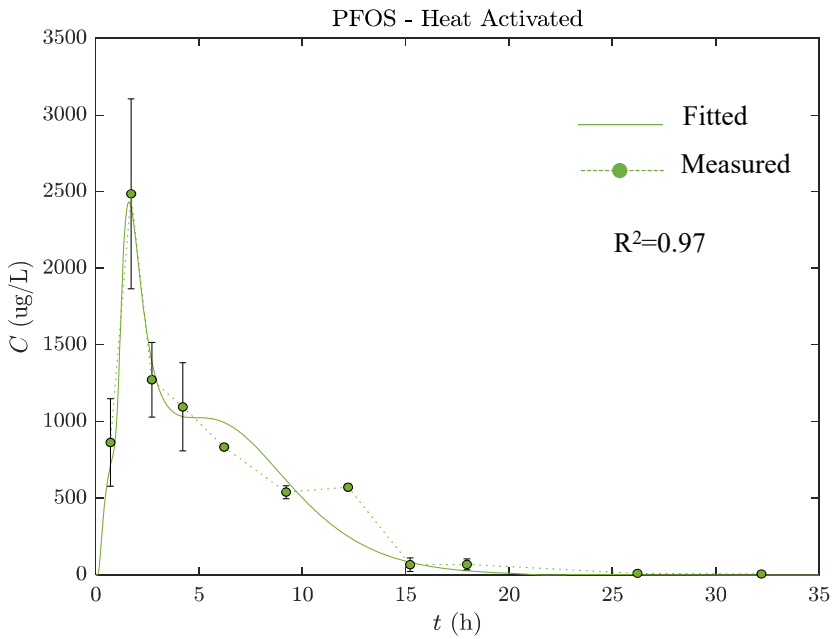

Figure 45. Predicted and measured PFOS breakthrough curves in Soil C columns.

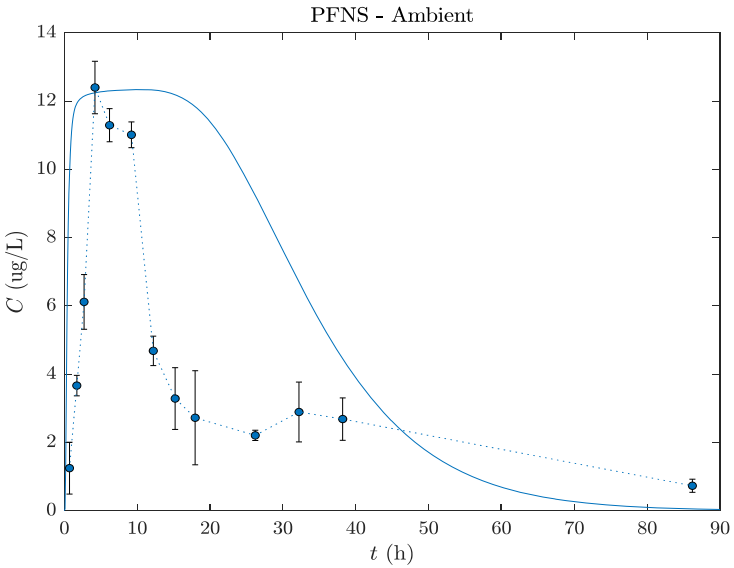
PFNS - Ambient
C (ug/L)
t (h)
0
2
4
6
8
10
12
14
0
10
20
30
40
50
60
70
80
90

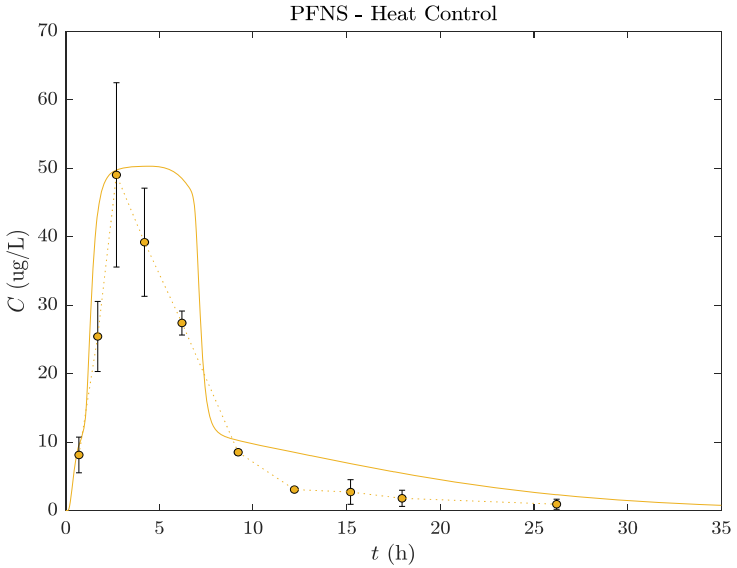
PFNS - Heat Control
C (ug/L)
t (h)
0
10
20
30
40
50
60
70
0
5
10
15
20
25
30
35

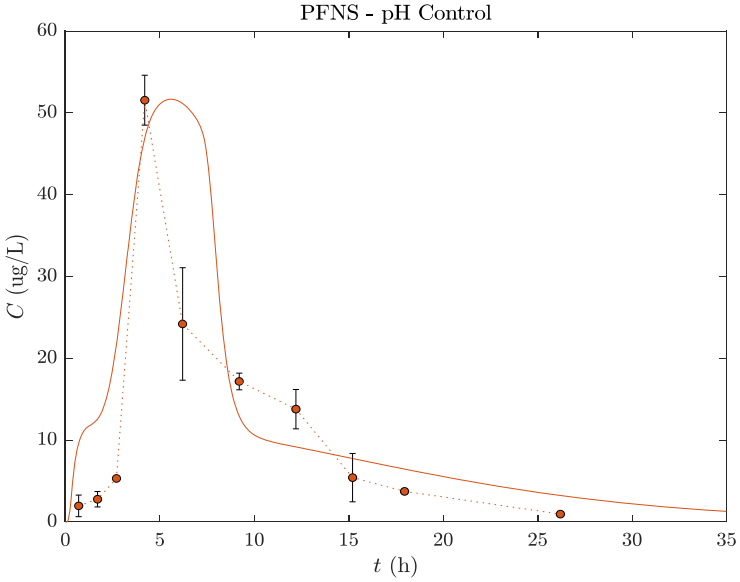
PFNS - pH Control
C (ug/L)
t (h)
0
10
20
30
40
50
60
0
5
10
15
20
25
30
35

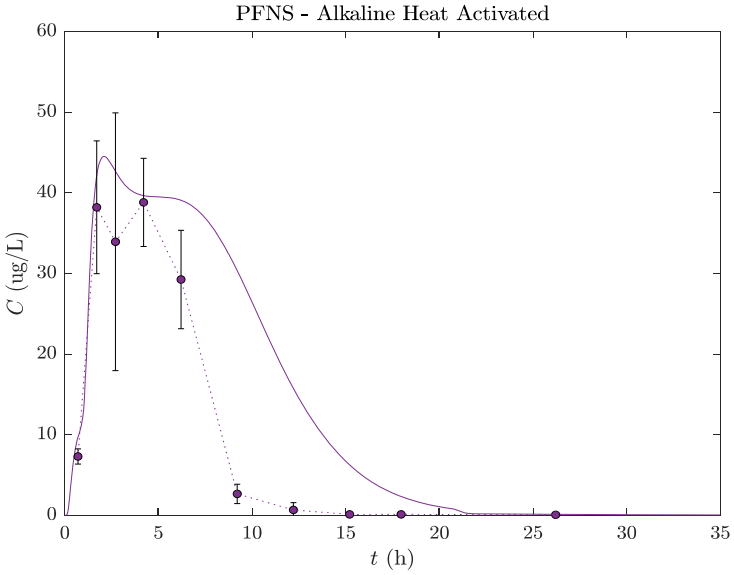
PFNS - Alkaline Heat Activated
C (ug/L)
t (h)
0
10
20
30
40
50
60
0
5
10
15
20
25
30
35

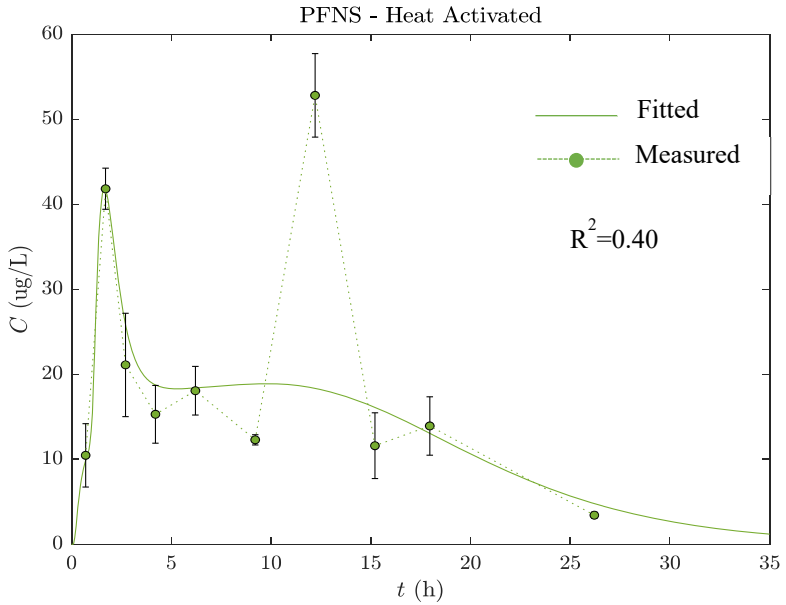

Figure 46. Predicted and measured PFNS breakthrough curves in Soil C columns.

Table 16. Calculated PFOS and PFNS K_d in Soil C columns.

Compounds	Ambient Control	Heat Control	pH Control	Alkaline Heat Activated	Heat Activated
PFOS	1.15	0.09	0.19	0.24	0.70
PFNS	3.50	0.70	0.85	1.35	1.80

Transport Cell Column Oxygen Sparging Oxidative Experiments. *PFAS Mass Balance.* Concentrations of PFAS measured in eluates and soils after the completion of column experiments were used to calculate mass balances on total PFAS recovery in column experiments. In Soil C, total PFAS mass balances in all columns were 70-100% (**Figure 47**), suggesting no PFAS losses during column experiments. PFSA mass balances were in the range 70-100%, so there was no evidence for generation of PFSAs, consistent with batch experiments. PFCA mass recoveries in Soil C were 121%, 138% and 143% in O_2-sparged, N_2-sparged, and ambient controls, respectively. Effluent mass recovery of perfluoropentanoic acid (PFPeA), perfluorohexanoic acid (PFHxA) and perfluoroheptanoic acid (PFHpA) in all column types and perfluorodecanoic acid (PFDA) in O_2- and N_2-sparged columns was greater than 140 %. Due to occurrence across multiple column conditions and early in the experimental duration (Days 1-2), over recovery of these PFCAs is not attributable to enhanced precursor biotransformation under O_2-sparged conditions. Mass balance of perfluorobutanoic acid (PFBA), perfluorooctanoic acid (PFOA) and perfluorononanoic acid (PFNA) were in the range of 95-130% (**Table 17**), indicating there was no significant generation resulting from biotransformation. Mass recoveries of precursors in Soil C were also in the range considered to be complete (70-85%) in all column types suggesting little to no precursor biotransformation. As mentioned, n:2 FTSs and FASAs are biotransformation intermediates (Harding-Marjanovic et al., 2015; Mejia-Avendaño et al., 2016), and their effluent mass recoveries were also complete. Recoveries of 6:2 FTS and 8:2 FTS were 80-120% and 121-137% respectively. Based on a student t-test, there was no statistical difference in 6:2 FTS mass results across column types ($p>0.05$). Similarly, mass balances of C6 and C8 FASAs in Soil C were in the range of 131-143% and 120-136%, respectively, and effluent concentrations in different column types were not statistically different from each other. Overall, column results were not consistent with batch results, and there was no evidence in the mass balances of enhanced biotransformation of precursors in O_2-sparged columns.

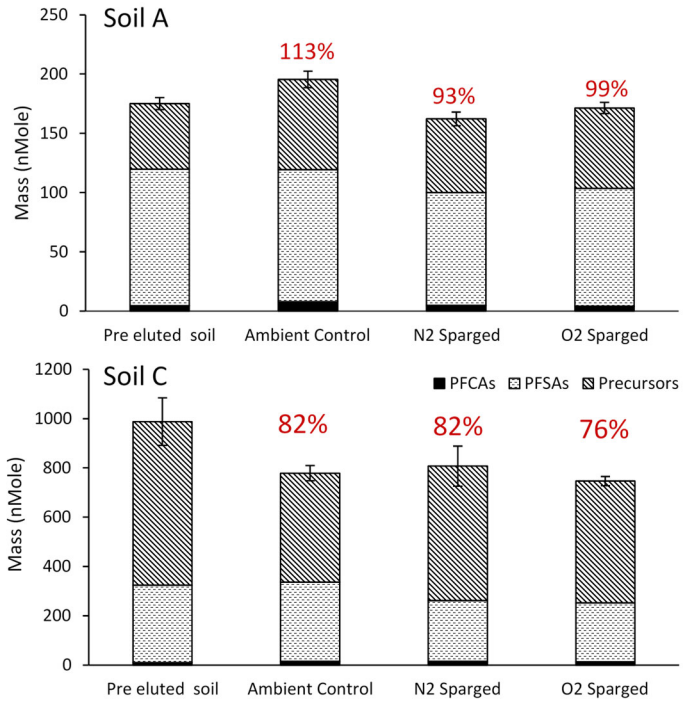

Figure 47. Composition of PFCAs, PFSAs, and precursors in Soil A and C pre- eluted soils, Ambient controls, N_2- sparged columns, and O_2-sparged columns. Percentage mass balance for each column shown in red numbers.

Table 17. Summary of % PFAAs mass balance relative to pre elution soil concentration in Ambient Control (AC), N_2- sparged (N_2), and O_2- sparged (O_2).

Compound	Soil C			Soil A		
	AC	N_2	O_2	AC	N_2	O_2
PFBA	130	146	146	170	88	81
PFPeA	179	176	163	295	100	67
PFHxA	199	207	180	241	152	97
PFHpA	180	235	207	182	94	117
PFOA	140	121	109	135	114	140
PFNA	105	113	99	108	138	142
PFDA	96	138	142	137	68	68
PFUdA	ND	ND	ND	26	28	52
PFDOA	ND	ND	ND	62	55	60
PFTrDA	ND	ND	ND	75	65	64
PFTeDA	ND	ND	ND	61	46	48
PFBS	138	145	118	148	117	108
PFPeS	130	121	104	135	101	92
PFHxS	155	134	127	136	94	105
PFHpS	58	60	61	134	139	120
PFOS	102	79	76	99	83	87
PFNS	70	51	47	72	77	83
PFDS	35	29	24	62	72	78

Results of total PFAS, PFSA, and PFCA mass balances in Soil A were similar to those in Soil C. Total PFAS mass balances in Soil A columns were between 90-110% (**Figure 47**). PFSA mass balance were in the range of 80-100%, and as shown in **Table 17**, mass balances of C4-C10 PFSAs were in the range of 50-100%, suggesting no PFSA generation due to biotransformation of ECF-based precursors with sulfonamide functionality (e.g., FASAs). PFCA mass balances in Soil A N_2- and O_2- sparged columns were 104% and 97% respectively, however the average mass balance in ambient control columns was 171%. High mass balance of PFCAs in ambient controls was attributable to over recovery of C3 (PFBA)-C6 (PFHpA) PFCAs. High recovery of C3-C6 PFCAs (147-278%) occurred in effluents collected on day 1, suggesting it was not caused by biotransformation in the control. Average concentration of replicate columns was used for mass balance calculations, higher variability of N_2- and O_2- sparged column duplicates led to lower PFCA mass balance in those column type in compare with ambient controls. However, considering standard deviation, result of student t.test showed measured PFCA mass in Soil A all column types were not statically different each other.

Similar to Soil C, TOP assay results demonstrated that total precursor mass balances in Soil A columns were 113%, 124%, and 139% in N_2-sparged, O_2-sparged and ambient control respectively, indicating no precursor transformation. Unlike Soil C, recovery of n:2 FTSs and FASAs suggested that partial biotransformation of parents to polyfluoroalkyl intermediates may have occurred. Specifically, 6:2 FTS mass balances showed 311%, 170%, and 61% recovery in ambient control, N_2-sparged and O_2-sparged columns respectively. This suggests generation of 6:2 FTS in ambient control and N_2-sparged columns and degradation of 6:2 FTS in O_2-sparged columns.

Based on biotransformation pathways reported in Harding-Marjanovic et al. (2015), biotransformation of 6:2 fluorotelomer thia propanoamido dimethyl ethyl sulfonate (6:2 FTTh-PrAD-DiMeEtS, 6:2 FtTAoS in

prior work (Harding-Marjanovic et al., 2015)) generates 6:2 FTS followed by transformation to 5:3 fluorotelomer carboxylic acid (5:3 FTCA) and 6:2 UFTCA. 6:2 FTTh-PrAD-DiMeEtS was not detected in Soil A; however Soil A contained 6:2 fluorotelomer sulfonyl propanoamido-dimethylethyl sulfonate (6:2 FTSO2PrAd-DiMeEtS), which is a transformation intermediate in the pathway proposed in prior work. [4] Moreover, Soil A contained structurally similar precursors such as 6:2 fluorotelomer thia ethanamido propyl dimethyl ammonium (6:2 FTTh-EtADPrAm), 6:2 fluorotelomer sulfonamido propyl dimethyl amine (6:2 FTSAPr-DiMeAn) and 6:2 fluorotelomer sulfinyl propanamido dimethyl ethyl sulfonate (6:2 FTSO-PrAd-DiMePrS) which may yield 6:2 FTS as an intermediate transformation product. Results of FTSO2PrAd-DiMeEtS showed slight mass decrease in both O_2- and N_2-sparged columns (63% and 50% recovery, respectively) relative to ambient controls (78% recovery). Notably only 7% of 6:2 FTSAPr-DiMeAn mass was measured in both O_2- and N_2- sparged columns and 14% in ambient control columns, suggesting it may have biotransformed to 6:2 FTS. 6:2 FTSO-PrAd-DiMePrs mass increased in O_2- and N_2- sparged columns potentially as a result of partial biotransformation of 6:2 FTTh-PrAD-DiMeEtS. Soil A has not contained 6:2 FTTh-PrAD-DiMeEtS, however it was detected just in increment 3 (**Figure 48**) of O_2- sparged post elution soil with concentration <LOQ, suggesting generation of this compound in O_2 Sparged columns. Therefore, it is possible generation of 6:2 FTTh-PrAD-DiMeEtS was followed by its degradation to 6:2 FTSO-PrAd-DiMePrs in O_2- sparged columns. Approximately 181%, 147% and 127% of 6:2 FTSO-PrAd-DiMePrs was recovered in O_2- sparged, N_2-sparged, and ambient controls, respectively. Other intermediates (e.g., 5:3 FTCA and 6:2 UFTS) were not detected in column effluents and post elution soils which may indicate that biotransformation did not proceed to these intermediates during the time frame of the column experiments.

PFAS Release. The fraction of PFAS eluted in effluent was calculated by measuring total mass recovered in aqueous column samples divided by the PFAS mass in pre-elution soil. In Soil C, 63%, 64%, and 65% of PFAS mobilized in ambient control, O_2-sparged and N_2-sparged columns respectively, further demonstrating that oxygen sparging did not increase PFAS mobility (**Figure 49 and Figure 50**). Total PFAS recovery included 122-143% elution of PFCAs and 75-90% elution of PFSAs and 41-59% elution of precursors with similar recovery in all column types considering standard deviations (**Table 18**, **Figure 50 and 51**). Similar to Soil C, the fraction of PFAS eluted from all three types of Soil A columns were similar and biosparging did not result in higher PFAS release in the Soil A O_2- Sparged columns (**Figure 49**). Similar fraction of PFSAs (67%-77%) and precursors (90-100%) were recovered in effluent of Soil A all column types (**Table 18**). Higher precursors concentration was measured in ambient control effluent in day 1 (**Figure 52c**, first 5 pore volumes) in relative to sparged columns, however, an earlier higher concentration does not necessarily correlate to a higher total mass eluted (**Figure 52c).** 50% of total eluted precursor recovered in first 6 days of experiments. Suspect screening result of effluent in all column types showed release of precursors in the first 10 days and after that no suspect PFAS detected in effluent. This could be because of slow release of precursors after day 10 which resulted in effluent concentration smaller than detection limit. For example, 6:2 FTSAPr-DiMeAn was the only suspect detected in O_2- sparged 106-576 pore volume (day13-79) which its concentration was <LOQ, this compound was not detected in N_2 sparged and ambient control effluents. Slow biotransformation of precursors to intermediate polyfluoroalkyl substances and their low concentration in effluents could be another possibility for inconsistency between effluent TOP and suspect screening results.

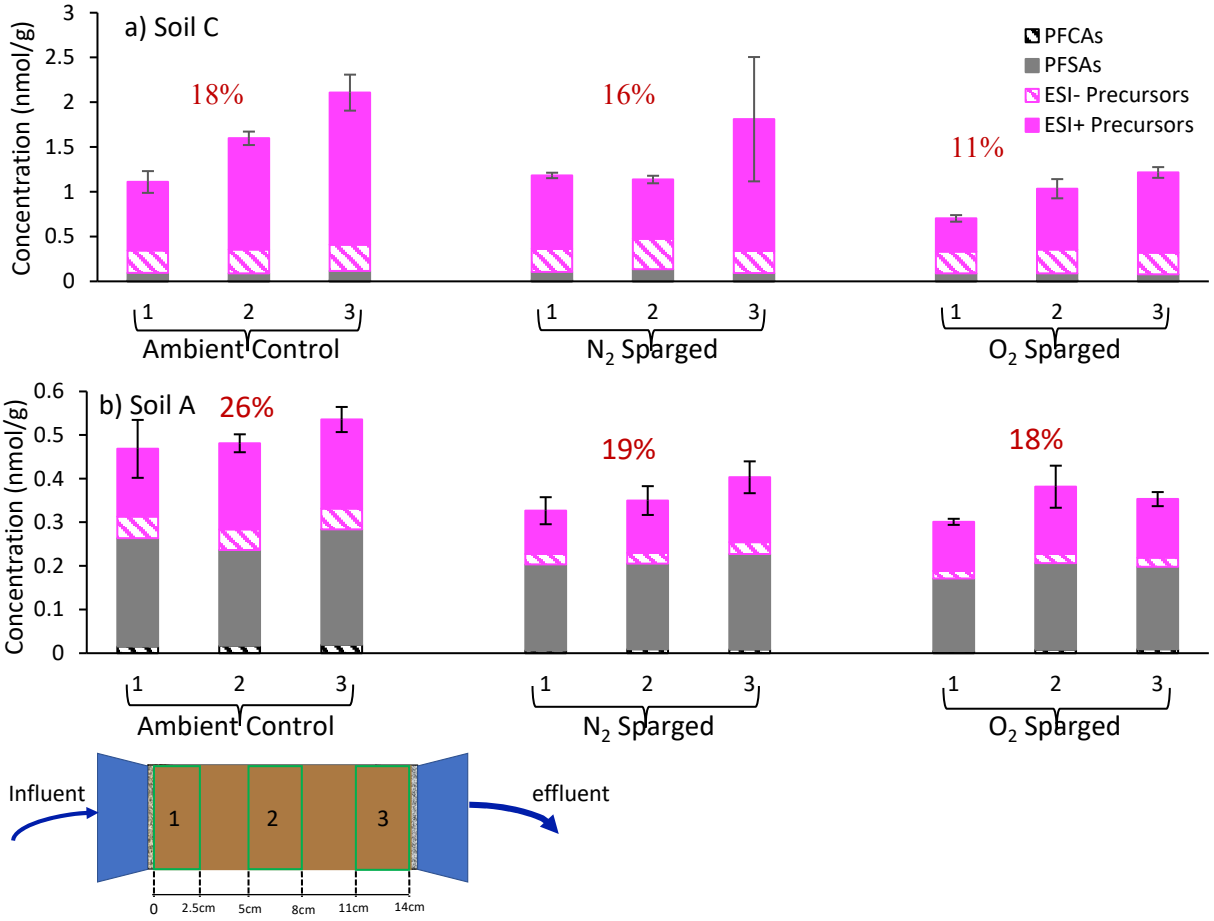

Figure 48. PFAS total Concentration in soil C (panel a) and soil A (panel b) in post elution soil. Percentages are fraction of total PFAS remained in post elution soils.

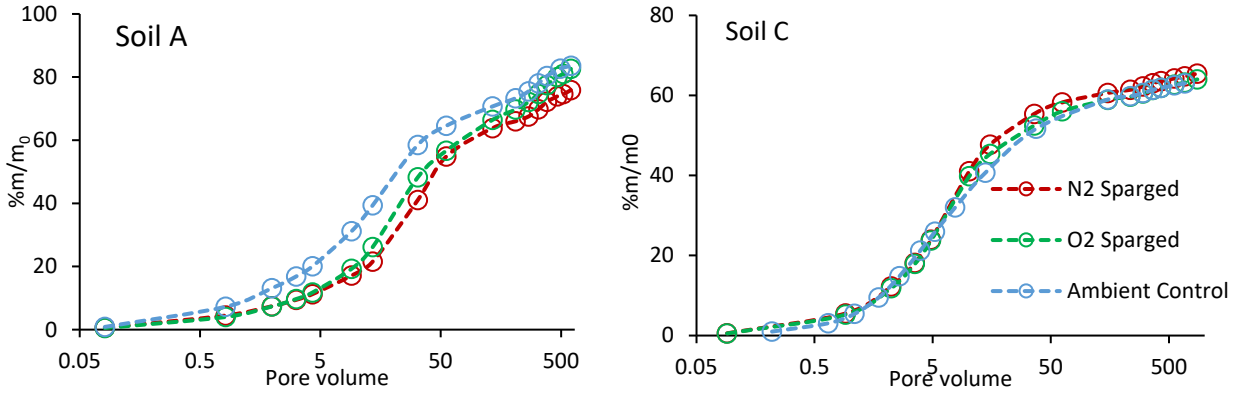

Figure 49. Fraction (m/m_0) of total PFAS recovered in Soil C and A column effluents.

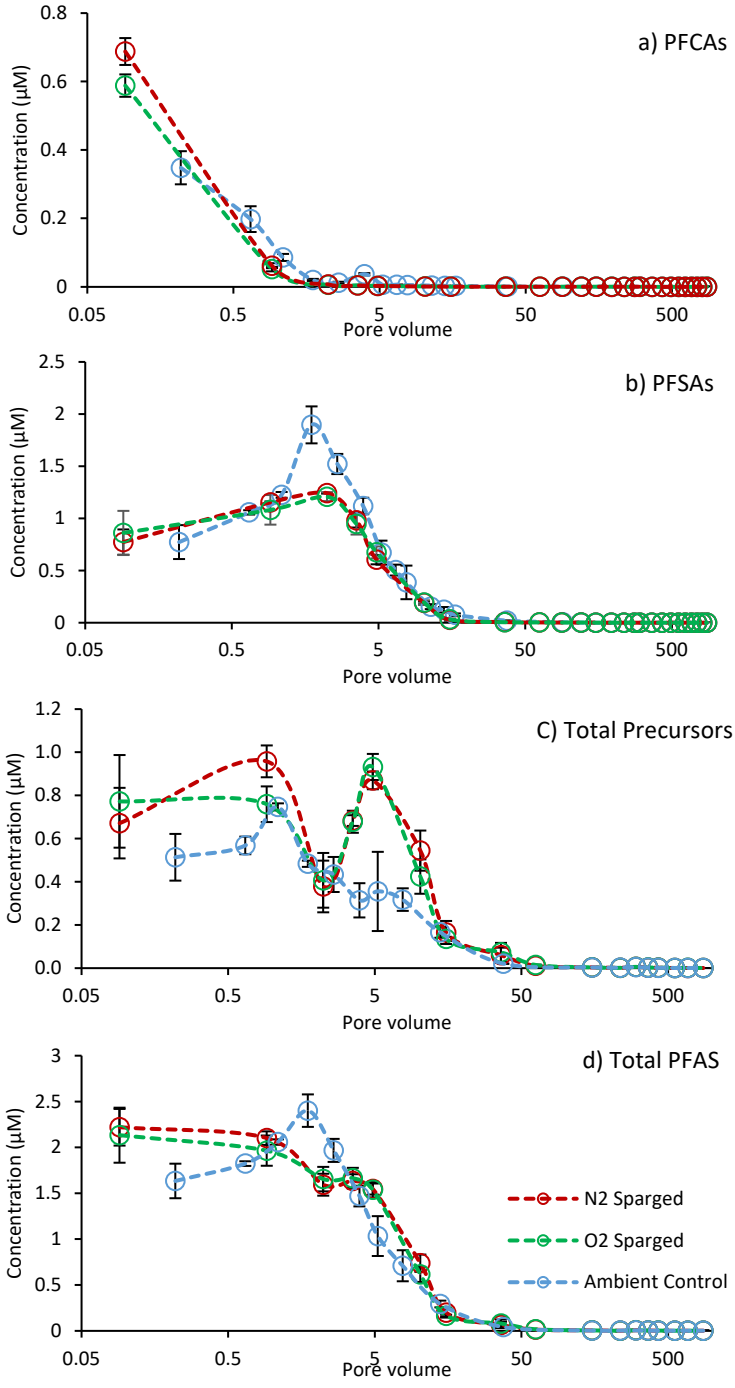

Figure 50. PFCA (panel a), PFSA (panel b) total precursors (panel c) and total PFAS (panel d) effluent concentration over pore volume in soil C columns.

Table 18. Summary of PFAS mass balance relative to pre elution soils in all column types.

PFAS	Ambient control (%)	N_2- sparged (%)	O_2- sparged (%)
Soil C			
PFCAs	156	152	136
PFSAs	102	78	76
Precursors	67	82	74
Total	82	82	76
Soil A			
PFCAs	171	103	91
PFSAs	97	83	87
Precursors	137	113	124
Total	113	93	99

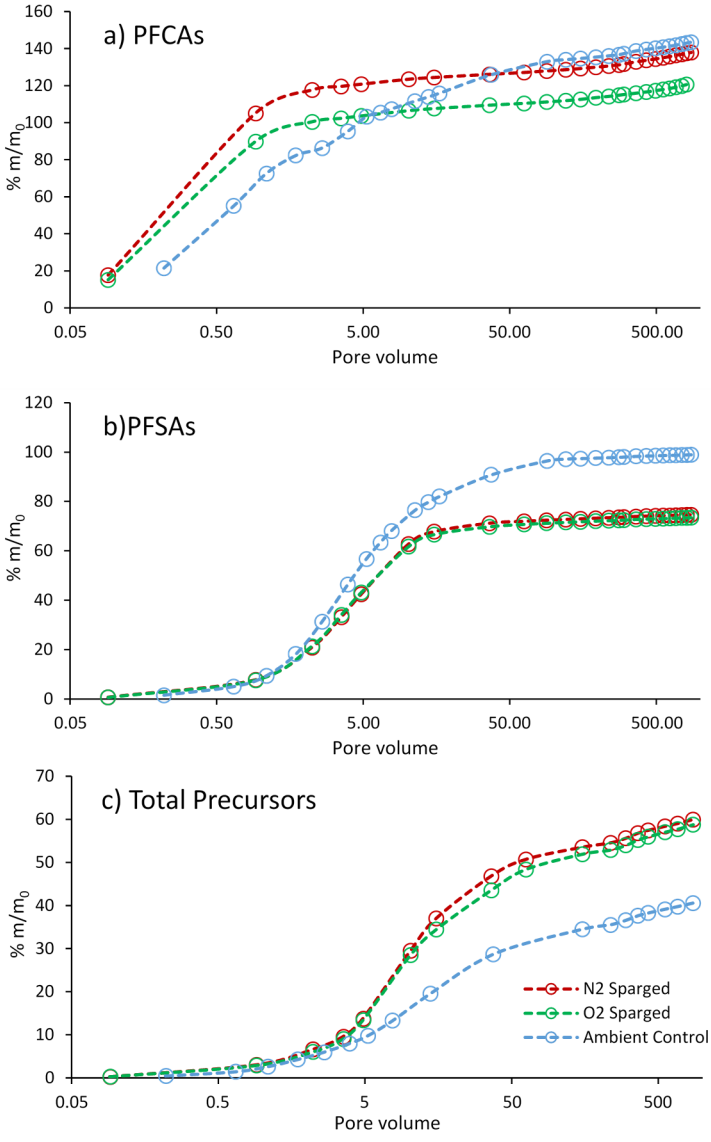

Figure 51. Percent PFCA (panel a), PFSA (panel b) and total precursors (panel c) mass eluted in soil C column effluents.

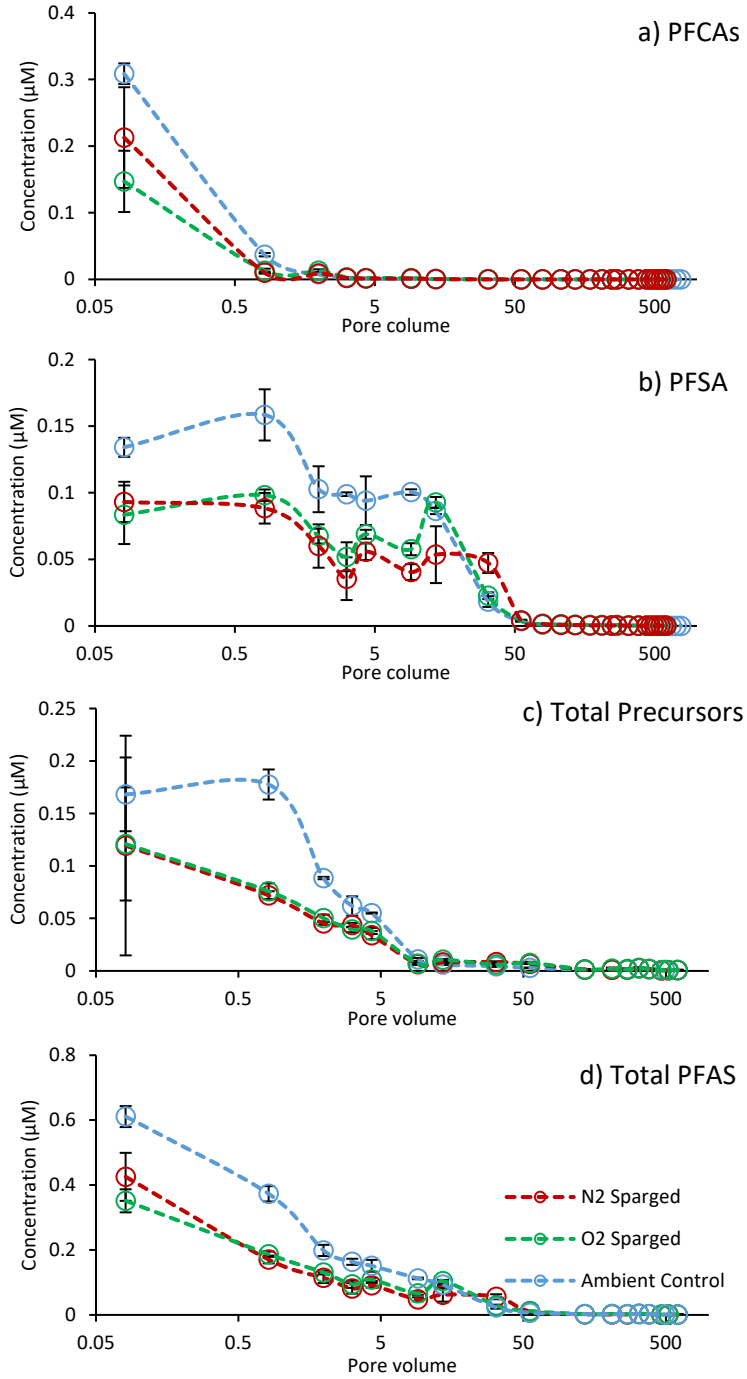

Figure 52. PFCA (panel a), PFSA (panel b) total precursors (panel c) and total PFAS (panel d) effluent concentration over pore volume in Soil A columns.

PFAS in Post Elution Soils. Characterization of post elution soils showed 18-29% (Soil A) and 12-19% (Soil C) of total PFAS remained soils at the conclusion of column experiments (**Figure 48**). Overall lower retention of total PFAS in Soil C is attributed to lower f_{oc} and clay content (**Table 6**) relative to Soil A, which would lead to weaker sorption of some PFAS (Guelfo and Higgins, 2013; Barzen-Hanson et al., 2017; Higgins and Luthy, 2006; Mejia-Avendaño et al., 2020). Whereas mass balances showed evidence for enhanced precursor transformation to intermediates in Soil A, the greatest evidence for PFAS mobilization was in PFAS soil concentrations measured in Soil C columns after completion of experiments (**Figure 48**). The fraction of PFAS remaining (11%) in Soil C O_2-sparged columns was lower than either N_2-sparged (16%) or ambient control (18%) columns. After completion of experiments, nearly all (91-94%) of the PFAS remaining in Soil C columns were precursors, and the majority of precursors remaining (70-76%) were ESI+ (i.e., zwitterionic and cationic) precursors. The greatest degree of precursor removal was observed in O_2-sparged soils, and this was primarily attributable to lower concentrations of cationic and zwitterionic precursors, which were approximately 47% and 33% lower in the O_2-sparged columns relative to the ambient control and N_2-sparged columns, respectively. This suggests that O_2-sparging enhanced transformation of less mobile precursors, but since a corresponding increase in PFCAs was not observed, it is likely that mobilization occurred due to generation of anionic, intermediate precursors.

Effluent concentration of ESI+ precursors in O2 sparged columns were not statistically different from N2 sparged and ambient control effluent results and no ESI+ precursors was detected in effluents after day 13 of experiment. The total recovery of ESI+ precursors in soil and effluent in N2 Sparged and ambient control columns was ~84% and in O2 Sparged columns was ~65%. 40% of O2 sparged ESI+ precursor mass was measured in post elution soils, this percentage increases to 50% in N2 sparged and ambient control columns. Differences between ESI+ total recoveries (84% vs. 65%) as it is mentioned above was because of their lower mass in O2 sparged post elution soil in relative to N2 sparged and ambient controls. Additionally, we need to mention that the total precursors recoveries in columns were in range of 67-82%.

In addition to total PFAS results in Soil C, data for individual precursors also suggested enhanced biotransformation in O_2-sparged columns. Lower 6:2 FTS and 8:2 FTS mass remained in O_2-sparged relative to N_2-sparged and ambient control columns (**Figure 53**). Specifically, the mass of 8:2 FTS remaining in O_2-sparged columns was 30 % lower than the mass remaining in N_2-sparged and ambient control columns, However Considering standard deviation on 8:2 FTS mass showed result of columns are not statically different from each other (**Figure 53**). The mass of 6:2 FTS remaining in O_2-sparged columns was 30% and 50% lower than the mass remaining in N_2-sparged and ambient control columns, respectively. The same or lower 6:2 FTS mass recovered in O_2- sparged column effluents, therefore lower 6:2 FTS mass in O_2- sparged column post elution soil could be because of its higher biotransformation as a result of O_2- sparging.

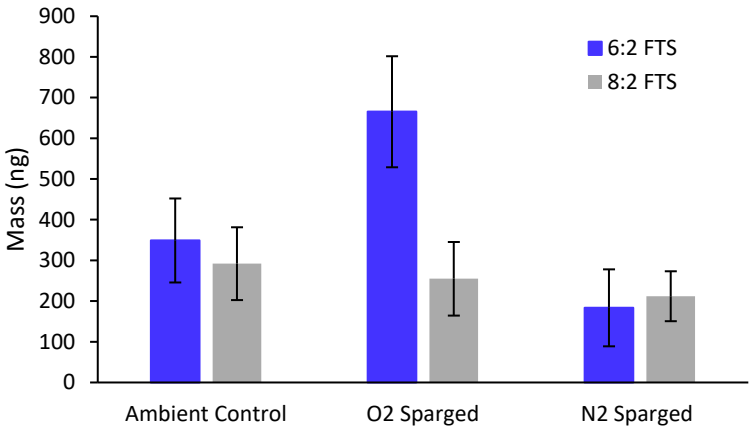

Figure 53. 6:2 and 8:2 FTS mass retained in Soil C post elution column soils.

In contrast to Soil C, post elution PFAS soil concentration in Soil A columns did not show evidence for enhanced mobilization in O_2-sparged columns (**Figure 48**). Across all column types PFSAs were the dominant PFAS class (44-57%) remaining in post elution soils, and the primary homologue was PFOS (84-91%), which is a relatively stronger sorbing PFAS (Guelfo and Higgins, 2013; Umeh et al., 2021; Kabiri et al., 2022) that will not undergo enhanced mobilization under sparged conditions. Post-elution soils in Soil A columns also contained 41-53% precursors, which were dominated by ESI+ PFAS, as seen in Soil C. Also similar to Soil C, the greatest retention of PFAS (26%) occurred in ambient control columns, but unlike Soil C, similar retention (18-19%) was observed in O_2-sparged and N_2-sparged columns (**Figure 48**).

Differences in the PFAS remaining in ambient controls and O_2-sparged and N_2-sparged Soil A columns were attributable to lower retention of ESI+ PFAS in the latter two column types. Outside of sparging, the primary difference in ambient control columns was that they sustained a higher flow rate over the experimental duration. Flow rate of N_2- and O_2-sparged columns decreased to 0.1 mL/min after day 49 as a result of clogging. Biotransformation predominantly occurs in the aqueous phase of subsurface (Zhao and Voice, 2000). Higher pour water velocity or lower the residence time may decrease the degradation rate of organic contaminants in the subsurface by higher transport of biomass (Gaber, 2004; Zheng et al., 2002). Two times higher AGW residence time in Soil A sparged columns may have led to faster precursor biotransformation and, as a result, lower precursor mass remaining in sparged soils.

Column vs. Batch Results. Results of preliminary batch experiments, clearly showed enhanced precursor loss and PFCA generation in O_2-sparged reactors, and some evidence for enhanced transformation during O_2-sparging of columns was evident in Soil A mass balances and post-elution soil PFAS concentrations in Soil C. In general, an increase in dissolved oxygen alone cannot account for enhanced biotransformation. However, if O_2-sparging is coupled with a source of nutrients, rates of aerobic biotransformation may increase (Li et al., 2019). No nutrient source was supplied during this study; however, study soils were field-collected from fire training areas, and may contain co-contaminants (e.g., hydrocarbons) that could serve as a nutrient source.

If biotransformation is occurring, the mixture of ECF- and FT-based precursors in Soils A and C could ultimately yield a mixture of terminal PFSAs and PFCAs (Harding-Marjanovic et al., 2015; Mejia-Avendaño et al., 2016; Liu and Mejia-Avendaño, 2013; Chen et al., 2020). There was no evidence for generation of terminal transformation products in column studies, but batch studies showed evidence of PFCA generation. The lack of PFSA generation may be attributable to differences in rates of biotransformation of ECF- vs. FT-based precursors as the latter are anticipated to undergo more rapid

biotransformation (Nickerson et al., 2021). However, this may also suggest a mechanism other than biotransformation. O_2-sparging may also increase concentrations of ROS, which could oxidize precursors to intermediate precursors and terminal PFCAs. Oxidation via ROS would not generate PFSAs (Plumlee et al., 2009), and this is consistent with the gain of PFCAs observed in batch reactors. Additional studies are needed to understand the role of ROS in precursor transformation during O_2-sparging.

Overall, evidence for enhanced transformation in O_2-sparged columns was less clear relative to O_2-sparged batch reactors. It is notable that a similar lack of enhanced transformation was observed in O_2-sparged columns conducted in a very similar manner in prior work (Nickerson et al., 2021). In that study, similarities in the elution of PFAS from both N_2- and O_2-sparged columns were attributed to either a greater degree of anaerobic transformation than previously suspected would occur or to the presence of enough residual DO in N_2-sparged columns to allow ongoing aerobic transformation (Nickerson et al., 2021). Based on analysis of DO levels in the current study, trends observed here and in prior work are more likely attributable to oxygen concentrations in ambient controls, N_2- sparged and O_2-sparged columns. Specifically, the data suggest that dissolved oxygen levels introduced into ambient, N_2- sparged and O_2-sparged columns in both this study prior work were much more similar than intended, leading to similar transformation and transport in all column types. This is further discussed below.

Column DO. As a result of discrepancies between observed PFAS transformation in batch reactors vs. transformation observed in column results here and in prior work, the column experimental design was further evaluated. The goal of the experimental design was to simulate anaerobic and hyperoxygenation conditions in columns by sparging N_2 and O_2 in separate influent reservoirs. Sparging was continuous resulting in DO concentrations < 0.9 mg/L in the N_2 sparged reservoir and ~ 32 mg/L in the O_2 sparged reservoir throughout the experiment. DO of the ambient control reservoir (i.e., no sparging) was ~7.2 mg/L.

A flow through DO meter was purchased to monitor oxygen concentrations in the influent and effluent ends of the columns. A standard DO meter could not be used because slow column flow rates led to extended periods required collect sufficient sample volume for the measurement, and oxygen exchange occurring during this time led to concentrations that were not representative of the effluent (i.e., O_2 was lost or gained from O_2-sparged and N_2-sparged samples, respectively). The flow-through meter was delayed in distribution to the extent that column studies were nearly complete by the time of arrival. Effluent DO concentrations were monitored with the DO sensor in the last two weeks of experiment, and showed that DO concentrations dropped in O_2-sparged columns from 32.00 mg/L to 15.59 mg/L between the reservoir and the influent end of the column (**Figure 54, Table E8**). Conversely, DO concentrations increased in N_2-sparged columns from 0.86 mg/L to 6.51 mg/L between the sparged reservoir and the column inlet (**Figure 54, Table 19**). This data demonstrate that significant oxygen exchange was occurring across the walls of the tubing used in column experiments. While the O_2-sparged were still higher in DO than other column types, differences were smaller than anticipated. N_2-sparged columns had DO concentrations similar to the ambient control columns (7.2 mg/L) and were not anoxic. The reduced differences in the DO concentrations amongst the various column types is likely the reason for similarities in the data across column types within each soil used in this study. Additionally, since O_2-sparged reactors were directly and constantly sparged, they had higher DO concentrations than O_2-sparged columns, and this likely explains differences in batch vs. column results.

The flow-through DO sensor also was used to measure the DO of column effluents. Concentrations of DO in Soil C columns did not change between the influent and effluent end of the column (**Table 20**). In Soil A all column types, however, effluent DO levels were 40-50% of influent DO. This suggests greater oxygen depletion in O_2-sparged columns compared to N_2-sparged and ambient control columns. Higher oxygen consumption might be because of higher microbial activity in O_2-sparged columns or generation of more ROS. Additionally, algae growth was observed in all column types in both soils, so some oxygen consumption in Soil A could be attributable to the algae although this was not observed in Soil C.

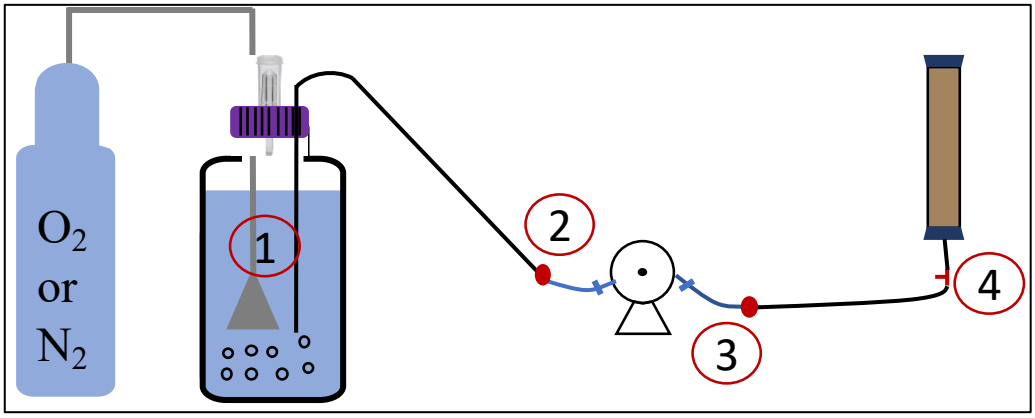

Figure 54. Sparged column flow diagram.

Table 19. DO of sparged column influents flow through PVC tubing (current study experimental set up) and PEEK tubing (Nickerson et. al, 2021, set up).

Position	PVC tubing set up		PEEK tubing set up	
	O_2 Sparged DO (mg/L)	N_2 Sparged DO (mg/L)	O_2 Sparged DO (mg/L)	N_2 Sparged DO (mg/L)
1	32.00	0.85	32	0.85
2	24.76	4.24	30.62	1.26
3	20.97	5.84	26.81	4.62
4	15.59	6.51	24.84	4.88

Table 20. DO (mg/L) of effluent in Soil A and C column effluents using flow through DO sensor.

Position	O_2 Sparged	N_2 Sparged	Ambient Control
Soil A	7.11	3.20	3.51
Soil C	15.4	6.52	7.15

TASK 4: IX REGENERANT SELECTION

Regenerant Solution Testing. 15 regeneration solutions were tested using a proprietary regenerant solution and varying solvent and salt concentrations. For each Task 4 regeneration test, 100 ml of PFAS loaded SORBIX A3F resin was transferred to a 12-inch long by 1-inch diameter SCH40 Clear PVC chromatography column. Ten bed volumes (BV) or 1000 ml of regenerant solution was pumped through 1/8-inch HDPE tubing to the column (down flow), using a Stenner Model 85MHP5 peristaltic pump at a flow rate of 3.33 ml/min, yielding an empty bed contact time of 30 minutes. The spent regenerant was pushed through a second 1/8-inch HDPE tubing and collected in a clean 1000 ml PFAS free HDPE container. Fifty ml were transferred to a 60 ml HDPE PFAS free container and shipped to Clarkson University for PFAS analysis. All regenerant solutions were prepared by dissolving a specified percent-by-weight salt and/or percent-by-volume solvent in laboratory generated deionized water. **Table 21** summarizes the regenerant solutions tested.

Table 21. Regenerant solution composition.

Test	Salt (wt %)	Solvent (vol %)
1	None	None (DI water only)
2	2.6% MIO	None (DI water only)
3	2% NaCl	None (DI water only)
4	10% NaCl	None (DI water only)
5	2.6% MIO + 5% NaCl	None (DI water only)
6	10% NaOH	None (DI water only)
7	None	100% Methanol
8	2% NaOH	90% Methanol
9	2% NaCl	50% Methanol
10	1.1% NaCl	100% Methanol
11	2% NaCl	70% Methanol
12	2% NaCl	70% Isopropanol
13	2% NaCl	70% Ethanol
14	2% NaBr	90% Methanol
15	2.5% NaBr	100% Methanol
16	2% NaCl	90% Methanol

PFAS in Regenerant Solutions. The analytical results for the thirteen PFAS compounds identified, for each regenerant solution tested, are summarized in **Table 22**. **Figure 55** compares the recoveries for summed PFAS precursors, perfluorinated carboxylic acids (PFCAs), perfluorinated sulfonic acids (PFSAs) and total PFAS. Individual PFAS compound and PFAS compound class mass recoveries are presented as a stoplight table (**Table 23**) to more easily identify the most effective regenerant solution.

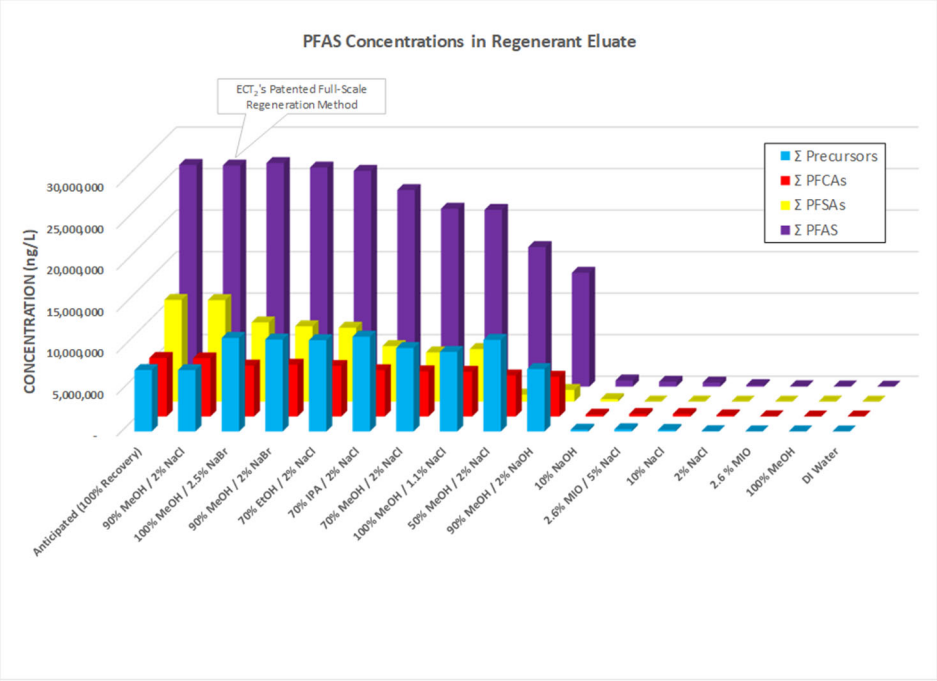

Figure 55. PFAS concentrations in regenerant eluate.

Key take-a-ways of the regenerant solution testing are that salt or solvent alone are ineffective at desorbing PFAS. Higher solvent or higher salt concentrations are more effective at PFAS desorption. There is very little difference between the effectiveness of methanol, ethanol, or isopropanol as the solvent, however, methanol is preferred because salts are more soluble in methanol than either ethanol or ispropanol. Additionally, ethanol and isopropanol form azeotropes with water, making solvent recovery more difficult; methanol does not form an azeotrope with water. Based on performance, regenerants 14, 15, & 16 will be moved into reproducibility testing (Task 5).

Table 22. Regenerant eluate composite concentration results.

Test	Regenerant	Precursors			Perfluorcarboxylic acids (PFCAs)						Perfluorosulfonic acids (PFSAs)				∑ Precursors	∑ PFCAs	∑ PFSAs	∑ PFAS
		6:2 FTS	8:2 FTS	PFOSA	PFBA	PFPeA	PFHxA	PFHpA	PFOA	PFNA	PFBS	PFHxS	PFHpS	PFOS				
Anticipated PFAS Concentration for 100% Recovery		*7,000,000*	*260,000*	*140,000*	*330,000*	*1,400,000*	*2,000,000*	*520,000*	*2,800,000*	*10,000*	*400,000*	*3,510,000*	*230,000*	*8,100,000*	*7,400,000*	*7,050,000*	12,240,000	*26,690,000*
1	DI Water	ND (<10)	ND (<10)	ND (<10)	48	102	52	ND (<10)	ND (<10)	ND (<10)	ND (<10)	24	ND (<10)	24	-	202	48	250
2	100% MeOH	9,200	ND (<10)	ND (<10)	ND (<10)	100	2,200	900	4,000	ND (<10)	ND (<10)	1,000	ND (<10)	1,300	9,200	7,200	2,300	18,700
3	2.6 % MIO	12,500	ND (<10)	ND (<10)	5,600	16,900	8,100	ND (<10)	1,600	ND (<10)	ND (<10)	1,100	700	ND (<10)	12,500	32,200	1,800	46,500
4	2% NaCl	42,700	ND (<10)	ND (<10)	32,300	75,700	30,600	2,300	4,300	ND (<10)	ND (<10)	1,400	700	ND (<10)	42,700	145,200	2,100	190,000
5	10% NaCl	191,300	ND (<10)	ND (<10)	73,900	162,200	51,300	ND (<10)	16,200	ND (<10)	ND (<10)	2,800	800	800	191,300	303,600	4,400	499,300
6	2.6% MIO / 5% NaCl	269,700	ND (<10)	ND (<10)	67,600	150,700	65,200	5,500	25,000	ND (<10)	ND (<10)	5,200	900	1,500	269,700	314,000	7,600	591,300
7	10% NaOH	60,000	ND (<10)	160,000	70,000	ND (<10)	90,000	ND (<10)	70,000	ND (<10)	90,000	120,000	80,000	ND (<10)	220,000	230,000	290,000	740,000
8	90% MeOH / 2% NaOH	7,030,000	370,000	110,000	90,000	530,000	1,130,000	470,000	2,570,000	ND (<10)	80,000	250,000	90,000	990,000	7,510,000	4,790,000	1,410,000	13,710,000
9	50% MeOH / 2% NaCl	10,810,000	220,000	ND (<10)	370,000	1,250,000	1,560,000	350,000	1,410,000	ND (<10)	ND (<10)	310,000	130,000	400,000	11,030,000	4,940,000	840,000	16,810,000
10	100% MeOH / 1.1% NaCl	9,370,000	210,000	ND (<10)	370,000	1,260,000	1,570,000	390,000	1,800,000	ND (<10)	ND (<10)	1,830,000	250,000	4,240,000	9,580,000	5,390,000	6,320,000	21,290,000
11	70% MeOH / 2% NaCl	10,040,000	10,000	ND (<10)	380,000	1,250,000	1,620,000	400,000	1,790,000	ND (<10)	ND (<10)	1,660,000	210,000	4,060,000	10,050,000	5,440,000	5,930,000	21,420,000
12	70% IPA / 2% NaCl	11,410,000	10,000	ND (<10)	380,000	1,240,000	1,690,000	430,000	1,830,000	ND (<10)	ND (<10)	1,760,000	280,000	4,640,000	11,420,000	5,570,000	6,680,000	23,670,000
13	70% EtOH / 2% NaCl	10,980,000	10,000	ND (<10)	380,000	1,400,000	1,840,000	410,000	2,060,000	ND (<10)	ND (<10)	2,650,000	320,000	5,930,000	10,990,000	6,090,000	8,900,000	25,980,000
14	90% MeOH / 2% NaBr	11,070,000	ND (<10)	ND (<10)	340,000	1,610,000	1,780,000	380,000	2,130,000	30,000	170,000	2,490,000	240,000	6,170,000	11,070,000	6,240,000	9,070,000	26,380,000
15	100% MeOH / 2.5% NaBr	10,990,000	270,000	ND (<10)	410,000	1,360,000	1,840,000	480,000	2,040,000	ND (<10)	ND (<10)	2,940,000	300,000	6,290,000	11,260,000	6,130,000	9,530,000	26,920,000
16	90% MeOH / 2% NaCl	6,990,000	260,000	140,000	330,000	1,380,000	2,000,000	520,000	2,780,000	ND (<10)	390,000	3,500,000	230,000	8,100,000	7,390,000	7,010,000	12,220,000	26,620,000

concentration units = ng/L

Table 23. Regenerant eluate composite concentration stoplight.

Test	Regenerant	Precursors			Perfluorcarboxylic acids (PFCAs)						Perfluorosulfonic acids (PFSAs)				Σ Precursors	Σ PFCAs	Σ PFSAs	Σ PFAS
		6:2 FTS	8:2 FTS	PFOSA	PFBA	PFPeA	PFHxA	PFHpA	PFOA	PFNA	PFBS	PFHxS	PFHpS	PFOS				
1	DI Water	<0.0001%	<0.004%	<0.007%	0.015%	0.007%	0.003%	<0.0019%	<0.0004%	<0.1000%	<0.0025%	0.001%	<0.0043%	0.0003%	0.0000%	0.003%	0.000%	0.001%
2	100% MeOH	0.13%	<0.004%	<0.007%	<0.003%	0.007%	0.11%	0.17%	0.14%	<0.1000%	<0.0025%	0.03%	<0.0043%	0.02%	0.12%	0.10%	0.02%	0.07%
3	2.6 % MIO	0.18%	<0.004%	<0.007%	1.7%	1.2%	0.41%	<0.0019%	0.06%	<0.1000%	<0.0025%	0.03%	0.30%	<0.0001%	0.17%	0.46%	0.01%	0.17%
4	2% NaCl	0.61%	<0.004%	<0.007%	10%	5.4%	1.5%	0.44%	0.15%	<0.1000%	<0.0025%	0.04%	0.30%	<0.0001%	0.58%	2.1%	0.02%	0.71%
5	10% NaCl	2.7%	<0.004%	<0.007%	22%	12%	2.6%	<0.0019%	0.58%	<0.1000%	<0.0025%	0.08%	0.35%	0.01%	2.6%	4.3%	0.04%	1.9%
6	2.6% MIO / 5% NaCl	3.9%	<0.004%	<0.007%	20%	11%	3.3%	1.1%	0.89%	<0.1000%	<0.0025%	0.15%	0.39%	0.02%	3.6%	4.5%	0.06%	2.2%
7	10% NaOH	0.9%	<0.004%	114%	21%	<0.0007%	4.5%	<0.0019%	2.5%	<0.1000%	23%	3.4%	35%	<0.0001%	3.0%	3.3%	2.4%	2.8%
8	90% MeOH / 2% NaOH	100%	142%	79%	27%	38%	57%	90%	92%	<0.1000%	20%	7.1%	39%	12%	101%	68%	12%	51%
9	50% MeOH / 2% NaCl	154%	85%	<0.007%	112%	89%	78%	67%	50%	<0.1000%	<0.0025%	8.8%	57%	4.9%	149%	70%	6.9%	63%
10	100% MeOH / 1.1% NaCl	134%	81%	<0.007%	112%	90%	79%	75%	64%	<0.1000%	<0.0025%	52%	109%	52%	129%	76%	52%	80%
11	70% MeOH / 2% NaCl	143%	3.8%	<0.007%	115%	89%	81%	77%	64%	<0.1000%	<0.0025%	47%	91%	50%	136%	77%	48%	80%
12	70% IPA / 2% NaCl	163%	3.8%	<0.007%	115%	89%	85%	83%	65%	<0.1000%	<0.0025%	50%	122%	57%	154%	79%	55%	89%
13	70% EtOH / 2% NaCl	157%	3.8%	<0.007%	115%	100%	92%	79%	74%	<0.1000%	<0.0025%	75%	139%	73%	149%	86%	73%	97%
14	90% MeOH / 2% NaBr	158%	0.004%	<0.007%	103%	115%	89%	73%	76%	300%	43%	71%	104%	76%	150%	89%	74%	99%
15	100% MeOH / 2.5% NaBr	157%	104%	<0.007%	124%	97%	92%	92%	73%	<0.1000%	<0.0025%	84%	130%	78%	152%	87%	78%	101%
16	90% MeOH / 2% NaCl	100%	100%	100%	100%	99%	100%	100%	99%	<0.1000%	98%	100%	100%	100%	100%	99%	100%	100%

Relative Mass Recovery Ranking Criteria	
	X ≥ 90%
	70 < x < 90
	x ≤ 70%

TASK 5: IX REGENERANT REPLICATION

PFAS Loaded IX Resin. Regeneration testing was conducted using PFAS loaded SORBIX A3F resin obtained from a pilot test conducted at the Former Pease AFB – Site 8 location, hereafter referred to as Site A. A second sample of PFAS loaded SORBIX A3F was obtained from an operating full-scale regenerable PFAS ion exchange treatment system for a confidential client, hereafter referred to as Site B. **Figure 56** shows the test apparatus utilized. Based on extensive characterization of this resin, by ECT, the sorbed PFAS concentration for 13 compounds is known, allowing for an estimate of the effectiveness of each regenerant solution tested. Task 4 identified the regenerant solutions for Task 5 (**Table 21**), which included (1) a mixture of 90% methanol and 2% NaCl, (2) a mixture of 100% methanol with 2.5% NaBr, and (3) a mixture of 90% methanol and 2% NaBr.

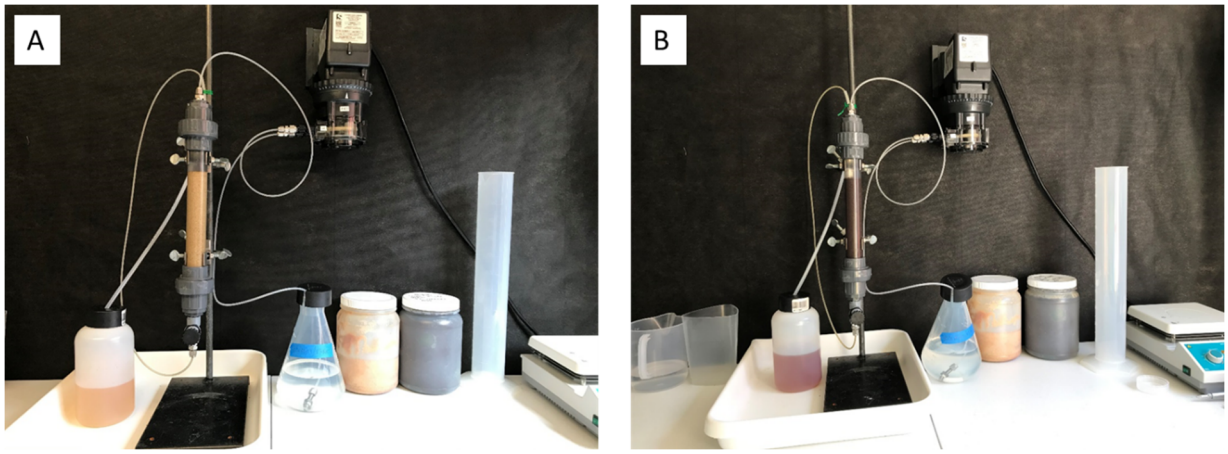

Figure 56. Site A (left) and Site B (right) regenerant test column.

Figures 57 and **58** present results of the triplicate tests for Resin A and Resin B, respectively. Results of replicate runs with both resins show excellent replication as indicated by the small error bars. While the specific compounds detected, and their concentrations, differ for the two resins, for both the three regeneration solutions offer similar results, consistent with those found in Task 4 – in other words, there is very little difference in regeneration results for the three different test regenerant solutions. There may be small differences in the precursors 4:2 FTS, 6:2 FTS, and 8:2 FTS for resin B, however their concentrations are low and differences from a practical standpoint are negligible.

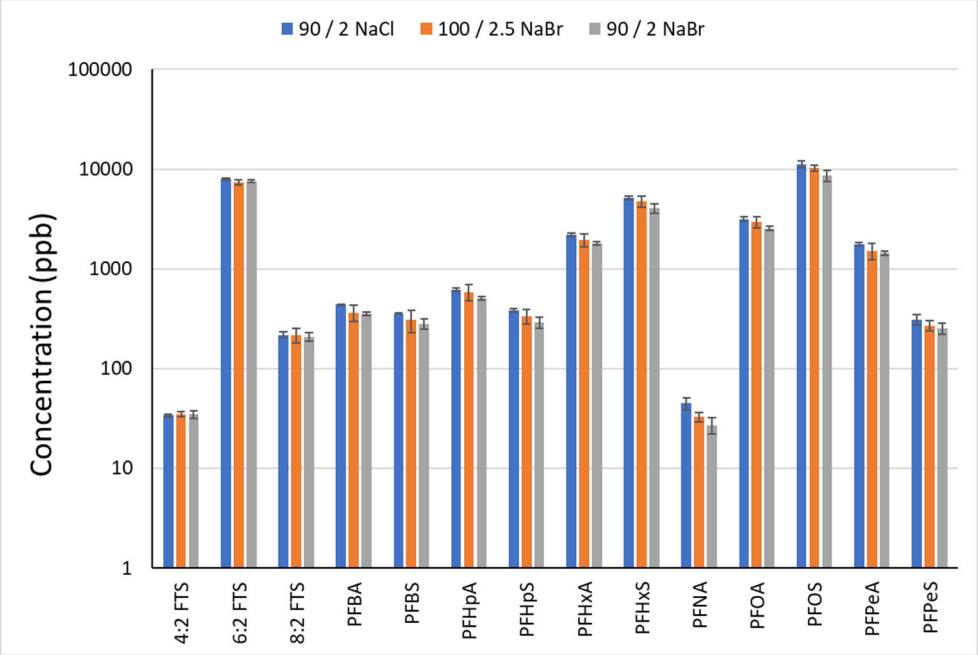

Figure 57. Regeneration results for Resin A.

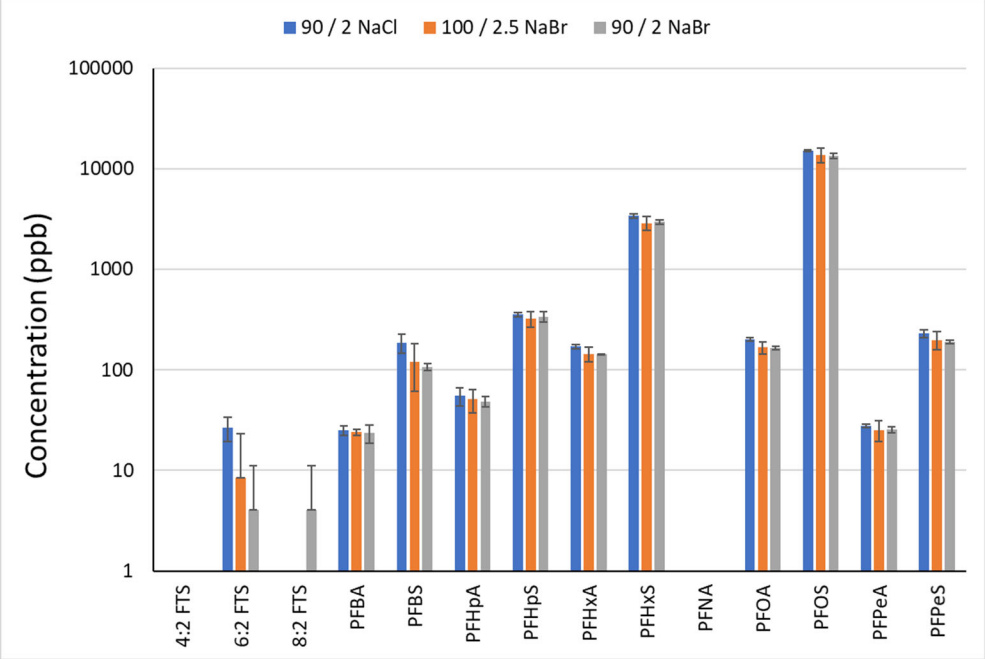

Figure 58. Regeneration results for Resin B.

TASK 6: OPTIMIZATION OF TOP PERFORMING REGENERANT FOR MULTIPLE TREATMENT CYCLES

IX Regenerant Distillation Recovery. Twelve different recovery techniques were applied to the regenerant solutions selected from Task 5. The primary recovery techniques tested are distillation and membrane separation. Variables for the distillation recovery approach included, 1) distillation column height between the still pot and condenser, 2) distillation column type (e.g., none, open extension, perforated Hempel and Vigreux), and 3) distillation column packing material. Distillation was only performed on regenerant solution from one site (Site A) that was also used in previous tasks. Distillation results, summarized in **Table 24**, show minimal PFAS carryover into the distillate as a function of distillation column height, type and packing material.

Table 24. PFAS carryover to the distillate.

Test #	Distillation Column Type	Distillation Column Height (cm)	Packing Type	Matrix	Precursors (µg/L)	PFCAs (µg/L)	PFSAs (µg/L)	ΣPFAS (µg/L)
				Spent Regenerant	8,200	8,300	17,411	33,911
1	None	0	None	Distillate	3.16	1.10	14.7	18.9
				% Carryover	0.039%	0.013%	0.084%	0.056%
2	Open Extension	12	None	Distillate	5.52	2.35	22.37	30.2
				% Carryover	0.067%	0.028%	0.129%	0.089%
3	Perforated Hempel	22	None	Distillate	5.69	2.14	22.34	30.2
				% Carryover	0.069%	0.026%	0.128%	0.089%
4	Vigreux	24	None	Distillate	6.07	2.48	21.80	30.4
				% Carryover	0.074%	0.030%	0.125%	0.090%
5	Perforated Hempel	22	Berl Porcelain Saddles	Distillate	7.97	2.78	31.17	41.9
				% Carryover	0.097%	0.033%	0.179%	0.124%
6	Vigreux	24	SS Wool	Distillate	5.21	2.35	28.09	35.6
				% Carryover	0.064%	0.028%	0.161%	0.105%

IX Regenerant Membrane Separation Recovery. Variables for membrane separation approach included: 1) membrane type (i.e., reverse osmosis or nanofiltration), 2) molecular weight cut-off, 3) percent salt rejection, and 4) flux rating (i.e., production rate vs applied pressure. The membranes were tested in a dead-end filtration mode as 47 mm flat sheet disks housed in a pressure rated housing. **Table 25** shows the properties of the membranes tested. Regenerant solution was placed in a vessel and 90 psi compressed nitrogen was used to push the regenerant solution through the flat sheet membrane. Regenerant solution from both Site A and Site B were tested with all six (2) membranes. Laboratory analysis showed salt rejection consistent with the values in **Table 25**. In addition, results also show no rejection of methanol and unacceptable PFAS rejection levels (**Table 26**) for solvent reuse. The current data indicate that distillation is the best performing recovery method (e.g. maximum regenerant solution recovery and minimum PFAS carry over) for each of the regenerant solutions.

Table 25. Membranes tested.

Manufacturer	Name	Class	MWCO (Da) (Pore Size (µm))	Rejection MgSO4% (NaCl%)	Flux (GFD/psi)	Material
DOW FilmTec	BW30XFR	Reverse Osmosis	NA	(99.7%)	28-33/225	polyamide-TFC
DOW FilmTec	NF90	Nanofiltration	200-400	99.0%	46-60/130	polyamide-TFC
DOW FilmTec	NF270	Nanofiltration	200-400	99.2%	72-98/130	polyamide-TFC
SUEZ (GE)	AK	Reverse Osmosis	NA	(99.0%)	26/115	polyamide-TFC
Synder Filtration	NFX	Nanofiltration	150-300	99.0 (40%)	20-25/110	polyamide-TFC
TriSep	TS80	Nanofiltration	150	99% (80-90%)	20/110	polyamide-TFC

Table 26. Summary of PFAS Leakage.

		SITE A				SITE B			
MEMBRANE	TYPE	Precursors (µg/L)	PFCAs (µg/L)	PFSAs (µg/L)	ΣPFAS (µg/L)	Precursors (µg/L)	PFCAs (µg/L)	PFSAs (µg/L)	ΣPFAS (µg/L)
Spent Regenerant		8,200	8,300	17,411	33,911	87	499	19,242	19,828
BW30XFR	RO	338	3,867	7,631	11,836	58	113	2,915	3,086
% Rejection		95.9%	53.4%	56.2%	65.1%	32.6%	77.3%	84.9%	84.4%
NF90	NF	320	3,399	6,221	9,940	9.2	69	2,319	2,397
% Rejection		96.1%	59.1%	64.3%	70.7%	89.3%	86.1%	88.0%	87.9%
NF270	NF	346	4,427	8,260	13,032	38	369	14,062	14,469
% Rejection		95.8%	46.7%	52.6%	61.6%	55.9%	26.0%	26.9%	27.0%
AK	RO	414	6,241	11,713	18,368	0.06	75	2,392	2,467
% Rejection		94.9%	24.8%	32.7%	45.8%	99.9%	85.0%	87.6%	87.6%
NFX	NF	469	8,339	16,225	25,033	0.05	99	3,733	3,832
% Rejection		94.3%	-0.5%	6.8%	26.2%	99.9%	80.1%	80.6%	80.7%
TS80	NF	281	3,356	3,506	7,143	41	189	4,164	4,394
% Rejection		96.6%	59.6%	79.9%	78.9%	52.6%	62.0%	78.4%	77.8%

TASK 7: DESTRUCTIVE PLASMA TREATMENT

Plasma Conditions. Groundwater treatment experiments were carried using an enhanced contact plasma reactor. Operational parameters tested include voltage (30-40 kV), frequency (30-120 Hz), and argon circulation rate (12 and 17 L/min). The plasma reactor was operated in batch mode. Samples were collected at 30 sec and 5 min time periods.

Plasma treatment of IDW samples. During treatment of the 4L samples, PFOA and PFOS concentrations decreased rapidly and were below 2016 HAL concentrations within one minute for IDW 1 - 9, 10 minutes for IDW 10 and 11, 15 minutes for IDW 12, and 50 minutes for IDW 13 (**Figure 59a** and **b**). For long-chain PFAAs (PFOA and PFOS), plasma treatment achieved a removal efficiency > 93% within 5 minutes for IDW 1 – 9, 30 minutes for IDW 10 – 12, and 60 minutes for IDW 13 (**Figure 60**). Removal efficiencies were also higher for long-chain PFAAs than for short-chain PFAAs. In general, PFSAs were more rapidly removed than PFCAs of similar chain-length and similar initial concentrations, a result that agrees with our previous findings. This is likely due to PFSAs' higher surface activity due to the presence of an extra CF_2 group in the molecule.

For the ten identified precursors (10:2 FTS, 4:2 FTS, 6:2 FTS, 8:2 FTS, EtFOSA, FOSA-1, FOSAA, MeFOSAA, MeFOSAA, and EtFOSAA) removal efficiencies were 92 ± 17, 94 ± 20, 90 ± 32, 91 ± 12, 92 ± 16, 95 ± 9, 79 ± 5, and 65 ± 64 %, respectively. These removal efficiencies were higher than those observed for TOP (65 ± 20%, Figure 4) which should be considered for all PFAS destruction technologies since any TOP not removed can be broken down to PFAAs in the environment. Negative removal (increasing concentrations) were observed for PFPeA, PFBA and MeFOSA (-14, -562 and -159 %, respectively) which is likely due to the formation of short-chain PFCAs (PFPeA and PFBA) from the degradation of long-chain PFAAs and the oxidation of their precursors, as discussed in the subsequent section. MeFOSA could be a degradation product of other precursors such as MeFOSAA, EtFOSA, EtFOSAA, and N-methyl perfluorooctane sulfonamidoethanol (MeFOSE) and formed by the terminal cleavage of $–CH_3COO^-$, $–CH_3$, and/or $–CH_3OH$ group from the parent molecules or from the degradation of unknown precursors.[9] The lower degradation efficiency for some precursors could be attributed to their lower initial concentration relative to most other PFAAs as the degradation followed pseudo first order kinetics. Also, high TOP concentrations measured indicate the presence of many unknown precursors which could also be the potential source of the identified precursors. Final PFAS concentrations, and initial and final fluoride, and VOC concentrations in individual IDW samples are shown in **Tables 27** and **28**.

Of the 13 IDWs, only IDW samples 1, 3, 10, 12, and 13 were above the fluoride detection limit of 0.1 mg/L following the treatment (**Table 27**). For those samples, there was a significant increase in fluoride concentrations post-treatment (from 260 to 2490 μg/L), which accounted for 33 ± 14% of the organically bound fluorine in the measured PFAAs and their precursors. However, the fluoride mass balance in this study was difficult to perform because the measured total PFAS concentration was low (ranged between tens and few hundreds of μg/L) compared to the minimum concentration of fluoride required by both F electrode and IC (low ppm level).

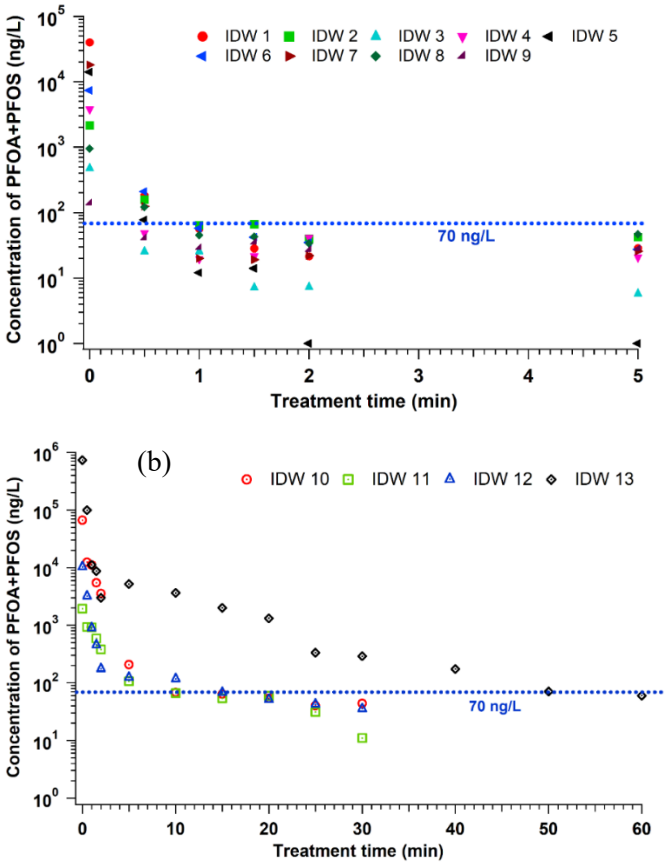

Figure 59. Degradation profiles of combined PFOA and PFOS concentrations in: (a) IDW samples 1 to 9 plotted for treatment time of 5 minutes and (b) IDW samples 10 to 13 plotted for treatment time of 60 minutes. The IDW treatment volume is 4 L. Blue horizontal dotted lines represent USEPA's HAL. Detection limits were approximately 9 ng/L.

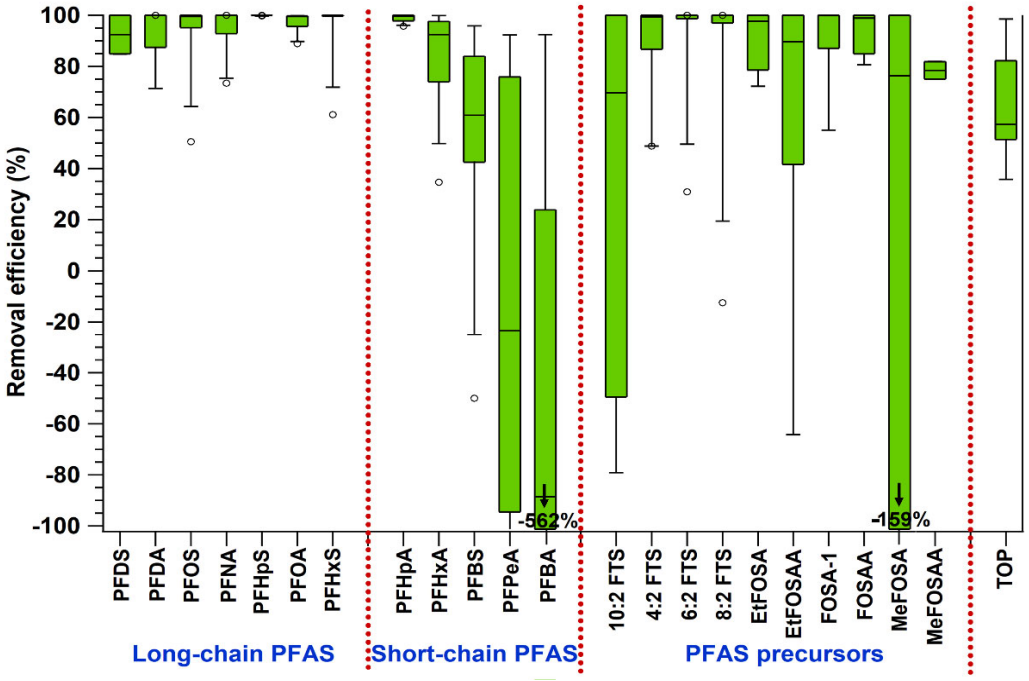

Figure 60. Removal efficiency of PFAS in plasma treatment. Box and Whisker plot showing the removal efficiency (%) of several long-chain PFAS, short-chain PFAS, PFAS precursors, and total oxidizable precursors (TOP) in unidentified GW samples treated in pilot-scale plasma reactor. Removal efficiency is shown between +100 and -100%, where negative removal efficiency is due to the formation of short-chain PFAS from degradation products of long-chain PFAS. PFBA and MeFOSA have shown negative removal efficiency of -562 and -159%, respectively, which are indicated by down arrows in the figure. The IDW treatment volume was 4 L and treatment time was 60 minutes.

Table 27. Fluoride Concentrations for 13 Unidentified GW Samples before and after Plasma Treatment.

Sample	Untreated (mg/L)	Treated (mg/L)	% increase
IDW1	BDL*	0.55	31.1
IDW2	BDL	BDL	-
IDW3	0.74	1.03	39.5
IDW4	BDL	BDL	-
IDW5	BDL	BDL	-
IDW6	BDL	BDL	-
IDW7	BDL	BDL	-
IDW8	BDL	BDL	-
IDW9	BDL	BDL	-
IDW10	0.71	1.22	71.9
IDW11	BDL	BDL	-
IDW12	1.12	1.38	23.2
IDW13	2.75	5.24	90.7

**BDL – Below detection limit.*

Table 28. Concentration of Volatile Organic Compounds (VOCs) before and after Plasma Treatment.

Sample	VOCs	Concentration (µg/L)	Detection limit (µg/L)
IDW1	Methyl ter-butyl ether	0.26	0.25
	1,2 -dichloroethane	28.0	0.15
IDW4	1,1-dichloroethane	0.72	0.14
	Bromodichloromethane	0.17	0.17
	Chloroform	2.70	0.16
IDW7	1,2 -dichloroethane	0.33	0.15
IDW8	1,1-dichloroethane	0.31	0.14
	1,2 -dichloroethane	2.50	0.15
	Benzene	1.60	0.16
	Ethylbenzene	2.20	0.16
IDW10	1,1-dichloroethane	0.26	0.14
	1,2 - dichloroethane	15.0	0.15
	Trichloroethane	24.0	0.16
IDW12	Acetone	13.0	1.90
	m-xylene & p-xylene	0.44	0.34
	o-xylene	0.27	BDL 0.19

**BDL – Below detection limit; VOCs concentrations were BDL in IDW 2, 3, 5, 6 and 11; VOCs concentrations in IDW 9 and 13 were not analyzed.*

Plasma Treatment of Groundwater Generated from Contaminated Soils. Oxidative pre-treatment using heat activated persulfate was compared to non-treated soil samples to determine whether this pre-treatment step makes a difference in the plasma treatment of PFCAs. Plasma work focusing on treating PFAS in groundwater from Jacksonville, Willow Grove are shown in **Figure 61** and results suggest the need for a treatment duration for longer than 60 minutes to address the concentrations of PFAS in these samples, which are orders of magnitude greater than 2016 EPA HAL.

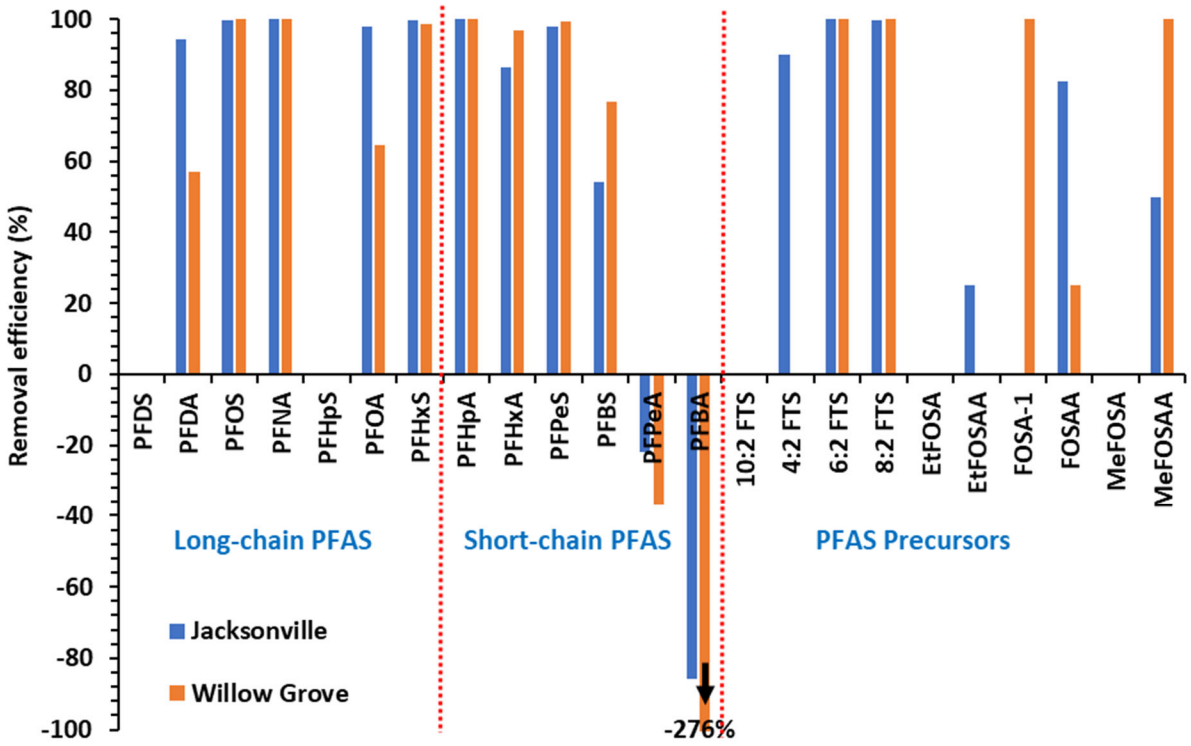

Figure 61. Results for plasma treatment of Jacksonville and Willow Grove field site groundwater.

Oxidative Pre-treatment before Plasma Treatment. To determine the efficiency of oxidative pretreatment of PFAS-contaminated groundwater using heat-activated persulfate, a persulfate concentration of 50 mM was used to pretreat soil/water mixtures from Willow Grove (1 g soil/ 1 mL water) before plasma treatment. Efficiency of the oxidative pretreatment option before plasma treatment was evaluated by considering >99% oxidative transformation of precursors to PFAAs and comparing the TOP reduction after plasma treatment. Six hundred mL of water were isolated from each soil/water mixture and used for plasma treatment in a batch reactor.

Plasma treatment efficiency of contaminated untreated and pre-treated groundwater. For both untreated and pretreated samples, 6:2 FTS had the highest concentration of remaining precursors (**Figures 62a and 63a**). Complete precursor degradation occurred within 30 minutes for both untreated and pretreated water (**Figures 62a and 63a**). Long chain PFAS were completely degraded whereas short chain PFAS remained after plasma treatment and increased in concentration due to byproducts formed from the degradation of longer chains and precursors (**Figures 62b-d; Figures 63b-d**). The percent reduction in TOP in the untreated and pretreated samples were 77% and 80%, respectively, indicating that oxidative pretreatment has a minor influence on the TOP reduction (**Figure 64a**). In both samples PFAS degraded in a similar timeframe during plasma treatment (**Figure 64b**) indicating that there was no significant difference in plasma treatment efficiency for untreated (control) and pretreated (heat + persulfate) water samples.

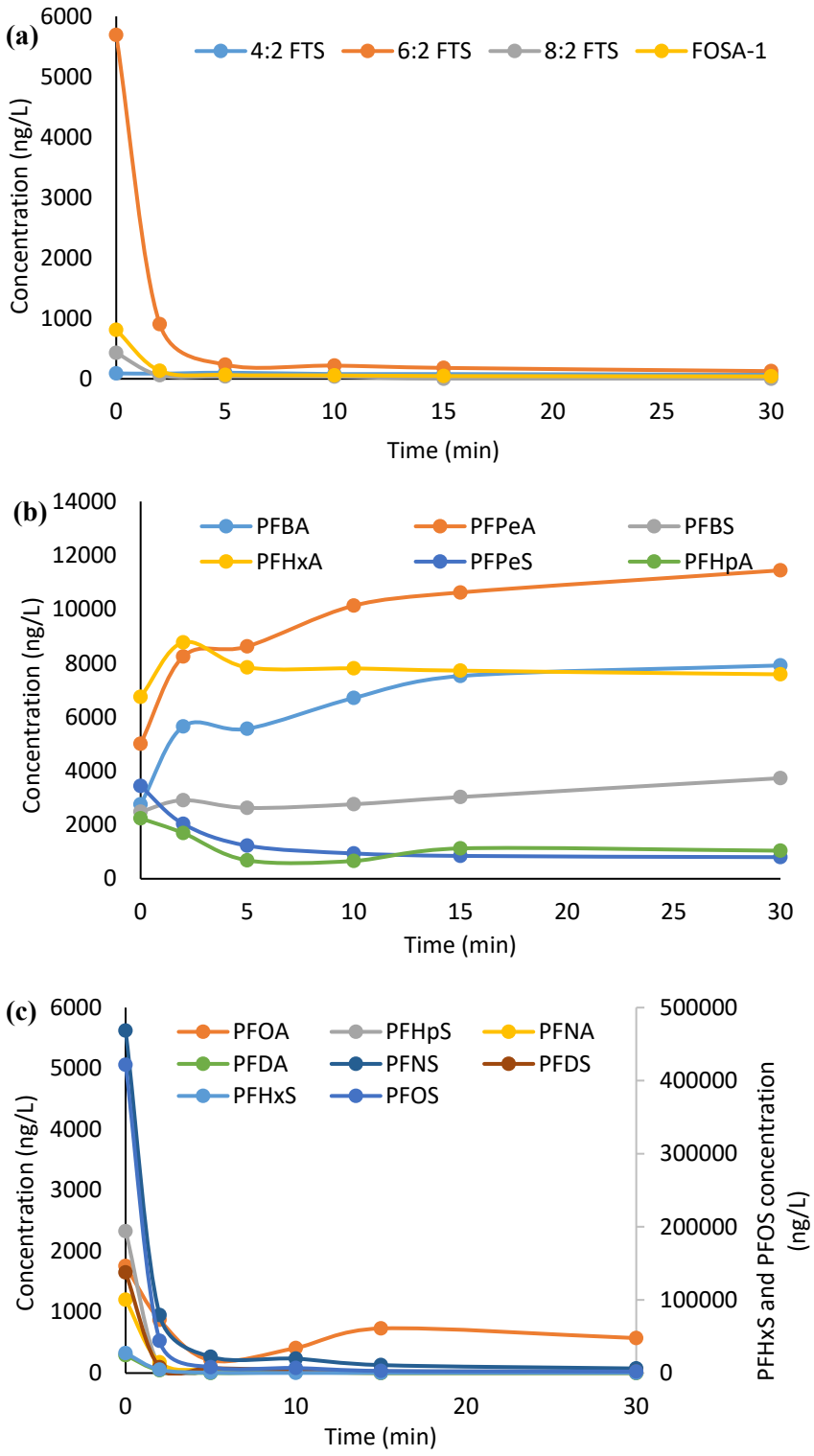

Figure 62. Concentrations of (a) precursors, (b) short chain PFAS, and (c) long chain PFAS in untreated water during plasma treatment.

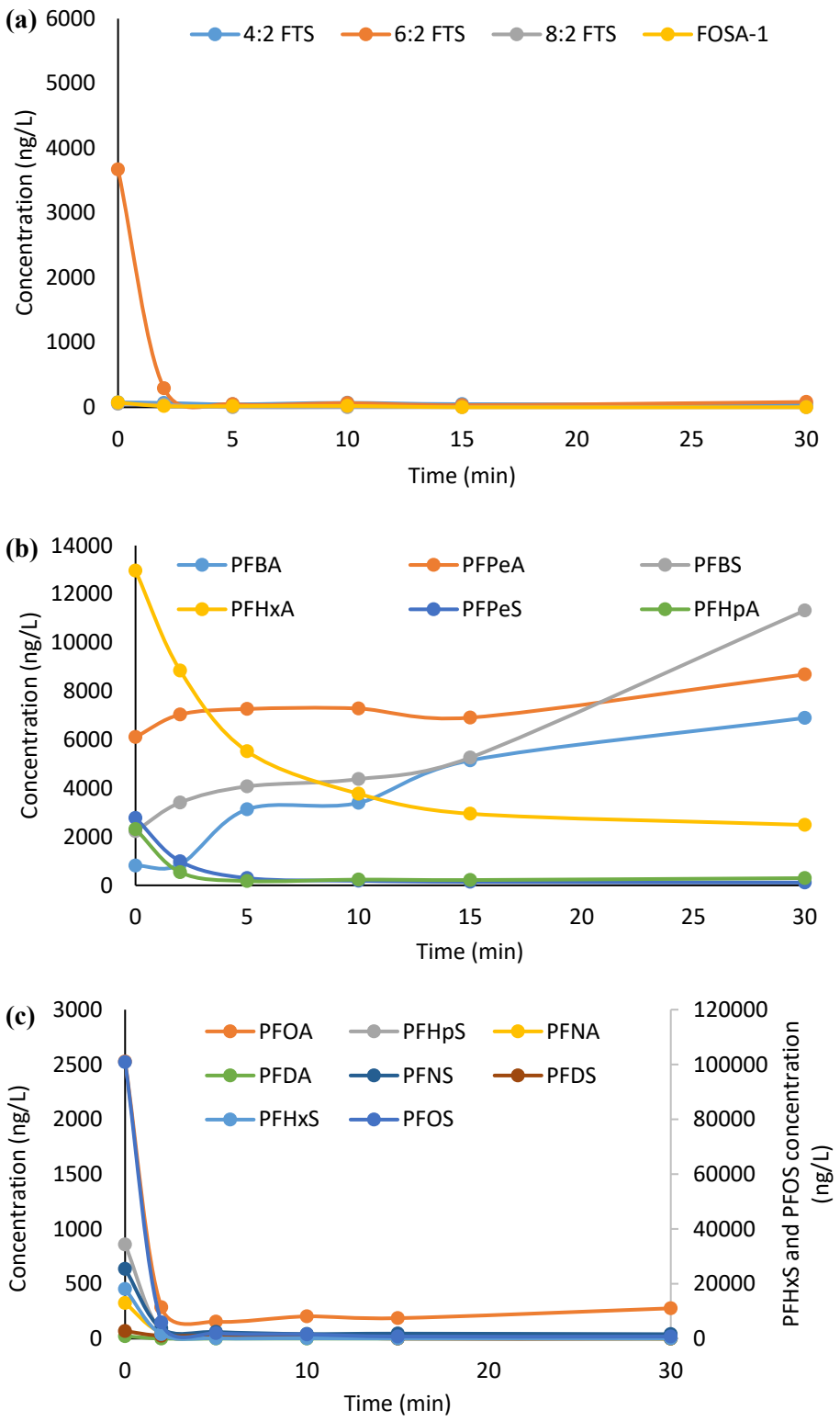

Figure 63. Concentrations of (a) precursors, (b) short chain PFAS, and (c) long chain PFAS in water pretreated with heated persulfate during plasma treatment.

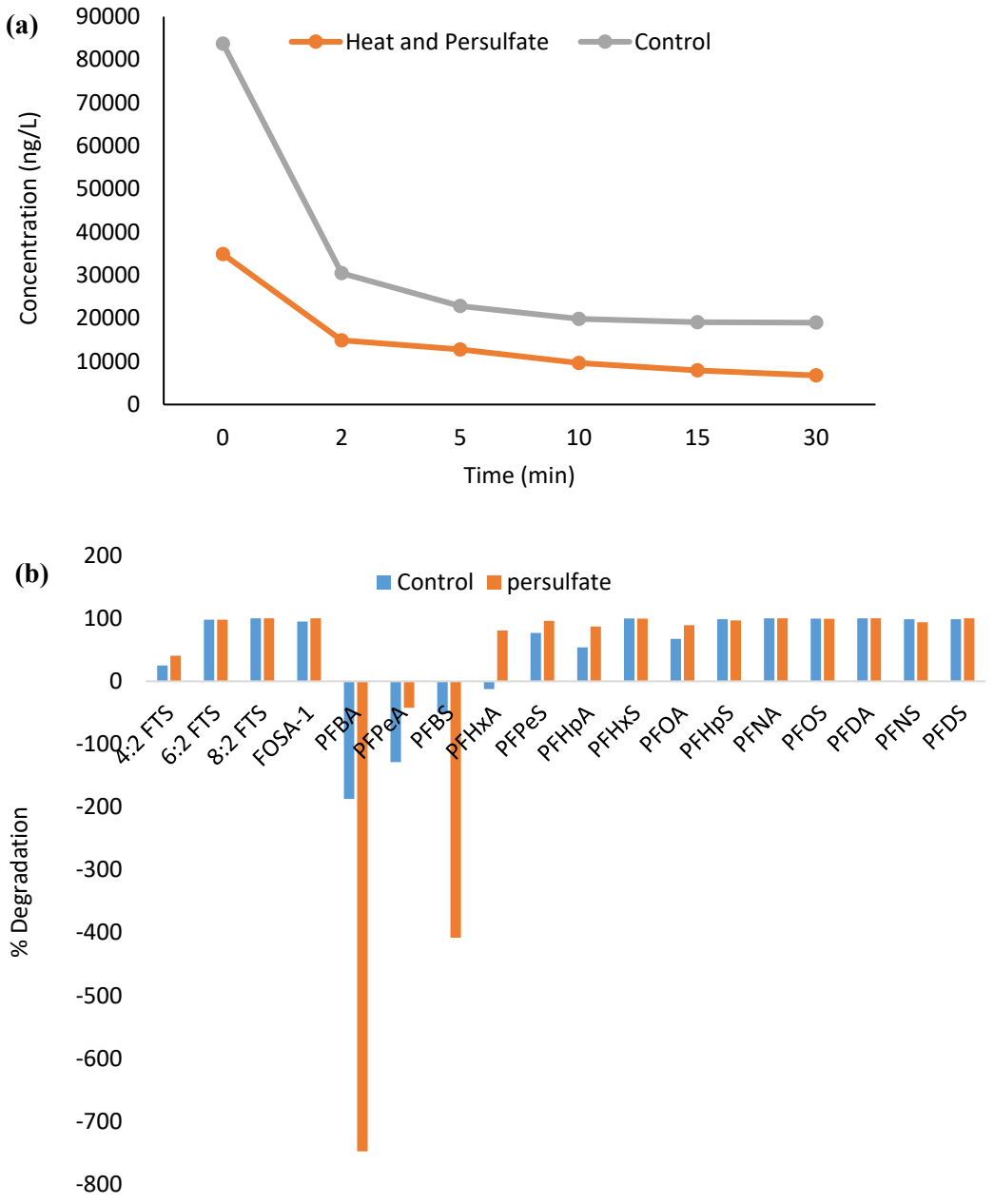

Figure 64. Comparisons of (a) TOP reduction during plasma treatment and (b) percent degradation of precursors and PFAS compounds after plasma treatment. The IDW treatment volume was 600 mL and treatment time was 30 minutes.

Fluorine Mass Balance. A fluoride mass balance was not possible because the measured total PFAS concentration was low (ranged between tens and few hundreds of µg/L) compared to low ppm F detection limit of the F electrode and ion chromatography (IC).

***Characterization of Still Bottom Samples*.** ECT2 provided Clarkson with six different SBs (conductivity range from 50 to 80 mS/cm) generated at a field site. Of the 27 PFAS analyzed for, seven long-chain (C ≥ 6 for PFSA and C ≥ 8 for PFCA) PFAAs (PFHxS, PFOA, PFHpS, PFNA, PFOS, PFDA and PFNS), six short-chain (C < 6 for PFSA and C < 8 for PFCA) PFAAs (PFBA, PFPeA, PFBS, PFHxA, PFPeS and PFHpA) and four precursors (4:2 FTS, 6:2 FTS. 8:2 FTS and FOSA-1) were found in all the SB samples in very high concentrations: ΣPFAAs concentrations ranged from 180 to 770 mg/L; Σshort-chain PFAAs ranged from 20 to 60 mg/L; Σlong-chain PFAAs ranged from 160 to 770 mg/L; ΣPFCAs ranged from 110 to 190 mg/L and ΣPFSAs ranged from 80 to 640 mg/L (**Table 29**). Total identified precursors ranged from 20 to 50 mg/L. TOP concentrations ranged between 3800 to 9400 mg/L, approximately 10 times higher than the total PFAAs concentration (**Table 30**).

Table 29. Concentrations of PFAS Precursors, Short-chain and Long-chain PFAAs in Six Different IX Brine Regenerant Still Bottom Samples. Concentrations are represented in µg/L in six SB samples.

Still bottom samples →		HC1A	HC1B	HC1C	A3FA	A3FB	A3FC
PFAS Precursors	4:2 FTS	95	96	200	100	161	133
	6:2 FTS	39500	28600	18600	19700	14100	47200
	8:2 FTS	1360	200	270	810	710	1900
	FOSA-1	30	40	35	23	50	40
Short-chain PFAAs	PFBA	2120	2330	2030	2060	940	2220
	PFPeA	6180	5250	6050	6810	5870	5070
	PFBS	4310	3900	7770	4170	6080	3700
	PFHxA	21400	15000	21800	1300	19800	19300
	PFPeS	7700	6440	8030	6630	9600	6160
	PFHpA	11900	1800	10300	920	15900	4130
Long-chain PFAAs	PFHxS	110900	25700	28700	8000	104500	157500
	PFOA	80300	99600	91600	95500	148000	94300
	PFHpS	50	1620	1230	2270	5680	3000
	PFNA	200	110	60	260	410	330
	PFOS	156900	70900	64300	55800	105000	68800
	PFDA	BDL	BDL	15	15	20	13
	PFNS	5	55	77	126	80	97

Table 30. Reduction of Total Oxidizable Precursor (TOP) Concentrations in Still Bottom Samples.

	TOP Initial (mg/L)	TOP final (mg/L)	TOP removal (%)
HC1A*	3870	2	99.9
HC1B	9260	34	99.6
HC1C**	6870	13	99.8
A3FA	4380	10	99.9
A3FB	6360	11	99.8
A3FC	9440	15	99.8

TOP concentrations are normalized to initial (without dilution) in SB samples. HC1A* was undiluted, HC1C** was diluted 50 times, and other SB samples were diluted 10 times.

Initial tests of undiluted SB solutions exhibited excessive foaming for extended periods (>3 hr), at all argon flow rates tested. Since excessive foaming is detrimental to the plasma process, 10-fold and 50-fold dilution of as received SB solutions, was conducted to determine how much dilution was needed before plasma treatment. After numerous tests, a minimum of 10-fold dilution was selected for continuous operation of plasma treatment. Two bench-scale batch plasma reactors, a "high-concentration (~100 mg/L)" and a "low-concentration (< 1 µg/L)" were used.

High Concentration Reactor Results. Results for the degradation of precursors, long-chain, and short-chain PFAAs are shown in **Figure 65**. In all the SBs, plasma degradation efficiencies were higher for long-chain PFAAs than short-chain PFAAs, which is consistent with what was found for the treatment of contaminated groundwater. For long-chain PFAAs (PFNS, PFDA, PFOS, PFNA, PFHpS, PFOA and PFHxS), plasma treatment resulted in >99% degradation within 120 minutes and the extent of removal was independent of the PFAA chain length. For short-chain PFAAs (PFHpA, PFPeS, PFHxA, and PFBS)), removal efficiencies were >99% after 6 hours of treatment except for PFPeA (96.7 ± 5.4%) and PFBA (23 ± 42%). For the four identified precursors, 8:2 FTS and FOSA-1 were removed to below detection limits (BDL) of approximately 30 ng/L and removal efficiencies for 6:2 FTS and 4:2 FTS were 99.9 ± .07%, and 90 ± 25%, respectively. Inorganic fluoride concentrations increased by 1 to 3 orders of magnitude post-treatment (**Table 31**) indicating significant defluorination of PFAS molecules.

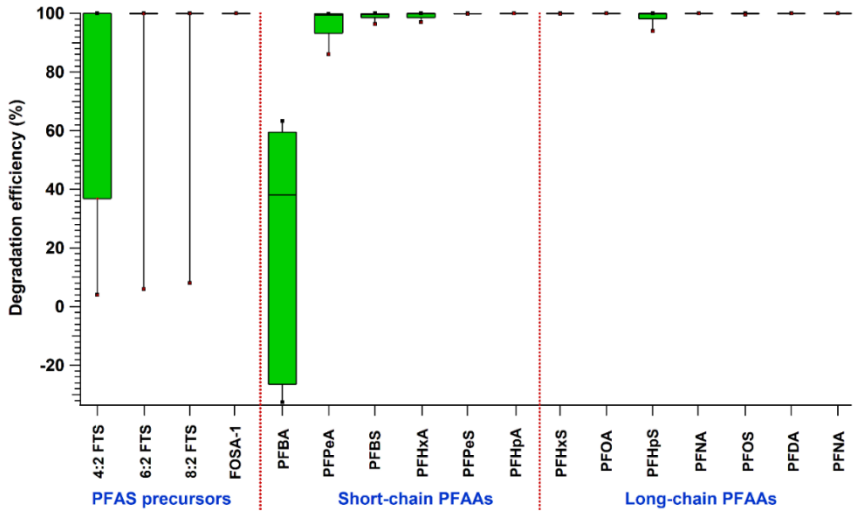

Figure 65. Box and whisker plot showing the plasma degradation efficiency (average ± SD %) for PFAS precursors, short-chain PFAAs, and long-chain PFAAs in six different SB samples in the high concentration reactor. Removal efficiencies were calculated from initial and final samples after six hours of treatment time (3 hours for HC1(C) SB sample) from 750 mL treatment volume.

Table 31. Fluoride Production in Six Different IX Brine Regenerant Still Bottom Samples. Initial Concentrations are reported (without dilution).

	Initial (mg/L)	Final (mg/L)
HC1A*	340	7890
HC1B	1670	8420
HC1C**	4700	16800
A3FA	1600	10700
A3FB	360	14400
A3FC	570	8800

Low Concentration Reactor Results. To further reduce PFAAs treatment continued in the low concentration reactor. All the long-chain PFAAs were removed to BDL after 30 minutes of additional treatment, except for short-chain PFAAs (**Figure 66a**). PFOA and PFOS concentrations were removed to below 2016 USEPA heath advisory level (HAL) of 70 ng/L for drinking water. The MDLs of both compounds (PFOA: 3 ng/L; PFOS: 7 ng/L) were above the 2022 HAL for both compounds (PFOA: 0.004 ng/L; PFOS: 0.02 ng/L) so it could not be determined whether the 2022 HAL was met. To remove short-chain PFAAs, an additional experiment was performed in which the cationic surfactant CTAB was added initially and after every 30 minutes of treatment (**Figure 66b**) for another 210 minutes of treatment. Dosing every 30 minutes was needed to maintain a CTAB concentration of 0.2 mM since it is readily degraded by the plasma. In this experiment all the short-chain PFAAs were removed to BDL in 90 minutes of treatment time, expect PFBA whose concentration decreased from 6000 to 260 ng/L.

Because there is a high salt (NaCl) concentration in SB samples, formation of perchlorate was investigated. Perchlorate concentrations in all untreated and treated still bottoms were below detection limits of 0.2 mg/L. Recovery of perchlorate in a standard addition experiment performed by adding 3.3 mg/L to a treated sample was 102%, indicating there were no matrix effects that interfered with perchlorate analysis.

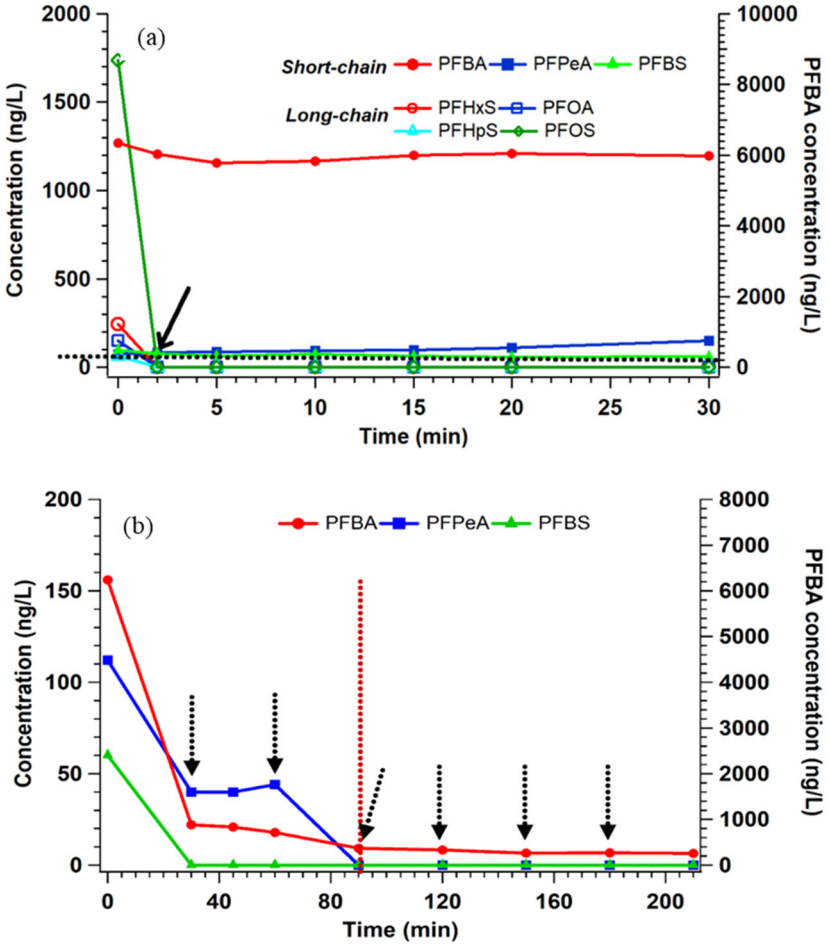

Figure 66. PFAAs concentration profiles during additional plasma treatment of a SB sample in the low concentration reactor in the (a) absence of CTAB; dotted black line showing the 2016 USEPA HAL (70 ng/L) for PFOA and PFOS which was achieved within 5 minutes (black arrows) of treatment, and (b) presence of CTAB (cationic surfactant); CTAB concentration was increased to 0.2 mM at every 30

minutes (black arrows). Red vertical dotted line at 90 min mark indicates the time that all short-chain PFAAs reached to BDL except PFBA.

Fluorine Mass Balance for SB samples. The total fluorine mass was determined by summing the masses of the organically bound and free inorganic F. Free inorganic fluoride was measured using IC, whereas the bound liquid phase organic fluorine was calculated using the measured concentrations of the PFAAs and TOP. For all the SB samples, the organically bound fluorine concentration decreased, and free inorganic fluoride ion concentration increased after treatment time of six hours (**Figure 67**). Overall, a range of 47-117% fluorine mass balance closure was achieved. The lower fluorine recovery could be attributed to volume loss due to evaporation, sputtering of droplets onto the reactor components, and adsorption on reactor components. The higher ionic strength of SB solutions caused significant liquid heating and evaporation loss compared to low-conductivity liquid. In addition, small amounts of smaller molecules like perfluoropropionic acid and trifluoroacetate which were not measured, could also have accounted for some of the missing F.

Effect of Water Matrices on PFAS Removal. To understand the influence of groundwater conditions on treatment of PFAS, a Pearson's correlation analysis was performed to investigate the impact of IDW characteristics on pseudo first order removal rate constants for PFOA and PFOS ($k_{PFOA+PFOS}$). The integration of the kinetic rate expression was carried out between time zero and the time required for the concentration of PFOA+PFOS to drop below the 2016 HAL of 70 ng/L. The impact of total PFAAs concentration (ng/L), combined initial PFOA and PFOS concentration (ng/L), total identified precursor (TIP) concentration (ng/L), TOP concentration (ng/L), PFAS+TOP concentration (ng/L), PFAAs+TIP (ng/L), solution conductivity (µS/cm), TOC (mg/L) and total fluorine (µg/L) on combined PFOA and PFOS (PFOA+PFOS) removal were investigated.

Of these variables, the removal rate of PFOA+PFOS was significantly correlated only with TIP ($r = -0.55$, $p = 0.049$) and marginally correlated with total fluorine ($r = -0.49$, $p = 0.087$). Other parameters such as total PFAAs+TIP ($r = -0.45$, $p = 0.127$), total PFAAs ($r = -0.44$, $p = 0.131$), conductivity ($r = -0.42$, $p = 0.152$), PFAAs+TOP ($r = -0.39$, $p = 0.186$) and total PFOA+PFOS ($r = -0.39$, $p = 0.188$) were also negatively correlated with PFOA+PFOS removal rates, however, they were not statistically significant (**Table 32**). TIP was the most influential parameter suggesting that the concentrations of precursors can decrease the PFAAs degradation rate by scavenging reactive species generated by the plasma and also by generating PFOA and PFOS as byproducts. In addition, no correlation with TOC was observed ($r = -0.18$, $p = 0.55$) indicating that the presence of natural organic matter such as VOCs, humic acid, and fulvic acid does not affect the removal rates of PFAS. This result is because the removal of PFOA and PFOS is taking place at the gas-liquid interface where (non-surfactant) co-contaminants are least likely to interfere, as explained in detail in our publication (Stratton et al., 2017). Some studies also reported the co-occurrence of non-PFAS surfactants such as hydrocarbons with PFAS in groundwaters. Although these hydrocarbons might compete with PFAS for the sites and reactive species at the gas-liquid interface, their presence is not expected to lower the PFAS treatment effectiveness because surfactant compounds (PFAS) are degraded directly in the plasma via "above-surface" reactions which proceed at extremely high rates; rates of reactions that occur beneath or at the plasma-liquid interface (e.g., hydrocarbons) are significantly lower (Mededovic et al., 2016).

Scaled-Up Plasma Reactors. Scaled-up plasma reactors were developed for large volume treatment of concentrated IX regenerant solutions (still bottoms (SB)). Still bottom samples were collected from ECT2 and treated in two batches in two 35-gallon identical plasma reactors. Each sample was first treated in the "high-concentration reactor" and further in the "low-concentration reactor." SB samples were diluted 17 times prior to treatment. A 0.2 mM concentration of the cationic surfactant cetrimonium bromide (CTAB) was used for the removal of short-chain PFAAs and was added at 21.5 and 16 hours in batch 1 and 2, respectively.

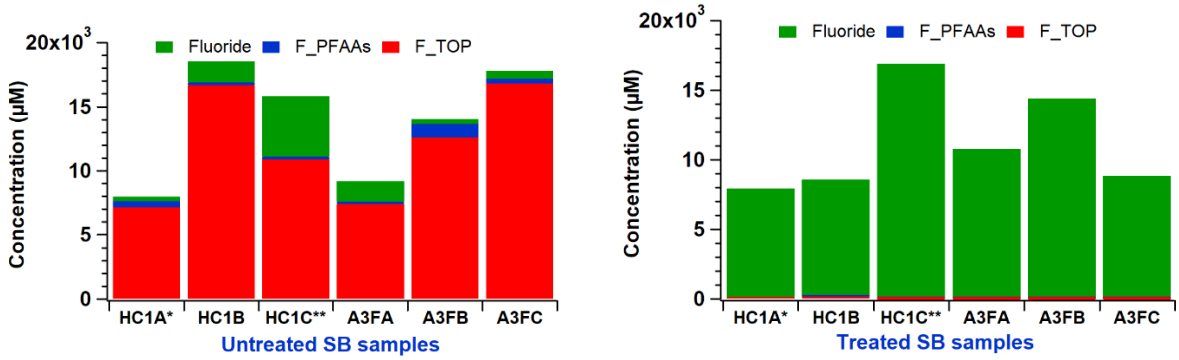

Figure 67. Fluorine mass balance in untreated (left) and plasma treated (right) still bottom samples. HC1A* was undiluted, HC1C** was diluted 50 times, and other SB samples were diluted 10 times. The concentrations shown here are normalized to their initial dilutions.

Table 32. Pearson's Correlation Matrix Showing the Effect of Different Water Matrices on the PFOA and PFOS Removal Rate. Statistically significantly ($p < 0.05$) correlations are in bold.

	k (min^{-1})	Total PFAS (ng/L)	TOP (ng/L)	PFOA+ PFOS (ng/L)	TIP (ng/L)	PFAS+ TOP (ng/L)	PFAS+ TIP (ng/L)	Cond. (µS/cm)	TOC (mg/L)
k (min^{-1})	1								
Total PFAS (ng/L)	-0.44	1							
TOP (ng/L)	-0.27	0.87	1						
PFOA+PFOS (ng/L)	-0.39	1.00	0.88	1					
TIP (ng/L)	-0.55	0.92	0.73	0.89	1				
PFAS+TOP (ng/L)	-0.39	0.98	0.95	0.99	0.88	1			
PFAS+TIP (ng/L)	-0.45	1.00	0.87	1.00	0.92	0.98	1		
Cond. (µS/cm)	-0.42	0.01	0.26	-0.01	-0.06	0.10	0.00	1	
TOC (mg/L)	-0.18	-0.09	-0.16	-0.07	-0.13	-0.12	-0.09	-0.09	1

High-Concentration Plasma Treatment Results. For the three identified precursors to PFAA (8:2, 6:2 and 4:2 FTS) from both batches, 8:2 FTS and 6:2 FTS were removed by ~99%, however, 4:2 FTS (a short-chain precursor) was not removed in 12 hours of treatment **(Figure 68a and 69a)**. Plasma degradation efficiencies were higher for long-chain PFAAs than for short-chain PFAAs, which is consistent with what was found earlier for our small batch (~750 mL) SBs treatment. For long-chain PFAAs (PFNS, PFDA, PFOS, PFNA, PFHpS, PFOA and PFHxS), plasma treatment resulted in >99% degradation within 12 hours, and the extent of removal was higher for longer PFAA chain length (**Figure 68b and 69b**). For short-chain PFAAs, removal efficiencies were not appreciable within 21.5 hours of treatment in batch 1. To remove short-chain PFAAs and 4:2 FTS, CTAB was added at 21.5 hours and after every 2 additional hours of treatment (**Figure 68c**, black arrows). Dosing at every 2 hours was needed to maintain a CTAB concentration of approximately 0.2 mM since it is readily degraded by the plasma (CTAB concentration was not measured during the treatment). The frequency of CTAB addition was determined by the visual inspection of the depletion rate of the foam layer in the reactor. After CTAB addition, a significant decrease in short-chain PFAAs (PFHpA, PFPeS, PFHxA, and PFBS) except PFBA and PFPeA was observed (**Figure 68c**) within 3 hours of treatment (between 21.5th and 24.5th hour). During batch 1 treatment, there was a insignificant decrease of all PFAS concentration between 16 and 21.5 hours due to release of sorbed PFAS from contaminated diffusers. Therefore, CTAB was added at 16th hour for batch 2 treatment (**Figure 69c**). Treated SB samples were transferred to the low-concentration reactor for further treatment.

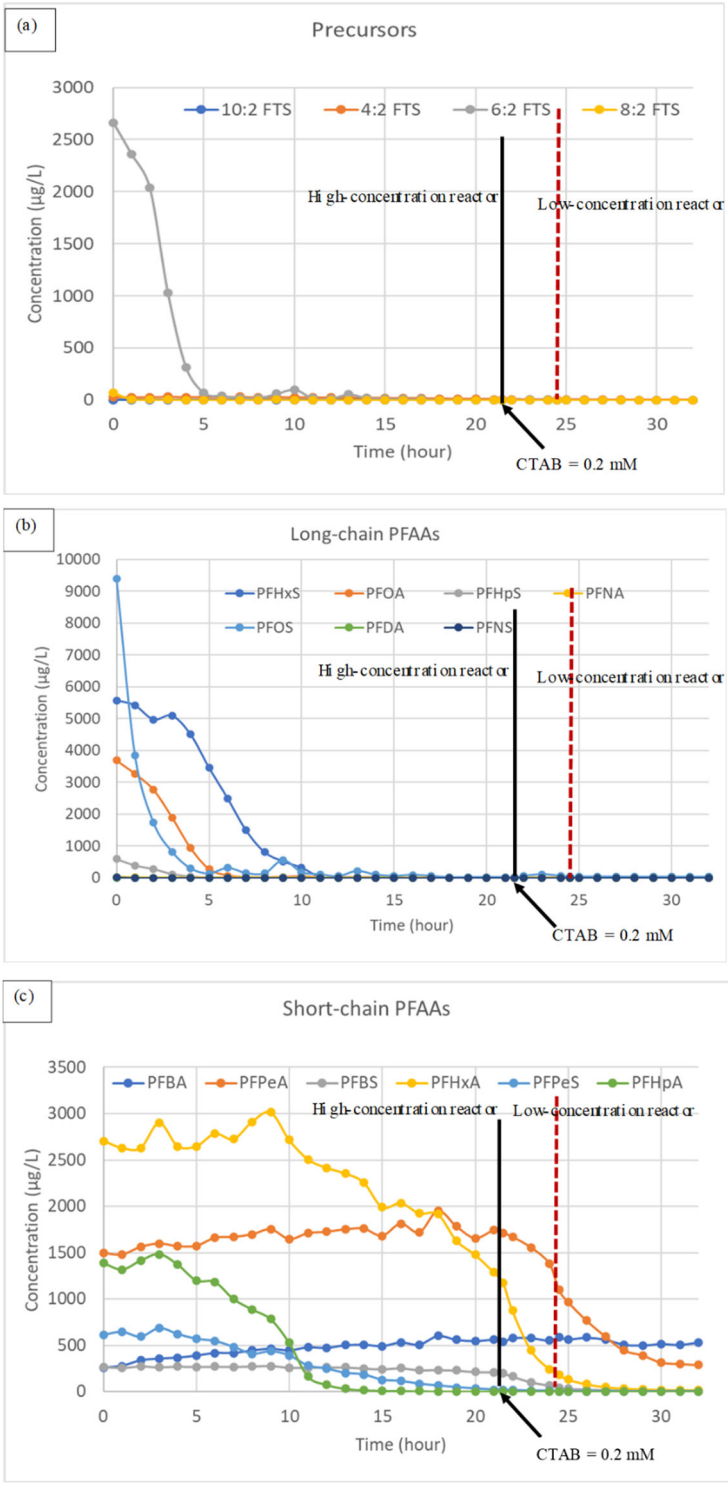

Figure 68. Concentration profiles of (a) precursors, (b) long-chain PFAAs and (c) short-chain PFAAs during plasma treatment of the batch 1 of SB sample in the high- and low-concentration reactor; solid black line represents the point (21.5th hour) of CTAB addition and CTAB concentration was increased to 0.2 mM at every 2 hours. The red dotted line at 24.5th hour mark indicates the time at which the sample was transferred from high-concentration reactor to low-concentration reactor.

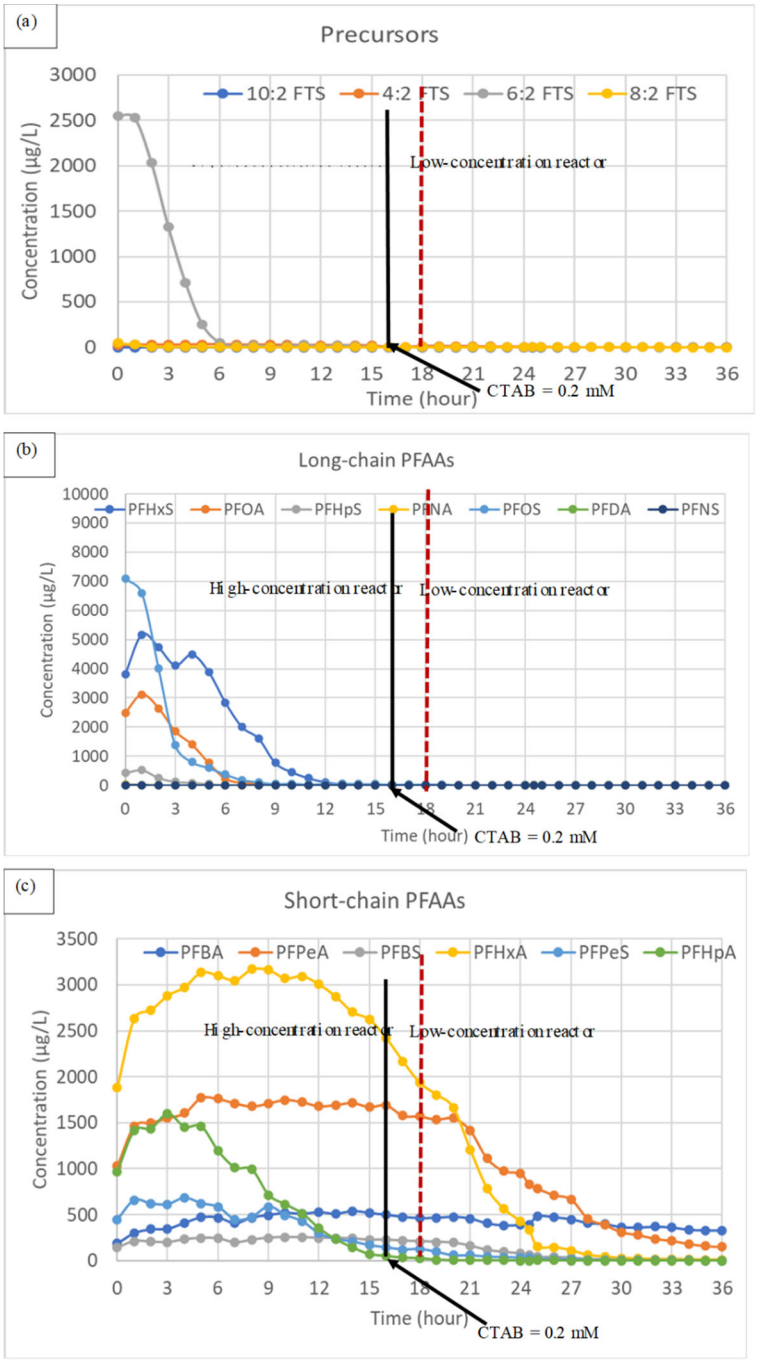

Figure 69. Concentration profiles of (a) precursors, (b) long-chain PFAAs and (c) short-chain PFAAs during plasma treatment of the batch 1 of SB sample in the high- and low-concentration reactor; solid black line represents the point (16th hour) of CTAB addition and CTAB concentration was increased to 0.2 mM at every 2 hours. The red dotted line at 18th hour mark indicates the time at which the sample was transferred from high-concentration reactor to low-concentration reactor.

Low-Concentration Plasma Treatment Results. By continuing plasma treatment, all the identified precursors were removed by ~99.9%, however, they were not removed to below detection limit (BDL, ~90 ng/L). This could be due to desorbed precursors from diffusers (**Figure 68a and 69a**). There was no significant removal of long-chain PFAAs observed, which could be due to the interference of CTAB that was present at much higher concentration compared to long-chain PFAAs. On the other hand, a significant decrease (~99%) in short-chain PFAAs (PFHpA, PFPeS, PFHxA, and PFBS) except PFBA and PFPeA was observed (**Figures 68c and 69c**). Our additional analysis confirmed that CTAB decreases the degradation efficiency of long-chain PFAAs, but improve the degradation efficiency for short-chain PFAAs.

TASK 8: CONCEPTUAL DESIGNS FOR IN SITU AND EX SITU TREATMENT TRAINS

Conceptual Designs. Conceptual designs for potential coupled treatment systems to manage the challenge of PFAA precursors, to efficiently separate PFAS from contaminated groundwater using media that can be regenerated and reused, and to ultimately destroy PFAS on site were prepared to explore their integrated technical feasibility and implementation challenges.

Three treatment scenarios were developed based on data from two example sites (**Table 33**). A key difference between the two sites is that Site A has been the basis of both laboratory and pilot study treatability projects conducted under the Environmental Security Technology Certification Program (ESTCP ER18-5015) and has an existing regenerable ion exchange P&T system. Site B neither has a P&T system nor any treatability data available related to ex-situ treatment of groundwater from the Site. Therefore a "Base Case" was established using the available data from Site A in order to develop three additional treatment scenarios. These additional scenarios include one scenario for Site A and two scenarios for Site B.

One of the primary challenges to implementation of a combined P&T PFAS treatment system is pretreatment of contaminated groundwater. Groundwater may contain metals or compounds that would foul the PFAS treatment technologies and degrade treatment performance; common examples include iron, manganese, total organic carbon (TOC), and other suspended or dissolved solids. For example, iron fouling has been a common problem at the existing Site A treatment plant. While Site B does not have an existing P&T system or PFAS treatability data, the available TOC data for the site suggests pretreatment of TOC to prevent fouling of a potential PFAS treatment system will likely be required.

Another challenge to implementation of a combined P&T PFAS treatment system is the additional health, safety, and environmental requirements associated with the technologies in the PFAS treatment system. For example, the regenerable resin technology uses flammable solvents (e.g. methanol, ethanol, or isopropyl alcohol) or potentially toxic solvents (methanol) to regenerate the ion exchange resin. The use of these solvents requires additional engineering measures (e.g. explosion-proof electrical requirements for electrical equipment near the regeneration and distillation process units) and health and safety measures (e.g. sensors, alarms, fire suppression) to protect the P&T system facility and workers.

Approach. *Site A.* Site A is located at the former fire training area (also called as Site 8) at the former Pease Air Force Base (Pease) in Portsmouth, New Hampshire (NH). Site A has been the basis of both laboratory and pilot study treatability projects conducted under the Environmental Security Technology Certification Program (ESTCP ER18-5015) and has an existing regenerable ion exchange P&T system. A pilot test was conducted at Site A under the ESTCP program to prove the effectiveness and develop scale-up criteria for integrating PFAS treatment and destruction technology into existing or new groundwater treatment systems. The pilot test had a lower flowrate (2-3 gallons per minute [gpm]) than the scaled-up scenarios (100 gpm) developed as part of this evaluation. The pilot scale PFAS treatment and destruction train consisted of four treatment steps that complement each other to remove PFAS from treated water with reusable media, reduce the volume of the PFAS-contaminated waste stream, and destroy that waste stream on-site.

Table 33. Site A and Site B characteristics used for scaled up conceptual designs.

	Site A	Site B
Perfluorobutanoic acid (PFBA)	0.57 ug/L	40 ug/L
Perfluorobutanesulfonic acid (PFBS)	0.5 ug/L	69 ug/L
Perfluoroheptanoic acid (PFHpA)	1.3 ug/L	40 ug/L
Perfluoroheptanesulfonic Acid (PFHpS)	2 ug/L	28 ug/L
Perfluorohexanoic acid (PFHxA)	4.5 ug/L	230 ug/L
Perfluorohexanesulfonic acid (PFHxS)	19 ug/L	446 ug/L
Perfluorononanoic acid (PFNA)	0.1 ug/L	1.1 ug/L
Perfluorooctanoic acid (PFOA)	11 ug/L	175 ug/L
Perfluorooctanesulfonic acid (PFOS)	60 ug/L	791 ug/L
Perfluoropentanoic acid (PFPeA)	2.6 ug/L	120 ug/L
6:2 Fluorinated telomer sulfonate(6:2 FTS)	23 ug/L	258 ug/L
8:2 Fluorinated telomer sulfonate(8:2 FTS)	0.3 ug/L	6.5 ug/L
Total PFAS	125 ug/L	1945 ug/L
PFOS+PFOA	71 ug/L	259 ug/L
Alkalinity	170 mg/L	190 mg/L
Hardness	170 mg/L	230 mg/L
Total Organic Carbon	Low	High
pH	N/A	6.3
Conductivity	N/A	284 uS/cm
Total Dissolved Solids	340 mg/L	N/A
Total Iron	15000 ug/L	N/A
Total Manganese	4800 ug/L	N/A
Phosphorous	0.5 mg/L	N/A
Site flowrate	2-3 gpm	N/A
Scale up to 100 gpm based on	Ex situ treatability data	Groundwater characterization, no ex situ treatability data

As described above, one of the primary drivers of the Site A conceptual design has been the removal of iron before PFAS treatment by the ion exchange resin. This has required pilot testing technologies and retrofitting the full-scale plant over its first several years of operations.

Site A Treatment Scenarios. Site A is the base case P&T system which entails groundwater extraction, pretreatment for iron, granular activated carbon (GAC), regenerable IX with distillation and super loader (large single use IX vessel) for still bottoms treatment (**Figure 70**). Option 1 is based on a site 8 scenario with plasma destruction in place of super loader for the treatment of still bottoms where the P&T system entails groundwater extraction, pretreatment for iron, GAC, regenerable IX with distillation, and plasma destruction for still bottoms treatment (**Figure 71**).

Site B. The second site is referred to as "Site B" which is modeled after a real site with some known and some unknown characteristics which were assumed for conceptual design. This site neither has a P&T system nor any treatability data available related to ex-situ treatment of groundwater from the site.

Based on the high TOC, it's expected pretreatment of the groundwater would be necessary; the pretreatment technology would depend on the speciation of organic carbon compounds in the water. The high levels of PFAS, including PFOS and PFOA at almost 1 mg/L combined, may require extended contact times with the ion exchange resin to remove to target effluent concentrations in the water. Extended contact times would require more ion exchange resin and therefore a larger regeneration system.

Site B Treatment Scenarios. Site B is the extrapolated case based on information from the base case in Site A which can be treated using two different options. Option 1 P&T system entails groundwater extraction, GAC, regenerable IX with distillation, and plasma destruction for the treatment of still bottoms (**Figure 72**). Option 2 P&T entails in situ chemical oxidation (ISCO), groundwater extraction, GAC, regenerable IX with distillation, and plasma destruction for the treatment of still bottoms (**Figure 73**).

Viable Treatment Trains and Treatment Scenarios. The Site A, base case entails an extraction well network with pretreatment of iron with accompanying sludge treatment, organic carbon treatment, ion exchange resins with assumed direct discharge of treated water; the resins are regenerated with a solvent brine solution, followed by distillation and treatment of the still bottoms with superloader (**Figure 70**).

- Site A, option 1 differs from the base case by treating the distilled solution with plasma instead of the superloader (**Figure 71**).
- Site B, option 1 differs from Site A, option 1 by forgoing iron pretreatment with accompanying sludge treatment (**Figure 72**); and
- Site B, option 2 introduces the ISCO well and injection network before the extraction well network (**Figure 73**).

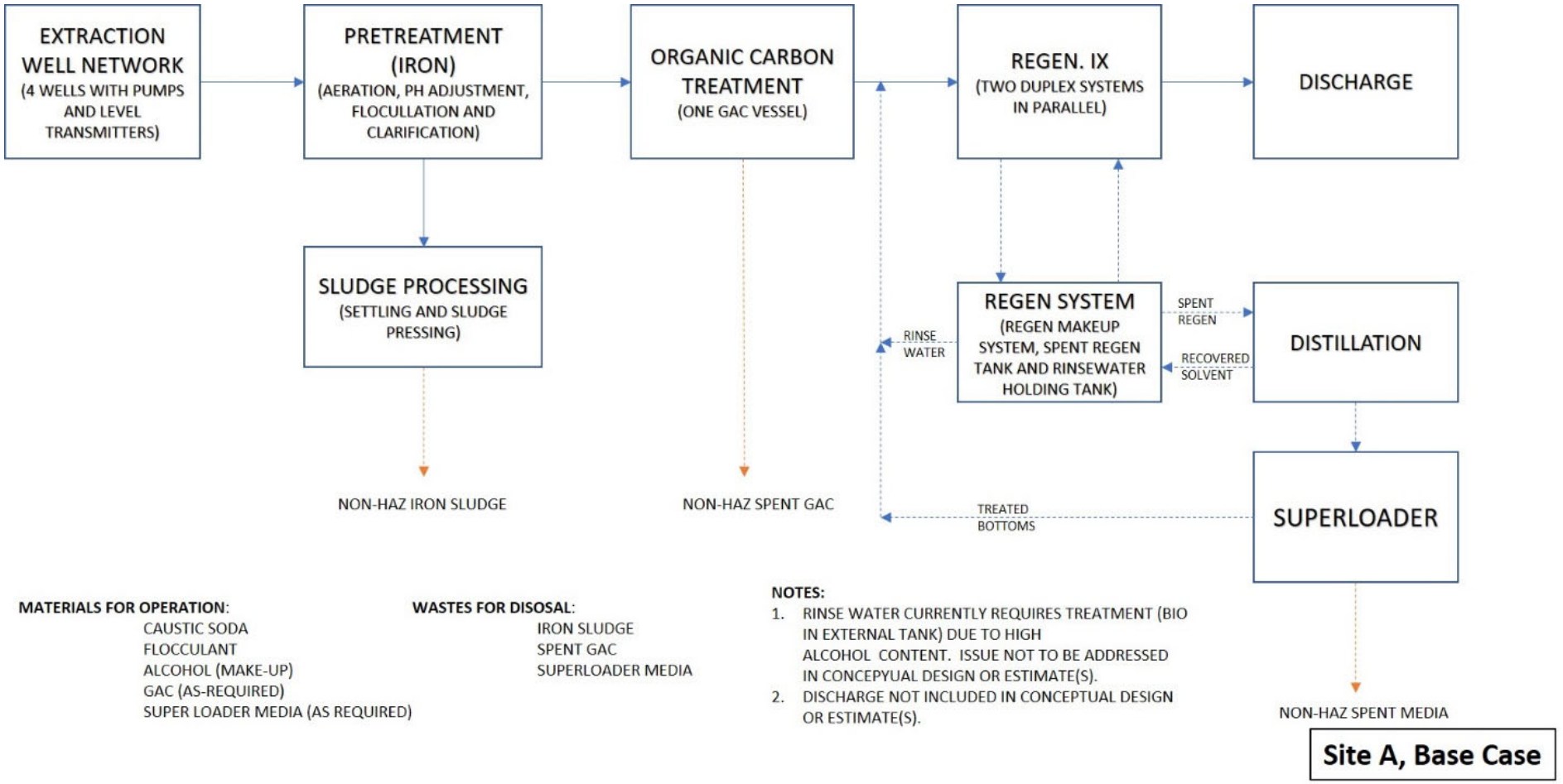

Figure 70. Site A, Base Case.

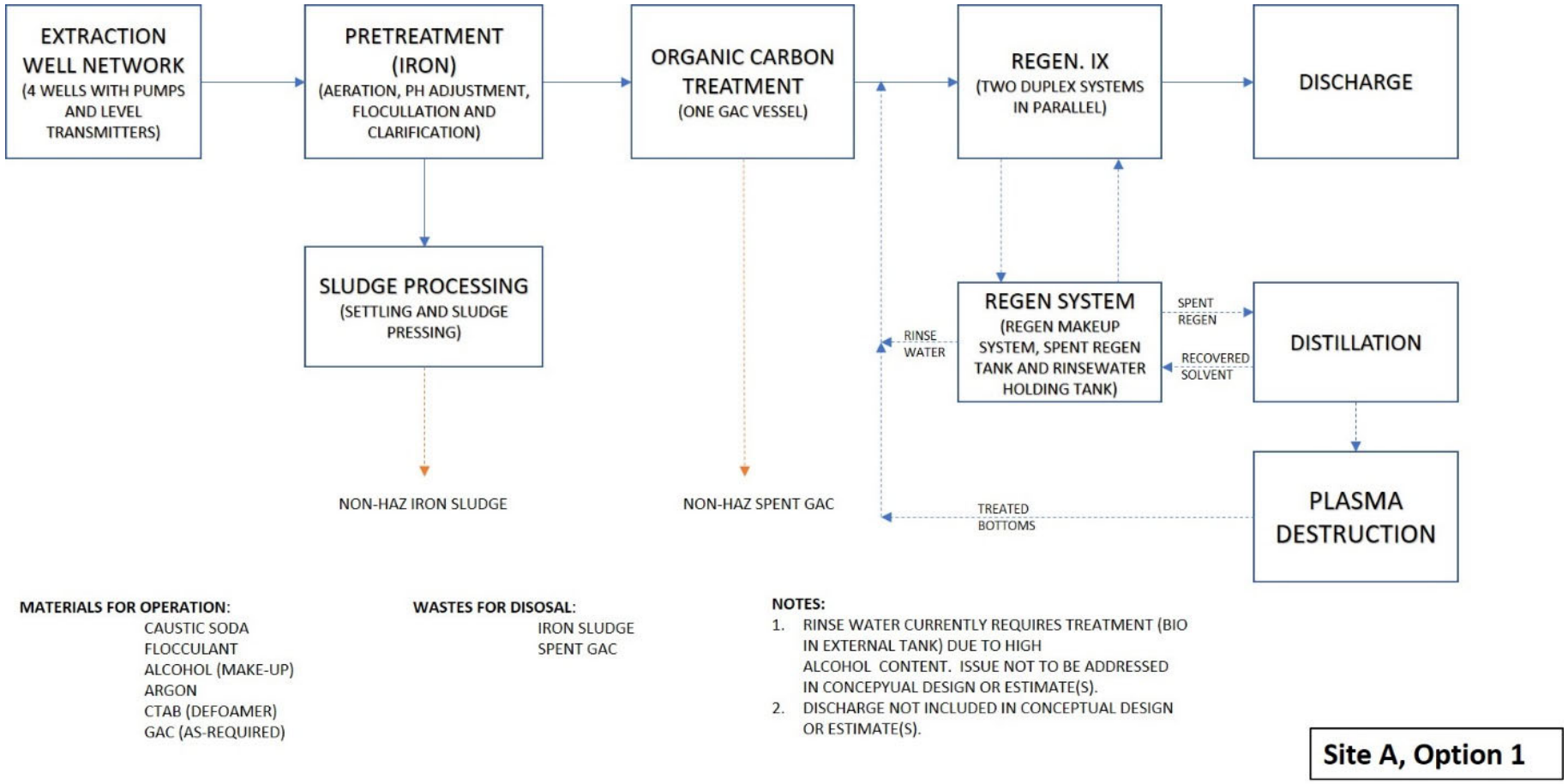

Figure 71. Site A, Option 1.

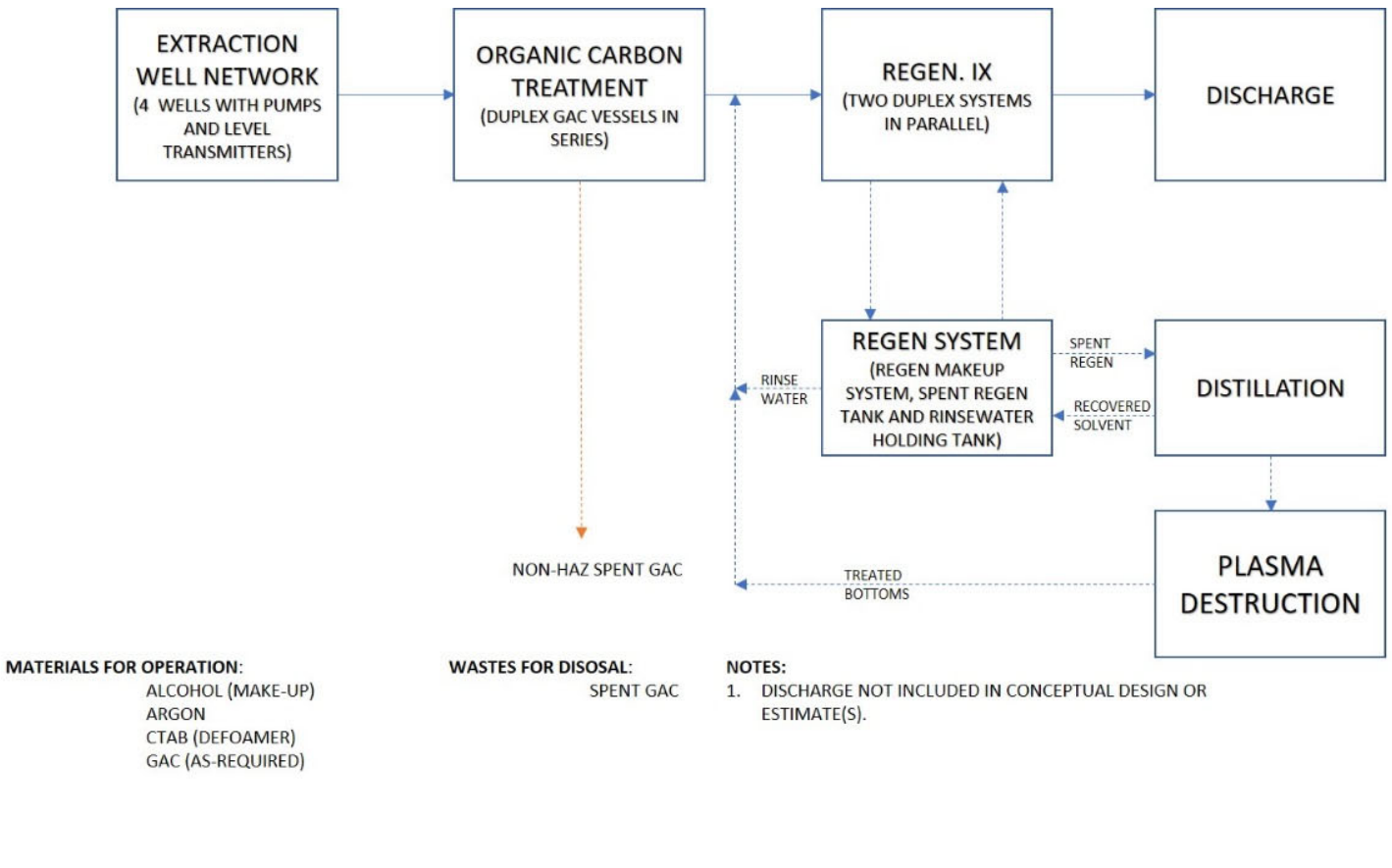

Figure 72. Site B, Option 1.

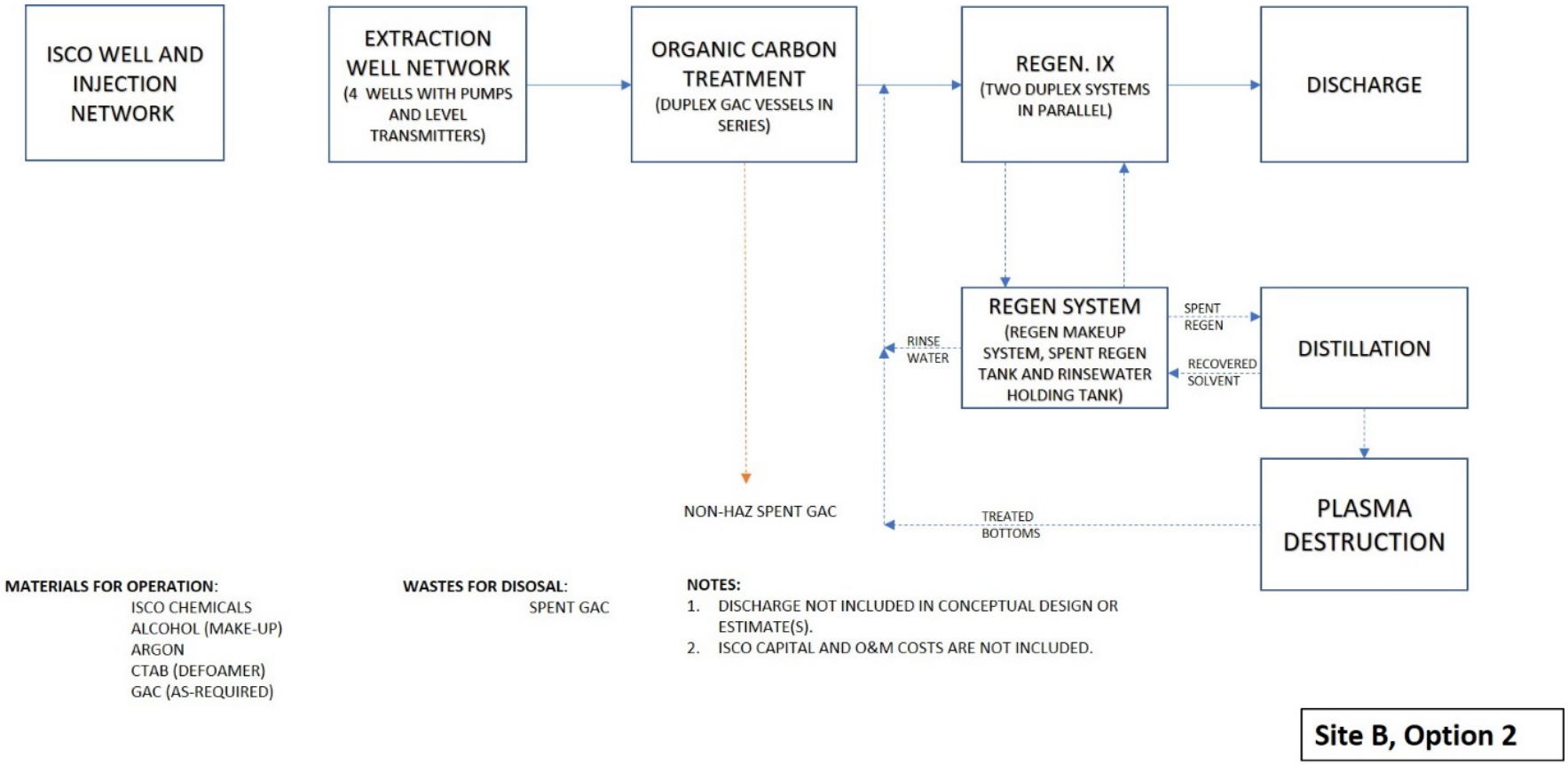

Figure 73. Site B, Option 2.

Implementation Challenges and Considerations. Additional work is required to understand how either persulfate or air sparge could be applied in the field to accelerate mobilization of precursors. These issues are presented below to help with additional design considerations:

- It is clear from both batch and column experiments that persulfate has the potential to convert PFAA precursors to more mobile intermediate and terminal degradation products. However, additional work is needed to understand oxidant dose and the need for multiple rounds of oxidant application.
- Any type of flushing technique needs to be executed with proper hydraulic controls in place to ensure that the plume is mobilized towards downgradient receptors, and some types of subsurface hydrogeology may not be suitable for effective application of in situ chemical oxidation.
- Experiments in a truly anoxic condition are needed and experiments with a nutrient amendment to help better understand the potential for enhanced transformation using air sparging to accelerate precursor conversion.

Items that need to be considered based on the operational experience during the pilot test and current operations at the full-scale system at Site 8 are presented below to help aid design decisions:

- Pretreatment for co-contaminants (metals, TOC, TSS, TDS, VOCs etc.): Based on the site-specific co-contaminants, pretreatment requirement can add to increased building size and larger pretreatment vessels footprint. These need to be carefully evaluated prior to design of any full-scale system.
- Downflow versus up-flow operation of the resin beds and the ability to backwash as required. Any full-scale system should be designed with adequate pretreatment so as not to require backwashing of the resin, which will disrupt the mass transfer zone of the resin bed. However, if a challenging water source makes it likely that the resin may be fouled, then down flow operation allows backwashing to remove foulants from the media. Based on the pilot and full-scale observations the treatment system should be fitted with downflow and up-flow valving to reduce operations and maintenance costs.
- Biofouling can be observed in any IX/GAC system, especially during long periods of down time required by maintenance activities, leading to pressure drop. Treatment equipment should include provisions for addressing these issues (backwashing and/or biocide addition) that could possibly negatively affect the resin/GAC performance.
- Consider the use of single pass IX after regenerable IX as a polishing step (based on pilot and full-scale Site 8 operations data). This should be considered if the influent stream has short chain PFAS compounds which require removal to meet regulatory requirements (especially PFAS with less than 6 carbons, e.g., PFBA). Alternatively, the regeneration cycle length can be reduced to accommodate enhanced removal of short chain PFAS.
- Waste minimization may be reduced if pretreatment before regenerable IX and tertiary treatment after plasma destruction are required. These wastes could potentially include spent filters, sludge as well as spent media (as applicable) requiring disposal as PFAS containing wastes.
- If regeneration and distillation cannot be performed outside (dependent on geographical system location) the equipment building, equipment, and related infrastructure must be explosion-proof.
- Identify discharge requirements for the system effluent to select appropriate regenerant (e.g., methanol may be regulated in the discharge permit, but IPA may not). This would be dependent on the regulatory authority's requirements.

- Spent regenerant after distillation through super loader and/or plasma destruction treatment has a high salt concentration and must be bled back into the system to avoid off-site disposal. The waste stream would be highly diluted depending on full-scale system flow; however, the high salt content may pose discharge concerns depending on discharge location (e.g., sewer, on-site reinjection or surface water).
- The distillation system should be appropriately designed to account for foaming (observed during the pilot study) to minimize PFAS carryover in the distillate.
- Application of plasma for PFAS destruction in still bottoms has been shown to be viable, however it has not been deployed at the scale required for full-scale, stand-alone treatment. While technologically there are no significant barriers to overcome, significant engineering would be required to design a system that was reliable, could operate largely unattended and was able to meet the treatment goals. Implementation challenges may include equipment reliability and maintenance requirements.

Cost Drivers. Key cost drivers for these sites and for evaluation of any potential site for this PFAS treatment system include: 1) design flow rates, PFAS concentrations, and presence of foulants or competing ionic species; 2) PFAS treatment capacity of the treatment media; and 3) regulated PFAS for the specific site.

Design flow rates, PFAS concentrations, and presence of foulants or competing ionic species affect ISCO treatment to degrade PFAS precursors in the groundwater, the volume of treatment media required for IX along with media vessel sizing which dictates facility size, the consequent volume of regeneration solution required and the size of major equipment items such as solution makeup tanks, the distiller, and the PFAS destruction unit, and the energy demand for ISCO and plasma treatment.

PFAS treatment capacity of the treatment media drives the frequency of media regeneration, the size of major equipment items such as solution makeup tanks and especially the distiller and the PFAS destruction unit, and energy requirements for system O&M, especially the distiller and the PFAS destruction unit.

Regulated PFAS for the specific site drives the PFAS treatment media sizing wherein lower treatment goals or goals that include harder to treat short chain PFAS may require more media and longer contact times to remove. This would result in larger treatment vessels, and upsizing of regeneration and destruction equipment sizing and O&M energy costs wherein more stringent treatment goals may require more frequent regenerations and therefore greater volumes of regenerant solution processed by the distiller and the PFAS destruction unit.

CONCLUSIONS AND IMPLICATIONS FOR FUTURE RESEARCH/IMPLEMENTATION

OVERALL RESULTS AND CONCLUSIONS

Pre-treatment in situ. Groundwater and soil from contaminated sites were found to have PFAA precursors, short-chain and long-chain PFAS including PFOS and PFOA. Precursor transformation was deemed effective using persulfate and oxygen amendment in both batch tests and transport cells and were found to reduce PFAA source zones through the optimization of treatment conditions, however this did not significantly decrease the time associated with subsequent ex situ plasma treatment.

Ion-exchange ex situ. IX regenerant solutions were tested and three different solutions were explored in depth: (1) a mixture of 90% methanol and 2% NaCl, (2) a mixture of 100% methanol with 2.5% NaBr, and (3) a mixture of 90% methanol and 2% NaBr. Regenerant solution performance was comparable between the solutions even in different resins. There is very little difference in regeneration results for the three different test regenerant solutions. Distillation was found to be the best performing recovery method (e.g. maximum regenerant solution recovery and minimum PFAS carry over) for each of the regenerant solutions.

Plasma treatment ex situ. Plasma was found to be successful in the treatment of PFAS in groundwater, pre-oxidized groundwater, and in concentrated IX regenerant solution, including precursors, long-chain, and short-chain compounds, has been achieved under optimized reactor conditions/configurations and under a broad range of groundwater conditions. The incorporation of plasma into treatment trains that include pre-oxidation and concentration by ion exchange individually or combined is appropriate and effective and plasma treatment of PFAS in concentrated IX still bottoms necessitates two reactors – an initial "high concentration" reactor followed by a "low concentration" polishing reactor.

Treatment train. Conceptual design and remedial guidance were developed based on Site A which has been the basis of both laboratory and pilot study treatability projects conducted under the Environmental Security Technology Certification Program (ESTCP ER18-5015) and has an existing regenerable ion exchange P&T system, and Site B which neither has a P&T system nor any treatability data available related to ex-situ treatment of groundwater from the Site. From these sites, three viable treatment trains were identified and process flow schematics were developed resulting in a protective remediation approach that can be implemented fully on-site which seeks to manage the challenge of PFAS precursors, to efficiently separate PFAS from contaminated groundwater using media that can be regenerated and reused, and to ultimately destroy PFAS. As no single treatment technique can address all of these challenges, implementation challenges and considerations based on these two sites and developed treatment trains provide guidance for Sites A and B, and for evaluation of any potential site for a holistic PFAS treatment train. Major cost drivers for a holistic treatment approach were identified to be design flow rates, PFAS concentrations, and presence of foulants or competing ionic species, PFAS treatment capacity of the treatment media, and regulated PFAS for specific sites.

RESOLUTION OF KNOWLEDGE GAPS AND IDENTIFICATION OF REMAINING RESEARCH QUESTIONS

The conceptual designs highlight feasible combinations of in situ and ex situ treatment trains that close PFAS treatment gaps of managing the challenge of PFAS precursors, to efficiently separate PFAS from contaminated groundwater using media that can be regenerated and reused, and to ultimately destroy PFAS implemented fully on-site. The developed treatment trains provide guidance for Sites A and B, and for evaluation of any potential site for a holistic PFAS treatment train that extends beyond what a single

treatment technique can do alone. Due to the fundamental nature of this work, a site-specific pilot testing guided by these conceptual designs is recommended for remedial technology selection and additional treatment scenarios should be evaluated on a case-by-case basis.

DIRECT IMPLEMENTATION BY DOD AND OTHERS

Discovering and demonstrating an effective and efficient treatment approach for PFAS is essential as the Navy alone has identified over 300 sites with likely plumes, and over a dozen sites that have drinking water extraction wells within one mile downgradient. Ex situ plasma treatment in combination with precursor transformation and IX treatment using regenerable resin can be used as a more efficient and cost-effective approach in terms of destructive treatment and both the resin and regenerant solutions can be reused, extending treatment time and minimizing both cost and waste relative to more conventional GAC treatment. By replacing the established technologies, such as granular activated carbon (GAC), or by combining multiple technologies, a more cost-effective overall treatment system can be obtained that results in no waste product, can be implemented fully on site, and will result in a more protective and efficient treatment option for the DoD and others.

LITERATURE CITED

Ahrens, L.; Bundschuh, M. Fate and Effects of Poly- and Perfluoroalkyl Substances in the Aquatic Environment: A Review: Fate and Effects of Polyfluoroalkyl and Perfluoroalkyl Substances. Environmental Toxicology and Chemistry 2014, 33 (9), 1921–1929. https://doi.org/10.1002/etc.2663.

Appleman, T.D., E.R.V. Dickenson, C. Bellona, C.P. Higgins (2013). Nanofiltration and granular activated carbon treatment of perfluoroalkyl acids. Journal of hazardous materials 260 (2013): 740-74.

ASTM. Standard Test Method for Measuring the Exchange Complex and Cation Exchange Capacity of Inorganic Fine-Grained Soils. ASTM D7503-10 2010.

Barzen-Hanson, K. A.; Davis, S. E.; Kleber, M.; Field, J. A. Sorption of Fluorotelomer Sulfonates, Fluorotelomer Sulfonamido Betaines, and a Fluorotelomer Sulfonamido Amine in National Foam Aqueous Film-Forming Foam to Soil. Environmental Science & Technology 2017, 51 (21), 12394–12404. https://doi.org/10.1021/acs.est.7b03452.

Barzen-Hanson, K. A.; Roberts, S. C.; Choyke, S.; Oetjen, K.; McAlees, A.; Riddell, N.; McCrindle, R.; Ferguson, P. L.; Higgins, C. P.; Field, J. A. Discovery of 40 Classes of Per- and Polyfluoroalkyl Substances in Historical Aqueous Film-Forming Foams (AFFFs) and AFFF-Impacted Groundwater. Environ. Sci. Technol. 2017, 51 (4), 2047–2057. https://doi.org/10.1021/acs.est.6b05843.

Bräunig, J.; Baduel, C.; Heffernan, A.; Rotander, A.; Donaldson, E.; Mueller, J. F. Fate and Redistribution of Perfluoroalkyl Acids through AFFF-Impacted Groundwater. Science of The Total Environment 2017, 596–597, 360–368.

Bruton, T. A.; Sedlak, D. L. Treatment of Aqueous Film-Forming Foam by Heat-Activated Persulfate Under Conditions Representative of In Situ Chemical Oxidation. Environmental Science & Technology 2017, 51 (23), 13878–13885. https://doi.org/10.1021/acs.est.7b03969.

Bruton, T. A.; Sedlak, D. L. Treatment of Perfluoroalkyl Acids by Heat-Activated Persulfate under Conditions Representative of in Situ Chemical Oxidation. Chemosphere 2018, 206, 457–464. https://doi.org/10.1016/j.chemosphere.2018.04.128.

Buck, R. C.; Franklin, J.; Berger, U.; Conder, J. M.; Cousins, I. T.; de Voogt, P.; Jensen, A. A.; Kannan, K.; Mabury, S. A.; van Leeuwen, S. P. Perfluoroalkyl and Polyfluoroalkyl Substances in the Environment: Terminology, Classification, and Origins. Integrated Environmental Assessment and Management 2011, 7 (4), 513–541. https://doi.org/10.1002/ieam.258.

Calafat, A. M.; Kuklenyik, Z.; Reidy, J. A.; Caudill, S. P.; Tully, J. S.; Needham, L. L. Serum Concentrations of 11 Polyfluoroalkyl Compounds in the U.S. Population: Data from the National Health and Nutrition Examination Survey (NHANES) 1999−2000. Environmental Science & Technology 2007, 41 (7), 2237–2242. https://doi.org/10.1021/es062686m.

Chen, H.; Liu, M.; Munoz, G.; Duy, S. V.; Sauvé, S.; Yao, Y.; Sun, H.; Liu, J. Fast Generation of Perfluoroalkyl Acids from Polyfluoroalkyl Amine Oxides in Aerobic Soils. Environ. Sci. Technol. Lett. 2020, 7 (10), 714–720. https://doi.org/10.1021/acs.estlett.0c00543.

Chen, J., P. Zhang, (2006). Photodegradation of perfluorooctanoic acid in water under irradiation of 254 nm and 185 nm light by use of persulfate. Water science and technology, 54(11-12):317-325.

Cheng, T.; Saiers, J. E. Colloid-Facilitated Transport of Cesium in Vadose-Zone Sediments: The Importance of Flow Transients. Environmental Science & Technology 2010, 44 (19), 7443–7449. https://doi.org/10.1021/es100391j.

Crownover, E.; Oberle, D.; Kluger, M.; Heron, G. Perfluoroalkyl and Polyfluoroalkyl Substances Thermal Desorption Evaluation. Remediation 2019, 29 (4), 77–81. https://doi.org/10.1002/rem.21623.

Cuypers, C.; Grotenhuis, T.; Nierop, K. G. J.; Franco, E. M.; de Jager, A.; Rulkens, W. Amorphous and Condensed Organic Matter Domains: The Effect of Persulfate Oxidation on the Composition of

Soil/Sediment Organic Matter. Chemosphere 2002, 48 (9), 919–931. https://doi.org/10.1016/S0045-6535(02)00123-6.
D'Agostino, L. A.; Mabury, S. A. Identification of Novel Fluorinated Surfactants in Aqueous Film Forming Foams and Commercial Surfactant Concentrates. Environ. Sci. Technol. 2014, 48 (1), 121–129. https://doi.org/10.1021/es403729e.
Dauchy, X.; Boiteux, V.; Colin, A.; Hémard, J.; Bach, C.; Rosin, C.; Munoz, J.-F. Deep Seepage of Per- and Polyfluoroalkyl Substances through the Soil of a Firefighter Training Site and Subsequent Groundwater Contamination. Chemosphere 2019, 214, 729–737. https://doi.org/10.1016/j.chemosphere.2018.10.003.
DeWitt, J. C.; Copeland, C. B.; Strynar, M. J.; Luebke, R. W. Perfluorooctanoic Acid–Induced Immunomodulation in Adult C57BL/6J or C57BL/6N Female Mice. Environmental Health Perspectives 2008, 116 (5), 644–650. https://doi.org/10.1289/ehp.10896.
Du, Z.; Deng, S.; Bei, Y.; Huang, Q.; Wang, B.; Huang, J.; Yu, G. Adsorption Behavior and Mechanism of Perfluorinated Compounds on Various Adsorbents—A Review. Journal of Hazardous Materials 2014, 274, 443–454. https://doi.org/10.1016/j.jhazmat.2014.04.038.
De Silva, A. O.; Spencer, C.; Scott, B. F.; Backus, S.; Muir, D. C. G. Detection of a Cyclic Perfluorinated Acid, Perfluoroethylcyclohexane Sulfonate, in the Great Lakes of North America. Environ. Sci. Technol. 2011, 45 (19), 8060–8066. https://doi.org/10.1021/es200135c.
Eschauzier, C.; Beerendonk, E.; Scholte-Veenendaal, P.; De Voogt, P. Impact of Treatment Processes on the Removal of Perfluoroalkyl Acids from the Drinking Water Production Chain. Environmental Science & Technology 2012, 46 (3), 1708–1715. https://doi.org/10.1021/es201662b.
Even-Ezraa, I., A. Mizrahia, D. Gerrity, S. Snyder, A. Salveson, O. Lahav O., Application of a novel plasma-based advanced oxidation process for efficient and cost-effective destruction of refractory organics in tertiary effluents and contaminated groundwater. Desalination and Water Treatment, 11:236-244.
Gaber, H. Bioavailability of Organic Contaminants Suring Transport: Impact of Initial Soil Environment Conditions. Journal of Soil Sciences and Agricultural Engineering 2004, 29 (4), 2137–2155.
Gerrity, D. B.D. Stanford, R.A. Trenholm, S.A. Snyder, (2010). An evaluation of a pilot-scale nonthermal plasma advanced oxidation process for trace organic compound degradation. Water Research 44(2):493-504.
Guelfo, J.L., C.P. Higgins (2013). Subsurface transport potential of perfluoroalkyl acids at aqueous film-forming foam (AFFF)-impacted sites. Environmental science & technology 47(9):4164-4171.
Guelfo, J. L.; Marlow, T.; Klein, D. M.; Savitz, D. A.; Frickel, S.; Crimi, M.; Suuberg, E. M. (2018) Evaluation and Management Strategies for Per- and Polyfluoroalkyl Substances (PFASs) in Drinking Water Aquifers: Perspectives from Impacted U.S. Northeast Communities. Environmental Health Perspectives, 126 (6), 065001. https://doi.org/10.1289/EHP2727.
Harding-Marjanovic, K. C.; Houtz, E. F.; Yi, S.; Field, J. A.; Sedlak, D. L.; Alvarez-Cohen, L. Aerobic Biotransformation of Fluorotelomer Thioether Amido Sulfonate (Lodyne) in AFFF-Amended Microcosms. Environmental Science & Technology 2015, 49 (13), 7666–7674. https://doi.org/10.1021/acs.est.5b01219.
Higgins, C. P.; Luthy, R. G. Sorption of Perfluorinated Surfactants on Sediments. Environmental Science & Technology 2006, 40 (23), 7251–7256. https://doi.org/10.1021/es061000n.
Higgins, C. P.; Luthy, R. G. Modeling Sorption of Anionic Surfactants onto Sediment Materials: An a Priori Approach for Perfluoroalkyl Surfactants and Linear Alkylbenzene Sulfonates. Environmental Science & Technology 2007, 41 (9), 3254–3261. https://doi.org/10.1021/es062449j.
Hori, H.; Murayama, M.; Inoue, N.; Ishida, K.; Kutsuna, S. Efficient Mineralization of Hydroperfluorocarboxylic Acids with Persulfate in Hot Water. Catalysis Today 2010, 151 (1–2), 131–136. https://doi.org/10.1016/j.cattod.2010.02.023.

Houtz, E. F. Oxidative Measurement of Perfluoroalkyl Acid Precursors: Implications for Urban Runoff Management and Remediation of AFFF-Contaminated Groundwater and Soil, UC Berkeley, 2013.
Houtz, E.F., D.L. Sedlak (2012). Oxidative Conversion as a Means of Detecting Precursors to Perfluoroalkyl Acids in Urban Runoff. Environmental Science & Technology, 46:9342-9349.
Houtz, E.F., C.P. Higgins, J.A. Field, D.L. Sedlak (2013). Persistence of perfluoroalkyl acid precursors in AFFF-impacted groundwater and soil." Environmental science & technology 47(15):8187-8195.
Hu, X. C.; Andrews, D. Q.; Lindstrom, A. B.; Bruton, T. A.; Schaider, L. A.; Grandjean, P.; Lohmann, R.; Carignan, C. C.; Blum, A.; Balan, S. A.; Higgins, C. P.; Sunderland, E. M. Detection of Poly- and Perfluoroalkyl Substances (PFASs) in U.S. Drinking Water Linked to Industrial Sites, Military Fire Training Areas, and Wastewater Treatment Plants. Environmental Science & Technology Letters 2016, 3 (10), 344–350. https://doi.org/10.1021/acs.estlett.6b00260.
Javed, H.; Lyu, C.; Sun, R.; Zhang, D.; Alvarez, P. J. J. Discerning the Inefficacy of Hydroxyl Radicals during Perfluorooctanoic Acid Degradation. Chemosphere 2020, 247, 125883. https://doi.org/10.1016/j.chemosphere.2020.125883.
Kabiri, S.; Tucker, W.; Navarro, D. A.; Bräunig, J.; Thompson, K.; Knight, E. R.; Nguyen, T. M. H.; Grimison, C.; Barnes, C. M.; Higgins, C. P.; Mueller, J. F.; Kookana, R. S.; McLaughlin, M. J. Comparing the Leaching Behavior of Per- and Polyfluoroalkyl Substances from Contaminated Soils Using Static and Column Leaching Tests. Environ. Sci. Technol. 2022, 56 (1), 368–378. https://doi.org/10.1021/acs.est.1c06604.
Kannan, K.; Corsolini, S.; Falandysz, J.; Fillmann, G.; Kumar, K. S.; Loganathan, B. G.; Mohd, M. A.; Olivero, J.; Wouwe, N. V.; Yang, J. H.; Aldous, K. M. Perfluorooctanesulfonate and Related Fluorochemicals in Human Blood from Several Countries. Environmental Science & Technology 2004, 38 (17), 4489–4495. https://doi.org/10.1021/es0493446.
Kim, M. H.; Wang, N.; Chu, K. H. 6:2 Fluorotelomer Alcohol (6:2 FTOH) Biodegradation by Multiple Microbial Species under Different Physiological Conditions. Applied Microbiology and Biotechnology 2014, 98 (4), 1831–1840. https://doi.org/10.1007/s00253-013-5131-3.
Krause, H., B. Schweiger, E. Prinz, J. Kim, U. Steinfeld (2011). Degradation of persistent pharmaceuticals in aqueous solutions by a positive dielectric barrier discharge treatment. Journal of Electrostatics, 69(4):333-338.
Lakshminarasimman, N.; Gewurtz, S. B.; Parker, W. J.; Smyth, S. A. Removal and Formation of Perfluoroalkyl Substances in Canadian Sludge Treatment Systems – A Mass Balance Approach. Science of The Total Environment 2021, 754, 142431. https://doi.org/10.1016/j.scitotenv.2020.142431.
Lange, C. The Aerobic Biodegradation of N-EtFOSE Alcohol by the Microbial Activity Present in Municipal Wastewater Treatment Sludge. For 3M Company 2000.
Lazcano, R.K. ; Perre, C.; Mashtare, M. L.; Lee, L. S. Per- and Polyfluoroalkyl Substances in Commercially Available Biosolid-based Products: The Effect of Treatment Processes. Water Environment Research 2019, 91 (12), 1669–1677. https://doi.org/10.1002/wer.1174.
Li, R.; Munoz, G.; Liu, Y.; Sauvé, S.; Ghoshal, S.; Liu, J. Transformation of Novel Polyfluoroalkyl Substances (PFASs) as Co-Contaminants during Biopile Remediation of Petroleum Hydrocarbons. Journal of Hazardous Materials 2019, 362, 140–147. https://doi.org/10.1016/j.jhazmat.2018.09.021.
Li, Y.; Oliver, D. P.; Kookana, R. S. A Critical Analysis of Published Data to Discern the Role of Soil and Sediment Properties in Determining Sorption of per and Polyfluoroalkyl Substances (PFASs). Science of The Total Environment 2018, 628–629, 110–120. https://doi.org/10.1016/j.scitotenv.2018.01.167.
Liang, C.; Su, H.-W. (2009). Identification of Sulfate and Hydroxyl Radicals in Thermally Activated Persulfate. Industrial & Engineering Chemistry Research, 48 (11), 5558–5562. https://doi.org/10.1021/ie9002848.

Liu, J.; Mejia Avendaño, S. Microbial Degradation of Polyfluoroalkyl Chemicals in the Environment: A Review. Environment International 2013, 61, 98–114. https://doi.org/10.1016/j.envint.2013.08.022.

Loi, E. I. H.; Yeung, L. W. Y.; Taniyasu, S.; Lam, P. K. S.; Kannan, K.; Yamashita, N. Trophic Magnification of Poly- and Perfluorinated Compounds in a Subtropical Food Web. Environ. Sci. Technol. 2011, 45 (13), 5506–5513. https://doi.org/10.1021/es200432n.

Maizel, A. C.; Shea, S.; Nickerson, A.; Schaefer, C.; Higgins, C. P. Release of Per- and Polyfluoroalkyl Substances from Aqueous Film-Forming Foam Impacted Soils. Environ. Sci. Technol. 2021, 55 (21), 14617–14627. https://doi.org/10.1021/acs.est.1c02871.

McGuire, M.E., C. Schaefer, T. Richards, W.J. Backe, J.A. Field, E. Houtz, D.L. Sedlak, J.L. Guelfo, A. Wunsch, C. Higgins (2014). Evidence of Remediation-Induced Alteration of Subsurface Poly- and Perfluoroalkyl Substance Distribution at a Former Firefighter Training Area. Environmental Science & Technology, 48:6644-6652.

McKenzie, E.R., R.L. Siegrist, J.E. McCray, C.P. Higgins (2015). Effects of chemical oxidants on perfluoroalkyl acid transport in one-dimensional porous media columns. Environmental science & technology 49(3):1681-1689.

Mejia Avendaño, S.; Liu, J. Production of PFOS from Aerobic Soil Biotransformation of Two Perfluoroalkyl Sulfonamide Derivatives. Chemosphere 2015, 119, 1084–1090. https://doi.org/10.1016/j.chemosphere.2014.09.059.

Mejia-Avendaño, S.; Munoz, G.; Vo Duy, S.; Desrosiers, M.; Benoît, P.; Sauvé, S.; Liu, J. Novel Fluoroalkylated Surfactants in Soils Following Firefighting Foam Deployment During the Lac-Mégantic Railway Accident. Environ. Sci. Technol. 2017, 51 (15), 8313–8323. https://doi.org/10.1021/acs.est.7b02028.

Mejia-Avendaño, S.; Vo Duy, S.; Sauvé, S.; Liu, J. Generation of Perfluoroalkyl Acids from Aerobic Biotransformation of Quaternary Ammonium Polyfluoroalkyl Surfactants. Environmental Science & Technology 2016, 50 (18), 9923–9932. https://doi.org/10.1021/acs.est.6b00140.

Mejia-Avendaño, S.; Zhi, Y.; Yan, B.; Liu, J. Sorption of Polyfluoroalkyl Surfactants on Surface Soils: Effect of Molecular Structures, Soil Properties, and Solution Chemistry. Environ. Sci. Technol. 2020, 54 (3), 1513–1521. https://doi.org/10.1021/acs.est.9b04989.

Mededovic Thagard, S.; Stratton, G. R.; Dai, F.; Bellona, C. L.; Holsen, T. M.; Bohl, D. G.; Paek, E.; Dickenson, E. R. Plasma-based water treatment: development of a general mechanistic model to estimate the treatability of different types of contaminants. J. Phys. D: Appl. Phys. 2016, 50, 014003.

Munoz, G.; Duy, S. V.; Labadie, P.; Botta, F.; Budzinski, H.; Lestremau, F.; Liu, J.; Sauvé, S. Analysis of Zwitterionic, Cationic, and Anionic Poly- and Perfluoroalkyl Surfactants in Sediments by Liquid Chromatography Polarity-Switching Electrospray Ionization Coupled to High Resolution Mass Spectrometry. Talanta 2016, 152, 447–456. https://doi.org/10.1016/j.talanta.2016.02.021.

Nickerson, A.; Maizel, A. C.; Kulkarni, P. R.; Adamson, D. T.; Kornuc, J. J.; Higgins, C. P. Enhanced Extraction of AFFF-Associated PFAS from Source Zone Soils. Environ. Sci. Technol. 2020, 54 (8), 4952–4962. https://doi.org/10.1021/acs.est.0c00792.

Nickerson, A.; Maizel, A. C.; Olivares, C. I.; Schaefer, C. E.; Higgins, C. P. Simulating Impacts of Biosparging on Release and Transformation of Poly- and Perfluorinated Alkyl Substances from Aqueous Film-Forming Foam-Impacted Soil. Environ. Sci. Technol. 2021, 55 (23), 15744–15753. https://doi.org/10.1021/acs.est.1c03448.

Nickerson, A.; Rodowa, A. E.; Adamson, D. T.; Field, J. A.; Kulkarni, P. R.; Kornuc, J. J.; Higgins, C. P. Spatial Trends of Anionic, Zwitterionic, and Cationic PFAS at an AFFF-Impacted Site. Environ. Sci. Technol. 2021, 55 (1), 313–323. https://doi.org/10.1021/acs.est.0c04473.

Pan, L. W.; Siegrist, R. L.; Crimi, M. Effects of In Situ Remediation Using Oxidants or Surfactants on Subsurface Organic Matter and Sorption of Trichloroethene. Ground Water Monitoring & Remediation 2012, 32 (2), 96–105. https://doi.org/10.1111/j.1745-6592.2011.01377.x.

Park, S., L.S. Lee (2016). Heat-activated persulfate oxidation of PFOA, 6: 2 fluorotelomer sulfonate, and PFOS under conditions suitable for in-situ groundwater remediation. Chemosphere 145 (2016): 376-383.
Place, Benjamin J., and Jennifer A. Field (2012). Identification of novel fluorochemicals in aqueous film-forming foams used by the US military. Environmental science & technology 46:7120-7127.
Plumlee, M. H.; McNeill, K.; Reinhard, M. Indirect Photolysis of Perfluorochemicals: Hydroxyl Radical-Initiated Oxidation of N -Ethyl Perfluorooctane Sulfonamido Acetate (N -EtFOSAA) and Other Perfluoroalkanesulfonamides. Environ. Sci. Technol. 2009, 43 (10), 3662–3668. https://doi.org/10.1021/es803411w.
Qian, Y.; Guo, X.; Zhang, Y.; Peng, Y.; Sun, P.; Huang, C.-H.; Niu, J.; Zhou, X.; Crittenden, J. C. Perfluorooctanoic Acid Degradation Using UV–Persulfate Process: Modeling of the Degradation and Chlorate Formation. Environmental Science & Technology 2016, 50 (2), 772–781. https://doi.org/10.1021/acs.est.5b03715.
Rak, A., C.M. Vogel (2009). Increasing regulation of perfluorinated compounds and the potential impacts at Air Force installations, in, Prepared by Noblis for the U.S. Air Force and the Office of the Deputy Under Secretary of Defense Installations and Environment, Chemical and Material Risk Management Directorate.
Ryan, J. N.; Illangasekare, T. H.; Litaor, M. I.; Shannon, R. Particle and Plutonium Mobilization in Macroporous Soils during Rainfall Simulations. Environmental Science & Technology 1998, 32 (4), 476–482. https://doi.org/10.1021/es970339u.
Schaefer, C. E.; Choyke, S.; Ferguson, P. L.; Andaya, C.; Burant, A.; Maizel, A.; Strathmann, T. J.; Higgins, C. P. Electrochemical Transformations of Perfluoroalkyl Acid (PFAA) Precursors and PFAAs in Groundwater Impacted with Aqueous Film Forming Foams. Environ. Sci. Technol. 2018, 52 (18), 10689–10697. https://doi.org/10.1021/acs.est.8b02726.
Schultz, M.M., D.F. Barofsky, J.A. Field (2004). Quantitative determination of fluorotelomer sulfonates in groundwater by LC MS/MS. Environmental Science & Technology, 38:1828-1835.
Schymanski, E. L.; Jeon, J.; Gulde, R.; Fenner, K.; Ruff, M.; Singer, H. P.; Hollender, J. Identifying Small Molecules via High Resolution Mass Spectrometry: Communicating Confidence. Environ. Sci. Technol. 2014, 48 (4), 2097–2098. https://doi.org/10.1021/es5002105.
Sepulvado, J.G., A.C. Blaine, L.S. Hunda., C.P. Higgins (2011). Occurrence and fate of perfluorochemicals in soil following the land application of municipal biosolids. Environmental science & technology 45(19):8106-8112.
Shojaei, M.; Kumar, N.; Chaobol, S.; Wu, K.; Crimi, M.; Guelfo, J. Enhanced Recovery of Per-and Polyfluoroalkyl Substances (PFAS) from Impacted Soils Using Heat Activated Persulfate. Environmental Science & Technology 2021.
Siegrist, R.L., M. Crimi, T.J. Simpkin (2011). In Situ Chemical Oxidation for Groundwater Remediation. Spring Science+Business Media, LLC, New York, NY. A volume in SERDP/ESTCP Remediation Technology Monograph Series, C.H. Ward (Series ed.).
Simunek, J., Sejna, M., Van Genuchten, M. T., Šimůnek, J., Šejna, M., Jacques, D., ... & Sakai, M. (1998). HYDRUS-1D. Simulating the one-dimensional movement of water, heat, and multiple solutes in variably-saturated media, version, 2.
Sörengård, M.; Lindh, A.; Ahrens, L. Thermal Desorption as a High Removal Remediation Technique for Soils Contaminated with Per-and Polyfluoroalkyl Substances (PFAS). PloS one 2020, 15 (6), e0234476.
Standard, A. Standard Test Method for PH of Soils. ASTM International, West Conshohocken, PA 2016.
Stratton, G., Bellona, C., Dai, F., Holsen, T., Dickenson, E., Mededovic Thagard, S. (2015). Plasma-based Water Treatment: Conception and Application of a New General Principle for Reactor Design. Chemical Engineering Journal, 273: 543-550.
Stratton, G. R.; Dai, F.; Bellona, C. L.; Holsen, T. M.; Dickenson, E. R. V.; Mededovic Thagard, S. Plasma-based water treatment: Efficient transformation of perfluoroalkyl substances in prepared solutions and contaminated groundwater. Environ. Sci. Technol. 2017, 51, 1643 – 1648.

Stratton, G.R., F. Dai, C. L. Bellona, T. M. Holsen, E. R. V. Dickenson and S. Mededovic Thagard (2016). Plasma-based water treatment: Demonstration of efficient perfluorooctanoic acid (PFOA) degradation and identification of key reactants. Environmental Science & Technology, accepted.

Stratton, G. R., F. Dai, C. Bellona, T. Holsen, E.R.V. Dickenson E. R. V. S. Mededovic Thagard, (2017). Plasma-Based Water Treatment: Efficient Transformation of Perfluoroalkyl Substances in Prepared Solutions and Contaminated Groundwater. Environmental Science & Technology 2017, 51(3):1643-1648.

Sun, B.; Ma, J.; Sedlak, D. L. Chemisorption of Perfluorooctanoic Acid on Powdered Activated Carbon Initiated by Persulfate in Aqueous Solution. Environmental Science & Technology 2016, 50 (14), 7618–7624. https://doi.org/10.1021/acs.est.6b00411.

Suthersan S., J. Quinnan, J. Horst, I. Ross, E. Kalve, C. Bell, T. Pancras (2016). Making Strides in the Management of "Emerging Contaminants". Groundwater Monitoring & Remediation, 36(1):15-25.

Tavakkoli, E.; Rengasamy, P.; Smith, E.; McDonald, G. K. The Effect of Cation-Anion Interactions on Soil PH and Solubility of Organic Carbon: Cation-Anion Interaction and DOC Solubility. Eur J Soil Sci 2015, 66 (6), 1054–1062. https://doi.org/10.1111/ejss.12294.

Tebes-Stevens, C.; Patel, J. M.; Jones, W. J.; Weber, E. J. Prediction of Hydrolysis Products of Organic Chemicals under Environmental PH Conditions. Environ. Sci. Technol. 2017, 51 (9), 5008–5016. https://doi.org/10.1021/acs.est.6b05412.

Tucker, D. K.; Macon, M. B.; Strynar, M. J.; Dagnino, S.; Andersen, E.; Fenton, S. E. The Mammary Gland Is a Sensitive Pubertal Target in CD-1 and C57Bl/6 Mice Following Perinatal Perfluorooctanoic Acid (PFOA) Exposure. Reproductive Toxicology 2015, 54, 26–36. https://doi.org/10.1016/j.reprotox.2014.12.002.

Umeh, A. C.; Naidu, R.; Shilpi, S.; Boateng, E. B.; Rahman, A.; Cousins, I. T.; Chadalavada, S.; Lamb, D.; Bowman, M. Sorption of PFOS in 114 Well-Characterized Tropical and Temperate Soils: Application of Multivariate and Artificial Neural Network Analyses. Environ. Sci. Technol. 2021, 55 (3), 1779–1789. https://doi.org/10.1021/acs.est.0c07202.

USEPA. Drinking Water Health Advisory for Perfluorooctanoic Acid (PFOA); EPA 822-R-16-005; Office of Water Health and Ecological Criteria Division: Washington, DC, 2016.

USEPA. Drinking Water Health Advisory for Perfluorooctane Sulfonate (PFOS); EPA 822-R-16-004; Office of Water Health and Ecological Criteria Division: Washington, DC, 2016.

USEPA. Interim Recommendations to Address Groundwater Contaminated with PFOA and PFOS https://www.epa.gov/pfas/interim-recommendations-addressing-groundwater-contaminated-pfoa-and-pfos (accessed Oct 28, 2020).

Vecitis, C., H. Park, J. Cheng, B. Mader, M. Hoffmann (2008). Enhancement of perfluorooctanoate and perfluorooctanesulfonate activity at acoustic cavitation bubble interfaces. The Journal of Physical Chemistry C, 112(43):16850-16857.

Washington, J. W.; Jenkins, T. M. Abiotic Hydrolysis of Fluorotelomer-Based Polymers as a Source of Perfluorocarboxylates at the Global Scale. Environ. Sci. Technol. 2015, 49 (24), 14129–14135. https://doi.org/10.1021/acs.est.5b03686.

Washington, J. W.; Jenkins, T. M.; Rankin, K.; Naile, J. E. Decades-Scale Degradation of Commercial, Side-Chain, Fluorotelomer-Based Polymers in Soils and Water. Environ. Sci. Technol. 2015, 49 (2), 915–923. https://doi.org/10.1021/es504347u.

Weber, W. J.; Huang, W.; LeBoeuf, E. J. Geosorbent Organic Matter and Its Relationship to the Binding and Sequestration of Organic Contaminants. Colloids and Surfaces A: Physicochemical and Engineering Aspects 1999, 151 (1–2), 167–179. https://doi.org/10.1016/S0927-7757(98)00820-6.

Weiner, B.; Yeung, L. W. Y.; Marchington, E. B.; D'Agostine, L. A.; Mabury, S. A. Organic fluorine content in aqueous film forming foams (AFFFs) and biodegradation of the foam component 6 : 2 fluorotelomermercaptoalkylamido sulfonate (6 : 2 FTSAS). Environmental Chemistry 2013 10(6) 486-493. https://doi.org/10.1071/EN13128.

Xiao, F.; Jin, B.; Golovko, S. A.; Golovko, M. Y.; Xing, B. Sorption and Desorption Mechanisms of Cationic and Zwitterionic Per- and Polyfluoroalkyl Substances in Natural Soils: Thermodynamics and Hysteresis. Environ. Sci. Technol. 2019, 53 (20), 11818–11827. https://doi.org/10.1021/acs.est.9b05379.

Xiao, X.; Ulrich, B. A.; Chen, B.; Higgins, C. P. Sorption of Poly- and Perfluoroalkyl Substances (PFASs) Relevant to Aqueous Film-Forming Foam (AFFF)-Impacted Groundwater by Biochars and Activated Carbon. Environmental Science & Technology 2017, 51 (11), 6342–6351. https://doi.org/10.1021/acs.est.7b00970.

Yasuoka, K., K. Sasaki, R. Hayashi, (2011). An energy-efficient process for decomposing perfluorooctanoic and perfluorooctane sulfonic acids using dc plasmas generated within gas bubbles. Plasma Sources Science and Technology, 20(3):034009.

Yeung, L. W. Y.; De Silva, A. O.; Loi, E. I. H.; Marvin, C. H.; Taniyasu, S.; Yamashita, N.; Mabury, S. A.; Muir, D. C. G.; Lam, P. K. S. Perfluoroalkyl Substances and Extractable Organic Fluorine in Surface Sediments and Cores from Lake Ontario. Environment International 2013, 59, 389–397.

You, C.; Jia, C.; Pan, G. Effect of Salinity and Sediment Characteristics on the Sorption and Desorption of Perfluorooctane Sulfonate at Sediment-Water Interface. Environmental Pollution 2010, 158 (5), 1343–1347. https://doi.org/10.1016/j.envpol.2010.01.009.

You, S.-J.; Yin, Y.; Allen, H. E. Partitioning of Organic Matter in Soils: Effects of PH and Water/Soil Ratio. Science of The Total Environment 1999, 227 (2–3), 155–160. https://doi.org/10.1016/S0048-9697(99)00024-8.

Zareitalabad, P.; Siemens, J.; Hamer, M.; Amelung, W. Perfluorooctanoic Acid (PFOA) and Perfluorooctanesulfonic Acid (PFOS) in Surface Waters, Sediments, Soils and Wastewater – A Review on Concentrations and Distribution Coefficients. Chemosphere 2013, 91 (6), 725–732. https://doi.org/10.1016/j.chemosphere.2013.02.024.

Zhang, Y.; Liu, J.; Moores, A.; Ghoshal, S. Transformation of 6:2 Fluorotelomer Sulfonate by Cobalt(II)-Activated Peroxymonosulfate. Environ. Sci. Technol. 2020, 54 (7), 4631–4640. https://doi.org/10.1021/acs.est.9b07113.

Zhao, X.; Voice, T. C. Assessment of Bioavailability Using a Multicolumn System. Environ. Sci. Technol. 2000, 34 (8), 1506–1512. https://doi.org/10.1021/es991100b.

Zheng, Z.; Aagaard, P.; Breedveld, G. D. Sorption and Anaerobic Biodegradation of Soluble Aromatic Compounds during Groundwater Transport. 1. Laboratory Column Experiments. Environmental Geology 2002, 41 (8), 922–932.

APPENDICES

Supporting Data:

***PFAS Analytical Method*:** A hybrid targeted/non-targeted analytical method will be employed to quantify the loss of target compounds (PFASs) and identify degradation products (Crimmins et al., 2014). Specifically, samples will be analyzed using a Waters Acquity Ultra-high Pressure Liquid Chromatograph coupled to a Xevo G2 S Quadrupole Time of Flight mass spectrometer (UPLC-QToF) with electrospray ionization (ESI) operated in a data independent MS/MS mode. This feature allows for the indiscriminant production of exact mass (5 ppm mass error) precursor and product ions for unknown identification and confirmation. The sensitivity of this method rivals tradition triple quadrupole mass spectrometers with sensitivities with a signal to noise ratio of >10 for PFOS at 0.1 pg on-column. Initial experiments will utilize "dilute and shoot" or basic liquid-liquid extractions to isolate the amphiphilic PFSAs from hydrocarbon co-contaminants. Solid phase extraction (SPE) enrichment usage will be used as a last resort to minimize selecting against degradation products. If needed for low level samples, a mixed mode C18/weak ion exchange column (Waters Corp.) will be used. Target compounds (Table C-1) and degradation products will be quantified relative to a series of isotopically labelled perfluoroalkyl acids with chain lengths ranging C4 to C16 added prior to analysis. An automated search algorithm will be deployed to screen for atypical polyfluoroalkyl products (Baygi et al., 2016) potentially assisting in reactor byproduct mass closer.

Potential semi- and non-volatile products will be identified using the UPLC-QToF. The ElectroSpray Ionization (ESI) source, operated in data independent MS/MS mode, will provide precursor/product pairs for improved species identification. Low molecular weight compounds will be identified and quantified in headspace samples introduced into a gas chromatographic system via direct injection or a canister/desorption tube system (Markes Thermal Desorption).

Peak identifications will be performed by spectral library matching and/or molecular formula determination using the high resolution MS data. Byproduct identities will be confirmed with neat standards where available. Sample enrichment via solid phase extraction (SPE) will be employed when direct injection is not possible using EPA 537 and canister/desorption tube (Park et al., 2009) for UPLC and volatile GC-MS amenable organic byproducts, respectively. We have shown the utility of the UPLC-QToF for trace level PFAA analysis and non-targeted chemical screening by identifying several novel polyfluorinated contaminants in Great Lakes fish using a screening algorithm capable of efficiently searching chromatographic/mass spectrometric data for unknown compounds (Crimmins et al, 2014; Baygi et al., 2016). A similar analysis will be performed on the UPLC-QToF data due to the absence of commercially available ESI spectral libraries. The LECO GCxGC HRT-TOFMS provides unmatched compound resolution (multidimensional GC) and identification (HRT) allowing for the detection and confirmation of hundreds-to-thousands of compounds at trace concentrations. The traditional electron impact ionization (EI) allows for the use of commercial spectral libraries (NIST and Wiley) containing 100,000s of compounds for volatile byproduct identification. When unacceptable candidates are suggested using the library screens alone, exact mass measurements allow for molecular formula determinations.

Table A 1. Target PFAS compounds, method detection limits, and labeled species.

Target Analytes		Method Detection Limits (MDL)
PFBA	Perfluoro-n-butanoic acid	5
PFPeA	Perfluoro-n-pentanoic acid	2
PFHxA	Perfluoro-n-hexanoic acid	4
PFHpA	Perfluoro-n-heptanoic acid	4
PFOA	Perfluoro-n-octanoic acid	3
PFNA	Perfluoro-n-nonaoic acid	3
PFDA	Perfluoro-n-decanoic acid	3
PFUdA	Perfluoro-n-undecanoic acid	16
PFDoA	Perfluoro-n-dodecanoic acid	5
PFTrDA	Perflluoro-n-tridecanoic acid	4
PFTeDA	Perflluoro-n-tetradecanoic acid	7
PFBS	Potassium perfluoro-1-butanesulfonate	3
PFPeS	Sodium perfluoro-1-pentanesulfonate	3
PFHxS	Sodium perfluoro-1-hexanesulfonate	4
PFHpS	Sodium-perfluoro-1-heptanesulfonamide	7
PFOS	Sodium perfluoro-1-octanesulfonate	7
PFNS	Sodium perfluoro-1-nonanesulfonate	8
PFDS	Sodium-perfluoro-1-decanesulfonate	9
4:2 FTS	Sodium 1H,1H,2H,2H-perfluorohexane sulfonate	3
6:2FTS	Sodium 1H,1H,2H,2H-perfluorooctane sulfonate	7
8:2 FTS	Sodium 1H,1H,2H,2H-perfluorodecane sulfonate	6
10:2 FTS	Sodium 1H,1H,2H,2H-perfluorododecane sulfonate	9
FOSA-1	Perfluoro-1-octanesulfonamide	4
FOSAA	Perfluoro-1-octanesulfonamidoacetic acid	5
N-MeFOSAA	N-methylperfluoro-1-octanesulfonamidoacetic acid	17
N-MeFOSA-M	N-methylperfluoro-1-octanesulfonamide	11
N-EtFOSAA	N-ethylperfluoro-1-octanesulfonamidoacetic acid	13
N-EtFOSA-M	N-ethylperfluoro-1-octanesulfonamide	10

Labeled Species	
MPFBA	Perfluoro-n-[$^{13}C_4$]butanoic acid
MPFHxA	Perfluoro-n-[1,2-$^{13}C_2$]hexanoic acid
MPFHxS	Pefluoro-1-hexane[$^{18}O_2$]sulfonate
MPFOA	Perfluoro-n-[1,2,3,4-$^{13}C_4$]octanoic acid
MPFOS	Perfluoro-n-[1,2-$^{13}C_2$] undecanoic acid
MPFNA	Perfluoro-n-[1,2,3,4,5-$^{13}C_2$] undecanoic acid
MPFDA	Perfluoro-n-[1,2-$^{13}C_2$]decanoic acid
MPFUnA	Perfluoro-n-[1,2-$^{13}C_2$] undecanoic acid
MPFDoA	Perfluoro-n-[1,2-$^{13}C_2$]dodecanoic acid

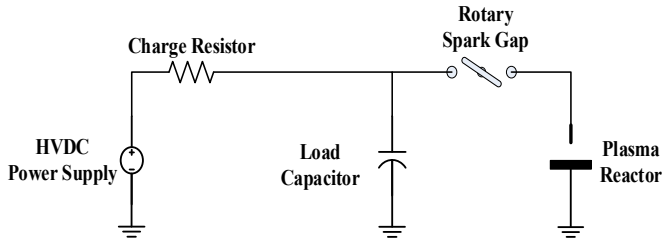

Figure A 1. The plasma-generating electrical network schematic. High voltage power supply (HVDC) produces a high voltage output but at low power. Load capacitor is charged by the HVDC. The rotary spark gap allows the capacitor to discharge upon alignment, such that an electrical pulse with high voltage and high power is delivered to the high voltage electrode in the reactor and produces plasma. For each pulse, the plasma is only present for a few microseconds followed by 10-50 milliseconds during which the capacitor is charged and the plasma is absent.

Table A 2. Mass spectra library results for peaks in the Total Current Ion Chromatogram of the gas phase sample from the PFOA degradation experiments.

RT	NIST Mass Spectral ID[1]
2.94	perfluorohexane
3	perfluorohexane
3.12	Hexadecafluorooctyl fluorosulfate[3]
3.32	Pentadecafluorooctanoic acid[3]
3.61	1H,1H-Perfluoro-1-heptanol[3]
3.66	Hexadecafluoroheptane
4.1	Hexadecafluorooctyl fluorosulfate[3]
[1]Library result, [2]Forward/reverse match score out of 1000, [3]ID not consistent with instrument conditions	

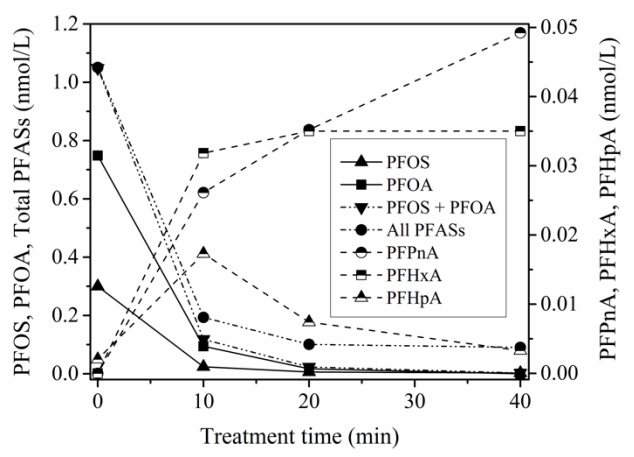

Figure A 2. Concentration profiles showing the reduction in concentrations of PFOA and PFOS, and a corresponding increase in concentrations of PFHpA, PFHxA and PFPnA.

List of Scientific/Technical Publications:

A. Articles in peer-reviewed journals (specify whether in print, accepted for publication, or submitted for publication).

- Singh, R. K., Multari, N., Nau-Hix, C., Anderson, R. H., Richardson, S. D., Holsen, T. M., & Mededovic Thagard, S. (2019). Rapid removal of poly-and perfluorinated compounds from investigation-derived waste (IDW) in a pilot-scale plasma reactor. *Environmental science & technology*, *53*(19), 11375-11382.
- Singh, R. K., Multari, N., Nau-Hix, C., Anderson, R. H., Richardson, S. D., Holsen, T. M., & Mededovic Thagard, S. (2019). Rapid removal of poly-and perfluorinated compounds from investigation-derived waste (IDW) in a pilot-scale plasma reactor. *Environmental science & technology*, *53*(19), 11375-11382.
- Shojaei, M., Kumar, N. and Guelfo, J. An Integrated Approach for Improved Liquid Chromatography Mass Spectrometry Based Determinations of Total PFAS in AFFF and AFFF-impacted Soils. In Preparation.
- Shojaei, M., Joyce, A., Ferguson, P.L. and Guelfo, J. Novel Per- and Polyfluoroalkyl Substances in an Active-Use C6-based Aqueous Film Forming Foam. *Journal of Hazardous Materials Letters*. In Review.
- Shojaei, M., Kumar, N., Chaobol, S., Wu, K, Crimi, M, and Guelfo, J. (2021) Enhanced recovery of per- and polyfluoroalkyl substances (PFAS) from impacted soils using heat activated persulfate. *Environmental Science & Technology*. (55)14, 9805-9816. https://doi.org/10.1021/acs.est.0c08069

B. Technical reports (specify whether in print, accepted for publication, or submitted for publication).

- N/A

C. Conference or symposium proceedings scientifically recognized and referenced (other than abstracts).

- N/A

D. Conference or symposium abstracts.

- **Guelfo, J.*** and Shojaei, M. Breaking Up is Complicated: Strategies to Simplify PFAS Remediation. American Chemical Society (ACS) North American Spring Meeting. 20-24 Mar 2022, San Diego, CA (Platform).
- **Guelfo, J.***, Kumar, N., and Shojaei, M. An Integrated Approach for Determination of Total PFAS. American Chemical Society (ACS) North American Spring Meeting. 20-24 Mar 2022, San Diego, CA (Platform).
- Guelfo, J.L. and Shojaei, M. Breaking Up is Complicated: Strategies to Simplify PFAS Remediation, Duke University Environmental Engineering Seminar, 27 Sept 2021. Durham, NC.
- **Crimi M.** (2021). Remediation of Chlorinated and Fluorinated Organic Contaminants. RemTECH Europe. Online. September 2021.
- Shojaei, M., Guelfo, J., & **Crimi, M**. (2021). Enhanced Total PFAS Recovery From AFFF-Impacted Soils Using In Situ Pre-Treatment. In *SETAC North America 41st Annual Meeting*. SETAC.
- **Crimi M.** (2021). PFAS Remediation Options and Case Study. LASTFIRE Foam Summit. September 2021.
- Shojaei, M., Guelfo, J., and Crimi, M. Combined In Situ / Ex Situ Treatment Train for Remediation of PFAS Contaminated Groundwater, SERDP-ESTCP Annual Project Meeting: PFAS Ecotoxicity, Analyses, Fate, Transport, and Treatment, 19-22 July 2021,San Pedro, CA. (Poster)

- Shojaei, M., Crimi, M., and Guelfo, J. Enhanced Total PFAS Recovery From AFFF-Impacted Soils Using In Situ Pre-Treatment, SERDP-ESTCP Symposium, 30 November-4 December 2020, Virtual. (Poster).
- Kumar, N.,* Shojaei, M., Chaobol, S. and **Guelfo, J.,** What PFAS are Present in Samples After the Total Oxidized Precursor (TOP) Assay? Application of High-Resolution Mass Spectrometry (HRMS) for Improved Understanding of TOP, SETAC North American Annual Meeting, 15-19 Nov 2020, Virtual. (Platform)
- Shojaei, M.,* Crimi, M., and **Guelfo, J.** Enhanced Total PFAS Recovery from AFFF-Impacted Soils Using In Situ Pre-Treatment, SETAC North American Annual Meeting, 15-19 Nov 2020, Virtual. (Platform)
- Guelfo, J. Enhanced PFAS Recovery from Impacted Soil Using In Situ Pre-Treatment, Addressing the next generation of persistent contaminants: Per- and polyfluoroalkyl substances (PFAS), University Consortium Fall Focus Meeting, 29 Sept - 1 Oct 2020. Virtual
- Guelfo, J. Oxidation of Forever Chemicals: Applications for Analysis and Remediation, University of Minnesota Environmental Engineering Seminar, 25 Sept 2020. Virtual
- **Crimi M.**, T.M. Holsen, S. Mededovic Thagard, J. Guelfo, S. Woodward, N. Hagelin, D. Woodward, J. Heath (2020). Optimization of Regenerable Ion-Exchange for PFAS. Groundwater Treatment - Outcomes from Two SERDP & ESTCP Projects. Northeast PFAS Science Conference: Public Health and the Environment. Framingham, MA. April 2020.
- **Crimi M.** (2020). Treatment of PFAS Contaminated Soil and Groundwater. 2020 Soil and Groundwater Practical Remediation Technology Symposium. SG RemTech Symposium, Taiwan.
- Shojaei, M. and **Guelfo, J.*** Enhanced PFAS Recovery from Impacted Soil Using In Situ Pre-Treatment, 2020 Emerging Contaminants Summit, 10-11 Mar 2020, Westminster, CO. (Platform)
- **Crimi M.** (2019). Review of Potential PFAS Remediation Options and Case Study. LASTFIRE/API/DFW Joint Meetings and Demonstrations. November 2019. Dallas, TX.
- **Crimi M.** (2019). Remediation Options for PFAS-Contaminated Groundwater (2019). SERDP & ESTCP Webinar Series. October 2019.
- **Crimi M.** (2019). Panelist: PFAS Remediation Research. PFAS Experts Symposium. May 2019. Washington, D.C.
- **Crimi M.** (2019). Remediation of PFAS-Contaminated Groundwater. Clarkson University Center for Advanced Materials Processing Annual Meeting. May 2019. Syracuse, NY.
- **Crimi M.** (2019). PFAS Remediation – The Next Frontier. PFAS Experts Symposium. May 2019. Arlington, VA.
- **Crimi M.**, T.M. Holsen, S. Mededovic Thagard, J. Guelfo, S. Woodward, N. Hagelin, D. Woodward, J. Heath (2019). Combined In Situ/Ex Situ Treatment Train for Remediation of PFAS Contaminated Groundwater. SERDP-ESTCP Symposium, Enhancing DoD's Mission Effectiveness. Dec. 2019. Washington D.C.
- **Crimi M**., T.M. Holsen, S. Mededovic Thagard, J. Guelfo, S. Woodward, N. Hagelin, D. Woodward, J. Heath (2019). Combined In Situ / Ex Situ Treatment Train for Remediation of PFAS Contaminated Groundwater. SERDP-ESTCP PFAS Project Meeting. July 2019. San Diego, CA.
- **Crimi M.**, T.M. Holsen, S. Mededovic Thagard, D. Siriwardena, J. Guelfo, S. Woodward, N. Hagelin, D. Woodward, J. Heath (2019). Combined In Situ / Ex Situ Treatment of Per- and Polyfluoroalkyl Substance (PFAS)-Contaminated Groundwater. Fifth International Symposium on Bioremediation and Sustainable Environmental Technologies. April 2019. Baltimore, MD.

- **Crimi M.**, T.M. Holsen, S. Mededovic Thagard, D. Siriwardena, J. Guelfo, S. Woodward, N. Hagelin, D. Woodward, J. Heath (2019). Treatment of Per- and Polyfluoroalkyl Substance (PFAS) Contaminated Groundwater Using an In Situ / Ex Situ Combined Remedy. ACS National Meeting & Expo. April 2019. Orlando, FL.
- **Crimi M.**, T. Holsen, S. Thagard Mededovic, J. Guelfo, J. Heath, N. Hagelin, D. Woodward, M. Malyk, S. S. Woodward, J. Berry, M. Nickelsen, J. Kornuc (2018). Combined In Situ / Ex Situ Treatment Train for Remediation of PFAS Contaminated Groundwater. SERDP-ESTCP Symposium, Enhancing DoD's Mission Effectiveness. Nov. 2018. Washington D.C.

E. Text books or book chapters.
- N/A

Other Supporting Materials:

A. Patents
- N/A

B. Protocols/user guides
- N/A

C. Scientific or technical awards or honors
- Environmental Restoration ESTCP Project of the Year Award for their work titled: "Demonstration and Validation of the Horizontal Reactive Media Treatment Well (HRX Well®) for Managing Contaminant Plumes in Complex Geological Environments." (December 2020)
- Outstanding Presentation Award of the ACS Spring 2019 National Meeting ENVR Symposium of Innovative & Practical Approaches for the Treatment of PFAS (April 2019)